Mathematical Assessment of Control Measures Against Mosquito-borne Diseases

by

Enahoro A. Iboi

A Dissertation Presented in Partial Fulfillment
of the Requirements for the Degree
Doctor of Philosophy

Approved April 2020 by the
Graduate Supervisory Committee:

Abba B. Gumel, Chair
Carl Gardner
Krijn Paaijmans
Yang Kuang
Yun Kang

ARIZONA STATE UNIVERSITY

May 2020

ABSTRACT

Mosquitoes are the greatest killers of mankind, and diseases caused by mosquitoes continue to induce major public health and socio-economic burden in many parts of the world (notably in the tropical sub-regions). This dissertation contributes in providing deeper qualitative insights into the transmission dynamics and control of some mosquito-borne diseases of major public health significance, such as malaria and dengue. The widespread use of chemical insecticides, in the form of long-lasting insecticidal nets (LLINs) and indoor residual spraying, has led to a dramatic decline in malaria burden in endemic areas for the period 2000-2015. This prompted a concerted global effort aiming for malaria eradication by 2040. Unfortunately, the gains recorded are threatened (or not sustainable) due to *Anopheles* resistance to all the chemicals embedded in the existing insecticides. This dissertation addresses the all-important question of whether or not malaria eradication can indeed be achieved using insecticides-based control. A novel mathematical model, which incorporates the detailed *Anopheles* lifecycle and local temperature fluctuations, was designed to address this question. Rigorous analysis of the model, together with numerical simulations using relevant data from endemic areas, show that malaria elimination in meso- and holo-endemic areas is feasible using moderate coverage of moderately-effective and high coverage of highly-effective LLINs, respectively. Biological controls, such as the use of sterile insect technology, have also been advocated as vital for the malaria eradication effort. A new model was developed to determine whether the release of sterile male mosquitoes into the population of wild adult female *Anopheles* mosquito could lead to a significant reduction (or elimination) of the wild adult female mosquito population. It is shown that the frequent release of a large number of sterile male mosquitoes, over a one year period, could lead to the effective control of the targeted mosquito population. Finally, a new model was designed and used to study the trans-

mission dynamics of dengue serotypes in a population where the *Dengvaxia* vaccine is used. It is shown that using of the vaccine in dengue-naive populations may induce increased risk of severe disease in these populations.

DEDICATION

"Every good gift and every perfect gift is from above, and cometh down from the Father of lights, with whom is no variableness, neither shadow of turning" James 1:17.

"As long as the earth remains, there will be planting and harvest, cold and heat, summer and winter, day and night" Genesis 8:22.

To my late Dad Sylvester Ekoh Iboi

With tears in my eyes and joy in my heart, I would like to thank you for all your sacrifices to make me whom I am today. You saw the future and gave your life in order for me to achieve greatness in life. As long as I remain on earth, I will forever be indebted to you. I will proclaim to generations to come the sacrifices you made for them to have a good life.

ACKNOWLEDGMENTS

My appreciation first of all goes to God Almighty the giver of life. I would like to thank my advisor Professor Abba B. Gumel for his fatherly role during my studies. I am very thankful for your understanding, patience during the early stage of my graduate studies and for your constructive criticism that has very much improved me in all facets of life. During my academic journey, you taught me not just to be great academically but to be a good person in life. Sir, I will forever be indebted to you for standing by me during my difficult times. I would like to thank my dissertation committee members: Professor Yang Kuang, Professor Carl Gardner, Professor Yun Kang and Professor Krijn Paaijmans, for their insightful comments, support and guidance during the writing of this thesis. I am also very thankful to Dr. Steffen Eikenberry for his support, mentor-ship and collaborations during my graduate studies.

I would like to thank my amiable wife (Oiza Oluwabukola Aliu) and the wonderful kids God blessed us with (Vania Omozele Iboi & Nuel Oseremhen Iboi) for their love, understanding, encouragement during my graduate studies. I would not have come this far if not for the strength I draw in your support. I would like to thank my mother (Mrs Mercy Iboi: Nee Inegbenijie) for those sleepless nights praying and fasting on my behalf. Indeed, I can attest to the fact that those prayers brought me this far. Also, I would like to thank my brothers (Mr Osagie Iboi & Mr Emhenya Iboi) and my only sister (Mrs Gloria Fasayo: Nee Iboi) for all your prayers, support, and encouragement during my graduate studies. I am thankful for the bond that has kept us together. I also want to thank my mother in-law (Mrs Florence Aliu) for your constant prayers and encouragement during my studies. I am very much indebted to my reliable friend (Kehinde Onadipe). You stood by me and supported me during my entire studies. I am also thankful to Dr. Benard Ikhimwin (trustworthy and

reliable) for your friendship all through these years and also for the valuable insight you provided me when I was writing my MATLAB Codes. I am also indebted to Professor Daniel Okuonghae (my academic mentor) for introducing me to the field of mathematical biology. I will like to thank all the friends (that became part of my family) I made at Arizona State during my program. You all made my stay at Arizona State worth while. Finally, this dissertation will not be complete without specially acknowledging my fathers in the lord (Pastor Gbenga Oladiran & Pastor A.S. Ariyibi) for their prayers, support, encouragement from the first day they learn't of my desire for a graduate degree. I will forever be indebted to Pastor Gbenga Oladiran for your widows mite that brought me to the United States of America for my graduate studies.

TABLE OF CONTENTS

CHAPTER Page

CHAPTER Page

LIST OF TABLES

Table Page

LIST OF FIGURES

Figure Page

Figure Page

Figure Page

Figure Page

Chapter 1

INTRODUCTION

1.1 Mosquito-Borne Diseases (MBDs)

Mosquitoes are the principal vectors of numerous mosquito-borne diseases (MBDs) of major public health concern, including malaria (Cailly et al., 2012; Chitnis et al., 2008; Mordecai et al., 2013; WHO et al., 2017), dengue (Esteva and Vargas, 2000; Iboi and Gumel, 2018; Wu et al., 2009), West Nile virus (Abdelrazec and Gumel, 2017; Lewis et al., 2006; Wan and Zhu, 2010), Zika (Abdelrazec and Gumel, 2017; Yakob and Walker, 2016) and Chikungunya (Abdelrazec and Gumel, 2017; Yakob and Walker, 2016). Of the over 3,500 described species of mosquitoes, about 200 are known to be capable of transmitting infectious diseases to humans (CDC, 2019a). Malaria is the most devastating of all the MBDs, accounting for approximately 214 (149-303) million cases and 438,000 (236,000-635,000) deaths annually, with the majority of deaths occurring in children under the age of five and in pregnant women (WHO, 2018b). Dengue is another MBD of major public health importance. It accounts for an estimated 390 (284-528) million dengue infections each year with about half of the world's population now at risk of the infection (WHO, 2019). Overall, MBDs account for approximately 600 million cases and over 1 million deaths globally (WHO, 2019). Figure 1.1 depicts the global distribution of some MBDs.

The life-cycle of a mosquito alternates between the free-flying adult stage and several aquatic juvenile stages (eggs, larval, and pupae stages) (Abdelrazec and Gumel, 2017; Afrane et al., 2005; Bayoh and Lindsay, 2003; Dao et al., 2006). Adult female mosquitoes require a blood meal for the development of eggs. Upon successful de-

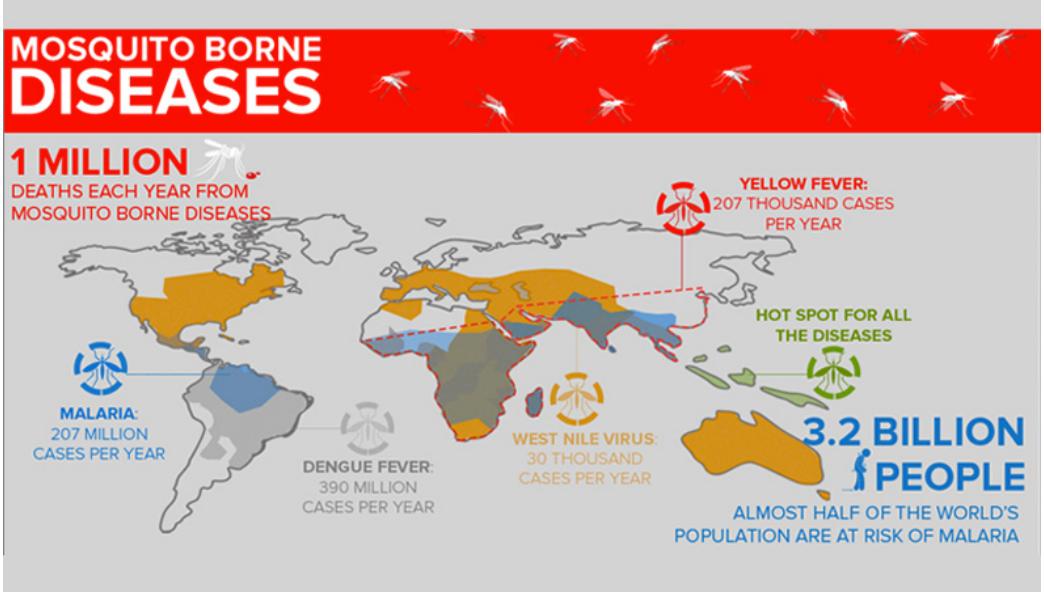

Figure 1.1: Global Distribution of Mosquito-Borne Diseases (Lyons, 2015).

velopment of the eggs, the adult female mosquito oviposits directly onto standing water, where the eggs hatch, releasing larvae that pass through four instars and then develop into pupae (Abdelrazec and Gumel, 2017; Afrane et al., 2005; Bayoh and Lindsay, 2003; Dao et al., 2006). Adult mosquitoes emerge from the pupae following metamorphosis and then fly away as depicted in Figure 1.2.

1.2 Transmission and Global Distribution of MBDs

1.2.1 Malaria

Malaria, the deadliest of all MBDs, is a parasitic disease caused by protozoan *Plasmodium* parasites (Carter and Mendis, 2002; Loy et al., 2017; WHO, 2016, 2017a). It spread between humans *via* the bite of infected adult female *Anopheles* mosquitoes. The disease is endemic in 91 countries, and caused 219 million cases and 435,000 deaths in 2017 (Camara et al., 2018; Gates, 2016; WHO, 2018b). Malaria burden is concentrated in the African Region, accounting for about 90% of cases and mortal-

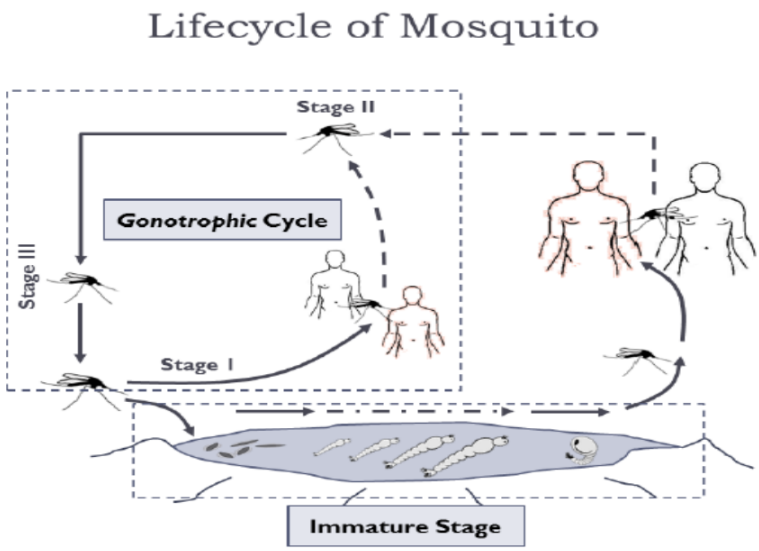

Figure 1.2: The Mosquito Lifecycle. Adapted from (Eikenberry and Gumel, 2018).

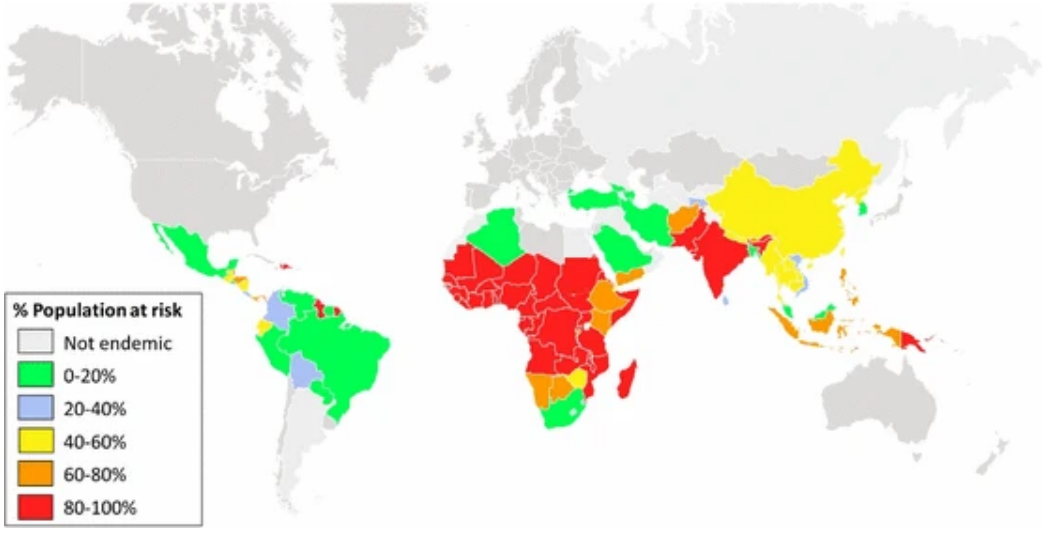

Figure 1.3: Malaria as a Tropical Disease (Eikenberry and Gumel, 2018; WHO, 2015a)

ity (with the majority of deaths occurring in children under the age of five) (WHO, 2017a). Other populations at high-risk of malaria include pregnant women and those living with HIV/AIDS (owing to their weakened immune systems) (Mohammed-Awel and Numfor, 2017; WHO, 2016). Malaria transmission dynamics is greatly affected by numerous abiotic and biotic factors, such as the increased mobility of people (the reservoir for the malaria parasite), the altered distribution of disease vectors (*Anopheles* mosquitoes) due to climate and environmental changes, and malaria's incursions into new areas (e.g., East African tropical highlands (Himeidan and Kweka, 2012)). Of the over 3500 *Anopheline* species, approximately 30-40 (species of this genus) have been shown to be efficient vectors of malaria (Cohuet et al., 2010; Sinka et al., 2010).

As noted by (Cohuet et al., 2010), to be efficient malaria vector, the *Anopheles* species must habitually bite humans (some anopheline species prefer to bite other non-human primates), must be susceptible to *Plasmodium* infection and must be able to live long enough to complete the *sporogonic cycle* (i.e., the maturation of the *Plasmodium* parasite in the mosquito). The dominant anopheline species in sub-Saharan Africa are *A. gambiae*, *A. arabiensis*, *A. funestus*, with *A. gambiae* by far the most important species, and, consequently the focal point of the over-whelming majority of malaria modeling efforts (Eikenberry and Gumel, 2018; Sinka et al., 2010).

There is significant heterogeneity in habitat preferences within the anopheline species. For instance, the *A. gambiae* complex tends to prefer conditions associated with anthropogenic (man-made) alteration of the environment (Sinka et al., 2010). Further, as noted by (Minakawa et al., 1999, 2004), the larvae of both *A. gambiae* and *A. arabiensis* prefer small, temporary, sunlit pools with little vegetation (the kind generated by deforestation, construction and livestock hoofprints). On the other hand, *A. funestus* (another major vector in sub-Saharan Africa), although also aided by deforestation, tends to prefer larger permant or semipermant habitats with estab-

lished vegetation (Eikenberry and Gumel, 2018; Minakawa et al., 2005). Figure 1.3 depicts the global distribution of malaria.

In the context of malaria, the adult mosquito (*Anopheles*) lifecycle is centered on the *gonotrophic cycle*, which entails the following three stages (Detinova et al., 1962; Okuneye et al., 2019):

Stage I : host-seeking and taking of a bloodmeal

Stage II : digestion of bloodmeal and egg maturation

Stage III : search for, and oviposition into, a suitable body of water

There are currently five *Plasmodium* species that transmit human malaria, namely *P. falciparum*, *P. vivax*, *P. Ovale*, *P. malariae* and *P. knowlesi* (Antinori et al., 2012). Of the five species, *P. falciparum* and *P. vivax* are dominant and responsible for nearly all of malaria deaths (Eikenberry and Gumel, 2018; Iboi et al., 2019a; Okuneye et al., 2019; WHO, 2015a, 2017a, 2018b). In particular, *P. falciparum* is responsible for over 90% of all malaria mortality in sub-Saharan Africa (WHO, 2015a, 2017a, 2018b).

1.3 Control Strategies

The control of malaria in endemic areas relies mainly on the implementation of vector-reduction strategies, such as adulticiding (use of pyrethroid-based long-lasting insecticidal nets (LLINs), indoor residual spraying (IRS)), larvacides (to kill immature mosquitoes) and treatment of confirmed cases using artemisinin-based therapy (Gerardin et al., 2015; Marsh, 1998; Yeung et al., 2004).The widespread *Anopheles* resistance to the insecticides embedded in LLINs and IRS, and also *Plasmodium* resistance to the artemisinin-therapy (Marsh, 1998; White et al., 1999; Yeung et al., 2004), prompted the call for anti-malarial biological control (such as the sterile insect technology (SIT), Wolbachia, larvivorous fish, genetically modified mosquitoes

(CRISPR-cas9)) (Eikenberry and Gumel, 2018; Iboi et al., 2019a,b; Mutabingwa, 2005).

Great successes have been recorded in the fight against malaria since about the year 2000, largely owing to concerted global public health efforts, such as the Roll Back Malaria initiative and the United Nations Millennium Development Goals (MDGs)(Huijben and Paaijmans, 2018; WHO, 2015b). Unfortunately, however, malaria remains a major public health challenge for about half of the world's population (Gething et al., 2016; WHO, 2012, 2015a).

New concerted global efforts, such as The Global Technical Strategy for Malaria 2016–2030 (approved by the World Health Assembly in May 2015 (WHO, 2015b)) and the Zero by 40 Initiative (an initiative of five chemical companies with the support of the Bill & Melinda Gates Foundation and the Innovative Vector Control Consortium (Gates, 2016; Willis and Hamon, 2018)), aimed at eradicating malaria by 2030 or 2040, respectively, are currently underway. Central to these laudable malaria eradication efforts is the widespread use of insecticide-based vector control interventions, including pyrethroid-based insecticide-treated nets (ITNs; LLINs), IRS and larvacides (WHO; Barbosa and Hastings, 2012; Huijben and Paaijmans, 2018; Okumu and Moore, 2011), complemented by artemisinin-based combination drug therapy. Five major classes of insecticides are used in malaria control efforts, namely *pyrethroids, organochlorines, organophosphates, carbamates* and the recent addition of *neonicotinoids*. Although all five are used in IRS (WHO, 2018a), only the pyrethroids is used in LLINs (owing to their low mammalian toxicity and irritant effect on mosquitoes) (Kabula et al., 2014).

It is notable that the earlier WHO's (World Health Organization's) Global Malaria Eradication Programme (1955–1969) relied almost exclusively on the use of DDT (*Dichlorodiphenyltrichloroethane*) and other insecticidal compounds for vector control,

with the theoretical goal of interrupting malaria transmission via decreasing adult *survival times*, rather than decreasing mosquito abundance *per se*, a goal largely based on the mathematical model of the malariologist George Macdonald (Macdonald, 1957; Nájera et al., 2011).

Long-lasting insecticidal bednets have been used to great success in reducing the global malaria burden (Bhatt et al., 2015). This success is partly attributed to community protection. In particular, if the coverage of bednet usage exceeds a certain threshold level, overall mosquito densities and malaria transmission are impacted sufficiently to also protect those individuals not using a bednet (Killeen and Smith, 2007; Levitz et al., 2018; Okumu and Moore, 2011).

1.3.1 Dengue

Dengue is a mosquito-borne viral disease caused by any of the four closely-related virus serotypes (DENV1-4) of the genus *Flavivirus*. The disease, which is endemic in over a hundred countries (mostly the tropical and sub-tropical regions of the world; Figures 1.4-1.7), accounts for over 50 million infections and 20,000 deaths annually (Andraud et al., 2012b; Chowell et al., 2007; Halstead, 1982; Shekhar, 2007). The disease is transmitted to humans *via* the bite of a dengue-infected adult female *Aedes aegypti* mosquito (Bancroft, 1906). The adult female *Aedes* mosquitoes bite humans in search of blood meal needed for eggs development. These mosquitoes typically reside in urban areas, where water-holding containers serve as their main breeding sites (Morales et al., 2017).

The incidence of dengue has consistently risen globally over the last five decades due to numerous factors, including the geographic expansion and transmission intensification in endemic tropical and subtropical regions (see Hladish et al. (2016) and some of the references therein). The disease causes life-threatening complications, such

as Dengue Hemorrhagic Fever (DHF) and Dengue Shock Syndrome (DSS) in some dengue-infected people (Gubler and Kuno, 1997; Halstead et al., 1970; Kawaguchi et al., 2003). These complications are often triggered due to immune responses to secondary infections (see, for instance, (Halstead et al., 1970; Halstead, 1982; Paul et al., 2016) for discussion on the *antibody-dependent enhancement* (ADE) in the context of dengue disease).

1.4 Control Strategies

The control of dengue disease in endemic areas relies mainly on vector-reduction strategies, such as larvacides (to kill immature mosquitoes) and adulticides (to kill adult mosquitoes), although biological controls (such as the sterile insect technology (SIT), Wolbachia, larvivorous fish, genetically modified mosquitoes (CRISPR-cas9)) (Eikenberry and Gumel, 2018; Iboi et al., 2019a,b; Mutabingwa, 2005) have also been suggested (and deployed in some settings). Another strategy is the use of vaccine against dengue (*Dengxavia*®, a recombinant chimeric live-attenuated DENV vaccine based on a yellow fever 17D vaccine backbone (Ferguson et al., 2016), developed by Sanofi Pasteur Ltd.) approved by the U.S. Food and Drug Administration (FDA) in 2019 (CDC, 2019b).

Dengue poses unique challenges for effective control owing to the fact that humans may be infected multiple times with different viral serotypes (and secondary infections are associated with an increased risk for severe disease) (Hladish et al., 2016). Infection with one dengue serotype induces lifelong immunity against acquiring infection from that serotype, and a temporary cross-immunity against the other serotypes (Burke et al., 1988; Halstead, 1982).

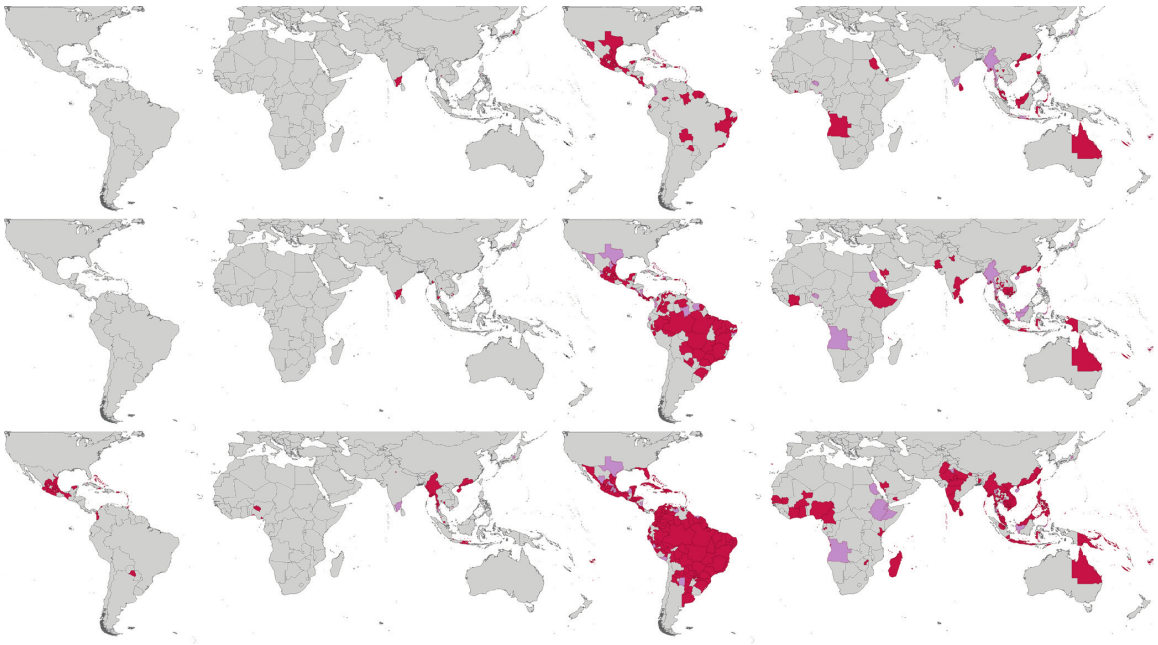

Figure 1.4: Spatial Distribution of Reported Confirmed Cases of DENV1 Since 1943. Darker-Colored Areas Represent Cases that were Confirmed in the Given Decade Under Consideration, Whereas Lighter-Colored Areas Represent Cases that had been Previously Reported but not in the Current Decade. Figure Taken from (Messina et al., 2014).

1.5 Research Objectives

The control of MBDs in endemic areas relies mainly on the implementation of mosquito-reduction strategies, such as the use of long-lasting insecticidal nets (LLINs) and indoor residual spraying (IRS) and treatment of confirmed cases (Mutabingwa, 2005). However, adult female mosquitoes have started developing resistance to the chemicals currently being used in the production of IRS and LLINs (Figure 1.8). Furthermore, in the context of malaria, the *Plasmodium* parasite has started developing resistance to the *artemisinin*-based therapy (Lubell et al., 2014; Ouji et al., 2018; Yeung et al., 2004). Hence, there is urgent need to explore other measures for vector control. Biological controls, such as sterile insect technology (SIT) (fre, 2017; Benelli et al., 2016;

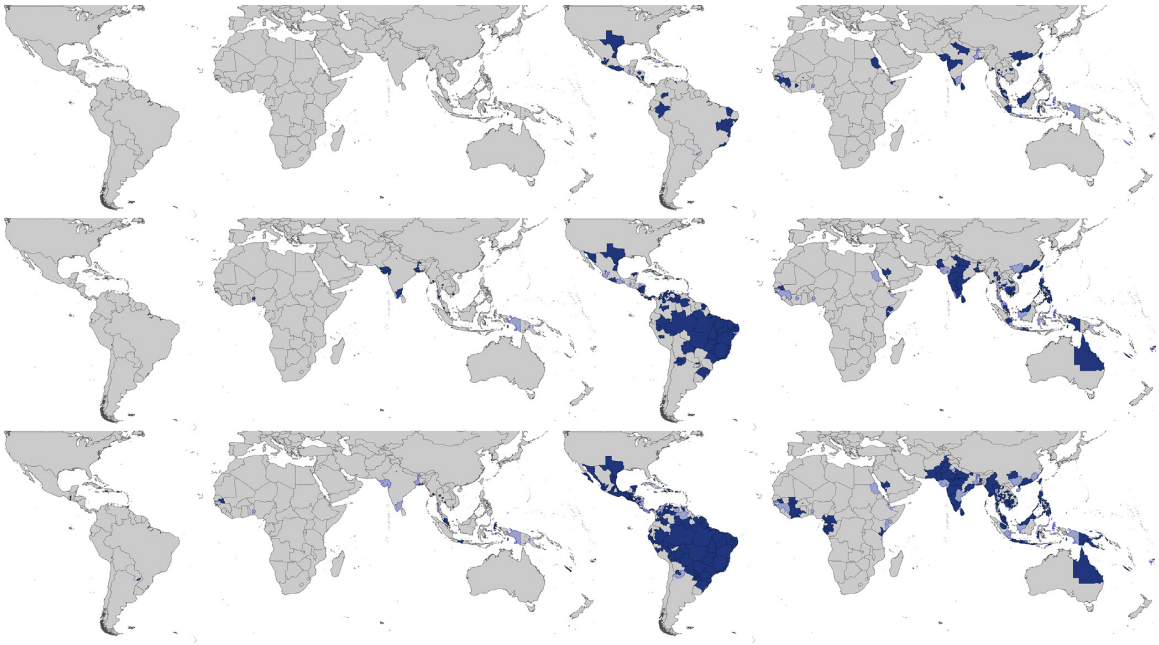

Figure 1.5: Spatial Distribution of Reported Confirmed Cases of DENV2 since 1943. Darker-Colored Areas Represent Cases that were Confirmed in the given Decade Under Consideration, Whereas Lighter-Colored Areas Represent Cases that had been Previously Reported but not in the Current Decade. Figure Taken from (Messina et al., 2014).

Cai et al., 2014; Huang et al., 2017; Patil et al., 2015; Thomé et al., 2010; Zheng et al., 2019), are being used to achieve this objective.

This dissertation work addresses three main research themes, namely:

1. The design of a modeling framework for assessing the population-level impact of the anti-dengue *Dengvaxia* vaccine (developed by Sanofi Pasteur Ltd.) on curtailing the spread of two dengue serotypes in a community.

2. The development a modeling framework for assessing the link between insecticide resistance and malaria epidemiology.

3. The development of a modeling framework for assessing the community-wide impact of SIT on malaria control. The effectiveness of SIT under various levels

Figure 1.6: Spatial Distribution of Reported Confirmed Cases of DENV3 Since 1943. Darker-Colored Areas Represent Cases that were Confirmed in the given Decade Under Consideration, Whereas Lighter-Colored Areas Represent Cases that had been Previously Reported but not in the Current Decade. Figure Taken from (Messina et al., 2014).

of local temperature fluctuations will also be assessed.

1.6 Outline of the Dissertation

The dissertation work is focused on the use of mathematical modeling approaches, coupled with dynamical systems analysis, computation and statistical data analytics, to gain insight into the population ecology of mosquitoes and the burden of the associated diseases they cause in humans. In particular, I studied the population ecology of two mosquito species, namely *Aedes* mosquitoes (which cause arboviral diseases, such as dengue fever, Chikungunya and Zika) and *Anopheles* mosquitoes (which causes malaria). Chapter 1 provides comprehensive introduction of the dissertation.

Chapter 2 of the dissertation contains material on modeling the population-level

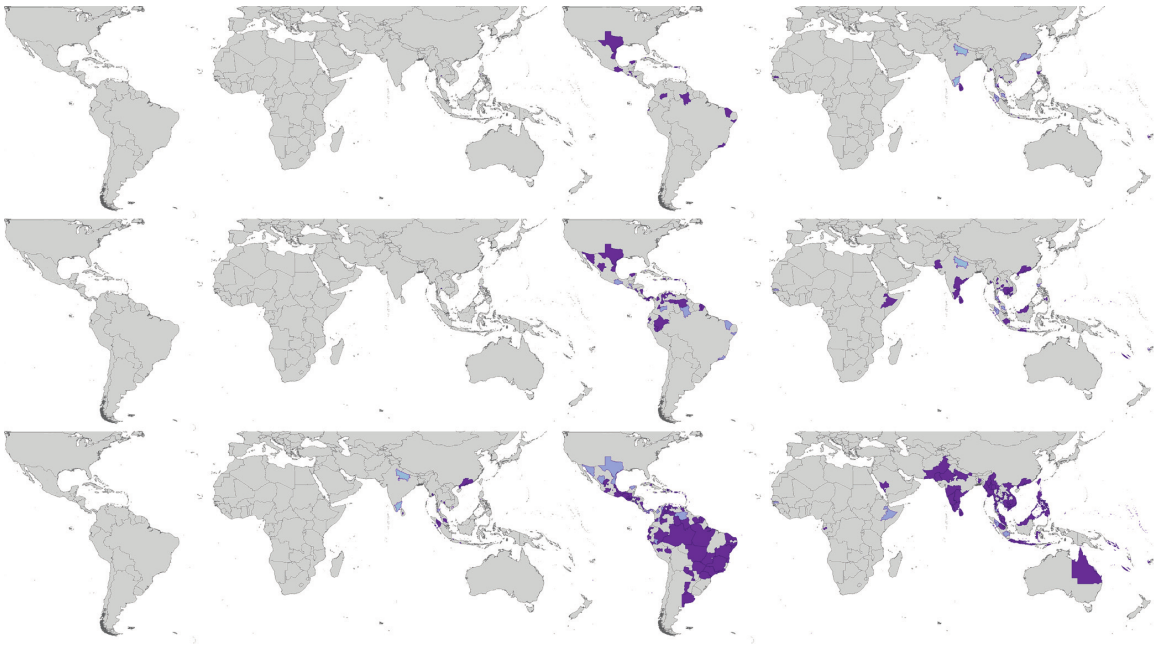

Figure 1.7: Spatial Distribution of Reported Confirmed Cases of DENV4 Since 1943. Darker-Colored Areas Represent Cases that were Confirmed in the Given Decade Under Consideration, Whereas Lighter-Colored Areas Represent Cases that had been Previously Reported but not in the Current Decade. Figure Taken from (Messina et al., 2014).

impact of the *Dengvaxia* vaccine against dengue (Iboi and Gumel, 2018). A new mathematical model for the dynamics of two dengue serotypes, in the presence of the vaccine, is developed. The model, which takes the form of a 27-dimensional deterministic system of nonlinear differential equations, is rigorously analysed to gain insight into its dynamical features. Detailed global uncertainty and sensitivity analyses of the parameters of the model, together with numerical simulations to assess the population-level impact of the vaccine are also reported.

Chapter 3 is based on modeling the impact of the use of long-lasting insecticidal nets (LLINs) and local temperature fluctuations on the transmission dynamics of malaria in an endemic setting. This work is motivated by the fact that the widespread use of LLINs (and, to a smaller extent, the indoor residual spray) has led to a dramatic

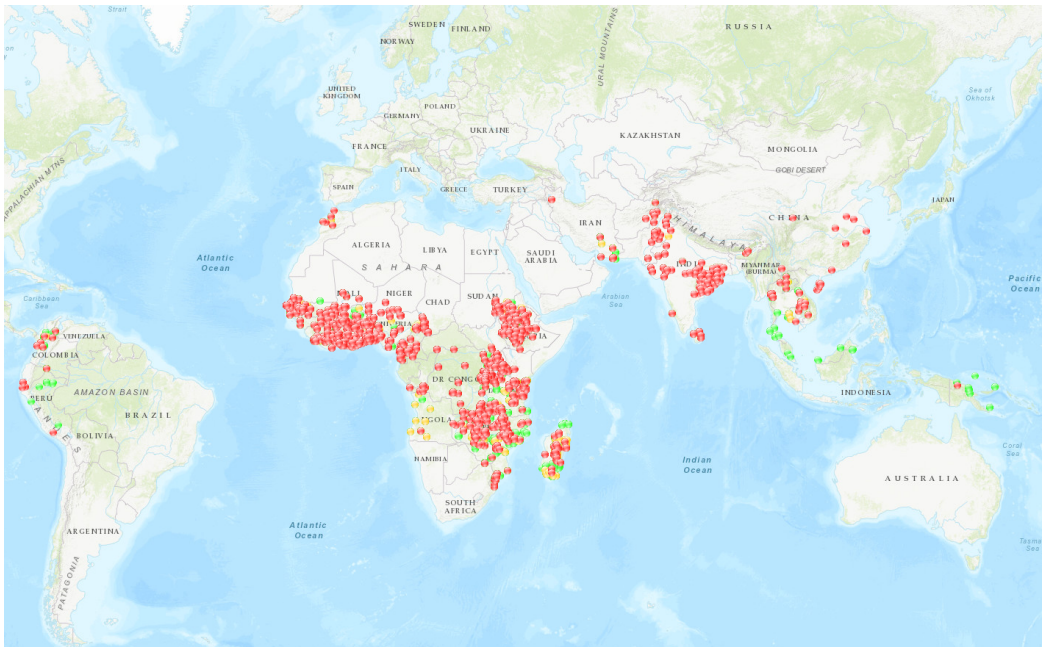

Figure 1.8: Red: Confirmed Resistance, Yellow: Possible Resistance and Green: Susceptibility (irmapper, 2019).

reduction in malaria incidence and burden globally for the period 2000-2015 (Huijben and Paaijmans, 2018; WHO, 2015b). Unfortunately, such widescale use of LLINs has also resulted in vector resistance to all five currently-available insecticides used in LLINs (WHO; Barbosa and Hastings, 2012; Huijben and Paaijmans, 2018; Okumu and Moore, 2011).

In chapter 4 of the dissertation, the possible population-level impact of the periodic release of sterile male mosquitoes on the local population abundance of mosquitoes is studied. The motivation for this work stems from the general thinking within the ecology community that, owing to the absence of a safe and effective vaccine against deadly mosquito-borne diseases (such as malaria) and vector insecticide resistance to all currently-available insecticides used in LLINs and IRS, the global effort to eliminate or eradicate malaria may have to hinge on using biological controls, such as the aforementioned sterile insect technology (SIT) approach.

Chapter 2

TRANSMISSION DYNAMICS OF DENGUE SEROTYPES: ROLE OF DENGVAXIA VACCINE

2.1 Introduction

As stated in chapter 1, dengue is a mosquito-borne viral disease that exudes significant public health burden in endemic areas (comprising of over 100 countries in the tropical and sub-tropical regions of the world). The disease, caused by any of the four closely-related virus serotypes (DENV1-4) of the genus *Flavivirus*, accounts for over 50 million infections and 20,000 deaths annually (Andraud et al., 2012b; Chowell et al., 2007; Halstead, 1982; Shekhar, 2007). It is transmitted to humans *via* the bite of an infected by adult female *Aedes* mosquitoes (Bancroft, 1906).

Although vector control (i.e., mosquito reduction), using larvacides (to kill mosquito larvae) and adulticides (to kill adult *Aedes* mosquitoes), has been the main option or strategy to combat the spread (and mitigate the impact) of dengue disease, these vector control programs are generally limited and unsustainable (Hladish et al., 2016). Consequently, a vaccine against dengue known as *Dengxavia*® vaccine, was developed by Sanofi Pasteur Ltd. in 2017 (CDC, 2019b). Dengvaxia, a recombinant chimeric live-attenuated DENV vaccine based on a yellow fever 17D vaccine backbone (Ferguson et al., 2016), developed by Sanofi Pasteur Ltd.) was approved for use by the U.S. Food and Drug Administration (FDA) in 2019 (CDC, 2019b). The vaccine was licensed for use in numerous countries, such as the US territories of American Samoa, Puerto Rico and the US Virgin Islands (CDC, 2019b). As noted by Ferguson et al. (2016), the development of this vaccine was considerably more chal-

lenging (in comparison to the development of vaccines for other *Flaviviruses*) because of the immunological interactions between the four dengue serotypes and the risk of antibody-dependent enhancement (ADE) (Halstead et al., 1970; Halstead, 1982; Paul et al., 2016).

Results from Phase III clinical trials of the Dengvaxia vaccine conducted in Latin America showed an estimated vaccine efficacy of 64.7% (95%CI [58.7, 69.8]), while the estimate from a trial in South East Asia was 56.5% (95%CI [43.8, 66.4]) (Hladish et al., 2016). Furthermore, as noted by (Hladish et al., 2016), pooled analysis of these two trials indicated vaccine efficacy was significantly higher for participants with pre-existing dengue neutralizing antibodies (81.9%; 95%CI [67.2, 90.0]) compared to those who were sero-negative at the time of vaccination (52.5%; 95%CI [5.9, 76.1]).

Vaccine efficacy against hospitalization for dengue in Latin America was 80.3% (95%CI [64.7, 89.5]) and in South East Asia was 67.2% (95%CI [50.3, 78.6]), and vaccine efficacy estimates varied by serotype in both trials (Capeding et al., 2014; Hadinegoro et al., 2015; Hladish et al., 2016; Villar et al., 2015) (in particular, DENV1 (50.2%, 95% CI 35.6%-61.5%), DENV2 (39.6%, 95% CI 18.7%-55.2%), DENV3 (74.9%, 95% CI 65.1%-82.0%) and DENV4 (76.6%, 95% CI 65.0%-84.4%)) WHO et al. (2017). Figures 1.4- 1.7 depicts the global distribution of the four serotypes, dating back to 1943 (Messina et al., 2014). Recent report by Sanofi Pasteur (Aguiar, 2018), based on a six-year clinical trial, show that while *Dengvaxia* provides long-term persistent protective benefit against dengue fever in people who had dengue infection prior to vaccination, the vaccine could induce more cases of severe disease (in the long-term) in dengue-naive populations. In fact, it is recently reported in the Philippines that up to three deaths may be attributable to the vaccine during a trial (Aguiar, 2018).

2.2 Literature Review on Mathematical Modeling of Dengue Serotypes

Numerous mathematical models have been designed and used to assess the potential impact of dengue vaccines (see, for instance, (Chao et al., 2012; Coudeville and Garnett, 2012; Ferguson et al., 2016; Garba et al., 2008; Hladish et al., 2016; Rodriguez-Barraquer et al., 2014)). Ferguson et al. (2016) used a PDE model that accounts for history of infection to assess the hypothesis that the Dengvaxia vaccine acts like a silent natural infection in priming or boosting host immunity. Hladish et al. (2016) used an agent-based dengue model to study the effectiveness of various vaccine scenarios on dengue transmission dynamics in Yucátan, Mexico. Coudeville and Garnett (2012) developed an age-structured compartmental model to study the impact of vaccination against the four dengue serotypes. Rodriguez-Barraquer et al. (2014) used a similar (age-stratified) model to evaluate the impact of a vaccine that is partially effective against three of the four dengue serotypes. Chao et al. (2012) showed, using compartmental and agent-based modeling approaches, that a dengue vaccine with efficacy between 70% to 90% against all four dengue serotypes has the potential to significantly reduce the frequency and magnitude of dengue epidemics in the short and medium terms (Morales et al., 2017). Using a deterministic compartmental model for two dengue strains, Morales et al. (2017) shows that vaccination and duration of cross immunity decrease the frequency and magnitude of dengue outbreaks (depending on vaccine interaction and dengue strain type). Garba et al. (2008) showed the presence of backward bifurcation in dengue transmission dynamics.

2.3 Main Objectives

The purpose of this chapter is to design, and rigorously analyse, an improved mechanistic model for assessing the population-level impact of the Sanofi *Dengvaxia* vaccine

against the four co-circulating dengue serotypes. In this chapter, the four dengue serotypes will be categorized as two vaccine-preventable dengue strains, where *strain* 1 consists of the three serotypes (DENV1, 3, 4) in whom the Sanofi vaccine is most effective, and *strain* 2 represents serotype 2 (the dengue strain for which the vaccine has reduced efficacy) (WHO et al., 2017). The model to be developed will also be used to evaluate the hypothesis that the *Dengvaxia* vaccine might increase the risk of severe disease in people who have never been exposed to the virus (i.e., dengue-naive populations).

2.4 Mathematical Formulation

The modeling work in this chapter is based on my paper (Iboi and Gumel, 2018). In particular, the model to be designed is for the transmission dynamics of the four dengue serotypes in a population in the presence of an anti-dengue vaccine. In this chapter, the three dengue serotypes with the highest vaccine efficacy (DENV1, 3 and 4) are categorized as "strain 1", while DENV2 is termed as "strain 2" (Hladish et al., 2016) ((Morales et al., 2017) also categorized the four dengue serotypes based on two strains, depending on which co-circulating serotypes are most dorminant).

The total human population at time t, denoted by $N_H(t)$, is sub-divided into the mutually-exclusive compartments of unvaccinated susceptible ($S_{UH}(t)$), vaccinated susceptible (S_{VH}), unvaccinated individuals who are exposed (infected but not symptomatic) to strain i (E_{UHi}), where $(i, j = 1, 2;\ i \neq j)$ represents the two strain classes, unvaccinated infectious (symptomatic) individuals with strain i and are susceptible to strain j (I_{UHi}), individuals who recovered from strain i and are now susceptible to strain j (W_{Uij}), individuals who recovered from strain i and are now exposed to strain j (E_{Uij}), unvaccinated infectious individuals with strain i and are now recovered from strain j (I_{Uij}), vaccinated individuals who are exposed (infected but not symptomatic)

to strain i (E_{VHi}), vaccinated infectious individuals with clinical symptoms of strain i and susceptible to strain j (I_{VHi}), vaccinated individuals who recovered from strain i and are now susceptible to strain j (W_{Vij}), vaccinated individuals who recovered from i and are now exposed to strain j (E_{Vij}), vaccinated infectious individuals with strain i and are now recovered from strain j (I_{Vij}), and individuals who recovered from both strains (W), so that (Iboi and Gumel, 2018)

$$N_H(t) = S_{UH}(t) + S_{VH}(t) + \sum_{i=1}^{2} [E_{VHi}(t) + E_{UHi}(t) + I_{UHi}(t) + I_{VHi}(t)]$$
$$+ \sum_{i=1}^{2} \sum_{\substack{j=1 \\ i \neq j}}^{2} [I_{Uij}(t) + I_{Vij}(t) + E_{Vij}(t) + E_{Uij}(t) + W_{Uij}(t) + W_{Vij}(t)] + W(t).$$

The total mosquito population at time t, denoted by $N_V(t)$, is sub-divided into sub-populations of immature ($L_M(t)$) and adult female ($N_M(t)$) mosquitoes, where $N_M(t)$ is split into adult female mosquitoes who are susceptible ($S_M(t)$), infected with strain 1 ($I_{M1}(t)$) and infected adult female mosquitoes with strain 2 ($I_{M2}(t)$). Hence,

$$N_V(t) = L_M(t) + N_M(t) = L_M(t) + S_M(t) + I_{M1}(t) + I_{M2}(t).$$

The model for dengue transmission dynamics in a population, in the presence of a vaccine against the four serotypes of dengue, is given by the following 27-dimensional ($i, j = 1, 2; i \neq j$) deterministic, non-linear differential equations (a dot represents differentiation with respect to time t) (Iboi and Gumel, 2018):

$$
\begin{aligned}
\dot{S}_{UH} &= \Pi_H + \omega S_{VH} - \sum_{i=1}^{2} \lambda_{Hi} S_{UH} - (\xi + \mu_H) S_{UH}, \\
\dot{S}_{VH} &= \xi S_{UH} - \sum_{i=1}^{2} \lambda_{Hi}(1-\varepsilon_i) S_{VH} - (\omega + \mu_H) S_{VH}, \\
\dot{E}_{UHi} &= \lambda_{Hi} S_{UH} - (\sigma_{Ui} + \mu_H) E_{UHi};\ i = 1, 2, \\
\dot{I}_{UHi} &= \sigma_{Ui} E_{UHi} - (\gamma_{Ui} + \mu_H + \delta_{UHi}) I_{UHi};\ i = 1, 2, \\
\dot{W}_{Uij} &= \gamma_{Ui} I_{UHi} - \eta_{Uij} \lambda_{Hj} W_{Uij} - \mu_H W_{Uij};\ i, j = 1, 2; i \neq j, \\
\dot{E}_{Uij} &= \eta_{Uij} \lambda_{Hj} W_{Uij} - (\alpha_{Uij} + \mu_H) E_{Uij};\ i, j = 1, 2; i \neq j, \\
\dot{I}_{Uij} &= \alpha_{Uij} E_{Uij} - (\tau_{Uij} + \mu_H + \delta_{Uij}) I_{Uij};\ i, j = 1, 2; i \neq j, \\
\dot{E}_{VHi} &= \lambda_{Hi}(1-\varepsilon_i) S_{VH} - (\sigma_{Vi} + \mu_H) E_{VHi};\ i = 1, 2, \\
\dot{I}_{VHi} &= \sigma_{Vi} E_{VHi} - (\gamma_{Vi} + \mu_H + \delta_{VHi}) I_{VHi};\ i = 1, 2, \\
\dot{W}_{Vij} &= \gamma_{Vi} I_{VHi} - \eta_{Vij} \lambda_{Hj}(1-\varepsilon_j) E_{Vij} - \mu_H W_{Vij};\ i, j = 1, 2; i \neq j, \\
\dot{E}_{Vij} &= \eta_{Vij} \lambda_{Hj}(1-\varepsilon_j) W_{Vij} - (\alpha_{Vij} + \mu_H) W_{Vij};\ i, j = 1, 2; i \neq j, \\
\dot{I}_{Vij} &= \alpha_{Vij} E_{Vij} - (\tau_{Vij} + \mu_H + \delta_{Vij}) I_{Vij};\ i, j = 1, 2; i = 1, 2, \\
\dot{W} &= \sum_{i=1}^{2} \sum_{\substack{j=1 \\ i \neq j}}^{2} (\tau_{Uij} I_{Uij} + \tau_{Vij} I_{Vij}) - \mu_H W, \\
\dot{L}_M &= \alpha_L \left(1 - \frac{L_M}{K_M}\right) N_M - \psi_L L_M - \mu_L L_M, \\
\dot{S}_M &= f \psi_L L_M - \sum_{i=1}^{2} \lambda_{Mi} S_M - \mu_M S_M, \\
\dot{I}_{M1} &= \lambda_{M1} S_M - \mu_M I_{M1}, \\
\dot{I}_{M2} &= \lambda_{M2} S_M - \mu_M I_{M2},
\end{aligned}
\tag{2.4.1}
$$

where,

$$\begin{aligned}
\lambda_{H1} &= \frac{\beta_H b_M I_{M1}}{N_H}, \quad \lambda_{H2} = \frac{\beta_H b_M I_{M2}}{N_H}, \\
\lambda_{M1} &= \frac{\beta_M b_M(\theta_{V1} I_{VH1} + I_{UH1} + \theta_{12} I_{U12} + \theta_1 I_{V12})}{N_H}, \\
\lambda_{M2} &= \frac{\beta_M b_M(\theta_{V2} I_{VH2} + I_{UH2} + \theta_{21} I_{U21} + \theta_2 I_{V21})}{N_H}.
\end{aligned} \tag{2.4.2}$$

A flow diagram of the model is depicted in Figure 2.1, and the state variables and parameters of the model are described in Tables 2.1-2.2.

In the model (2.4.1), with (2.4.2), the parameter Π_H is the recruitment (either by birth or by immigration) rate of individuals into the community (these individuals are assumed to be susceptible to both strains) and ω is the rate at which the vaccine wanes. Susceptible humans acquire infection, following an effective bite by an adult female *Aedes aegypti* mosquito, at a rate λ_{Hi} $(i = 1, 2)$. Similarly, b_M is the *per capita* biting rate of adult female *Aedes aegypti* mosquitoes, β_M is the probability that a susceptible mosquito acquires dengue infection *per* bite (from an infectious human carrying either of the two strains) and β_H is the probability that a susceptible human acquires dengue infection *per* bite (from an infected female mosquito carrying either of the two strains). The modification parameters θ_{V1}, θ_{12} and θ_1 account for the assumed variability in the infectiousness (i.e., transmissibility) of individuals in the I_{VH1}, I_{U12} and I_{V12} classes, respectively in comparison to those in the I_{UH1} class. Similarly, θ_{V2}, θ_{21} and θ_2 represent, respectively, modification parameters for the assumed variability of the infectiousness of individuals in the I_{VH2}, I_{U21} and I_{V21} classes, in relation to those in the I_{UH2} class.

Susceptible humans are vaccinated (against the two strains) at a rate ξ (it is assumed that the vaccine is imperfect, with protective efficacy $0 < \varepsilon_i < 1$ against strain i (Hladish et al., 2016)). Natural death rate occurs in all human compartments at a rate μ_H. Furthermore, $\sigma_{Ui}(\sigma_{Vi})$, with $i = 1, 2$, represents the rate at which individuals

in the $E_{UHi}(E_{VHi})$ class develop clinical symptoms of dengue, while the parameter $\gamma_{Ui}(\gamma_{Vi})$ represents the rate at which symptomatic individuals in the $I_{UHi}(I_{VHi})$ class recover. The parameter $\alpha_{Uij}(\alpha_{Vij})$ $(i, j = 1, 2; i \neq j)$ represents the rate at which individuals in the $E_{Uij}(E_{Vij})$ class develop clinical symptoms of the disease while $\tau_{Uij}(\tau_{Vij})$ is the rate at which individuals in the $I_{Uij}(I_{Vij})$ class recover from both strains. Individuals in the infectious (symptomatic) $I_{UHi}, I_{Uij}, I_{VHi}$ and I_{Vij} classes suffer additional dengue-induced mortality (at a rate) $\delta_{UHi}, \delta_{Uij}, \delta_{Vi}$ and δ_{Vij} (it is assumed that $\delta_{VHi} > \delta_{Vij}, \delta_{UHi}, \delta_{Uij}$) (Aguiar, 2018), respectively. Furthermore, $0 < \eta_{Uij}, \eta_{Vij} < 1$ is the modification parameter for the assumed reduction in the rate of acquisition of infection with strain j after recovery from infection with strain i (due to assumed partial cross immunity).

For computational convenience, the immature mosquito population is lumped into a single ecological compartment denoted by $L_M(t)$. Eggs are laid by adult female *Aedes aegypti* mosquitoes at a logistic growth rate $\alpha_L \left(1 - \frac{L_M(t)}{K_M}\right)$, where α_L is the eggs oviposition rate and it is assumed that the population of immature mosquitoes is limited by a carrying capacity, K_M (with $K_M > L_M(t)$ for all t; K_M depends on the available nutrients and breeding sites (Horsfall, 1955; Hoshen and Morse, 2004; Imbahale et al., 2011; Okuneye and Gumel, 2017)). The population of immature mosquitoes is decreased by the maturation (from eggs to larvae to pupae) of adult female *Aedes aegypti* mosquitoes (at a rate of ψ_L) and natural death (at a rate μ_L). Susceptible adult female *Aedes aegypti* mosquitoes acquire dengue infection with strain i, following an effective contact with an infectious human with strain i, at a rate λ_{Mi}, as defined in (2.4.2).

The model (2.4.1) is an extension of numerous models for dengue transmission dynamics in the literature (such as those in (Do et al., 2014; Feng and Velasco-Hernández, 1997; Garba and Gumel, 2010; Garba et al., 2008; Kyle and Harris, 2008;

Morales et al., 2017; Reich et al., 2013)). In particular,

(i) it extends the the two-strain dengue transmission model in (Garba and Gumel, 2010), by including an anti-dengue vaccine;

(ii) it extends the dengue vaccination models in (Garba et al., 2008; Morales et al., 2017), by including the dynamics of immature mosquitoes (i.e., the compartment L_M).

Furthermore, the 27-dimensional model (2.4.1) extends the 17-dimensional two-strain dengue transmission model with vaccination in (Morales et al., 2017) by, *inter alia*:

(i) including waning rate of the vaccine ($\omega \neq 0$) and disease-induced mortality in the host population ($\delta_{UHi}, \delta_{VHi}, \delta_{Uij}, \delta_{Vij} \neq 0$; $i, j = 1, 2$; $i \neq j$);

(ii) splitting the population of exposed (primary and secondary) individuals ($E_{UHi}, E_{VHi}; i = 1, 2$) into vaccinated exposed and unvaccinated exposed individuals with strain 1 or strain 2 (these populations are not categorized according to) vaccine status in (Morales et al., 2017). There is also similar extension with respect to the populations of individuals with disease symptoms (I_{VHi}, I_{UHi}; $i = 1, 2$);

(iii) splitting the population of individuals who recovered from strain i but are susceptible to strain j (W_{Vij}, W_{Uij}; $i, j = 1, 2$; $i \neq j$) according to vaccination status.

2.4.1 Basic Qualitative Properties of the Model

The basic properties of the model (2.4.1) will now be explored.

Let $\mu_V(t) = \min\{\mu_L(t), \mu_M(t)\}$. Consider, first of all, the equation for the rate of

change of the total human, immature mosquito and adult female mosquito populations, given, respectively, by

$$\dot{N}_H(t) = \Pi_H - \mu_H N_H(t) - \sum_{i=1}^{2} \delta_{UHi} I_{Ui}(t) - \sum_{i=1}^{2} \delta_{VHi} I_{Vi}(t) - \sum_{i=1}^{2} \sum_{\substack{j=1 \\ i \neq j}}^{2} \delta_{Uij} I_{ij}(t) - \sum_{i=1}^{2} \sum_{\substack{j=1 \\ i \neq j}}^{2} \delta_{Vij} I_{Vij}(t), \tag{2.4.3}$$

$$\dot{N}_M(t) = f\psi_L L_M(t) - \mu_M N_M(t), \tag{2.4.4}$$

and,

$$\dot{L}_M(t) = \alpha_L \left[1 - \frac{L_M(t)}{K_M}\right] N_M(t) - (\psi_L + \mu_L) L_M(t). \tag{2.4.5}$$

Lemma 2.4.1. *Consider the model* (2.4.1) *with non-negative initial data satisfying* $N_H(0) > 0$, $L_M(0) > 0$ *and* $N_M(0) > 0$. *Then, the model has a unique solution and all the state variables remain non-negative for all* $t > 0$.

Proof. The proof is based on the approach in (Hale and Verduyn Lunel, 1993; Hews et al., 2010). First, since the right-hand sides of the equations in (2.4.1) are continuous and Lipschitzian at $t = 0$, a solution of system (2.4.1), with non-negative initial conditions, exists and is unique on $[0, t^*)$ for some $t^* > 0$. Suppose there exists a t_1 such that $t^* > t_1 > 0$, $S_{UH}(t_1) = 0$ and each variable of the model (2.4.1) is positive at time t for $t \in (0, t_1)$. It follows from the first equation of the model (2.4.1) that:

$$\dot{S}_{UH}(t) > -\left[\sum_{i=1}^{2} \lambda_{Hi}(t) + \xi + \mu_H\right] S_{UH}(t).$$

Hence,

$$S_{UH}(t_1) > S_{UH}(0) \exp\left\{-\int_0^{t_1} \left[\sum_{i=1}^{2} \lambda_{Hi}(t) + \xi + \mu_H\right] dt\right\} > 0,$$

which contradicts $S_{UH}(t_1) = 0$. Furthermore, suppose there exists a t_1 such that $t^* > t_1 > 0$, $L_M(t_1) = 0$ and each variable of the model (2.4.1) is positive at time t for $t \in (0, t_1)$. It follows from the equation for the rate of change of the immature mosquito population ($\dot{L}_M(t)$) that:

$$\dot{L}_M(t) > -\left(\frac{\alpha_L N_M(t)}{K_M} + \psi_L + \mu_L\right) L_M,$$

so that,

$$L_M(t_1) > L_M(0) \exp\left\{-\int_0^{t_1} \left[\left(\frac{\alpha_L N_M(t)}{K_M} + \psi_L + \mu_L\right)\right] dt\right\} > 0,$$

which contradicts $L_M(t_1) = 0$. Similar contradictions can be obtained for the remaining variables of the model (2.4.1). Thus, for any non-negative initial data, the model (2.4.1) has a unique non-negative solution for all $t \in [0, t^*)$. □

It is convenient to define (for $i, j = 1, 2$; $i \neq j$):

$$\mathcal{X} = (S_{UH}, S_{VH}, E_{UHi}, E_{VHi}, E_{Uij}, E_{Vij}, I_{UHi}, I_{VHi}, I_{Uij}, I_{Vij}, W_{Uij}, W_{Vij}, W, L_M, S_M, I_{Mi}).$$

Further, let $\mathcal{D} = \{\mathcal{X} \in \mathbb{R}^{27}_+ \mid N_H(t) \leq \frac{\Pi_H}{\mu_H}, L_M(t) \leq K_M, N_M(t) \leq \frac{f\psi_L K_M}{\mu_M},$ for t $\geq 0\}$.

Lemma 2.4.2. *The region $\mathcal{D}$ is positively-invariant with bounded solutions.*

Proof. It follows from Equations (2.4.3), (2.4.4) and (2.4.5) that (noting that, in $\mathcal{D}$, $N_H(t) \leq \Pi_H/\mu_H$, $L_M(t) \leq K_M$ and $N_M(t) \leq f\psi_L K_M/\mu_M$ for all $t \geq 0$) :

$$\begin{aligned}\dot{N}_H(t) = \Pi_H - \mu_H N_H - \sum_{i=1}^{2} \delta_{UHi} I_{Ui} - \sum_{i=1}^{2} \delta_{VHi} I_{Vi} - \sum_{i=1}^{2} \sum_{\substack{j=1 \\ i \neq j}}^{2} \delta_{Uij} I_{ij} \\ - \sum_{i=1}^{2} \sum_{\substack{j=1 \\ i \neq j}}^{2} \delta_{Vij} I_{Vij} \leq \Pi_H - \mu_H N_H(t),\end{aligned} \tag{2.4.6}$$

$$\dot{N}_M(t) = f\psi_L L_M(t) - \mu_M N_M(t) \leq f\psi_L K_M - \mu_M N_M(t), \tag{2.4.7}$$

and,

$$\begin{aligned}\dot{L}_M(t) &= \alpha_L\left[1 - \frac{L_M(t)}{K_M}\right]N_M(t) - (\psi_L + \mu_L)L_M(t),\\ &\leq \alpha_L\left[1 - \frac{L_M(t)}{K_M}\right]N_M(t),\\ &\leq \frac{\alpha_L f\psi_L K_M}{\mu_M} - \frac{\alpha_L f\psi_L L_M}{\mu_M}.\end{aligned} \tag{2.4.8}$$

Thus, $N_H(t)$, $N_M(t)$ and $L_M(t)$ are decreasing functions of t if $N_H(t) > \frac{\Pi_H}{\mu_H}$, $N_M(t) > \frac{f\psi_L K_M}{\mu_M}$ and $L_M(t) > K_M$, respectively. Consider, next, the following upper solutions of the systems in (4.4.12), (2.4.7) and (2.4.8):

$$\begin{aligned}\dot{N}_H(t) &= \Pi_H - \mu_H N_H(t),\\ \dot{L}_M(t) &= \frac{\alpha_L f\psi_L K_M}{\mu_M} - \frac{\alpha_L f\psi_L L_M(t)}{\mu_M}\\ \dot{N}_M(t) &= f\psi_L K_M - \mu_M N_M(t).\end{aligned} \tag{2.4.9}$$

The general solutions of the equation in (2.4.9) are given, respectively, by:

$$\begin{aligned}N_H(t) &= \frac{\Pi_H}{\mu_H} + e^{-\mu_H t}\left[N_H(0) - \frac{\Pi_H}{\mu_H}\right],\\ L_M(t) &= K_M + e^{-\left(\frac{\alpha_L f\psi_L}{\mu_M}\right)t}\left[L_M(0) - K_M\right],\\ N_M(t) &= \frac{f\psi_L K_M}{\mu_M} + e^{-\mu_M t}\left[N_M(0) - \frac{f\psi_L K_M}{\mu_M}\right],\end{aligned} \tag{2.4.10}$$

from which it follows, by comparison principle (Lakshmikantham and Leela, 1969), that:

$$
\begin{aligned}
&N_H(t) \leq \frac{\Pi_H}{\mu_H}, \text{ if } N_H(0) \leq \frac{\Pi_H}{\mu_H}, \\
&L_M(t) \leq K_M, \text{ if } L_M(0) \leq K_M, \\
&N_M(t) \leq \frac{f\psi_L K_M}{\mu_M}, \text{ if } N_M(0) \leq \frac{f\psi_L K_M}{\mu_M}.
\end{aligned} \tag{2.4.11}
$$

Thus, the region $\mathcal{D}$ is positively-invariant with bounded solutions. Hence, it is sufficient to consider the dynamics of the model (2.4.1) in $\mathcal{D}$ (where, the usual existence, uniqueness and continuation results hold for the system (Forouzannia and Gumel, 2014; Hethcote, 2000)). □

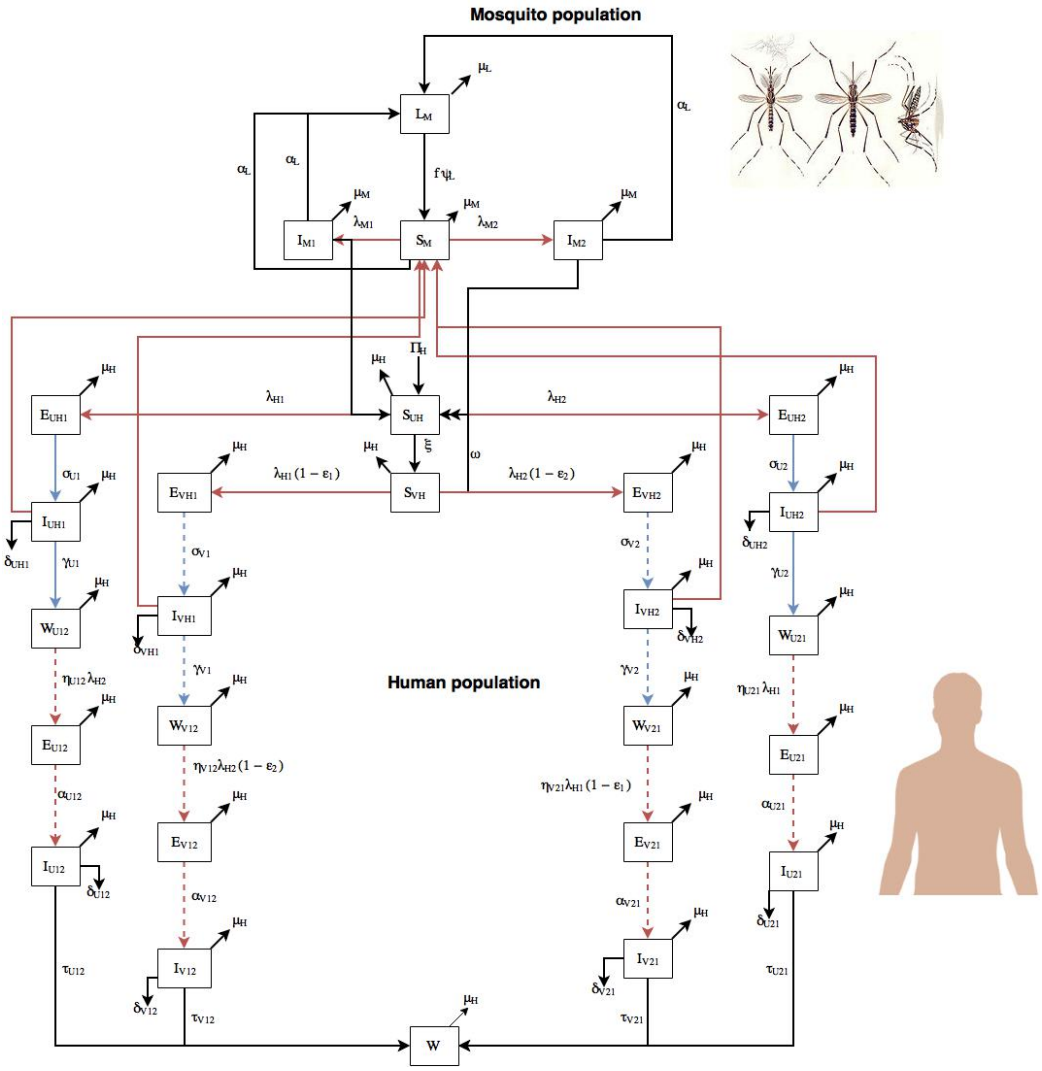

Figure 2.1: Flow Diagram of the Model (2.4.1).

2.5 Analysis of the Model

It is instructive to, first of all, analyze the dynamics of the model. It is convenient to define the quantity $r_0 = \dfrac{\alpha_L f \psi_L}{\mu_M(\psi_L + \mu_L)}$, the *production rate* of new adult female *Aedes aegypti* mosquitoes. The model has two disease free-equilibria, namely the trivial disease-free equilibrium (denoted by $\mathcal{T}_o$) and the non-trivial disease free-equilibrium (denoted by $\mathcal{T}_1$), given below (for $i, j = 1, 2;\ i \neq j$).

Table 2.1: Description of the State Variables of the Dengue Model (2.4.1)

State variables $(i, j = 1, 2; i \neq \text{j})$	**Interpretation**
S_{UH}	Population of unvaccinated individuals susceptible to both strains
S_{VH}	Population of susceptible individuals vaccinated against both strains
E_{VHi}	Population of vaccinated individuals exposed to strain i
E_{UHi}	Population of unvaccinated individuals exposed to strain i
E_{Uij}	Population of unvaccinated individuals who recovered from strain i and are exposed to strain j
E_{Vij}	Population of vaccinated individuals who recovered from strain i and are exposed to strain j
I_{VHi}	Population of vaccinated individuals symptomatic with strain i and are susceptible to strain j
I_{UHi}	Population of unvaccinated individuals symptomatic with strain i and are susceptible to strain j
I_{Uij}	Population of unvaccinated symptomatic individuals with strain i and exposed to strain j
I_{Vij}	Population of vaccinated symptomatic individuals with strain i and are exposed to strain j
W_{Vij}	Population of vaccinated individuals who recovered from strain i and are susceptible to strain j
W_{Uij}	Population of unvaccinated individuals who recovered from strain i and are susceptible to strain j
W	Population of individuals who recovered from both strains
L_M	Population of immature mosquitoes
S_M	Population of susceptible adult female *Aedes aegypti* mosquitoes
I_{Mi}	Population of infected adult female *Aedes aegypti* mosquitoes with strain i
$\lambda_j(j = Hi, Mi)$	Infection rate for susceptible humans and susceptible mosquitoes

Table 2.2: Description of Parameters of the Dengue Model (2.4.1)

Human Parameters	**Interpretation**
Π_H	Rate of recruitment of individuals into the community
μ_H	Natural mortality rate for humans
ξ	Vaccination rate
ω	Vaccine waning rate
ε_i	Vaccine efficacy against infection with strain i
δ_{UHi}, δ_{VHi}, δ_{Uij}, δ_{Vij}	Disease-induced death rate for humans
β_H	Probability of an infection from an infected human to a susceptible mosquito
β_M	Probability of an infection from an infected mosquito to a susceptible human
$\sigma_{Vi}(\sigma_{Ui})$	Progression rate from the exposed vaccinated(unvaccinated) class
	to symptomatic vaccinated(unvaccinated) class
$\alpha_{Vij}(\alpha_{Uij})$	Progression rate from the exposed vaccinated(unvaccinated) class
	to symptomatic vaccinated(unvaccinated) class
γ_{Vi}, γ_{Ui}	Progression rate from the symptomatic vaccinated(unvaccinated) class
	to the recovered vaccinated(unvaccinated) class
τ_{Vij}, τ_{Uij}	Progression rate from the infected vaccinated(unvaccinated) class
	to recovered vaccinated(unvaccinated) class
$\theta_{ij}, i \neq j$	Modification parameters for the reduction in infectiousness of individuals in I_{Uij}
	in relation to I_{UHi}
θ_{Vi}	Modification parameters for the reduction in infectiousness of individuals in I_{VHi}
	in relation to I_{UHi}
θ_i	Modification parameters for the reduction in infectiousness of individuals in I_{Vij}
	in relation to I_{Uij}
η_{Uij}, η_{Vij}	Modification parameters for the reduction in infectiousness due to cross-immunity
Vector Parameters	**Interpretation**
b_M	*Per capita* biting rate of mosquitoes on susceptible humans
α_L	*Per capita* egg deposition rate
ψ_L	Maturation rate of immature mosquitoes
μ_L	*Per capita* death rate for immature mosquitoes
μ_M	Natural death rate for adult female *Aedes aegypti* mosquitoes
K_M	Carrying capacity of immature mosquitoes
f	Proportion of new adult mosquitoes that are female

Table 2.3: Values and Ranges of the Parameters of the Dengue Model (2.4.1)

Parameters ($i, j = 1, 2; i \neq$j)	Range (*per* day)	Baseline values (*per* day)	Reference
Π_H	(50, 400)	155	Brinkhoff (2017)
μ_H	(0.0000315, 0.000043)	$1/(70 \times 365)$	[157]
ξ	(0.08, 0.41)	0.245	Estimated
ω	(0.15, 0.28)	0.215	[85]
ε_1	(0.6, 0.8)	0.7	Implied from [105]
ε_2	(0.2, 0.4)	0.3	Implied from [105]
δ_{UHi}, δ_{VHi}, δ_{Uij}, δ_{Vij}	(0.0009, 0.0011)	0.001	[85]
β_H	(0.66, 0.85)	0.76	Estimated
β_M	(0.68, 0.83)	0.75	Estimated
$\sigma_{Vi}(\sigma_{Ui})$	(0.125, 0.25)	0.19	[157]
$\alpha_{Vij}(\alpha_{Uij})$	(0.05, 0.083)	0.063	[157]
γ_{Vi}, γ_{Ui}	(0.067, 0.25)	0.16	[157]
τ_{Vij}, τ_{Uij}	(0.33, 0.5)	0.42	Estimated
$\theta_{ij}, i \neq j$	(0.6, 0.8)	0.7	Estimated
θ_{Vi}	(0.4, 0.7)	0.5	Estimated
θ_i	(0.4, 0.6)	0.5	Estimated
η_{Uij}, η_{Vij}	(0.45 ,0.55)	0.5	Estimated
b_M	(0.3, 1)	0.7	[14]
α_L	(200, 500)	300	[7]
ψ_L	(0.08, 0.35)	0.14	[57; 80]
μ_L	(0.07, 0.3)	0.18	[57; 80]
μ_M	(0.05, 0.07)	0.06	[157]
K_M	$(1 \times 10^6, 5 \times 10^6)$	3×10^6	[7]
f	(0.4, 0.6)	0.55	Estimated

Table 2.4: PRCC Values for the Parameters of the Model (2.4.1) Using Total Number of Unvaccinated Individuals who are Exposed to Strain i, Vaccinated Individuals who are Exposed to Strain i, Unvaccinated Individuals who Recovered From Strain i and are now Exposed to Strain j, Vaccinated Individuals who Recovered From Strain i and are now Exposed to Strain j as Output. The Top (most dominant) Parameters that Affect the Model with Respect to each of the Eight Response Function are Highlighted in Bold Font. Parameter Values and Ranges Used are as Given in Table 2.3 (with $\delta_H = 0$).

Parameters	E_{UH1}	E_{U12}	E_{U21}	E_{UH2}	E_{VH1}	E_{V12}	E_{VH2}	E_{V21}
Π_H	0.3019	0.2422	0.2318	-0.1142	-0.0084	0.0984	-0.0385	0.0643
μ_H	0.0152	0.0606	0.0214	0.0282	0.0597	0.0385	-0.0492	0.0836
ξ	0.5002	-0.0937	-0.0511	-0.0654	-0.0380	0.1129	0.0527	0.0663
ω	-0.1658	0.0567	0.0049	0.0166	-0.0789	-0.0859	0.0091	-0.0643
ε_1	0.4506	-0.0079	0.0359	-0.0045	-0.0068	-0.1606	0.0076	0.7915
ε_2	0.1982	-0.0534	0.0394	-0.0575	-0.0072	0.2265	-0.2065	-0.0395
δ_{UH1}	0.0872	0.0299	-0.0013	-0.0365	-0.0159	-0.0629	-0.0332	-0.0767
δ_{UH2}	-0.0414	0.0327	-0.0513	-0.1023	0.0090	0.0265	0.0396	0.0707
δ_{VH1}	-0.0429	0.0427	0.0154	0.0559	-0.0028	-0.0238	-0.0121	-0.0408
δ_{VH2}	0.0038	-0.0089	0.0362	-0.0090	0.0216	-0.0897	0.0184	0.0466
δ_{U12}	- 0.0257	-0.0869	-0.0156	-0.0074	0.0459	-0.0028	-0.0124	-0.0384
δ_{U21}	0.0302	0.0686	0.1154	-0.0186	0.0606	-0.0422	0.0905	-0.0036
δ_{V12}	-0.0330	-0.0116	-0.0360	-0.0111	0.0127	0.0389	-0.0242	0.0447
δ_{V21}	0.0241	0-0.0769	-0.0101	0.0649	0.0103	0.0141	-0.0294	-0.0359
β_H	-0.2628	-0.2869	-0.3003	0.1336	0.2101	-0.2566	0.1603	-0.0070
β_M	-0.1811	-0.2091	-0.1948	0.0860	0.2419	-0.2238	0.0988	-0.0808
σ_{V1}	-0.0203	-0.0201	-0.0131	0.0503	0.0599	0.1292	0.0519	-0.0425
σ_{V2}	-0.0139	-0.0033	0.0645	-0.0579	-0.1138	0.0384	-0.0256	0.3044
σ_{U1}	-0.0618	0.2571	-0.1672	0.0906	0.1485	-0.0104	0.0355	-0.0845
σ_{U2}	- 0.1128	-0.1521	0.1521	0.0413	0.0506	-0.1081	0.0890	0.0281
α_{V12}	-0.0293	-0.0463	-0.0736	0.0372	0.0297	0.0183	0.7826	0.0166
α_{V21}	0.0030	-0.0513	-0.0183	0.0781	0.0620	-0.0246	-0.0244	0.0497
α_{U12}	-0.0671	-0.0918	-0.0144	0.7899	0.0380	0.0407	-0.0035	-0.0215
α_{U21}	-0.0143	0.0107	0.0050	0.0694	0.8394	0.0016	0.0262	0.0563

Table 2.5: PRCC Values for the Parameters of the Model (2.4.1) Using Total Number of Unvaccinated Individuals who are Exposed to Strain i, Vaccinated Individuals who are Exposed to Strain i, Unvaccinated Individuals who Recovered from Strain i and are now Exposed to Strain j, Vaccinated Individuals who Recovered From Strain i and are now Exposed to Strain j as Output. The Top (most dominant) Parameters that Affect the Model with Respect to each of the Eight Response Function are Highlighted in Bold Font. Parameter Values and Ranges Used are as Given in Table 2.3 (with $\delta_H = 0$).

Parameters	E_{UH1}	E_{U12}	E_{U21}	E_{UH2}	E_{VH1}	E_{V12}	E_{VH2}	E_{V21}
γ_{V1}	-0.0241	-0.0075	0.0836	0.0078	-0.0266	0.6034	0.2545	0.1061
γ_{V2}	-0.0477	0.1394	0.0932	-0.0437	0.0798	0.0873	-0.0299	0.7787
γ_{U1}	0.0468	0.5680	0.2614	0.3673	-0.1668	0.0005	0.0449	0.1235
γ_{U2}	0.1783	0.3671	0.4735	-0.1163	0.4637	0.3115	-0.1635	-0.1174
τ_{V12}	0.0449	0.0532	0.0328	-0.0539	-0.0436	0.0355	-0.9312	0.0617
τ_{V21}	0.0818	-0.0846	-0.0050	-0.0445	0.0607	-0.0642	0.0216	-0.0188
τ_{U12}	-0.0744	-0.0746	0.0016	-0.9291	-0.0249	-0.0879	0.0062	0.0744
τ_{U21}	0.1006	0.0706	0.0224	-0.0376	-0.9445	0.0304	-0.0086	0.0458
θ_{12}	-0.0353	-0.0277	-0.0637	0.0351	-0.0165	-0.0110	-0.0067	0.0458
θ_{21}	0.0158	-0.0111	0.0258	0.0252	0.0005	-0.0407	-0.0058	-0.0386
θ_{V1}	-0.0536	-0.0014	-0.0840	0.0476	0.1163	-0.0273	-0.0515	-0.0601
θ_{V2}	-0.0331	-0.0879	0.0233	-0.0304	0.0378	-0.1409	0.6639	0.0669
θ_1	0.0443	-0.0005	0.0025	0.0392	-0.0909	0.0454	-0.0132	-0.0234
θ_2	-0.0655	-0.0259	0.1096	0.0365	0.0271	-0.0119	0.0962	0.0201
η_{U12}	-0.0445	-0.3050	0.0406	0.1444	-0.0991	-0.0718	-0.1124	-0.0447
η_{U21}	-0.0193	-0.0407	-0.1156	-0.0665	0.1841	0.0291	-0.0412	-0.0619
η_{V12}	0.0441	-0.0436	0.0019	0.0142	0.0611	-0.2247	0.1213	-0.0412
η_{V21}	-0.0328	-0.0243	0.0136	0.0838	0.0171	-0.0642	-0.0139	-0.0293
b_M	**-0.9235**	**-0.9304**	**-0.9225**	**0.8514**	**0.8743**	**-0.9041**	**0.8124**	**-0.6079**
α_L	-0.4926	-0.4504	-0.4125	0.3634	0.4528	-0.3855	0.3407	0.0868
ψ_L	**-0.9106**	**-0.8989**	**-0.9000**	**0.8215**	**0.8626**	**-0.8681**	**0.7992**	**-0.5292**
μ_L	0.0584	-0.0063	0.0187	-0.0607	-0.0300	0.1510	-0.0046	0.0157
μ_M	-0.0002	0.0676	0.0499	-0.1365	-0.0311	0.0433	0.0816	0.0399
K_M	**-0.7948**	**-0.7876**	**-0.8205**	**0.6214**	**0.6623**	**-0.7566**	**0.6246**	-0.3883
f	-0.4963	-0.5133	-0.04526	0.4611	0.4217	-0.4512	0.3904	-0.2559

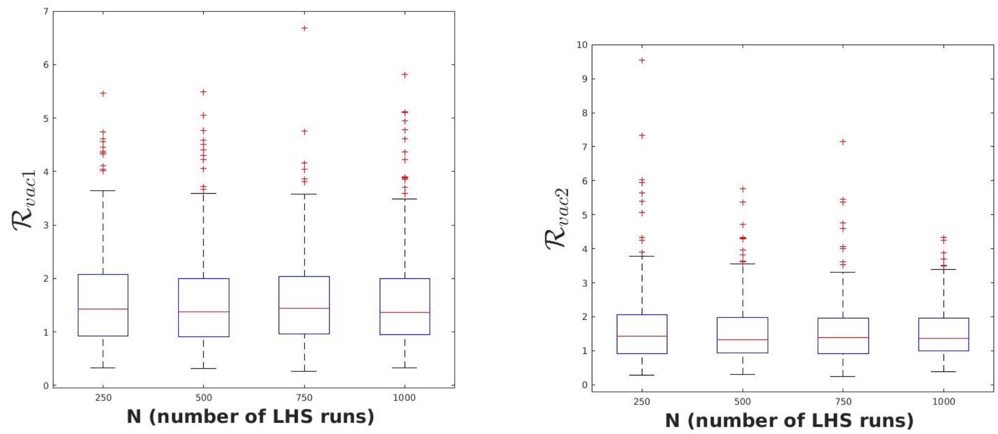

(a) (b)

Figure 2.2: Boxplots of the Vaccination Reproduction Numbers of the Model (2.4.1), as a Function of LHS Runs. (a) $\mathcal{R}_{vac1}$ (b) $\mathcal{R}_{vac2}$. Parameter Values and Ranges Used are as Given in Table 2.3.

(i) *TDFE*:

$$\begin{aligned}\mathcal{T}_o &= (S^o_{UH}, S^o_{VH}, E^o_{VHi}, E^o_{UHi}, E^o_{Uij}, E^o_{Vij}, I^o_{VHi}, I^o_{Vij}, I^o_{UHi}, I^o_{Uij}, W^o_{Vij}, W^o_{Uij}, W^o, L^o_M, S^o_M, I^o_{Mi}) \\ &= (a_{1o}, a_{2o}, 0, 0, 0, 0, 0, 0, 0, 0, 0, 0, 0, 0, 0, 0, 0, 0, 0, 0, 0, 0, 0, 0, 0, 0, 0)\,. \end{aligned} \tag{2.5.1}$$

(ii) *NDFE*:

$$\begin{aligned}\mathcal{T}_1 &= (S^*_{UH}, S^*_{VH}, E^*_{VHi}, E^*_{UHi}, E^*_{Uij}, E^*_{Vij}, I^*_{VHi}, I^*_{Vij}, I^*_{UHi}, I^*_{Uij}, W^*_{Vij}, W^*_{Uij}, W^*, L^*_M, S^*_M, I^*_{Mi}) \\ &= (a_{1o}, a_{2o}, 0, 0, 0, 0, 0, 0, 0, 0, 0, 0, 0, 0, 0, 0, 0, 0, 0, 0, 0, 0, 0, a_{3o}, a_{40}, 0, 0)\,, \end{aligned} \tag{2.5.2}$$

where $a_{1o} = \dfrac{\Pi_H(\omega+\mu_H)}{\mu_H(\omega+\xi+\mu_H)}$, $a_{2o} = \dfrac{\xi\Pi_H}{(\omega+\xi+\mu_H)}$, $a_{3o} = K_M\left(1-\frac{1}{r_0}\right)$ and $a_{40} = \dfrac{\psi_L K_M\left(1-\frac{1}{r_0}\right)}{\mu_M}$.

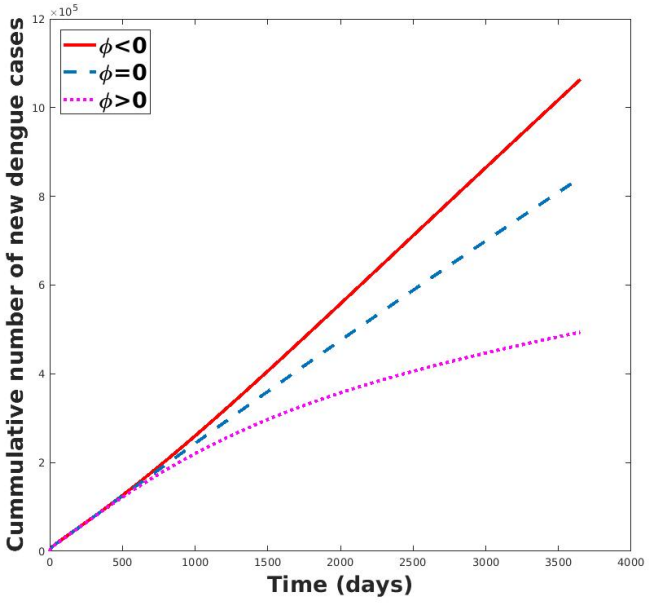

Figure 2.3: Simulations of Model (2.4.1), Showing the Total Number of Dengue Cases as a Function of Time with (a) $\phi < 0$ (Using $\varepsilon_1 = 0.2, \sigma_{U1} = 0.25, \sigma_{V1} = 0.19, \gamma_{U1} = 0.067, \gamma_{V1} = 0.16$ and $\theta_{V1} = 1$), (b) $\phi = 0$ (Using $\varepsilon_1 = 0.3$, $\sigma_{U1} = 0.25$, $\sigma_{V1} = 0.19$, $\gamma_{U1} = 0.067$, $\gamma_{V1} = 0.16$ and $\theta_{V1} = 1$) and (c) $\phi > 0$ (Using $\varepsilon_1 = 0.4$, $\sigma_{U1} = 0.25$, $\sigma_{V1} = 0.19$, $\gamma_{U1} = 0.067$, $\gamma_{V1} = 0.16$ and $\theta_{V1} = 1$). Parameter Values and Ranges Used are as Given in Table 2.3.

2.5.1 Asymptotic Stability of Disease-Free Equilibria

It follows from (2.5.2) that the NDFE exists if and only if $r_0 > 1$. Furthermore, it can be shown (by linearizing the model around the TDFE) that the TDFE is globally-asymptotically stable (GAS) whenever $r_0 \leq 1$ (see, for instance, (Dumont and Chiroleu, 2010; Okuneye and Gumel, 2017)).

Let $r_0 > 1$ (so that the NDFE exists). The local stability of the NDFE (in $C([0], \mathbb{R}^{27}_+) \setminus \{\mathcal{T}_o\}$) will now be explored using the next generation operator method (Diekmann et al., 1990; van den Driessche and Watmough, 2002). Using the notation

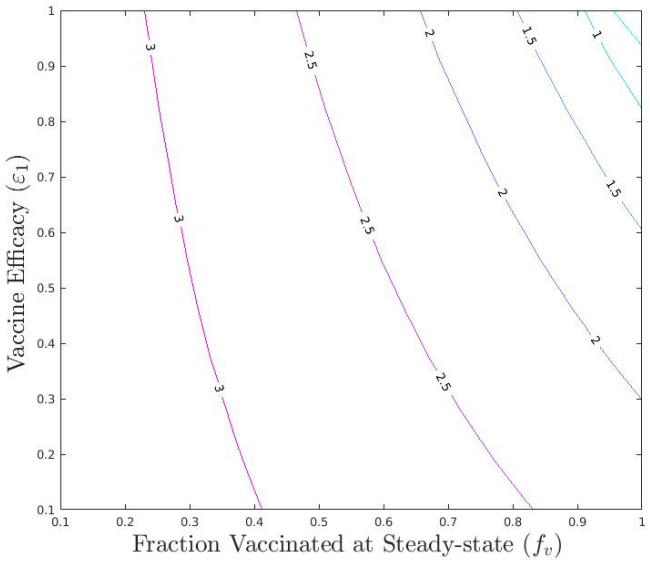

Figure 2.4: Simulations of the Model (2.4.1) Showing Contour Plots of $\mathcal{R}_{vac1}$, as a Function of the Fraction of Individuals Vaccinated Against Strain 1 at Steady-State ($f = \frac{S^*_{VH}}{N^*_H}$) and Vaccine Efficacy ($\varepsilon_1$). Parameter Values Used are as Given in Table 2.3 with $\varepsilon_1 = \varepsilon_2 = 1$, $\eta_{ij} = \eta_{Vij} = 0\,(i, j = 1, 2; i \neq j)$ and $\delta_H = 0$ (so that, by Theorem 2.5.4, Backward Bifurcation does not occur when $\mathcal{R}^{**}_{vac} = 1$).

in (van den Driessche and Watmough, 2002), it follows that the matrices $\mathcal{F}$ of new infection terms and $\mathcal{V}$ of the remaining transfer terms associated with the version of the model are given, respectively, by

$$\mathcal{F} = \begin{bmatrix} \mathbf{0}_{9\times 9} & F_1 \\ F_2 & F_3 \end{bmatrix}, \mathcal{V} = \begin{bmatrix} V_1 & \mathbf{0}_{9\times 9} \\ V_2 & V_3 \end{bmatrix},$$

where the matrices F_1, F_2, F_3, V_1, V_2 and V_3 are given in Appendix A (and $\mathbf{0}_{9\times 9}$ is the zero matrix of order 9). It is convenient to define: $N^*_H = \frac{\Pi_H}{\mu_H}, K_1 = \xi + \mu_H, K_2 = \omega + \mu_H, K_3 = \sigma_{U1} + \mu_H, K_4 = \gamma_{U1} + \mu_H + \delta_{UH1}, K_5 = \alpha_{12} + \mu_H, K_6 = \tau_{12} + \mu_H + \delta_{U12}, K_7 = \sigma_{U2} + \mu_H, K_8 = \gamma_{U2} + \mu_H + \delta_{UH2}, K_9 = \alpha_{21} + \mu_H, K_{10} = \tau_{21} + \mu_H + \delta_{U21}, K_{11} = \sigma_{V1} + \mu_H, K_{12} = \gamma_{V1} + \mu_H + \delta_{VH1}, K_{13} = \alpha_{V12} + \mu_H, K_{14} = \tau_{V12} + \mu_H + \delta_{V12}, K_{15} =$

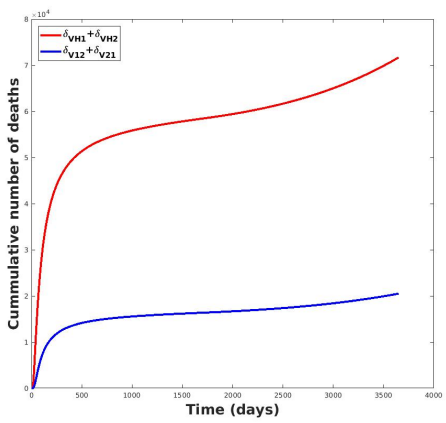

(a)

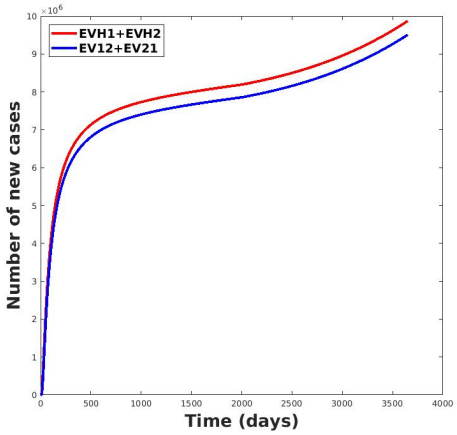

(b)

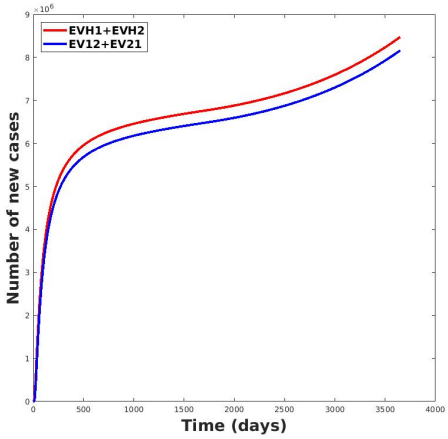

(c)

Figure 2.5: Simulations of the Model (2.4.1), Showing (a) The Cumulative Number of Deaths for Naive Population S_{VH} and Individuals with Prior Infection W_{Vij} with $\varepsilon_1 = 0.7$ and $\varepsilon_2 = 0.3$, (b) The Number of New Cases for Naive Population S_{VH} and Individuals with Prior Infection W_{Vij} with $\varepsilon_1 = 0.7$ and $\varepsilon_2 = 0.3$ and (c) The Number of New Cases for Naive Population S_{VH} and Individuals with Prior Infection W_{Vij} with $\varepsilon_1 = \varepsilon_2 = 0.8$. Parameter Values and Ranges Used are as Given in Table 2.3.

$\sigma_{V2} + \mu_H, K_{16} = \gamma_{V2} + \mu_H + \delta_{VH2}, K_{17} = \alpha_{V21} + \mu_H, K_{18} = \tau_{V21} + \mu_H + \delta_{V21}, K_{19} = \psi_L + \mu_L$. The *vaccination (effective) reproduction number* of the model, denoted by $\mathcal{R}_{vac}$, is given by

$$\mathcal{R}_{vac} = \max\{\mathcal{R}_{vac1}, \mathcal{R}_{vac2}\}, \tag{2.5.3}$$

where $\mathcal{R}_{vac1}$ and $\mathcal{R}_{vac2}$ are given, respectively, by

$$\mathcal{R}_{vac1} = \sqrt{g_1 g_3 + g_2 g_4}, \;\; \mathcal{R}_{vac2} = \sqrt{g_5 g_7 + g_6 g_8}, \tag{2.5.4}$$

with,

$$\begin{aligned}
g_1 &= \frac{\beta_M S^*_{UH} b_M \sigma_{U1}}{N^*_H K_3 K_4}, g_2 = \frac{\beta_M S^*_{VH} b_M \sigma_{V1}(1-\varepsilon_1)}{N^*_H K_{11} K_{12}}, \\
g_3 &= \left(\frac{\beta_H b_M S^*_M}{N^*_H}\right)\left(\frac{1}{\mu_M}\right), g_4 = \theta_{V1} g_3, \\
g_5 &= \frac{\beta_M S^*_{UH} b_M \sigma_{U2}}{N^*_H K_7 K_8}, g_6 = \frac{\beta_M S^*_{VH} b_M \sigma_{V2}(1-\varepsilon_2)}{N^*_H K_{15} K_{16}}, \\
g_7 &= \left(\frac{\beta_H b_M S^*_M}{N^*_H}\right)\left(\frac{1}{\mu_M}\right), g_8 = \theta_{V2} g_7.
\end{aligned}$$

The result below follows from Theorem 2 of (van den Driessche and Watmough, 2002).

Theorem 2.5.1. *The NDFE of the model* (2.4.1) *is locally-asymptotically stable (LAS) in* $C([0], \mathbb{R}^{27}_+) \setminus \{\mathcal{T}_0\}$ *if* $\mathcal{R}_{vac} < 1$, *and unstable if* $\mathcal{R}_{vac} > 1$.

The threshold quantity $\mathcal{R}_{vac}$, measures the average number of new dengue infections in the vector(host) generated by an infected host(vector) introduced into a community where a certain proportion of the susceptible host population is vaccinated against the two co-circulating dengue strains (Anderson and May., 1982, 1991; Diekmann et al., 1990; Hethcote, 2000). Similarly, the quantities $\mathcal{R}_{vac1}$ and $\mathcal{R}_{vac2}$ represent the average number of new cases generated by an infected host (vector) with strain 1 or 2, respectively.

Interpretation of the Vaccination Reproduction Number ($\mathcal{R}_{vac}$)

Interpretation of $\mathcal{R}_{vac1}$: The reproduction number of strain 1 ($\mathcal{R}_{vac1}$) is interpreted as follows. The term g_1 in $\mathcal{R}_{vac1}$ represents the average number of new unvaccinated symptomatic humans with strain 1 generated by a mosquito infected with strain 1. It is the product of the infection rate of unvaccinated susceptible humans ($\frac{\beta_M b_M S^*_{UH}}{N^*_H}$), the proportion of exposed humans that survived the unvaccinated exposed class (E_{UH1}) and move to the symptomatic I_{UH1} class ($\frac{\sigma_{U1}}{K_3}$) and the average duration in the I_{UH1} class ($\frac{1}{K_4}$). Similarly, g_2 is the average number of new vaccinated symptomatic humans with strain 1 generated by an infected mosquito with strain 1. It is the product of the infection rate of vaccinated susceptible humans ($\frac{\beta_M b_M (1-\varepsilon_1) S^*_{VH}}{N^*_H}$), the proportion that survived the vaccinated exposed class (E_{VH1}) and move to the I_{VH1} class ($\frac{\sigma_{V1}}{K_{11}}$), and the average duration in the I_{VH1} class ($\frac{1}{K_{12}}$). The term g_3 measures the average number of new infected mosquitoes generated by an unvaccinated symptomatic human with strain 1 (I_{UH1}). It is the product of the infection rate of susceptible mosquitoes with strain 1 ($\frac{\beta_H b_M S^*_M}{N^*_H}$) and the average lifespan of adult female mosquitoes ($\frac{1}{\mu_M}$). Finally, g_4 is the average number of new infected mosquitoes generated by a vaccinated symptomatic human with strain 1.

Interpretation of $\mathcal{R}_{vac2}$: The reproduction number of strain 2 ($\mathcal{R}_{vac2}$) is interpreted as follows. The term g_5 in $\mathcal{R}_{vac1}$ represents the average number of new unvaccinated symptomatic humans with strain 2 generated by a mosquito infected with strain 2. It is the product of the infection rate of susceptible humans ($\frac{\beta_M b_M S^*_{UH}}{N^*_H}$), the proportion of exposed humans that survived the unvaccinated exposed class (E_{UH2}) and move to the I_{UH2} class ($\frac{\sigma_{U2}}{K_7}$) and the average duration in the I_{UH2} class ($\frac{1}{K_8}$). Similarly, g_6 is the average number of new vaccinated symptomatic humans with strain 2 generated by an infected mosquito with strain 2. It is the product of infection rate of susceptible

humans ($\frac{\beta_M b_M(1-\varepsilon_2)S^*_{VH}}{N^*_H}$), the proportion that survived the vaccinated exposed class (E_{VH2}) and move to the I_{VH2} class ($\frac{\sigma_{V2}}{K_{15}}$), and the average duration in the I_{VH2} class ($\frac{1}{K_{16}}$). The term g_7 measures the average number of new infected mosquitoes generated by an unvaccinated symptomatic human with strain 2 (I_{UH2}). It is the product of the infection rate of susceptible mosquitoes ($\frac{\beta_H b_M S^*_M}{N^*_H}$) and the average lifespan of adult female mosquitoes ($\frac{1}{\mu_M}$). Finally, g_8 is the average number of new infected mosquitoes generated by a vaccinated symptomatic human with strain 2.

The maximum of $\mathcal{R}_{vac1}$ and $\mathcal{R}_{vac2}$ gives $\mathcal{R}_{vac}$. Theorem 2.5.1 shows that the use of the *Dengvaxia* vaccine can lead to the effective control of the disease in the community if the initial sizes of the infected human and vector populations are in the basin of attraction of the NDFE ($\mathcal{T}_1$). For such control to be independent of initial conditions, global asymptotic stability result must be established for the NDFE.

2.5.2 Backward Bifurcation Analysis

It is instructive, first of all, to characterize the type of bifurcation the model (2.4.1) may undergo. Typically, models for the spread of vector-borne diseases (such as dengue (Garba and Gumel, 2010; Garba et al., 2008), malaria (Feng et al., 2015; Niger and Gumel, 2008), leishmaniasis (Hussaini et al., 2016; Iboi et al., 2018) and West Nile virus (Blayneh et al., 2010; Jiang et al., 2009)) undergo a backward bifurcation when the associated reproduction number of the model is less than unity. The implication of backward bifurcation, which is characterized by the co-existence of a stable endemic equilibrium and the stable disease-free equilibrium when the reproduction number of the model is less than unity, is that the classical epidemiological requirement of having the reproduction number of the model to be less than unity, while necessary, is no longer sufficient for the effective control (or elimination) of the disease. The possibility for the presence of backward bifurcation in the model (2.4.1) is now explored.

For mathematical tractability, the analysis will be carried out for the special case of the model where the vaccine offers 100% protection against all four dengue serotypes (i.e., $\varepsilon_1 = \varepsilon_2 = 1$) and disease-induced mortality in the host population is the same (i.e., $\delta_{UHi} = \delta_{Uij} = \delta_{VHi} = \delta_{Vij} = \delta_H$ for $i, j = 1, 2; i \neq j$). It is convenient to define

$$\delta_H^c = \frac{-[2a_1(1+\mu_H)+a_4]-\sqrt{[2a_1(1+\mu_H)+a_4]^2-4a_1[a_1(1+\mu_H)^2+a_4(1+\mu_H)+a_2+a_3]}}{2a_1} > 0$$

(where the constants, a_1, a_2, a_3 and a_4, are given in Equation (B-4) in Appendix B1) and,

$$\tilde{\mathcal{R}}_{vac} = \mathcal{R}_{vac}|_{\eta_{ij}=\eta_{Vij}=0,\, \delta_{UHi}=\delta_{Uij}=\delta_{VHi}=\delta_{Vij}=\delta_H} \; (i, j = 1, 2;\; i \neq j).$$

Theorem 2.5.2. *The special case of the model* (2.4.1) *with* $\delta_{UHi} = \delta_{Uij} = \delta_{VHi} = \delta_{Vij} = \delta_H$, $\eta_{ij} = \eta_{Vij}\,(i, j = 1, 2; i \neq j) = 0$ *and* $\varepsilon_1 = \varepsilon_2 = 1$ *undergoes a backward bifurcation at* $\tilde{\mathcal{R}}_{vac} = 1$ *whenever* $\delta_H > \delta_H^c > 0$.

The proof of Theorem 2.5.2, based on using Center Manifold theory (Carr, 1981; Castillo-Chavez and Song, 2004; van den Driessche and Watmough, 2002), is given in Appendix B1. The analysis in Appendix B1 shows that the aforementioned special case of the model (2.4.1) exhibits a backward bifurcation at $\tilde{\mathcal{R}}_{vac} = 1$, whenever the disease-induced mortality in the host population (δ_H) exceeds the threshold value δ_H^c. That is, this study shows that the phenomenon of backward bifurcation occurs when the disease-induced mortality is high enough ($\delta_H > \delta_H^c$) and that this dynamic phenomenon persists even if the vaccine offers perfect protection against both strains (i.e., $\varepsilon_1 = \varepsilon_2 = 1$). It should further be mentioned that the backward bifurcation persists whenever $\varepsilon_1 \neq 1$ and $\varepsilon_2 \neq 1$ (regardless of the value of δ_H; see also Theorem 2.5.4).

Theorem 2.5.3. *The special case of the model* (2.4.1) *with* $\delta_H = 0$ *and* $\eta_{ij} = \eta_{Vij} = 0$ $(i, j = 1, 2; i \neq j)$ *undergoes a backward bifurcation at*
$\mathcal{R}^*_{vac} = \mathcal{R}_{vac}|_{\delta_H=\eta_{ij}=\eta_{Vij}\,(i,j=1,2;\,i\neq j)=0} = 1$ *if* $\varepsilon_1 \neq 1$ *and* $\varepsilon_2 \neq 1$.

The proof of Theorem 2.5.3 is given in Appendix B2. The results of Theorems 2.5.2 and 2.5.3 show that the backward bifurcation phenomenon persists in the model (2.4.1) if either the disease-induced mortality in the host population is high enough (i.e., $\delta_H > \delta_H^c$), or if the vaccine efficacy against each of the two strains is not perfect (i.e., $\varepsilon_1 \neq 1$ and $\varepsilon_2 \neq 1$).

Theorem 2.5.4. *The special case of the model* (2.4.1)*, with* $\varepsilon_1 = \varepsilon_2 = 1$*,* $\eta_{ij} = \eta_{Vij} = 0\,(i, j = 1, 2;\, i \neq j)$ *and* $\delta_H = 0$*, does not undergo a backward bifurcation at* $\mathcal{R}_{vac}^{**} = \mathcal{R}_{vac}^{*}|_{\varepsilon_1=\varepsilon_2=1} = 1$.

Proof. Setting $\varepsilon_1 = \varepsilon_2 = 1, \delta_H = 0$ and $\eta_{ij} = \eta_{Vij} = 0\,(i = 1, 2, i \neq j)$ in the expression for the backward bifurcation coefficient a (given by Equation (H.0.1) in Appendix B1), and simplifying, shows that the bifurcation coefficient (a) reduces to:

$$a = 2\,\frac{v_3\sigma_{U1}^2\beta_M^2(\beta_H^*)^2(x_{25}^*)^2\mu_H^4 x_1^* w_3^2 b_M^4 K_2}{\mu_M^2\Pi_H^4 K_4^2\,(\omega\,\xi - K_1K_2)} - 2\,\frac{\beta_H^* b_M^3 x_1^*\mu_H^3 v_3\sigma_{U1}^2 w_3^2\beta_M^2 x_{25}^*}{\mu_M^2\Pi_H^3 K_4^2}. \qquad (2.5.5)$$

Since the eigenvectors w_3 and v_3 (given in Appendix B1) are positive and $\omega\,\xi - K_1K_2 = -\mu_H(\xi+\omega+\mu_H) < 0$, it follows from (3.5) that the bifurcation coefficient $a < 0$ (ruling out backward bifurcation in this case, in line with Theorem 4.1 in (Castillo-Chavez and Song, 2004)). □

Thus, this study shows that the backward bifurcation phenomenon of the model (2.4.1) can be removed if the following conditions hold:

(i) disease-induced mortality in the host population (δ_H) is small enough (e.g., $\delta_H = 0$);

(ii) vaccine efficacy against each strain is perfect (i.e., $\varepsilon_1 = \varepsilon_2 = 1$).

In other words, the phenomenon of backward bifurcation persists in the model (2.4.1) if Item (i) or Item (ii) does not hold. To completely rule out backward bifurcation

when the aforementioned Conditions hold (i.e., when $\delta_H = 0$ and $\varepsilon_1 = \varepsilon_2 = 1$), a global asymptotic stability result is established for the NDFE of the model under this scenario (and also, for computational convenience, setting $\eta_{ij} = \eta_{Vij} = 0\,(i, j = 1, 2; i \neq j)$) below. It should be mentioned that the requirement $\eta_{ij} = \eta_{Vij} = 0\,(i, j = 1, 2; i \neq j)$ is not necessary for the removal of backward bifurcation in the model (it is only chosen to simplify the mathematical analysis; the backward bifurcation property persists regardless of the values of η_{ij} and $\eta_{Vij}\,(i, j = 1, 2; i \neq j)$ provided $\delta_H > \delta_H^c$ or $\varepsilon_1 \neq 1$ and $\varepsilon_2 \neq 1$).

Theorem 2.5.5. *Consider the model* (2.4.1) *with* $\varepsilon_1 = \varepsilon_2 = 1$, $\eta_{ij} = \eta_{Vij} = 0\,(i, j = 1, 2; i \neq j)$ *and* $\delta_H = 0$. *The NDFE* ($\mathcal{T}_1$) *of this special case of the model is GAS in* $C([0], \mathbb{R}_+^{27}) \setminus \{\mathcal{T}_o\}$ *whenever* $\mathcal{R}_{vac}^{**} < 1$.

The proof of Theorem 2.5.5, based on using the approach in (Dumont and Chiroleu, 2010; Kamgang and Sallet, 2008), is given in Appendix C. The epidemiological implication of Theorem 2.5.5 is that, for the special case of the model (2.4.1) with no disease-induced mortality in the host population (i.e., $\delta_H = 0$) and with perfect vaccine efficacy against the two strains (i.e., $\varepsilon_1 = \varepsilon_2 = 1$), bringing (and maintaining) the threshold quantity $\mathcal{R}_{vac}^{**}$ to a value less than unity will lead to the elimination of all four dengue serotypes from the community.

2.5.3 Uncertainty and Sensitivity Analyses

The model (2.4.1) contains 49 parameters, and uncertainty in their estimates are expected to arise. The effect of such uncertainties is assessed using uncertainty and sensitivity analysis (Cariboni et al., 2007). In particular Latin Hypercube Sampling (LHS) and Partial Rank Correlation Coefficients (PRCC) is used for the model (2.4.1) below. The purpose of sensitivity analysis is to determine effects of parameters on

model outcomes (Cariboni et al., 2007). A highly sensitive parameter should be more carefully estimated, since a small change in that parameter can cause a large quantitative changes in the result (Cariboni et al., 2007). On the other hand, a parameter that is not sensitive does not require as much attempt to estimate (because a small change in that parameter will not cause a large variation to the quantity of interest) (Blower and Dowlatabadi, 1994; Cariboni et al., 2007; Marino et al., 2008). We use the range and baseline values of the parameters in Table 2.3.

Figure 2.2 depicts boxplots of the reproduction number of the model against strain 1 in the absence of disease-induced mortality in the host population as a function of the number of LHS runs. The results obtained show a distribution of $\mathcal{R}_{vac1}$ in the range [0.2286, 6.7857] (with a mean of $\mathcal{R}_{vac1}$=1.5973) (Figure 2.2a), while the values of $\mathcal{R}_{vac2}$ lie in the range [0.2356, 8.2638] (with a mean of $\mathcal{R}_{vac2}$=1.5982) (Figure 2.2b). Since $\mathcal{R}_{vac} = \max\{\mathcal{R}_{vac1}, \mathcal{R}_{vac2} > 1\} = 1.5982$, it follows from these simulations that, although the use of the *Dengvaxia* vaccine will reduce the disease burden in the community, it is unable to lead to the effective control (or elimination) of the two dengue strains in the community (in other words, the singular use of a vaccination program, using *Dengvaxia*, will not lead to the effective control or elimination of the disease in Oaxaca, since the efficacy of *Dengvaxia* against the two strains ($\varepsilon_1 = 0.7, \varepsilon_2 = 0.3$ (Hladish et al., 2016)) is not sufficiently high enough to bring (and maintain) $\mathcal{R}_{vac}$ to a value less than unity). (Morales et al., 2017) reported a distribution of $\mathcal{R}_{vac}$ (the notation $\mathcal{R}_0$ is used in (Morales et al., 2017)) for their dengue model with vaccination in the range [0.4– 2].

Furthermore, using the population of unvaccinated individuals who are exposed to strain 1 (E_{UH1}) as the response function, it is shown in Tables 2.4-2.5 that the top PRCC-ranked parameters (with PRCC value ≥ 0.5 in magnitude) are the biting rate of mosquitoes (b_M), the maturation rate of immature mosquitoes (ψ_L) and the carry-

ing capacity of immature mosquitoes (K_M). It is further evident from Tables 2.4-2.5 that these three parameters remain the most dominant ones if the populations of unvaccinated individuals who are exposed to strain 2 (E_{UH2}), unvaccinated individuals who are exposed to strain 1 (E_{UH1}) and vaccinated individuals who are exposed to strain 2 (E_{VH2}) are used as the response functions, respectively. In summary, this study identifies three parameters that play the most dominated role on the transmission dynamics of the four dengue serotypes (i.e., strains 1 and 2) in the community, namely the mosquito biting rate (b_M), maturation rate of immature mosquitoes (ψ_L) and the carrying capacity of immature mosquitoes (K_M). It is worth noting that the human-related parameters of the model (including the vaccine parameters) do not feature prominently in the PRCC rankings.

2.6 Theoretical Assessment of Vaccine Impact

The model (2.4.1) will now be analysed to assess the population-level impact of the dengue vaccine against strain 1 (i.e., dengue serotypes 1, 3 and 4). Similar analysis can be used to assess the impact of the vaccine against strain 2 (i.e., dengue serotype 2). To achieve this, a threshold analysis is carried out on the vaccination threshold for dengue strain 1 in the absence of disease-induced mortality in the host population (i.e., $\mathcal{R}_{vac1}$). The quantity $\mathcal{R}_{vac1}$ is, first of all, expressed as a function of the fraction of susceptible individuals vaccinated at steady-state ($f_v = \frac{S^*_{VH}}{N^*_H}$). That is,

$$(\mathcal{R}_{vac1})^2 = (\mathcal{R}_{vac1})^2(f_v) = \frac{\beta_M \beta_H (1-f_v) b_M^2 \sigma_{U1} S^*_M}{\mu_M N^*_H K_3 K_4} + \frac{\beta_M \beta_H f_v b_M^2 \sigma_{V1}(1-\varepsilon_1)\theta_{V1} S^*_M}{\mu_M N^*_H K_{11} K_{12}}, \tag{2.6.1}$$

where, now, $K_4 = \gamma_{U1} + \mu_H$ and $K_{12} = \gamma_{V1} + \mu_H$. Differentiating $\mathcal{R}_{vac1}$ partially with respect to f_v gives

$$\frac{\partial \mathcal{R}_{vac1}}{\partial f_v} = \frac{(\Delta - 1)(\mathcal{R}_0)^2}{2\mathcal{R}_{vac1}}, \tag{2.6.2}$$

where,

$$\Delta = \frac{\sigma_{V1}(1-\varepsilon_1)\theta_{V1}K_3K_4}{\sigma_{U1}K_{11}K_{12}}, (\mathcal{R}_0)^2 = \frac{\beta_M\beta_H b_M^2\sigma_{U1}S_M^*}{\mu_M N_H^* K_3K_4},$$

and,

$$\mathcal{R}_{vac1}(f_v) = \sqrt{\frac{\beta_M\beta_H(1-f_v)b_M^2\sigma_{U1}S_M^*}{\mu_M N_H^* K_3K_4} + \frac{\beta_M\beta_H f_v b_M^2\sigma_{V1}(1-\varepsilon_1)\theta_{V1}S_M^*}{\mu_M N_H^* K_{11}K_{12}}}.$$

It follows from Equation (2.6.2) that $\frac{\partial \mathcal{R}_{vac1}}{\partial f_v} < (>)0$ whenever $\Delta < (>)1$. That is, $\mathcal{R}_{vac1}$ is a decreasing (increasing) function of the vaccinated fraction, f_v, whenever $\Delta < (>)1$. Furthermore, since a reduction in reproduction number implies a reduction in the burden of the disease, the above analyses shows that a dengue vaccine will have a positive (negative) impact in reducing (increasing) the disease burden whenever $\Delta < (>)1$. This result is summarized below.

Theorem 2.6.1. *Consider the model* (2.4.1). *The use of the Dengvaxia vaccine against strain 1 will have the following properties:*

(i) a positive population-level impact (i.e., reduce disease burden) if $\Delta < 1$;

(ii) no population-level impact if $\Delta = 1$;

(iii) a negative (detrimental) population-level impact (i.e., increase disease burden) if $\Delta > 1$.

The result of Theorem 2.6.1 can be expressed in terms of the vaccine efficacy against strain 1 (ε_1), by setting $\Delta = 1$ and solving for $\varepsilon_1 = \varepsilon_1^c$, giving

$$\varepsilon_1^c = 1 - \frac{H_1}{H_2}, \tag{2.6.3}$$

where $H_1 = \sigma_{U1}K_{11}K_{12}$ and $H_2 = \sigma_{V1}\theta_{V1}K_3K_4$ (it should be noted that $H_1 < H_2$ is needed to ensure $0 < \varepsilon_1^c < 1$). These results are summarized below.

Theorem 2.6.2. *Consider the model* (2.4.1). *The use of the Dengvaxia vaccine against strain 1 will have the following properties:*

(i) a positive population-level impact if $\varepsilon_1 > \varepsilon_1^c$;

(ii) no population-level impact if $\varepsilon_1 = \varepsilon_1^c$;

(iii) a negative population-level impact if $\varepsilon_1 < \varepsilon_1^c$.

Using the parameter values in Table 2.3 with $\sigma_{U1} = 0.25, \sigma_{V1} = 0.19, \theta_{V1} = 0.7, \gamma_{U1} = 0.067$ and $\gamma_{V1} = 0.16$ (Morales et al., 2017), the value of ε_1^c is computed to be $\varepsilon_1^c = 0.58 < \varepsilon_1 = 0.7$ (Hladish et al., 2016). Thus, since $\varepsilon_1^c = 0.58$ (i.e., 58% efficacy against strain 1) is less than the reported efficacy of the vaccine against strain 1 (i.e., $\varepsilon_1 = 0.7$ (Hladish et al., 2016)), it follows from Theorem 2.6.2 that the community-wide use of the *Dengvaxia* vaccine will induce a positive population-level impact against strain 1 (i.e., dengue serotypes 1, 3 and 4).

Furthermore, following (Blower et al., 1998; Podder and Gumel, 2010), the effectiveness of the vaccine can be measured in terms of the *vaccine impact factor* (denoted by $0 < \phi < 1$), by rewriting $\mathcal{R}_{vac1}$ as

$$(\mathcal{R}_{vac1})^2 = (\mathcal{R}_0)^2 \left\{ 1 - f_v \left[1 - \frac{(\mathcal{R}_{0V})^2}{(\mathcal{R}_0)^2} \right] \right\}, \tag{2.6.4}$$

where,

$$(\mathcal{R}_{0V})^2 = \frac{\beta_M \beta_H b_M^2 \sigma_{V1} (1 - \varepsilon_1) \theta_{V1} S_M^*}{\mu_M N_H^* K_{11} K_{12}}, \tag{2.6.5}$$

is the *reproduction number* of the model when every member of the community is vaccinated. Using the notation in (Blower et al., 1998; Podder and Gumel, 2010), it follows from (2.6.4) that the *vaccine impact factor* is given by

$$\phi = f_v \left[1 - \frac{(\mathcal{R}_{0V})^2}{(\mathcal{R}_0)^2} \right]. \tag{2.6.6}$$

It should be noted from (2.6.6) that if $\mathcal{R}_{0V} < (>)\mathcal{R}_0$, then the vaccine impact factor (ϕ) is positive (negative), so that the community-wide implementation of the vaccination program will reduce (increase) the reproduction number ($\mathcal{R}_{vac1}$). Hence, the vaccine will have positive (negative) impact (i.e., reduce (increase) disease burden) in this case. Furthermore, if $\mathcal{R}_{0V} > (<)\mathcal{R}_0$, then $\phi(> 0) < 0$, so that vaccination will have negative (positive) impact in the community. If $\phi = 0$, then $\mathcal{R}_{0V} = \mathcal{R}_0$, and the vaccine will have no population-level impact in this case. These results are summarized below.

Theorem 2.6.3. *Consider the model* (2.4.1). *The use of the Dengvaxia vaccine against strain 1 will have the following properties:*

(i) a positive population-level impact if $\phi > 0$ *(*$\mathcal{R}_{0V} < \mathcal{R}_0$*);*

(ii) no population-level impact if $\phi = 0$ *(*$\mathcal{R}_{0V} = \mathcal{R}_0$*);*

(iii) a negative population-level impact if $\phi < 0$ *(*$\mathcal{R}_{0V} > \mathcal{R}_0$*).*

The result of Theorem 2.6.3 is illustrated in Figure 2.3. Further, a contour plot of the reproduction number of strain 1 ($\mathcal{R}_{vac1}$), as a function of the vaccine efficacy against strain 1 (ε_1) and the function of susceptible individuals vaccinated at steady-state ($f_v = \frac{S^*_{VH}}{N^*_H}$), is depicted in Figure 2.4. This figure shows, with the 70% *Dengvaxia* efficacy against strain 1 (WHO et al., 2017), the vaccine is unable to bring the reproduction number to a value less than unity (even if 100% of the susceptible population is vaccinated). Hence, although routine vaccination using *Dengvaxia* vaccine reduces disease burden, it is unable to lead to the elimination of the disease (strain 1). Similar result is obtained for strain 2 (not repeated here).

The model (2.4.1) is simulated to test the recent report by Sanofi Pasteur Ltd. that the *Dengvaxia* vaccine may increase the risk of severe disease in people who

have never been exposed to the dengue virus (Aguiar, 2018). Figure 2.5*a* depicts the cumulative dengue-induced mortality for dengue-naive vaccinated individuals and individuals who recovered from dengue strain i and exposed to dengue strain j ($i \neq j$), showing that, indeed, the dengue-induced mortality is higher in the dengue-naive population than in the population with prior dengue infection (similar result is obtained for the cumulative new cases, as shown in Figure 2.5*b*). Thus, this study supports the recent claim that the use of *Dengvaxia* vaccine in dengue-naive populations could induce additional risk of severe disease in these populations. It is worth noting that the result does not change even if the efficacy of the dengue vaccine (against both strains) is significantly increased (Figure 2.5*c*).

2.7 Discussion and Conclusions

Dengue, a mosquito-borne disease that is endemic in over 100 countries in the tropical and sub-tropical regions of the world, continues to inflict major public heath burden in the affected areas (accounting for over 50 million infections and 20,000 deaths annually). This Chapter is based on the use of mathematical modeling approaches to assess the population-level impact of the *Dengvaxia* vaccine against the four dengue serotypes (DENV1, 2, 3, 4; but categorized into two strains, namely strain 1 and 2, in this study for computational convenience). A new deterministic model for the temporal dynamics of the two strains of the disease in the presence of the *Dengvaxia* vaccine, was designed.

Rigorous analysis of the model show that, as in other models for the transmission dynamics of vector-borne diseases (with disease-induced mortality in the host population), the model undergoes the phenomenon of backward bifurcation when the associated disease-induced mortality in the host population exceeds a certain threshold value (i.e., $\delta_H > \delta_H^c$) or the vaccine efficacy against the two dengue strains is not

high enough (i.e., $\varepsilon_1 \neq 1$ and $\varepsilon_2 \neq 1$). The public health implication of the backward bifurcation phenomenon (which is characterized by the co-existence of multiple stable attractors when the associated reproduction number of the model is less than unity) is that bringing the reproduction number to a value less than unity, while necessary, is no longer sufficient for the effective control of the disease. In such a scenario, more needs to be done (e.g., increase vaccine coverage) to decrease the reproduction number further below unity (outside the backward bifurcation range)to enhance the prospect of disease elimination.

It is shown that, in the absence of this dynamic phenomenon, the disease-free equilibrium of the model is globally-asymptotically stable whenever the associated reproduction number is less than unity. Hence, in this case, a routine vaccination program, based on using the *Dengvaxia* vaccine, can lead to the effective control (or elimination) of the disease.

Using data relevant to dengue transmission dynamics in Oaxaca, Mexico, our simulations for parameter uncertainty show that the reproduction number of strain 1 (strain 2) lie between $\mathcal{R}_{vac} \in [0.2286, 6.7857]$ ([0.2356, 8.2638]), with a mean $\mathcal{R}_{vac}$=1.5973 (1.5982). Thus, although the *Dengvaxia* vaccine can significantly reduce the burden of each of the two strains, it is unable to lead to the elimination of any of the two strains (since elimination of a strain requires the reproduction number of that strain to be less than unity).

Using clinical trial data from the Philippines, Sanofi Pasteur Ltd. (the makers of *Dengvaxia* vaccine) recently reported that the use of the vaccine in dengue-naive population can induce additional risk of severe disease in this population (Aguiar, 2018). The simulations strongly supports this claim. Thus, in a community this complication must be fully taken into account before a decision to deploy the vaccine is made.

Chapter 3

INSECTICIDE RESISTANCE AND MALARIA EPIDEMIOLOGY

3.1 Introduction

As stated in chapter 1, malaria is a deadly parasitic disease caused by the protozoan *Plasmodium* parasites. The disease, which is spread in humans *via* the bite of infected adult female *Anopheles* mosquitoes (WHO, 2016, 2017a), affect over 2.5 billion people who reside in tropical and sub-tropical regions of the world (Gething et al., 2011; Johnston et al., 2013). It is endemic in 91 countries, and causes 500,000 deaths annually (Camara et al., 2018; Gates, 2016; WHO, 2018b). Control efforts against malaria are largely focused on mosquito reduction strategies, such as larvaciding (to kill immature mosquitoes), adulticiding (using LLINs and IRS to kill adult *Anopheles* mosquitoes) and the use of artemisinin-based therapy to treat infected individuals (Alliance, 2018; Huijben and Paaijmans, 2018). Dramatic successes have been recorded in the fight aginst malaria in sub-Saharan Africa during 2000-2015, largely owing to the widespread use of insecticide-based interventions (notably LLINs and IRS).

It has been estimated that LLINs bednets and IRS accounted for 81% of the reduction in malaria burden recorded during the period 2000 and 2015 (with most of the benefits resulting from the use of bednets) (Bhatt et al., 2015). The dramatic success of pyrethroid-based LLINs (over IRS) is likely due to multiple factors, including the fact that LLINs target indoor-biting mosquitoes, are effective as a physical barrier to biting, and pyrthroids have an excito-repellent effect that may diverting mosquitoes before they feed on the (protected) human host. However, at the most basic level, the success of LLINs is likely simply due to the enormous scale of implementation in

endemic areas, especially in sub-Saharan Africa: Nearly 1.5 billion pyrethroid-based bednets have been deployed in endemic areas since 2010, with 1.25 billion distributed in sub-Saharan Africa (Alliance, 2018; Huijben and Paaijmans, 2018).

Unfortunately, this widespread and heavy use of insecticides has resulted in the emergence of vector resistance to nearly every currently-available agent used in the insecticides (Alout et al., 2017; Dondorp et al., 2009; Imwong et al., 2017; WHO, 2017b) with pyrethroid resistance via multiple molecular mechanisms now widely observed across the African continent (Hemingway et al., 2016). Given this, and the dominant role of LLINs in malaria mortality reductions, any threat to their efficacy via resistance is of foremost importance.

This chapter is based on the design, analysis and simulations of an improved mathematical model for assessing the impact of insecticide resistance on malaria epidemiology in malaria-endemic areas that adopt wide-scale use of LLINs.

3.2 Literature Review of Modeling of Insecticides and Malaria Epidemiology

A number of mathematical models have been designed and used to assess the impact of insecticide resistance on malaria transmission dynamics. For example, (Barbosa and Hastings, 2012) developed a genetic model to predict changes in mosquito fitness and resistance allele frequency (parameters that describe insecticide selection, fitness cost as well as LLINs and synergist (PBO) are incorporated). The results of their investigation suggested that resistance was most sensitive to selection coefficients, fitness cost and dominance coefficients.

Chitnis et al. (2008) developed and analysed a linear difference equation model for the dynamics of host-seeking adult female mosquitoes in a heterogeneous population of hosts in a community where ITNs are used. In addition to incorporating the gonotrophic cycle of the malaria vector and the aforementioned host heterogeneity,

other notable features of the model in (Chitnis et al., 2008) include stage-structure in *Anopheles* feeding cycle and that such cycle varies across mosquitoes as well as allowing for the assessment of various mosquito control interventions. Consistent with previous studies for the impact of ITNs on malaria epidemiology in both ITN-protected and unprotected hosts, the (Chitnis et al., 2008) study shows beneficial effects to unprotected humans at both, low and high, ITN coverage levels.

Birget and Koella (2015a) developed a population-genetic model of the spread of insecticide-resistance in *Anopheles* mosquitoes in response to ITNs and larvicides, which suggested indoor ITNs were less likely to select for resistance. Brown et al. (2013) developed a mathematical model to investigate optimal (cost-effective) strategies for mosquito control in the presence of insecticide resistance. Consistent with previous studies, their results show that fitness costs are the key elements in the computation of economically optimal resistance management strategies.

Mohammed-Awel and Gumel (2018) designed a novel deterministic model for assessing the population-level impact of mosquito insecticide resistance on malaria transmission dynamics and to evaluate the community-wide impact of the use ITNs, IRS and their combination. Their study showed that the prospect of the effective control of malaria spread in endemic settings (while minimizing the risk of insecticide resistance in the female adult mosquito population), using ITNs and IRS, is quite promising (provided the effectiveness and coverage levels are at optimal levels).

Birget and Koella (2015b) proposed a model to assess the relative importance in different epidemiological contexts of repellent and insecticidal properties of ITNs. Gu and Novak (2009) used an agent-based model that incorporated the killing and avoidance of individual mosquitoes exposed to ITNs in a hypothetical village setting with 50 houses and 90 aquatic habitats. Smith et al. (2009) used a mathematical model to establish the relationship between *P. falciparum* parasite rate ($PfPR$) and

ITNs coverage.

Killeen and Smith (2007) proposed a model that describes the interaction of a blood-seeking mosquito with either bednet-protected or unprotected hosts as a two-stage process, whereby mosquito are either diverted from the attempt, or engage in an attempt and then either die or succeed in taking a bloodmeal. Similar bednet-human interaction and feeding cycle models are described in (Glunt et al., 2018; Killeen et al., 2011; Le Menach et al., 2007; Okumu et al., 2013).

3.3 Main Objectives

The main objective of this chapter is to develop an improved mathematical modeling framework for assessing the impact of insecticide resistance on malaria epidemiology (in malaria-endemic areas that adopt wide-scale use of LLINs). The main motivation is twofold. The first motivation is the fact that LLINs are the core intervention (due to their superior success over IRS) for National Malaria Prevention Programs (WHO, 2015c, 2017c). The second motivation is the fact that the impact of pyrethroid resistance on malaria transmission/epidemiology is not well-understood and remains a subject for considerable debate within the malaria control community (Alout et al., 2017; Kleinschmidt et al., 2018; Protopopoff et al., 2018; Toe et al., 2018).

The model to be developed, which will take the form of a deterministic system of nonlinear differential equations, incorporates key features of aquatic and adult mosquito dynamics (including the aquatic developmental stages, adult mosquito gonotrophic cycle, parasite sporogony and schizogony in the hosts population), disease transmission in humans, and the use of bednets as the sole control strategy.

3.4 Mathematical Formulation

The model to be developed in this chapter describes the temporal dynamics of immature and adult mosquitoes and humans. The total immature mosquito population is split into compartments for eggs ($E(t)$), four larval instar stages ($L_i(t)$; $i = 1, 2, 3, 4$ and pupae ($P(t)$). As dicussed in chapter 1, the dynamics of the adult female *Anopheles* mosquito is governed by the following three gonotrophic cycle stages (Corbel et al., 2004; Okuneye et al., 2019):

Stage I : host-seeking and taking of a bloodmeal

Stage II : digestion of bloodmeal and egg maturation

Stage III : search for, and oviposition into, a suitable body of water

The populations of vectors in Stages I, II and III of the gonotrophic cycle at time t are denoted by $X(t)$, $Y(t)$ and $Z(t)$, respectively. With respect to *Plasmodium* infection and the sporogonic cycle, vectors in each gonotrophic stage is further subdivided into susceptible ($S_X(t), S_Y(t), S_Z(t)$), exposed (i.e., infected but not yet infectious) ($E_X(t), E_Y(t), E_Z(t)$) and infectious ($I_X(t), I_Y(t), I_Z(t)$) compartments. Thus, the total number of adult female *Anopheles* mosquitoes at time t, denoted by $N_M(t)$, is given by

$$N_M(t) = S_X(t) + E_X(t) + I_X(t) + S_Y(t) + E_Y(t) + I_Y(t) + S_Z(t) + E_Z(t) + I_Z(t).$$

The total human population at time t, denoted by $N_H(t)$, is split into the total number of humans who are protected by bednets (i.e., those who consistently sleep under an LLIN), denoted by $N_{H_p}(t)$, and those who are not protected, denoted by $N_{H_u}(t)$. The population of protected and unprotected individuals is further subdivided into susceptible $S_{H_p}(t)(S_{H_u}(t))$, exposed $E_{H_p}(t)(E_{H_u}(t))$, infectious $I_{H_p}(t)(I_{H_u}(t))$ and recovered $R_{H_p}(t)(R_{H_u}(t))$ humans, so that

$$N_H(t) = N_{Hp}(t) + N_{Hu}(t),$$

$$= S_{H_p}(t) + S_{H_u}(t) + E_{H_p}(t) + E_{H_u}(t) + I_{H_p}(t) + I_{H_u}(t) + R_{H_p}(t) + R_{H_u}(t).$$

The Flow Diagram of the Model to be Developed in This Chapter is Depicted in Figure 3.1.

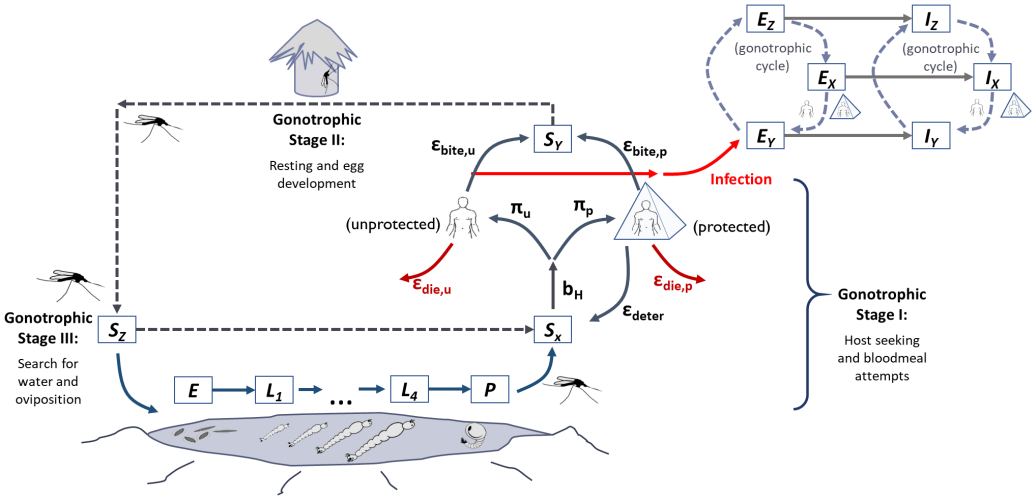

Figure 3.1: Flow Diagram of the Model {(3.4.1), (3.4.2), (3.4.4)}.

3.4.1 Equations for the Dynamics of Immature Mosquitoes

It is convenient to define $L = \sum_{j=1}^{4} L_j$. The equations for the dynamics of immature mosquitoes are given by (where a dot represents differentiation with respect to time t) (Iboi et al., 2019b)

$$\begin{aligned}
\dot{E} &= \psi_E \varphi_Z \left(1 - \frac{E}{K_E}\right)_+ (S_Z + E_Z + I_Z) - [\sigma_E(T_W) + \mu_E(T_W)]E, \\
\dot{L}_1 &= \sigma_E(T_W)E - [\sigma_{L_1}(T_W) + \mu_L(T_W) + \delta_L L]L_1, \\
\dot{L}_j &= \sigma_{Lj-1}(T_W)L_{j-1} - [\sigma_{L_j}(T_W) + \mu_L(T_W) + \delta_L L]L_j;\ j = 2, 3, 4, \\
\dot{P} &= \sigma_{L_4}(T_W)L_4 - [\sigma_P(T_W) + \mu_P(T_W)]P,
\end{aligned} \tag{3.4.1}$$

where T_A and T_W represent air and water, temperature, respectively. In (3.4.1), ψ_E is the number of eggs laid *per* oviposition, φ_Z is the rate at which female mosquitoes transition from Stage III to Stage I of the gonotrophic cycle (i.e., the rate of oviposition for mosquitoes in Stage III) and K_E is the environmental carrying capacity of eggs (the notation $r_+ = \max\{0, r\}$ is used to ensure the non-negativity of the logistic term). The quantity $\delta_L L$ represents the density-dependent larval mortality rate (Agusto et al., 2015). Further, μ_i and σ_i ($i = E, L, P$) represent the natural death and maturation rates of immature mosquitoes of type i, respectively. The temperature-dependence of the developmental and survival parameters is presented in Section 3.4.4.

3.4.2 Equations for the Dynamics of Adult Female *Anopheles* Mosquitoes

As stated above, the dynamics of the adult female *Anopheles* mosquitoes is governed by the gonotrophic cycle. The total vector population is split into the aforementioned nine compartments $(S_X, E_X, I_X, S_Y, E_Y, I_Y, S_Z, E_Z, I_Z)$ corresponding to the three gonotrophic cycle stages (Okuneye et al., 2019). We let π_p represent the proportion of humans that are protected by a bednet (i.e. consistently sleep under an LLIN), while $\pi_u = 1 - \pi_p$ is the unprotected portion. In other words, $0 < \pi_p \leq 1$ is the bednet coverage. Bednet-mosquito interactions are defined by three basic parameters: ε_{deter}, $\varepsilon_{die,i}$, and $\varepsilon_{bite,i}$, as described now. We let ε_{deter} represent the chance that an adult female mosquito is deterred from entering an LLIN-protected hut (or house), relative to an unprotected hut (or house). That is,

$$\varepsilon_{\text{deter}} = \frac{\text{Number of mosquitoes in control group} - \text{Number of mosquitoes in the protected hut}}{\text{Number of mosquitoes in the control group}}.$$

It should be emphasized that, in the context of this study, "deterrence" (as measured

by the parameter ε_{deter}) means that the mosquito is deterred from entering the house before any attempt is made to take a bloodmeal. Thus, the parameter ε_{deter} does not include any direct "barrier" property of the net.

We let $\varepsilon_{die,i}$ (with $i = \{p, u\}$; p=protected; u=unprotected) represent the probability that an adult female mosquito dies following entry into a protected (unprotected) house. The parameters $\varepsilon_{bite|die,i}$ and $\varepsilon_{bite|\sim die,i}$ represent, respectively, the probability that an adult female mosquito successfully takes a bloodmeal from the human host, given that the mosquito did or did not die, with i (p or u) indicating the bednet protection status of the targeted human (Figure 3.2 depicts the associated decision tree of the aforementioned probabilities).

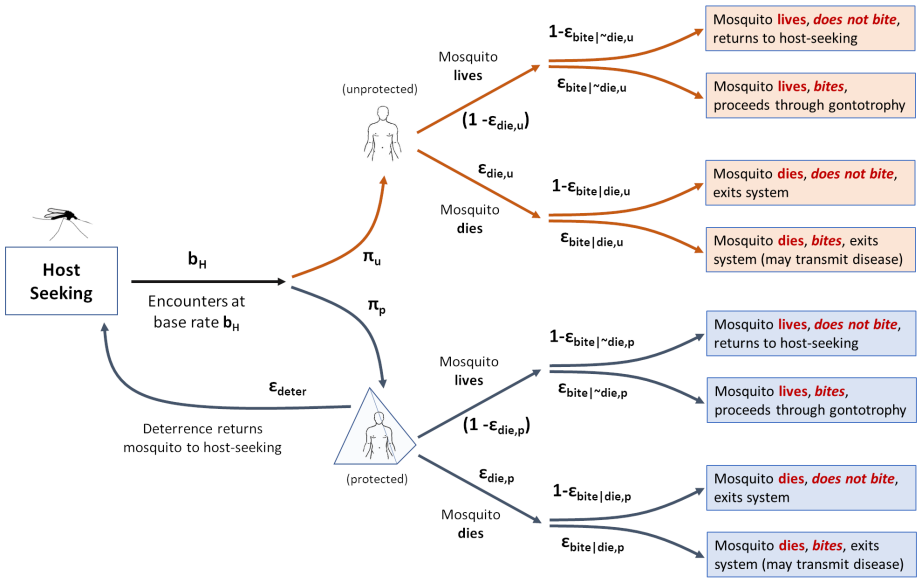

Figure 3.2: A Decision Tree of Probabilities of the Model {(3.4.1), (3.4.2), (3.4.4)}.

The (temperature-dependent) equations for adult female mosquito dynamics are

given by (Iboi et al., 2019b):

$$\text{Stage I}\begin{cases}\dot{S}_X &= f\sigma_P(T_W)P + \varphi_Z S_Z + b_H(Q_2+Q_3)S_X - [b_H Q_1 + \mu_X + \mu_M(T_A)]S_X,\\ \dot{E}_X &= \varphi_Z E_Z + b_H(Q_2+Q_3)E_X - [b_H Q_1 + \kappa_V(T_A) + \mu_X + \mu_M(T_A)]E_X,\\ \dot{I}_X &= \varphi_Z I_Z + \kappa_V(T_A)E_X + b_H(Q_2+Q_3)I_X - [b_H Q_1 + \mu_X + \mu_M(T_A)]I_X,\end{cases} \tag{3.4.2}$$

$$\text{Stage II}\begin{cases}\dot{S}_Y &= b_H[(1-\beta_V\omega_p)R_1 + (1-\beta_V\omega_u)R_2]S_X - [\theta_Y(T_A) + \mu_M(T_A)]S_Y,\\ \dot{E}_Y &= b_H(\beta_V\omega_p R_1 + \beta_V\omega_u R_2)S_X + b_H(R_1+R_2)E_X\\ &\quad -[\theta_Y(T_A) + \kappa_V(T_A) + \mu_M(T_A)]E_Y,\\ \dot{I}_Y &= \kappa_V(T_A)E_Y + b_H(R_1+R_2)I_X - [\theta_Y(T_A) + \mu_M(T_A)]I_Y,\end{cases}$$

$$\text{Stage III}\begin{cases}\dot{S}_Z &= \theta_Y(T_A)S_Y - [\varphi_Z + \mu_M(T_A)]S_Z,\\ \dot{E}_Z &= \theta_Y(T_A)E_Y - [\varphi_Z + \kappa_V(T_A) + \mu_M(T_A)]E_Z,\\ \dot{I}_Z &= \theta_Y(T_A)I_Y + \kappa_V(T_A)E_Z - [\varphi_Z + \mu_M(T_A)]I_Z.\end{cases}$$

where,

$$\begin{aligned} Q_1 &= \pi_p(1-\varepsilon_{deter}) + \pi_u,\\ Q_2 &= \pi_p(1-\varepsilon_{deter})(1-\varepsilon_{die,p})(1-\varepsilon_{bite|\sim die,p}),\\ Q_3 &= \pi_u(1-\varepsilon_{die,u})(1-\varepsilon_{bite|\sim die,u}),\\ R_1 &= \pi_p(1-\varepsilon_{deter})(1-\varepsilon_{die,p})\varepsilon_{bite|\sim die,p},\\ R_2 &= \pi_u(1-\varepsilon_{die,u})\varepsilon_{bite|\sim die,u},\\ \omega_p &= \frac{I_{H_p}}{N_{H_p}},\\ \omega_u &= \frac{I_{H_u}}{N_{H_u}},\end{aligned} \tag{3.4.3}$$

with ω_p (ω_u) representing the fractions of protected (unprotected) humans that are infectious.

In (3.4.2) and (3.4.2), the term $f\sigma_P$ $(0 < f < 1)$ represents the proportion of new adult mosquitoes that are females. Susceptible adult mosquitoes in Stage I of the gonotrophic cycle encounter hosts at a rate $b_H Q_1$ (where b_H is the mosquito-host encounter rate per unit time, and Q_1 is defined above). The rate $b_H(Q_2 + Q_3)$ represents failure to take a bloodmeal ending in survival (and thus a return to stage I of the gonotrophic cycle), while $b_H(R_1 + R_2)$ is the rate at which encounters result in successful bloodmeals and survival.

It should be emphasized that, in the formulation of the model (3.4.2) questing adult female mosquitoes that do not succeed in biting bednet-protected humans will not necessarily have to bite an unprotected human. They will simply look for a bloodmeal from another human who may be protected or not (see Figure 3.1). The parameter κ_V represents the maturation rate of malaria parasite in the mosquito (i.e., $\frac{1}{\kappa_V}$ is the average duration of the sporogonic cycle), while the parameter θ_Y is the progression rate from Stage II to Stage III of the gonotrophic cycle. Susceptible adult female mosquitoes in Stage II of the gonotrophic cycle acquire malaria infection at the rate $b_H(\beta_V \omega_p R_1 + \beta_V \omega_u R_2)$, where β_V is the transmission probability from infectious human to a susceptible mosquito, ω_p and ω_u are the fractions of protected and unprotected infectious humans, respectively, and μ_M is the natural mortality rate of adult female mosquitoes. Following Chitnis et al. (2008), we assume an additional mortality rate, μ_X, for adult female mosquitoes in the host-seeking stage, as this stage of the gonotrophic cycle is expected to be most hazardous to the adult female mosquitoes. Moreover, this helps account for a survival cost potentially incurred when the adult female mosquitoes are deterred from protected hosts and, thus, must expend more energy in questing for bloodmeal. Furthermore, as noted by Cator et al. (2012), sporozoite-infected *Anopheles gambiae* females are more likely than uninfected females to take bloodmeal from multiple hosts in the same night, and they

suffer higher feeding-associated mortality. It should, however, be mentioned that very little is known about adult mosquito mortality in the field, and the degree that mortality is associated with bloodfeeding events is unknown. Such valuable data, when available, will undoubtedly enhance the predictive power of malaria modeling studies.

From the above formulation, the (time-varying) entomological inoculation rates (EIRs; the average numbers of infectious bites per human per unit time (Eikenberry and Gumel, 2018)) for protected and unprotected hosts are given, respectively, by

$$\text{EIR}_p(t) = b_H \frac{I_X(t)}{N_{H_p}(t)} \pi_p (1 - \varepsilon_{deter}) \left[\varepsilon_{bite|die,p}\, \varepsilon_{die,p} + \varepsilon_{bite|\sim die,p} (1 - \varepsilon_{die,p}) \right],$$

$$\text{EIR}_u(t) = b_H \frac{I_X(t)}{N_{H_u}(t)} \pi_u \left[\varepsilon_{bite|die,u}\, \varepsilon_{die,u} + \varepsilon_{bite|\sim die,u} (1 - \varepsilon_{die,u}) \right].$$

Similarly, the biting (infectious or uninfectious) rates for protected and unprotected host are given, respectively, by

$$\text{biting}_p(t) = b_H \frac{[S_X(t)+E_X(t)+I_X(t)]}{N_{H_p}(t)} \pi_p (1 - \varepsilon_{deter}) \left[\varepsilon_{bite|die,p}\, \varepsilon_{die,p} + \varepsilon_{bite|\sim die,p} (1 - \varepsilon_{die,p}) \right],$$

$$\text{biting}_u(t) = b_H \frac{[S_X(t)+E_X(t)+I_X(t)]}{N_{H_u}(t)} \pi_u \left[\varepsilon_{bite|die,u}\, \varepsilon_{die,u} + \varepsilon_{bite|\sim die,u} (1 - \varepsilon_{die,u}) \right].$$

Estimation of Bednet-related Parameters: Clinical Hut Trial

The parameters related to the use of LLINs in the community (i.e., b_H, π_p, π_u, ε_{deter}, $\varepsilon_{bite|\sim die,p}$, $\varepsilon_{bite|\sim die,u}$, $\varepsilon_{bite|die,p}$, $\varepsilon_{bite|die,u}$, $\varepsilon_{die,p}$ and $\varepsilon_{die,u}$) have been estimated for various mosquito-bednet pairings using experimental hut trial data conducted in various parts of sub-Saharan Africa. We assume, in this chapter, that $\varepsilon_{bite|\sim die,i} = \varepsilon_{bite,i}$, for $i = u, p$. In brief, such trials typically include a control net and several treated nets that may be of different classes (conventional ITN vs. LLIN), subject to different degrees of wear (e.g. washing and/or artificial holing), and conducted in areas with different levels of local *Anopheline pyrethroid* resistance (or employ lab strains).

Volunteers sleep under nets in these trials, and the total number of mosquitoes collected in each hut, the total bloodfed, and the total dead are typically reported. We identified 26 publications conducted in Africa that reported sufficient detail to calculate the above metrics (Asale et al., 2014; Asidi et al., 2004, 2005; Bayili et al., 2017; Camara et al., 2018; Chandre et al., 2000; Corbel et al., 2004, 2010; Djènontin et al., 2015; Djènontin and Cédric, 2018; Fanello et al., 1999; Ketoh et al., 2018; Koffi et al., 2015; Kweka et al., 2017; Malima et al., 2013, 2008; N'Guessan et al., 2001; Ngufor et al., 2011, 2014, 2016; N'Guessan et al., 2007, 2010; Oxborough et al., 2013; Pennetier et al., 2013; Randriamaherijaona et al., 2015; Tungu et al., 2010),

Every mosquito-hut pairing reported in these trials gives a value for $\varepsilon_{die,p}$, $\varepsilon_{bite,p}$, and ε_{deter}. Moreover, each pairing represents some "effective" level of insecticide resistance (i.e. an ineffective net and a sensitive mosquito and effective net but highly resistant mosquito may both represent pairings of high effective resistance). These pairings can be used to estimate how $\varepsilon_{die,p}$ and $\varepsilon_{bite,p}$ systematically co-vary as effective resistance changes, and a functional relationship between $\varepsilon_{die,p}$ (the probability of death following encounter with a protected host) and $\varepsilon_{bite,p}$ (the probability of taking a bloodmeal from a protected host) can been estimated, as depicted in Figure 3.3. We choose the exponential relation,

$$\varepsilon_{bite,p} = a_0 \exp\left(-b_0 \, \varepsilon_{die,p}\right),$$

where the best-fit values of the constants a_0 and b_0 are found, using weighted nonlinear least squares (weighting by number of mosquitoes collected in each trial), to be $a_0 = 0.55$ and $b_0 = 2$. The value of this relationship is that it allows effective bednet resistance to be described by a single parameter, $\varepsilon_{die,p}$, with $\varepsilon_{bite,p}$ determined as a function of $\varepsilon_{die,p}$.

Following Randriamaherijaona et al. (Randriamaherijaona et al., 2015), we es-

timate the probability that a mosquito takes a bloodmeal from a person sleeping without a net or under an extremely holed untreated net is on the order of 70-80%, while the probability of death is $\leq 5\%$. Hence, we take $\varepsilon_{bite,u} = 0.7$ and $\varepsilon_{die,u} = 0.05$ as baseline parameters for encounters with unprotected hosts. The parameter ε_{deter} is assumed to vary between 0.01 to 0.4.

For simulation purposes, the following three effectiveness levels of the LLINs are considered (given in Table 3.4), as also highlighted in Figure 3.3:

(i) Weakly-effective net: this is a net that has low killing efficacy and high biting probability. For this setting, we choose $\varepsilon_{die,p} = 0.25, \varepsilon_{bite,p} = 0.33$. Here, the adult mosquitoes are highly resistant to the net.

(ii) Moderately-effective net: this is a net with moderate killing efficacy and moderate biting probability. Here, we set $\varepsilon_{die,p} = 0.5, \varepsilon_{bite,p} = 0.2$, and the adult mosquitoes are moderately resistant to the net.

(iii) Highly-effective net: this is a net with very high killing efficacy and very low biting probability. Here, we set $\varepsilon_{die,p} = 0.9, \varepsilon_{bite,p} = 0.1$. This corresponds to the case where the adult mosquitoes are weakly resistant to the net.

3.4.3 Equations for the Dynamics of Human Population

The equations for the dynamics of the human population are given by (Iboi et al., 2019b)

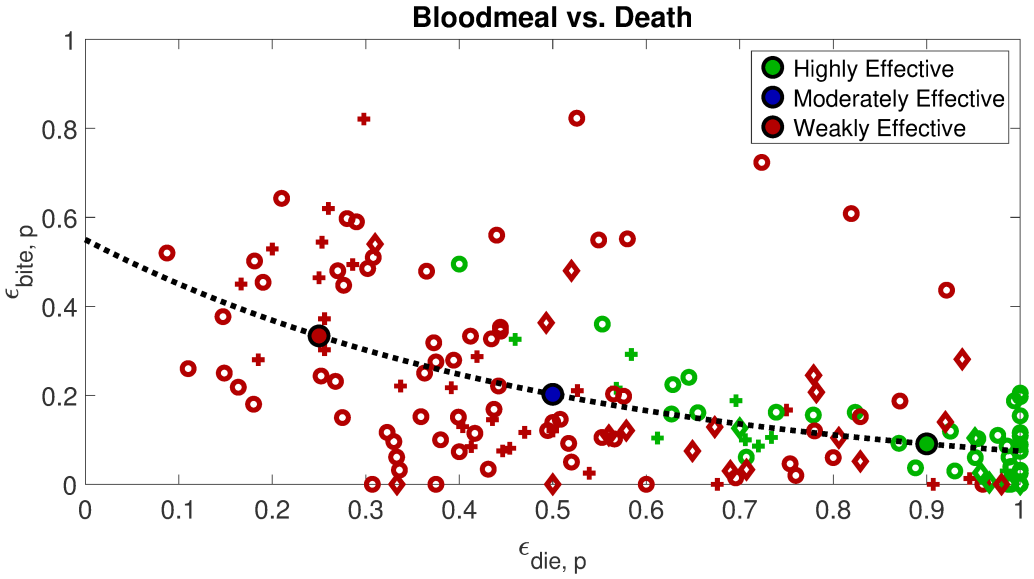

Figure 3.3: Data-Points Showing Probability of Death ($\varepsilon_{die,p}$) and Blood Feeding ($\varepsilon_{bite,p}$) for Various Mosquito-net Pairings Drawn from Experimental Hut Trial Data. Each Point is Coded According to Net Type by Symbol Shape, and According to Mosquito Resistance Class (Either Pyrethroid Resistant or Sensitive). Additionally, Representative Points on the Exponential Curve Fit Relating $\varepsilon_{bite,p}$ to $\varepsilon_{die,p}$ are Marked, Signifying Parameters for a Highly Effective ($\varepsilon_{die,p} = 0.9$, $\varepsilon_{bite,p} = 0.1$), Moderately Effective ($\varepsilon_{die,p} = 0.5$, $\varepsilon_{bite,p} = 0.2$), and Weakly Effective ($\varepsilon_{die,p} = 0.25$, $\varepsilon_{bite,p} = 0.33$) Bednet. Data for the Curves is Drawn from the References (Asale et al., 2014; Asidi et al., 2004, 2005; Bayili et al., 2017; Camara et al., 2018; Chandre et al., 2000; Corbel et al., 2004, 2010; Djènontin et al., 2015; Djènontin and Cédric, 2018; Fanello et al., 1999; Ketoh et al., 2018; Koffi et al., 2015; Kweka et al., 2017; Malima et al., 2013, 2008; N'Guessan et al., 2001; Ngufor et al., 2011, 2014, 2016; N'Guessan et al., 2007, 2010; Oxborough et al., 2013; Pennetier et al., 2013; Randriamaherijaona et al., 2015; Tungu et al., 2010), as Described Further in the Text.

$$
\begin{aligned}
\dot{S}_{H_p} &= \Pi\,\pi_p + \eta_H R_{H_p} - (\lambda_{VH_p} + \mu_H) S_{H_p}, \\
\dot{E}_{H_p} &= \lambda_{VH_p} S_{H_p} - (\gamma_H + \mu_H) E_{H_p}, \\
\dot{I}_{H_p} &= \gamma_H E_{H_p} - (\alpha_H + \mu_H + \delta_H) I_{H_p}, \\
\dot{R}_{H_p} &= \alpha_H I_{H_p} - (\eta_H + \mu_H) R_{H_p}, \\
\dot{S}_{H_u} &= \Pi\,\pi_u + \eta_H R_{H_u} - (\lambda_{VH_u} + \mu_H) S_{H_u}, \\
\dot{E}_{H_u} &= \lambda_{VH_u} S_{H_u} - (\gamma_H + \mu_H) E_{H_u}, \\
\dot{I}_{H_u} &= \gamma_H E_{H_u} - (\alpha_H + \mu_H + \delta_H) I_{H_u}, \\
\dot{R}_{H_u} &= \alpha_H I_{H_u} - (\eta_H + \mu_H) R_{H_u},
\end{aligned}
\tag{3.4.4}
$$

where, $\lambda_{VH_p}(t) = \beta_M\,\mathrm{EIR}_p(t)$ and $\lambda_{VH_u}(t) = \beta_M\,\mathrm{EIR}_u(t)$.

In (3.4.4), Π represents the recruitment rate of individuals (by birth or immigration) into the population (with π_p and π_u as defined in Section 2). The parameter η_H represents the loss of immunity by individuals who recovered from malaria. Susceptible protected humans acquire malaria infection from infectious mosquitoes at a rate $\lambda_{VHp}\,(\lambda_{VHu})$, with β_M being the probability of infection *per* bite and EIR_p (EIR_u) as defined in Section 2. Natural mortality occurs in all human compartments at a rate μ_H. Infected individuals develop clinical symptoms of malaria at a rate γ_H, and recover at a rate α_H. Finally malaria-induced death occurs in the infectious human population at a rate δ_H.

The model {(3.4.1), (3.4.2), (3.4.4)} is a modification of the model in Okuneye et al. (2019) by:

(i) explicitly including the dynamics of the adult mosquitoes under the influence of bednet usage (in Stages I and II of the gonotrophic cycle);

(ii) stratifying the human population in terms of bednets usage (only one class for

susceptible, exposed, infectious and recovered humans was used in Okuneye et al. (2019)).

The 23-dimensional nonlinear continuous-time model {(3.4.1), (3.4.2), (3.4.4)} is also an extension of the 3-dimenisonal, linear, difference equation model developed by Chitnis et al. (2008) by:

(i) explicitly including the dynamics of the immature mosquitoes (i.e., adding equations for the dynamics of eggs, the four larval instars and the pupal stages of the aquatic cycle; this was not included in Chitnis et al. (2008)) ;

(ii) explicitly incorporating the deterrence property of the bednet (this was not explicitly included in Chitnis et al. (2008));

(iii) explicitly including the dynamics of the adult mosquitoes under the influence of bednet usage (in Stages I and II of the gonotrophic cycle);

(iv) including the dynamics of humans *vis a vis* malaria transmission, and stratifying the human population in terms of bednets usage (the dynamics of humans is not explicitly incorporated in the model in Chitnis et al. (2008), making the model linear);

(v) explicitly incorporating the effect of temperature variability on the population ecology of immature and adult mosquitoes (this was not considered in Chitnis et al. (2008)).

Furthermore, unlike in the case of the model in Chitnis et al. (2008), the model {(3.4.1), (3.4.2), (3.4.4)} is simulated subject to three effectiveness levels (low, moderate and high) of the bednets used in the community. This allows for the assessment of various levels of insecticide resistance in the community (these bednets effectiveness levels are not considered in Chitnis et al. (2008)).

The state variables and parameters of the model {(3.4.1), (3.4.2), (3.4.4)} are described in Tables 3.1-3.3. Baseline values and ranges of the parameters of the model are tabulated in Table 3.5 (more detailed descriptions may be found in Okuneye et al. (2019)). All bednet-related parameters vary with net effectiveness, as described above, with the sole exception of ε_{deter}, which we fix at 0.1 for all simulation results, unless otherwise stated.

Table 3.1: Description of State Variables of the Model {(3.4.1), (3.4.2), (3.4.4)}.

Variables	**Interpretation**
E	Number of eggs
$L_j\,(j=1,2,3,4)$	Number of larvae at instar Stage j
P	Number of pupae
S_X, E_X, I_X	Number of susceptible, exposed, and infectious female mosquitoes in gonotrophic Stage I, respectively
S_Y, E_Y, I_Y	Number of susceptible, exposed, and infectious female mosquitoes in gonotrophic Stage II, respectively
S_Z, E_Z, I_Z	Number of susceptible, exposed, and infectious, female mosquitoes in gonotrophic Stage III, respectively
$S_{H_p}(S_{H_u})$	Number of protected (unprotected) susceptible humans
$E_{H_p}(E_{H_u})$	Number of protected (unprotected) exposed (infected but not yet infectious) humans
$I_{H_p}(I_{H_u})$	Number of protected (unprotected) infectious (symptomatic) humans
$R_{H_p}(R_{H_u})$	Number of protected (unprotected) recovered humans

3.4.4 Temperature-Dependent Parameters

Both vector and parasite are ectothermal (dependent on ambient temperature). Thus, their life histories are significantly affected by temperature. For instance, adult and immature aquatic mosquito survival is maximized for temperature values in the mid-20s (°C), with survival tailing off rather symetrically at higher and lower temperatures

Table 3.2: Description of Bednet-Independent Parameters of the Model {(3.4.1), (3.4.2), (3.4.4)}.

Parameters	**Interpretation**
μ_M	Mortality rate for the mosquito population
μ_X	Additional mortality rate for those mosquitoes deterred from entering the protected hut
δ_L	Density-dependent mortality rate of larvae
κ_V	Progression rate of exposed adult female mosquito to infectious stage
φ_Z	Oviposition rate for adult in Stage III of the gonotrophic cycle (Stage III to Stage I transition)
β_V	Transmission probability from infected human to a susceptible mosquito
β_M	Transmission probability from infected mosquito to a susceptible human
$\omega_p(\omega_u)$	Fraction of protected (unprotected) humans that are infectious
θ_Y	Progression rate for Stage II of the gonotrophic cycle
f	Proportion of adult mosquitoes that are females
ψ_E	Number of eggs per oviposition event (Stage III to Stage I transition)
K_E	Carrying capacity of eggs
σ_E	Maturation rate from egg to larvae
σ_L	Maturation rate from larvae to pupae
σ_P	Maturation rate from pupae to adult mosquitoes
μ_E	Mortality rate of eggs
μ_L	Mortality rate of larvae
μ_P	Mortality rate of pupae
Π	Recruitment rate of humans into the population
λ_{VH}	Infection rate of susceptible humans
γ_H	Progression rate of humans from exposed to infectious (symptomatic) class
δ_H	Malaria-induced mortality rate for humans
α_H	Recovery rate of infected humans
η_H	Rate of loss of infection-acquired immunity
μ_H	Natural mortality rate of humans

Table 3.3: Description of Bednet-Related Parameters of the Model {(3.4.1), (3.4.2), (3.4.4)}.

Parameters	**Interpretation**
π_p	Proportion of protected hosts
π_u	Proportion of unprotected hosts
ε_{deter}	Chance repelled before entering protected hut relative to unprotected
$\varepsilon_{bite\|\sim die,p}$	Probability of bloodmeal in protected houses
$\varepsilon_{bite\|\sim die,u}$	Probability of bloodmeal in unprotected houses
$\varepsilon_{bite\|die,p}$	Probability of bloodmeal, given death, in protected houses
$\varepsilon_{bite\|die,u}$	Probability of bloodmeal, given death, in unprotected houses
$\varepsilon_{die,p}$	Probability of death in protected houses
$\varepsilon_{die,u}$	Probability of death in unprotected houses

Table 3.4: Parameters for Bednet Effectiveness Levels.

Bednet effectiveness	$\varepsilon_{die,p}$	$\varepsilon_{bite,p}$
Weakly-effective net	0.25	0.33
Moderately-effective net	0.5	0.2
Highly-effective net	0.9	0.1

(Eikenberry and Gumel, 2018). Further, the development rates of *Plasmodium* parasites, immature *Anophelines* and mosquito eggs generally increase with increasing temperature to, at least, about 30°C (Eikenberry and Gumel, 2018; Paaijmans et al., 2010). Thermal response functions for temperature-dependent parameters are determined from experimental lab data as follows.

Death rate of adult female mosquitoes ($\mu_M(T_A)$). The mean survival times for adult *Anopheles gambiae* under laboratory conditions, and under constant ambient

Table 3.5: Ranges and Baseline Values of Temperature-Independent Parameters of the Model {(3.4.1), (3.4.2), (3.4.4)}. The Estimate for K_E is Defined in Terms of the Total Human Population at the Disease-Free Equilibrium ($\frac{\Pi}{\mu_H}$) to Ensure that the Mosquito: Host Ratio Falls within the Realistic Range of 0.1 to 10 Mosquitoes *per* Person *per* Day Typically Encountered in the Field (Macdonald, 1957).

Parameters	Range (per day)	Baseline Value (per day)	Reference
μ_M	0.0431—0.1000	0.0431	Adapted from Okuneye et al. (2019)
μ_X	0—0.1	0.05	Estimated
δ_L	0—0.0001	0.00002	Adapted from Okuneye et al. (2019)
κ_V	0.070—0.0973	0.0851	Adapted from Okuneye et al. (2019)
β_V	0.0200—0.2500 (dimensionless)	0.1500 (dimensionless)	(Charlwood et al., 1997; Lines et al., 1991)
β_M	0.0100—0.5000 (dimensionless)	0.5000 (dimensionless)	(Rickman et al., 1990; Smith et al., 2009)
θ_Y	0.4000—0.4964	0.2807	Adapted from Okuneye et al. (2019)
f	0.5000—0.8000 (dimensionless)	0.5000 (dimensionless)	Okuneye et al. (2019)
ψ_E	10—150 eggs per oviposition	65	Takken et al. (1998)
φ_Z	0.5000—4.000	2.000	Detinova et al. (1962)
K_E	1.0×10^4—1.0×10^6	$100\times\frac{\Pi}{\mu_H}$	Okuneye et al. (2019)
σ_E	0.3300—1.0000	0.4499	Dao et al. (2006)
$\sigma_{L_j}\,(j=1,2,3,4)$	0.3599—0.5399	0.4499	Adapted from Okuneye et al. (2019)
σ_P	0.3300—1.0000	0.4499	Bayoh and Lindsay (2003)
μ_E	0.0608—0.0912	0.0760	Adapted from Okuneye et al. (2019)
μ_L	0.0608—0.0912	0.0760	Adapted from Okuneye et al. (2019)
μ_P	0.0608—0.0912	0.0760	Adapted from Okuneye et al. (2019)
Π	4.000—5.5000 humans	4.5000	Okuneye et al. (2019)
γ_H	1/17—1/14	1/14	Okuneye et al. (2019)
δ_H	0.0001–0.0030	0.0021	(Alles et al., 1998; Dondorp et al., 2010; Reyburn et al., 2005)
α_H	1/1500—1/100	1/30	(Ashley and White, 2014; Jeffery and Eyles, 1954; Sama et al., 2004)
η_H	$1/(3\times365)-1/(7\times365)$	$1/(3\times365)$	Filipe et al. (2007)
μ_H	$1/(50\times365)-1/(70\times365)$	$1/(60\times365)$	Okuneye et al. (2019)

temperatures ranging from 5 to 40°C (5 °C intervals), are taken from (Bayoh, 2001).

$$\frac{1}{\mu_M(T_A)} = \max(0.01, a + bT_A + cT_A^2), \tag{3.4.5}$$

where a = -11.8239, b = 3.3292 and c = -0.0771.

Transition rate from Stage II to Stage III of gonotrophic cycle ($\theta_Y(T_A)$). We describe the rate at which mosquitoes complete Stage II of the gonotrophic cycle (that is, the transition from the Y to Z compartment(s)), using a Briere function

(Briere et al., 1999), such that

$$\theta_Y(T_A) = cT_A(T_A - T_A^0)(T_A^m - T_A)^{\frac{1}{2}}, \tag{3.4.6}$$

and parameter values are adopted from Mordecai et al. (Mordecai et al., 2013), with $c = 0.000203$, $T_A^m = 42.3^{\circ}$C and $T_A^0 = 11.7^{\circ}$C .

Sporogony ($\kappa(T_A)$). We follow Paaijmans et al. (Paaijmans et al., 2010) and use a Briere function for $\kappa(T_A)$, given by the right-hand side of (3.4.6) with parameters $c = 0.000112$, $T_A^m = 35^{\circ}$C , and $T_A^0 = 15.384^{\circ}$C .

Death rate of immature mosquitoes ($\mu_E(T_W)$, $\mu_L(T_W)$, $\mu_P(T_W)$). We assume that temperature-dependent death rates are equal for eggs, larvae, and pupae, and use laboratory larval survival times reported by Bayoh and Lindsay (Bayoh and Lindsay, 2004), to fit a *per-capita* death rate (inverse of survival time) with the fourth-order polynomial,

$$\mu_i(T_W) = 8.929\times10^{-6}T_W^4 - 0.0009271T_W^3 + 0.03536T_W^2 - 0.5814T_W + 3.509, i = E, L, P. \tag{3.4.7}$$

Development rate of immature mosquitoes ($\sigma_E(T_W)$, $\sigma_L(T_W)$, $\sigma_P(T_W)$). We adopt the relationship between water temperature and overall time from egg to adult, $l(T_W)$, given by Bayoh and Lindsay (Bayoh and Lindsay, 2003) (based on laboratory data),

$$l(T_W) = (a + bT_W + ce^{T_W} + de^{-T_W})^{-1}, \tag{3.4.8}$$

with $a = -0.05$, b = 0.005, c = -2.139×10^{-16} and $d = -281357.656$. We assume that the duration of all six immature stages (egg, four larval instars, and pupa) is equal, giving (Okuneye et al., 2019). We determined stage-specific development times as a function of temperature from Figure 1 of Bayoh and Lindsay (Bayoh and Lindsay, 2003), as shown in Figure 3.4. Development times are similar across all immature stages, with appreciable overlap in the temperature-dependent curves.

Therefore, we simply assume all stages have the same duration, and the uniform temperature-dependent development rates are given as

$$\sigma_E(T_W) = \sigma_P(T_W) = \sigma_L(T_W) = 6\frac{1}{l(T_W)}. \tag{3.4.9}$$

We have assumed, for this study, that near the surface of the water, air and water temperature are approximately equal ((Agusto et al., 2015; Iboi and Gumel, 2018)), giving $T_A = T_W$ (unless otherwise stated, a default value of $T_A = T_W = 25$ °C will be used to compute each of the aforementioned temperature-dependent parameters of the model). Further, since (by using fixed temperature values) the aforementioned temperature-dependent parameters take constant values, the model {(3.4.1), (3.4.2), (3.4.4)} is *autonomous*. This assumption is made for mathematical tractability.

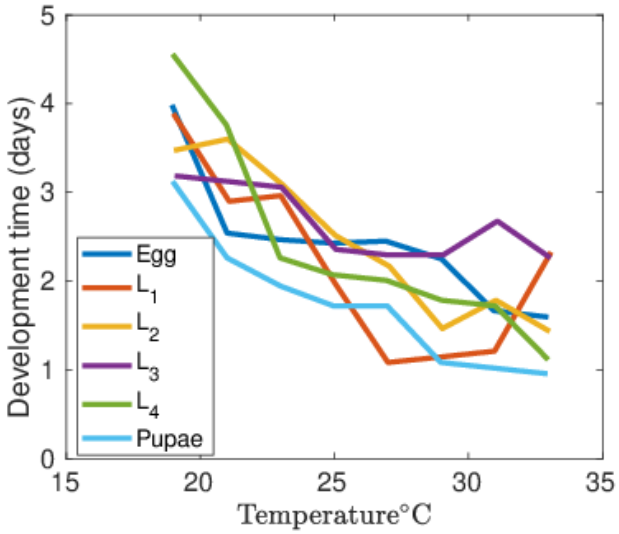

Figure 3.4: Development Times of the Dynamics of the Immature Mosquitoes. Adapted from Bayoh and Lindsay (2003).

3.4.5 Basic Qualitative Properties of the Model

The basic qualitative properties of the model {(3.4.1), (3.4.2), (3.4.4)} in the absence of density-dependent mortality rate in the larvae stage ($\delta_L = 0$) are explored in this section, with the positivity and boundedness of the solutions of the model established. Let,

$$A_X = S_X + E_X + I_X,$$

$$A_Y = S_Y + E_Y + I_Y,$$

$$A_Z = S_Z + E_Z + I_Z,$$

and,

$$N_M(t) = A_X(t) + A_Y(t) + A_Z(t).$$

Further, define

$$\big(E, L_1, L_2, L_3, L_4, P, S_X, E_X, I_X, S_Y, E_Y, I_Y, S_Z, E_Z, I_Z, S_{H_p}, E_{H_p}, I_{H_p}, R_{H_u}, S_{H_u}, E_{H_u}, I_{H_u}, R_{H_u}\big).$$

It is convenient to group the variables of the model {(3.4.1), (3.4.2), (3.4.4)} as follows:

$$\begin{aligned} \mathcal{B}_1 &= (E, L_1, L_2, L_3, L_4, P), \\ \mathcal{B}_2 &= (S_X, E_X, I_X, S_Y, E_Y, I_Y, S_Z, E_Z, I_Z), \\ \mathcal{B}_3 &= \big(S_{H_p}, E_{H_p}, I_{H_p}, R_{H_u}, S_{H_u}, E_{H_u}, I_{H_u}, R_{H_u}\big). \end{aligned} \tag{3.4.10}$$

Consider the feasible region $\Omega = \Omega_1 \times \Omega_2 \times \Omega_3$ for the model {(3.4.1), (3.4.2), (3.4.4)}, where:

$$\begin{aligned} \Omega_1 &= \left\{\mathcal{B}_1 \in \mathbb{R}^6_+ : E(t) \leq K_E, L_1(t) \leq L_1^\diamond, L_2(t) \leq L_2^\diamond, L_3(t) \leq L_3^\diamond, L_4(t) \leq L_4^\diamond, P(t) \leq P^\diamond\right\}, \\ \Omega_2 &= \left\{\mathcal{B}_2 \in \mathbb{R}^9_+ : N_M(t) \leq \frac{f\sigma_P P^\diamond}{\mu_M}\right\}, \ \Omega_3 = \left\{\mathcal{B}_3 \in \mathbb{R}^8_+ : N_H(t) \leq \frac{\Pi}{\mu_H}\right\}, \end{aligned} \tag{3.4.11}$$

with, $L_1^\diamond = \frac{\sigma_E K_E}{\sigma_{L_1}+\mu_L}$, $L_2^\diamond = \frac{\sigma_{L_1} L_1^\diamond}{\sigma_{L_2}+\mu_L}$, $L_3^\diamond = \frac{\sigma_{L_2} L_2^\diamond}{\sigma_{L_3}+\mu_L}$, $L_4^\diamond = \frac{\sigma_{L_3} L_3^\diamond}{\sigma_{L_4}+\mu_L}$ and $P^\diamond = \frac{\sigma_{L_4} L_4^\diamond}{\sigma_P+\mu_P}$.
We claim the following result.

Lemma 3.4.1. *Consider the model* {(3.4.1), (3.4.2), (3.4.4)}.

(a) Each component of the solution of the model, with non-negative initial conditions, remains positive and bounded for all time $t > 0$.

(b) The set Ω *is positively-invariant and attracting region for the model.*

The proof of Lemma 3.4.1 is given in Appendix C.

3.5 Mathematical Analysis

In this section, the model {(3.4.1), (3.4.2), (3.4.4)} is rigorously analysed to show the existence and asymptotic stability of its disease-free equilibrium, and to characterize the bifurcation structure of the model. We define the threshold quantity, $\mathcal{N}_0$, as

$$\mathcal{N}_0 = \frac{\psi_E \varphi_Z \sigma_E f \sigma_P \theta_Y C_2 \prod_{i=1}^{4} \sigma_{L_i}}{(C_1 K_9 K_{11} - C_2 \theta_Y \varphi_Z) \prod_{i=1}^{6} K_i}, \tag{3.5.1}$$

where $C_1 = K_7 - b_H(Q_2 + Q_3)$, $C_2 = b_H(R_1 + R_2)$, $K_1 = \sigma_E + \mu_E$, $K_j = \sigma_{L_{j-1}} + \mu_L \, (j = 2, ..., 5)$, $K_6 = \sigma_P + \mu_P$, $K_7 = b_H Q_1 + \mu_X + \mu_M$, $K_9 = \theta_Y + \mu_M$ and $K_{11} = \varphi_Z + \mu_M$. Furthermore (noting the definitions of C_9, C_{10} and C_{11} given in Appendix D), $C_1 K_9 K_{11} - C_2 \theta_Y \varphi_Z = \mu_M^3 + \mu_M^2 C_9 + \mu_M C_{10} + C_{11} > 0$. Hence, $\mathcal{N}_0 > 0$.

The quantity $\mathcal{N}_0$, which is the *extinction threshold* for the mosquito population of the model, measures the average number of new adult female mosquitoes produced by one reproductive mosquito during its entire reproductive period (Eikenberry and Gumel, 2018; Okuneye et al., 2019).

3.5.1 Existence of the Disease-Free Equilibria

The model {(3.4.1), (3.4.2), (3.4.4)} has the following disease-free equilibrium (DFE):

(i) A trivial disease-free equilibrium (*TDFE*), given by:

$$\begin{aligned}\mathcal{T}_1 &= \left(0,0,0,0,0,0,0,0,0,0,0,0,0,0,0,0,S^*_{H_p},0,0,0,S^*_{H_u},0,0,0\right),\\ &= \left(0,0,0,0,0,0,0,0,0,0,0,0,0,0,0,0,\frac{\Pi\,\pi_p}{\mu_H},0,0,0,\frac{\Pi\,\pi_u}{\mu_H},0,0,0\right).\end{aligned}$$

The *TDFE* is ecologically unrealistic (since it is associated with the total absence of mosquitoes in the community). Hence, it is not analysed.

(ii) A unique non-trivial disease-free equilibrium (*NDFE*), given by:

$$\mathcal{T}_2 = \left(E^*, L^*_1, L^*_2, L^*_3, L^*_4, P^*, S^*_X, 0, 0, S^*_Y, 0, 0, S^*_Z, 0, 0, \tfrac{\Pi\,\pi_p}{\mu_H}, 0, 0, 0, \tfrac{\Pi\,\pi_u}{\mu_H}, 0, 0, 0\right),$$

where,

$$\begin{aligned}&E^* = K_E\left(1-\frac{1}{\mathcal{N}_0}\right),\ L^*_1 = \frac{\sigma_E E^*}{K_2},\ L^*_2 = \frac{\sigma_{L_1} L^*_1}{K_3},\ L^*_3 = \frac{\sigma_{L_2} L^*_2}{K_4},\\ &L^*_4 = \frac{\sigma_{L_3} L^*_3}{K_5},\ P^* = \frac{\sigma_{L_4} L^*_4}{K_6},\ S^*_X = \frac{\left[f\sigma_E\sigma_P K_E\left(1-\frac{1}{\mathcal{N}_0}\right)K_9K_{11}\right]\prod_{i=1}^{4}\sigma_{L_i}}{(C_1K_9K_{11}-C_2\theta_Y\varphi_Z)\prod_{i=2}^{6}K_i},\\ &S^*_Y = \frac{C_2S^*_X}{K_9},\ S^*_Z = \frac{\theta_Y S^*_Y}{K_{11}}.\end{aligned} \tag{3.5.2}$$

It is clear from Equation (3.5.2) that the *NDFE* ($\mathcal{T}_2$) exists if and only if $\mathcal{N}_0 > 1$ (it is assumed from here on that $\mathcal{N}_0 > 1$, so that the non-trivial disease-free equilibrium, $\mathcal{T}_2$, exists). It is worth noting that the *NDFE* is the non-extinction equilibrium for the mosquito population coupled with the trivial disease-free equilibrium ($\mathcal{T}_1$) for the human population. Hence, in the absence of the vectors and the disease, the two subsystems ($\mathcal{T}_1$ and $\mathcal{T}_2$) are uncoupled.

3.5.2 Asymptotic Stability of the NDFE

Consider the model {(3.4.1), (3.4.2), (3.4.4)}. It can be shown, using the next generation operator method (van den Driessche and Watmough, 2002), that the associated

reproduction number $\mathcal{R}_0$ of the model is given by:

$$\mathcal{R}_0 = \sqrt{(\mathcal{R}_{H_pV} + \mathcal{R}_{H_uV}) \times \mathcal{R}_{VH}}, \tag{3.5.3}$$

where,

$$\mathcal{R}_{H_pV} = \frac{\gamma_H \beta_V N^*_{Hu} Q_p R_1}{K_{13} K_{14}},\ \mathcal{R}_{H_uV} = \frac{\gamma_H \beta_V N^*_{Hp} Q_u R_2}{K_{13} K_{14}}, \tag{3.5.4}$$

and,

$$\mathcal{R}_{VH} = \frac{b_H \beta_M S^*_X}{N^*_{Hp} N^*_{Hu}} \frac{\kappa_V \varphi_Z \theta_Y [(K_9 + K_{12}) C_3 + K_9 K_{11}]}{(C_3 K_{10} K_{12} - C_2 \theta_Y \varphi_Z)(C_1 K_9 K_{11} - C_2 \theta_Y \varphi_Z)}, \tag{3.5.5}$$

with,

$$\begin{aligned} Q_p &= b_H \pi_p (1 - \varepsilon_{deter}) \left[\varepsilon_{bite|die,p}\, \epsilon_{die,p} + \varepsilon_{bite|\sim die,p} (1 - \varepsilon_{die,p}) \right], \\ Q_u &= b_H \pi_u \left[\varepsilon_{bite|die,u}\, \varepsilon_{die,u} + \varepsilon_{bite|\sim die,u} (1 - \varepsilon_{die,u}) \right], \end{aligned}$$

$N^*_{Hp} = \frac{\Pi \pi_p}{\mu_H}$, $N^*_{Hu} = \frac{\Pi \pi_u}{\mu_H}$, $C_3 = K_8 - b_H(Q_2 + Q_3)$, $K_8 = b_H Q_1 + \kappa_V + \mu_X + \mu_M$, $K_{10} = \theta_Y + \kappa_V + \mu_M$, $K_{12} = \varphi_Z + \kappa_V + \mu_M$, $K_{13} = \gamma_H + \mu_H$ and $K_{14} = \alpha_H + \delta_H + \mu_H$.

It can be shown that $C_3 K_{10} K_{12} - C_2 \theta_Y \varphi_Z = b_H [C_4 \kappa_V^2 + 2\kappa_V \left(\mu_M + \frac{\theta_Y}{2} + \frac{\varphi_Z}{2}\right) C_5 + C_6 + C_7] + C_8 > 0$ (where the coefficients $C_i\,(i = 2, ..., 8)$ are constants, and are given in Appendix D). Hence, $\mathcal{R}_{VH} > 0$ (and thus $\mathcal{R}_0$ is also automatically positive).

Theorem 3.5.1. *Let $\mathcal{N}_0 > 1$. The NDFE, $\mathcal{T}_2$, of the model* {(3.4.1), (3.4.2), (3.4.4)} *is locally-asymptotically stable (LAS) in $\Omega \setminus \mathcal{T}_1$ if $\mathcal{R}_0 < 1$, and unstable if $\mathcal{R}_0 > 1$.*

The epidemiological implication of Theorem 3.5.1 is that malaria can be effectively controlled (or eliminated) from the population if the initial sizes of the subpopulations of the model {(3.4.1), (3.4.2), (3.4.4)} are in the basin of attraction of the non-trivial disease-free equilibrium ($\mathcal{T}_2$). In other words, in this case, a small influx of malaria-infected individuals into the community will not generate large outbreaks.

It is notable that the value of the reproduction number ($\mathcal{R}_0$) for the worst-case scenario (i.e., bednet coverage is zero), denoted by $\tilde{\mathcal{R}}_{0*}$ and computed using the baseline parameter values in Table 3.3, is $\tilde{\mathcal{R}}_{0*} \simeq 11.4$ (see Appendix E for the formulation of the special case of the model {(3.4.1), (3.4.2),(3.4.4)} with no bednet coverage). This high value of the reproduction number is typically seen in holo-endemic malaria regions (Gething et al., 2010). It should be mentioned that, for the computation of the value of the reproduction number for this (holo-endemic) setting, we assumed (in Table 3.3) that there are, on average, 100 eggs per human (which translates to about 10 adult mosquitoes per human). When we reduce the number of eggs per human to 10 per human, so that we have one mosquito per human (which is more typically the case in meso-endemic regions (Gething et al., 2010)), the value of $\mathcal{R}_0$ reduces to $\tilde{\mathcal{R}}_{0*} \simeq 4.2$. Hence, these computations (together with Theorem 3.5.1) show that, for the worst-case scenario (with no bednets used in the community), the disease will persist in both the holoendemic and the mesoendemic regions (since $\tilde{\mathcal{R}}_{0*} > 1$ in both cases), as expected.

3.5.3 Existence of Backward Bifurcation

The phenomenon of backward bifurcation has been observed in numerous models (such as those in Blayneh et al. (2010); Feng et al. (2015); Garba and Gumel (2010); Garba et al. (2008); Iboi et al. (2018); Iboi and Gumel (2018)) for spread of malaria and other vector-borne diseases that incorporated disease-induced death in the host population. A backward bifurcation is characterized by the co-existence of two asymptotically-stable equilibria when $\mathcal{R}_0 < 1$: an endemic equilibrium point (EEP) and a disease-free equilibrium point (DFE). Thus, the classical epidemiological requirement that $\mathcal{R}_0$ be less than one for elimination of the disease, while necessary, is no longer sufficient to eliminate malaria when it already exists in the population.

That is, while $\mathcal{R}_0 \geq 1$ remains a condition for malaria to spread within a previously unexposed population, pushing $\mathcal{R}_0 < 1$ via control measures does not necessarily guarantee elimination of the disease.

Theorem 3.5.2. *The model* {(3.4.1), (3.4.2), (3.4.4)} *undergoes a backward bifurcation at* $\mathcal{R}_0 = 1$ *whenever a bifurcation coefficient, denoted by a (given in Appendix F), is positive.*

Proof. The proof of Theorem 3.5.2, based on using Center Manifold theory (Carr, 1981; Castillo-Chavez and Song, 2004), is given in Appendix F. The result given by Theorem 3.5.2 is numerically illustrated by simulating the model {(3.4.1), (3.4.2), (3.4.4)} using parameter values such that the backward bifurcation condition, given in Appendix F, is satisfied (Figure 3.5). □

The range for backward bifurcation for a **weakly-effective net** (i.e., a net with $\varepsilon_{die,p} = 0.25$, $\varepsilon_{bite,p} = 0.33$) is $\beta_M \in (0.526394, \infty)$, a **moderately-effective net** (i.e., a net with $\varepsilon_{die,p} = 0.5$, $\varepsilon_{bite,p} = 0.2$) is $\beta_M \in (0.503682, \infty)$ and that for a **highly-effective net** (i.e., a net with $\varepsilon_{die,p} = 0.9$, $\varepsilon_{bite,p} = 0.1$) is $\beta_M \in (1.4009823, \infty)$, where β_M is the chosen backward bifurcation parameter (see Appendix F). Hence, this study shows that the phenomenon of backward bifurcation is more likely to occur using a moderately-effective net than when either a weak or highly-effective net is used.

Theorem 3.5.2 shows that elimination is dependent on the initial sizes of the infected vector and human populations. For elimination to be independent of the size of the infected populations, a global asymptotic stability property must be explored for the non-trivial disease-free equilibrium ($\mathcal{T}_2$). We claim the following.

Theorem 3.5.3. *The NDFE,* $\mathcal{T}_2$*, of the model* {(3.4.1), (3.4.2), (3.4.4)}*, with* $\delta_H = 0$ *and* $\mathcal{N}_0 > 1$*, is globally-asymptotically stable (GAS) in* $\Omega \setminus \mathcal{T}_1$ *if* $\tilde{\mathcal{R}}_0 = \mathcal{R}_0|_{\delta_H=0} < 1$.

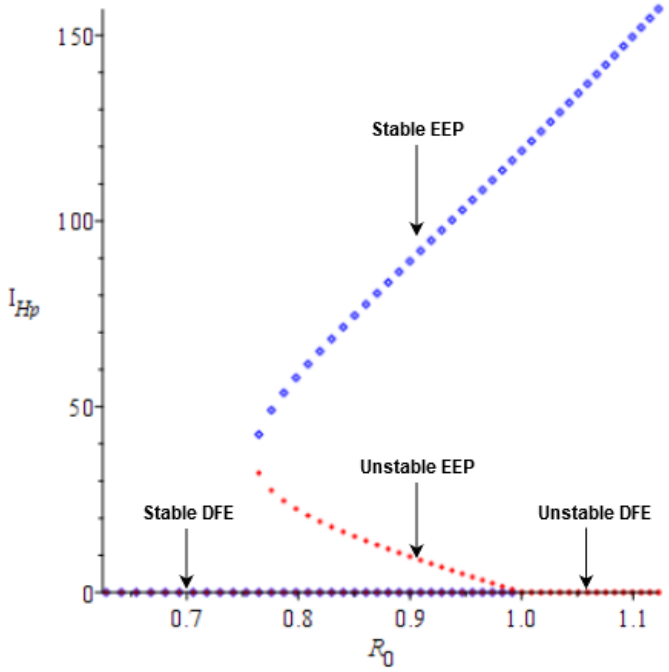

Figure 3.5: Backward Bifurcation Diagram of the Model {(3.4.1), (3.4.2), (3.4.4)}, Showing a Plot of $I_{Hp}(t)$ as a Function of the Reproduction Number $\mathcal{R}_0$, Where β_M is the Chosen Bifurcation Parameter. Parameter Values Used are as Given in Table 3.5 with: $\pi_p = 0.5, \pi_u = 0.5, \varepsilon_{deter} = 0.75, \varepsilon_{bite|\sim die,p} = 0.1, \varepsilon_{bite|\sim die,u} = 0.7, \varepsilon_{bite|die,p} = 0.1, \varepsilon_{bite|die,u} = 0.7, \varepsilon_{die,p} = 0.9, \varepsilon_{die,u} = 0.05, b_H = 2, \mu_X = 0.005, \psi_E = 5, \delta_H = 0.0005, \eta_H = 1/14, \beta_V = 0.5, \Pi = 1$ and $K_E = \frac{\Pi}{\mu_H}$ (so that the Bifurcation Coefficient, a (Defined in Appendix F), is Given by a=5.42 $\times 10^{-6} > 0$ and $\mathcal{R}_0 = 1$). It Should be Mentioned that in order to Generate this Figure, the Values of Five Parameters ($\alpha_H, \eta_H, \delta_H, \beta_V$ and Π) have to be Chosen Outside their Biologically-Feasible Ranges Given in Table 5.

The proof of Theorem 3.5.3, based on using Lyapunov function theory and LaSalle's Invariance Principle, is given in Appendix G. The epidemiological implication of Theorem 3.5.3 is that, for the special case of the model {(3.4.1), (3.4.2), (3.4.4)} with no disease-induced mortality in the host population (i.e., $\delta_H = 0$), bringing and maintaining the associated reproduction threshold ($\tilde{\mathcal{R}}_0$) to a value less than one is necessary and sufficient for complete elimination of malaria in the community, regardless of initial conditions.

3.6 Numerical Simulations: Populations at Equilibrium

3.6.1 Interaction Between Bednet Coverage and Bednet Efficacy Parameters

To assess the population-level impact of bednets on malaria transmission dynamics in the community under equilibrium conditions (i.e., the model is numerically simulated until an endemic equilibrium is reached), the model {(3.4.1), (3.4.2), (3.4.4)} is simulated using various bednet coverage and effectiveness levels, where bednet effectiveness is jointly defined by $\varepsilon_{bite,p}$ and $\varepsilon_{die,p}$. Unless otherwise stated, all simulations use the baseline parameter values in Table 3.5, and temperature is fixed at 25°C (i.e., the values of all the temperature-dependent parameters of the model are obtained by evaluating each of the functional forms in Section 2 at the fixed temperature T=25°C).

Figure 3.6 illustrates the nonlinear relationships between bednet coverage fraction, π_p, disease prevalence in the two human populations (bednet-protected and unprotected), $\tilde{\mathcal{R}}_0$ (i.e., $\mathcal{R}_0$ for the case when the disease-induced mortality in the human population, δ_H, is set to zero), and EIR (again, in the bednet-protected and unprotected populations), at endemic equilibrium and for baseline parameters. Notably, this figure shows that EIR decreases with increasing bednet coverage (top right

panel). This result is consistent with that reported in the modeling study by chitnis et al. (Chitnis et al., 2008), which used data relevant to malaria transmission dynamics in Ifakara, Tanzania (i.e., data for *Anopheles gambiae* feeding on a heterogenous human population, with no cattle), to show that bednets are effective in reducing malaria transmission. Our result is also consistent with the results of the field trials on *permethrin*-treated bednets in western Kenya reported by Hawley et al. (Hawley et al., 2003).

Further, as evident from the graph in the lower left panel of Figure 3.6, human disease prevalence varies hyperbolically with EIR (i.e., prevalence increases with increasing EIR), such that, for a high baseline EIR, a large reduction in EIR is required before any meaningful malaria control is realized. A five-fold reduction in overall EIR, however, is achieved with roughly 20% bednet coverage (see upper right panel of Figure 3.6). Thus, although even a relatively low bednet coverage can aid somewhat in malaria control, the simulations in Figure 3.6 show that much higher bednet coverage (and a decrease in EIR of two orders of magnitude) is needed to achieve malaria elimination. Finally, there is a similar, although less marked, hyperbolic relationship between increasing $\tilde{\mathcal{R}}_0$ and increasing disease prevalence (bottom right panel).

We explore how changes in $\varepsilon_{bite,p}$ and $\varepsilon_{die,p}$ (i.e. net effectiveness) affect $\tilde{\mathcal{R}}_0$, starting from either a baseline $\tilde{\mathcal{R}}_0$ value of 13.7, presumably representing holoendemic malaria, or 4.3, which is more appropriate for mesoendemic malaria. In particular, we generate contour plots of $\tilde{\mathcal{R}}_0$ as a function of $\varepsilon_{bite,p}$ and $\varepsilon_{die,p}$, for either low (20%) or high (80%) bednet coverage levels (Figure 3.7). The inscribed curve on each contour plot of Figure 3.7 shows how $\varepsilon_{bite,p}$ and $\varepsilon_{die,p}$ co-vary, based upon the experimental hut data discussed in Section 3.4.2. In these plots, the highlighted points indicate highly, moderately, and weakly effective nets. It follows from Figure 3.7 that, for the mesoendemic baseline, even a moderately effective net is capable of pushing $\tilde{\mathcal{R}}_0$

to a value less than one when bednet coverage is high (80%). Further, for this (mesoendemic baseline scenario) even low bednet coverage (20%) may substantially improve malaria control.

In the holoendemic baseline, on the other hand, only a highly effective net with high coverage can have a chance to approach malaria elimination. Thus, these simulations show that our study only supports the claim in the malaria modeling study by (Chitnis et al., 2008) (based on data relevant to malaria dynamics in Ifakara, Tanzania) and the *permethrin*-treated bednets field trial in western Kenya by (Hawley et al., 2003) that bednets reduce malaria transmission if the malaria region being considered is mesoendemic. For holoendemic malaria regions, our study shows that only a highly-effective net, coupled with very high coverage, can lead to effective control of malaria. Ifakara and western Kenya are considered regions of high malaria endemicity (Githeko et al., 1992; Holzer et al., 1993).

Figure 3.7 also suggests that high coverage of weakly effective (i.e. low killing efficiency) nets is better than low coverage with highly effective (i.e. high killing efficiency) nets. For example, in the holoendemic setting, 20% coverage with a highly effective net pushed $\tilde{\mathcal{R}}_0$ from 11.7 to 5.5, while 80% coverage with a weakly effective net gives $\tilde{\mathcal{R}}_0$ of 3.6. Given the nonlinear relationship between $\tilde{\mathcal{R}}_0$ and disease prevalence, widespread use of even marginally effective bednets may better control malaria than lower coverage rates with better (more effective) nets. Finally, Figure 3.8 shows the nonlinear relationship between $\tilde{\mathcal{R}}_0$ and EIR, such that EIR must be pushed very close to zero before $\tilde{\mathcal{R}}_0$ drops below one. In other words, Figure 3.8 shows that a significant reduction in EIR is needed in order to bring the reproduction number $\tilde{\mathcal{R}}_0$ to a value less than 1 (so that, by Theorem 3.5.3, malaria elimination can be achieved).

We also examine how deterrence, as measured in the model by ε_{deter}, interacts

with bednet coverage and net effectiveness to determine $\tilde{\mathcal{R}}_0$, as shown in the contour plots in Figure 3.9. Perhaps surprisingly, increasing deterrence generally results in an *increase* in $\tilde{\mathcal{R}}_0$. This is likely because increasing ε_{deter} focuses mosquito biting upon the unprotected subpopulation, resulting in more intense malaria transmission among this subpopulation and an overall increase in $\tilde{\mathcal{R}}_0$.

It should be emphasized here that this increased biting on unprotected persons is not an assumption directly imposed on the model, but is a natural consequence of the fact that, if a mosquito does not attempt a bloodmeal on a net-protected human she has encountered, due to deterrence, she will continue in her search and likely ultimately encounter an unprotected person (although this comes at an increased mortality, denoted by μ_X in the model 3.4.2).

3.6.2 Effects of Temperature

We examine the effect of changing mean ambient temperature (assumed equal to water temperature) upon $\tilde{\mathcal{R}}_0$ and EIR, as shown in Figure 3.10. We see an asymmetric increase in $\tilde{\mathcal{R}}_0$ and EIR from low temperatures to peaks around 29–30°C, followed by rapid drop-offs at higher temperatures. In other words, malaria burden is maximized for temperature values in the range 29–30°C, and such burden decreases for increasing temperatures thereafter. This peak is similar to that reported by (Okuneye et al., 2019), but higher than the reported value by the well-known (Mordecai et al., 2013) study. Furthermore, although the results in Figure 3.10 are obtained using a highly effective net with $K_E = 100 \times \Pi/\mu_H$, it should be stated that qualitatively similar results are obtained regardless of net type and K_E value.

To determine if temperature alters the qualitative interaction between bednet efficacy, bednet coverage, and control, we have generated a series of contour plots showing $\tilde{\mathcal{R}}_0$ as a function of $\varepsilon_{die,p}$ and $\varepsilon_{bite,p}$, for different ambient temperatures;

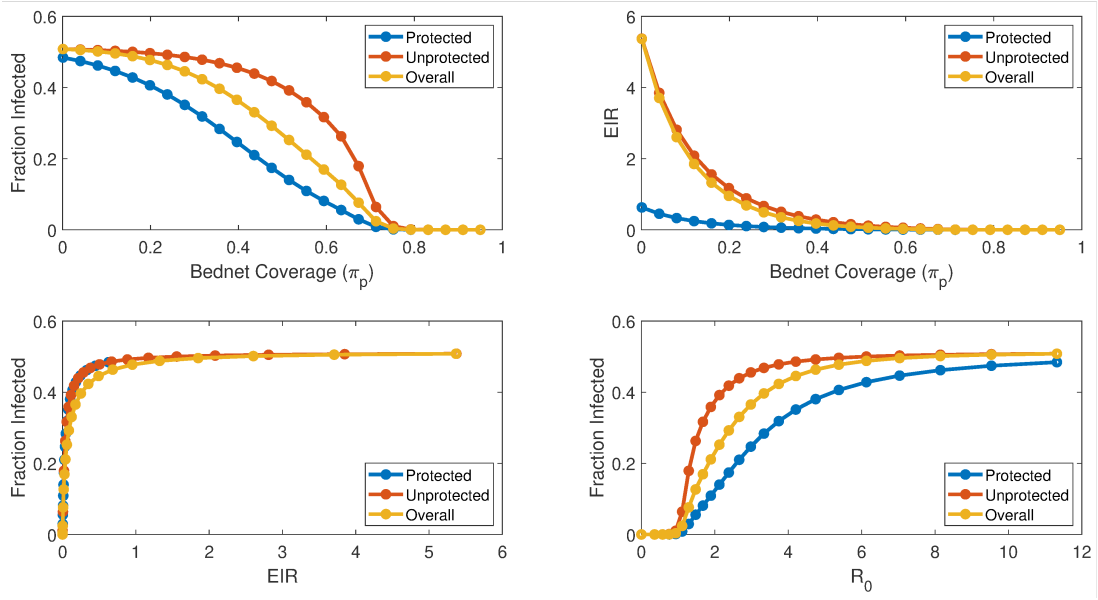

Figure 3.6: Relationships Among EIR, Fraction of Infected Humans, Bednet Coverage Level, and $\tilde{\mathcal{R}}_0$, at the Endemic Equilibrium, as Determined from Numerical Simulation of the Model {(3.4.1), (3.4.2), (3.4.4)}, and for Fixed Temperature (25°C). Results are Disaggregated Between the Protected, Unprotected, and Overall (Bednet-Protected and Unprotected human) Populations. Results are Determined Using Baseline Parameter Values with a Highly Effective Net in a Holoendemic Setting ($K_E = 100\frac{\Pi}{\mu_H}$, $\tilde{\mathcal{R}}_0 = 11.7$ with no Bednet Coverage).

several surfaces are given in Figure 3.11. While altering the maximum $\tilde{\mathcal{R}}_0$ value, changes in temperature have no meaningful effect upon the qualitative contour shape. That is, while maximum $\tilde{\mathcal{R}}_0$ varies between about 1.3 and 4.5 in the contours shown in Figure 3.11, the surface shapes are essentially invariant. Mirroring Figure 3.10, maximum $\tilde{\mathcal{R}}_0$ increases up to nearly 30°C and then falls off. Thus, it is concluded that bednet coverage and temperature independently affect malaria risk.

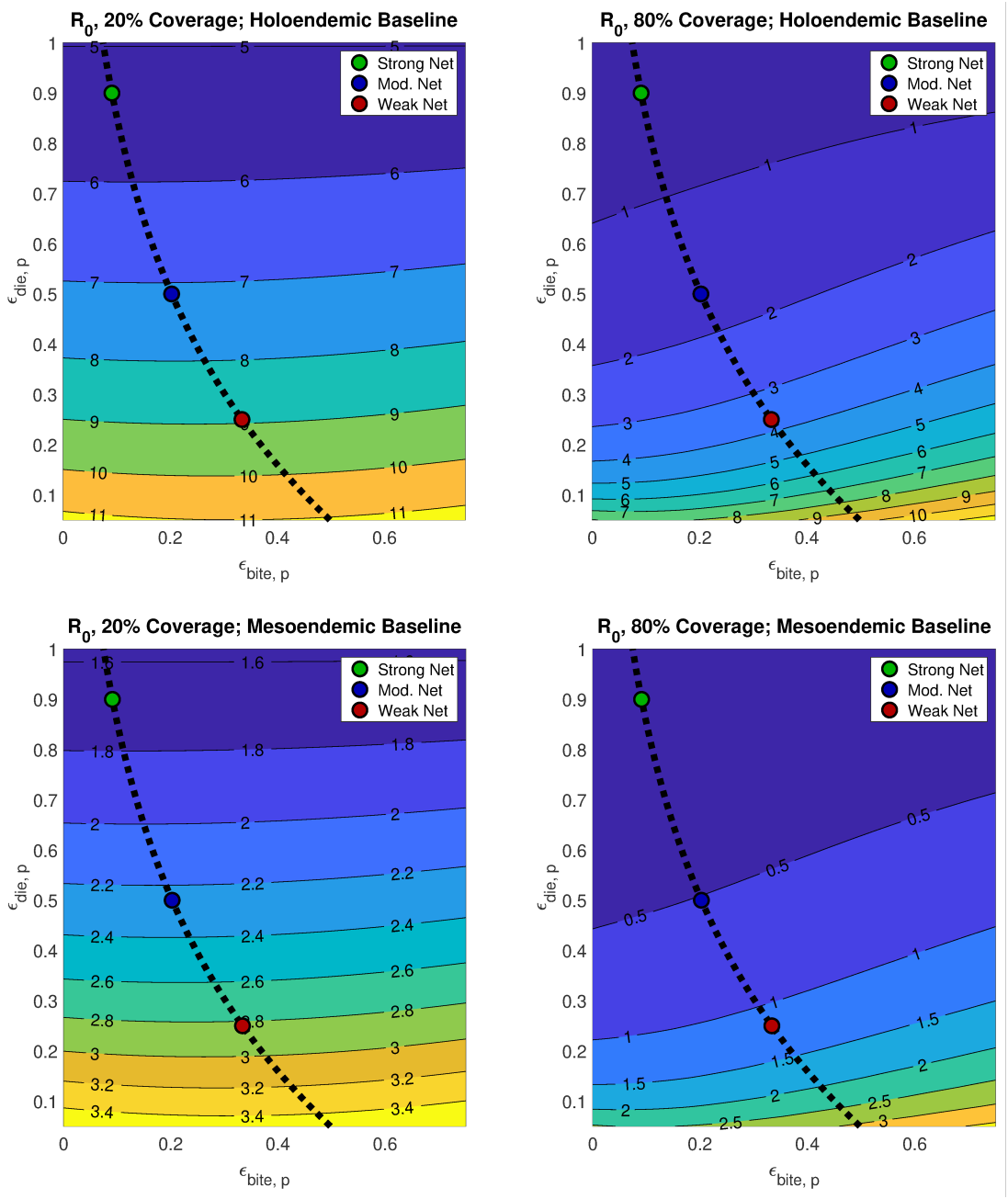

Figure 3.7: Contour Plots of the $\tilde{\mathcal{R}}_0$ of the Model $\{(3.4.1), (3.4.2), (3.4.4)\}$, as a Function of $\varepsilon_{die,p}$ and $\varepsilon_{bite,p}$ (the Respective Probabilities that a Mosquito Dies or takes a Blood Meal Upon Encountering a Protected Human), for Four Different Permutations of Bednet Coverage and Baseline $\tilde{\mathcal{R}}_0$. The Top Panels use $K_E = 100\frac{\Pi}{\mu_H}$ to Approximate a Holoendemic Baseline, while the Bottom Panels use $K_E = 10\frac{\Pi}{\mu_H}$ as an Approximation of a Mesoendemic Baseline. Bednet Coverage is Either 20% (left) or 80% (right).

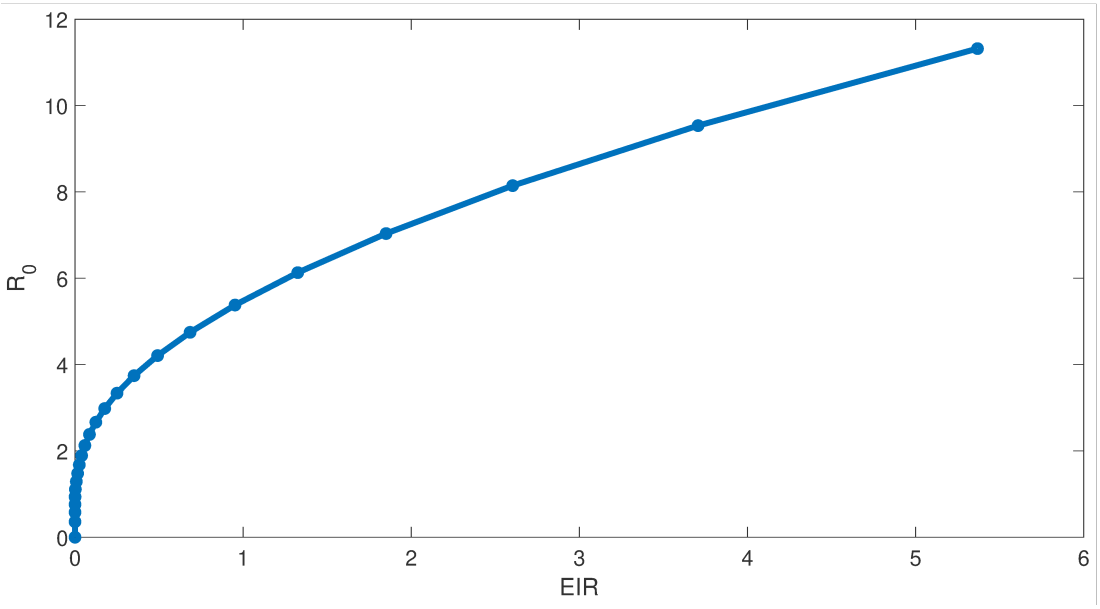

Figure 3.8: Numerically Determined Relationship Between Overall EIR and $\tilde{\mathcal{R}}_0$ at the Endemic Equilibrium, where Variability in EIR is Generated by Changing Bednet Coverage, π_p. For Larger EIR, $\tilde{\mathcal{R}}_0$ Decreases Nearly Linearly with Falling EIR, while for Very Small EIR, $\tilde{\mathcal{R}}_0$ decreases dramatically with Falling EIR. Thus, EIR Must be Pushed Very Close to Zero for Malaria Elimination. Results are Generating Using Baseline Parameter Values with a Highly Effective Net in a Holoendemic setting ($K_E = 100\frac{\Pi}{\mu_H}$).

3.7 Discussion and Conclusions

Great successes have been recorded in the concerted global effort against malaria between the year 2000 to 2015, thanks largely to the large-scale use of long-lasting insecticidal bednets (LLINs) and indoor residual spraying (IRS) in malaria-endemic regions within sub-Saharan Africa. There is now a strong global push to eradicate malaria (particularly the "Zero by 40" initiative of five chemical companies, with support of the Bill & Melinda Gates Foundation and the Innovative Vector Control Consortium (Gates, 2016; Willis and Hamon, 2018)). Given the widespread emergence of vector resistance to pyrethroid-based insecticides (the only chemical agent approved

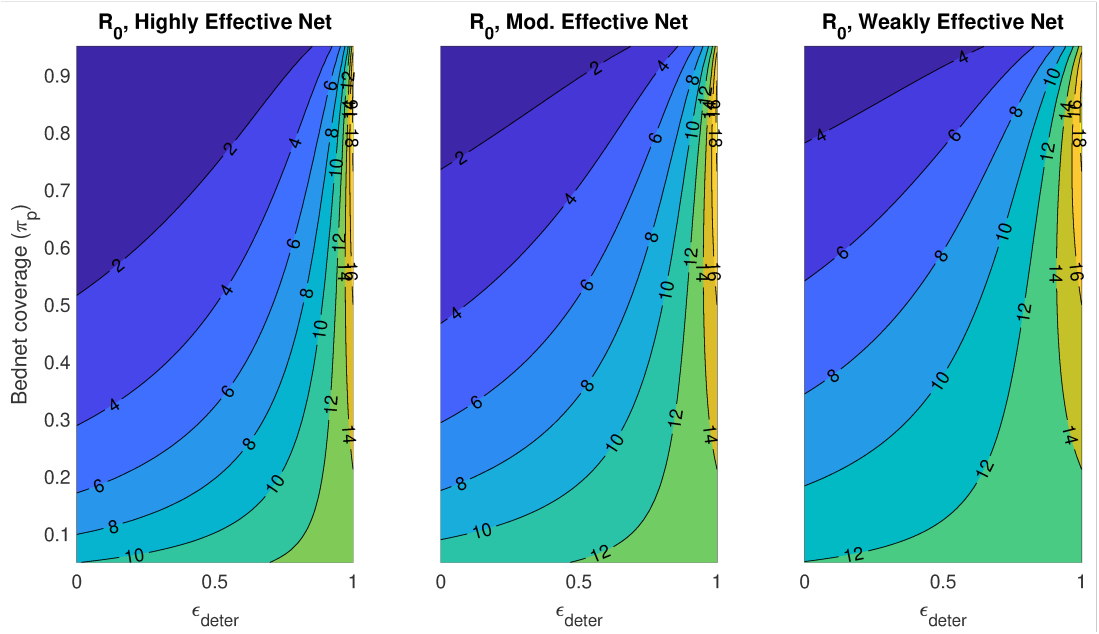

Figure 3.9: Contour Plots Showing $\tilde{\mathcal{R}}_0$ as a Function of ε_{deter} and π_p (Bednet Coverage), for Weakly, Moderately, and Highly Effective Nets. For this Figure, We use $K_E = 100\frac{\Pi}{\mu_H}$ to Approximate a Holoendemic Baseline.

for use in LLINs), and the uncertainty surrounding how this affects (and will affect) malaria epidemiology, mathematical modeling studies are a promising to examine the interaction between bednet resistance and malaria epidemiology.

This chapter presents a novel mathematical model, of the form of deterministic system of nonlinear differential equations, for gaining insight into the transmission dynamics of malaria in a population where a certain percentage of the populace use LLINs (consistently and correctly). In addition to incorporating many critical features of malaria disease (e.g., the four main cycles associated with malaria disease, namely immature mosquito life cycle, adult mosquito gonotrophic cycle, parasite sporogony in the mosquito and schizogony in humans; stratifying human population according to bednet usage; etc.), the model allows for the assessment of the killing and deterrence properties of the LLINs (in particular, in addition to killing adult mosquitoes (with

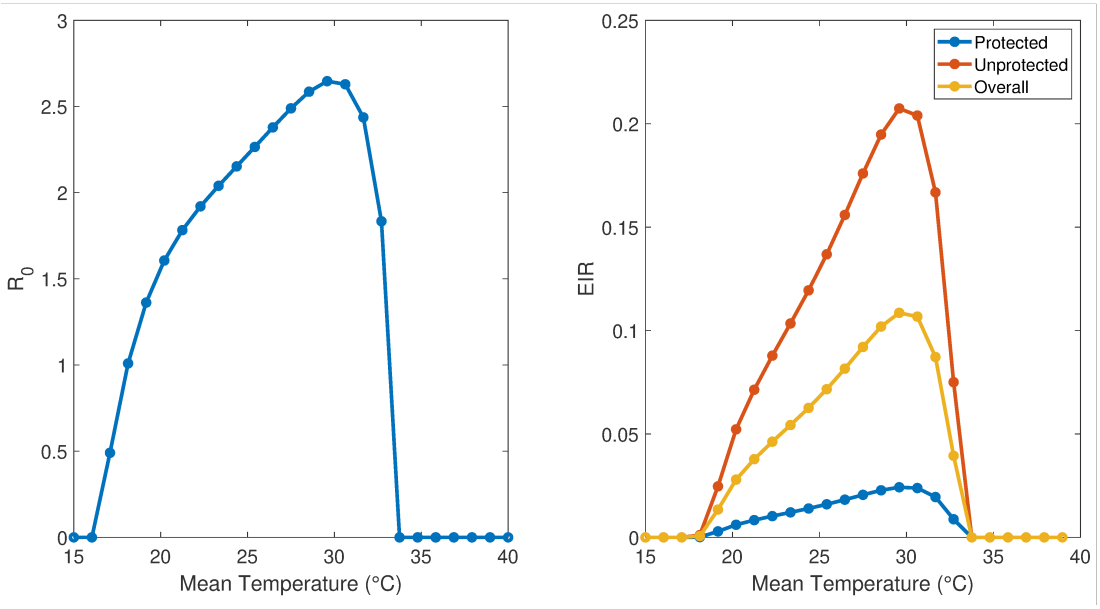

Figure 3.10: The Left Panel Shows how $\tilde{\mathcal{R}}_0$ Varies with Mean Temperature, Using a Fixed $\pi_p = 0.5$, $K_E = 100\frac{\Pi}{\mu_H}$, and a Highly Effective Net. The Right Shows the Numerically Determined Equilibrium Values of EIR for Protected, Unprotected, and Overall Human Populations as a Function of Temperature (and for the Same Parameter Values). Both $\tilde{\mathcal{R}}_0$ and EIR, Across Populations, Peak Around 29°C.

some efficacy) upon encounter, the nets can also deter the mosquito from entering the house and/or from biting the human host). The model has been parametrized using ecological data and parameter values relevant to malaria transmission dynamics in holo- and meso-endemic regions of sub-Saharan Africa, and was used to evaluate the population-level impact of various LLINs coverage and effectiveness levels. For numerical simulation purposes, the effectiveness levels of the bednets described in Section 3.4.2 are considered.

The model {(3.4.1), (3.4.2), (3.4.4)} was rigorously analysed to gain insight into its dynamical features (thereby allowing for the determination of important ecological and epidemiological thresholds that govern the persistence, effective control and/or

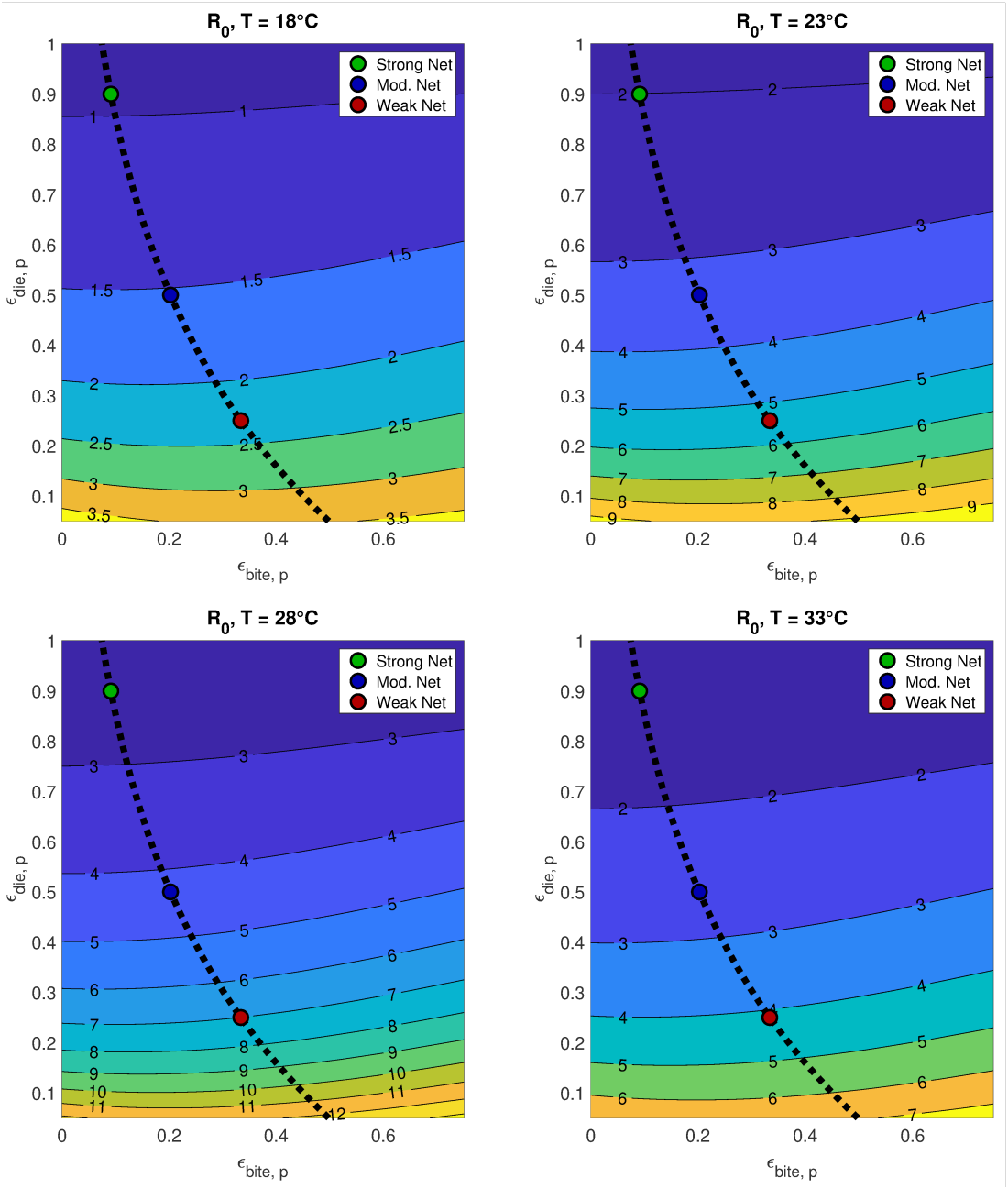

Figure 3.11: Contours of $\tilde{\mathcal{R}}_0$ as a Function of $\varepsilon_{die,p}$ and $\varepsilon_{bite,p}$ for Four Different Ambient Temperatures, and for Different Net at 50% Bednet Coverage (with $K_E = 100\frac{\Pi}{\mu_H}$). The Qualitative Shape of the Contour Plots does not Appreciably Vary with Temperature.

elimination of the disease in a population). It is, first of all, shown, using the theory of center manifold (LaSalle and Lefschetz, 1976), that the model undergoes the phenomenon of backward bifurcation, when the reproduction number of the model is less than 1, whenever a certain bifurcation coefficient attains positive values. This condition is associated with the disease-induced mortality in the host population being set to zero (Iboi et al., 2018; Iboi and Gumel, 2018). The epidemiological implication of this phenomenon is that the usual epidemiological requirement of having the reproduction number of the model being less than 1, while necessary, is no longer sufficient for the effective control of the disease. Thus, when a backward bifurcation exists, greater control effort is needed to eradicate disease.

However, the phenomenon of backward bifurcation does not exist in the model developed in this study if all the values of the parameters are chosen from their biologically realistic ranges in Table 3.5, for a holoendemic setting, with five parameter values chosen outside the given range to illustrate a backward bifurcation. Thus, the study in this Chapter shows that, for a holoendemic malaria setting, the backward bifurcation phenomenon in the developed model is essentially a mathematical artifact which may not be realizable using realistic data (or set of parameter values). This result is consistent with those reported in (Garba and Gumel, 2010; Garba et al., 2008; Iboi et al., 2018; Iboi and Gumel, 2018), which also showed that backward bifurcation is not realizable using realistic parameters.

The backward bifurcation phenomenon is known to exist in vector-borne disease models that incorporate disease-induced death in the host(s) population(s). This is confirmed, in this Chapter, by showing that such bifurcation does not occur in the special case of the model with no disease-induced death in the human population (we showed, using Lyapunov function theory together with LaSalle's Invariance Principle, that the disease-free equilibrium of the special case of the model with no disease-

induced death rate and no density-dependent larval mortality is, indeed, globally-asymptotically stable whenever the associated reproduction number is less than 1).

The impact of coverage level of the LLINs is monitored by simulating the model using various coverage levels. The simulation results obtained show, expectedly, that the disease prevalence in the host population (including those protected, by sleeping under a net, and the unprotected ones who do not sleep under a net) decreases with increasing coverage levels.

We observe LLINs at 20% coverage to reduce the reproduction number, at the holoendemic baseline (approximated by $K_E = 100 \times \Pi/\mu_H$), from a baseline value of about 13.7 to either 10.7, 8.3, or 6.1, under weakly, moderately, or highly effective bednets, respectively. Increasing coverage to 80% yields $\tilde{\mathcal{R}}_0$ values of 4.3, 1.9, and 0.8, for the same respective net efficacies. Thus, malaria elimination in holoendemic regions will require highly effective nets at high coverage levels. At the mesoendemic baseline, approximated by $K_E = 10 \times \Pi/\mu_H$ and giving $\tilde{\mathcal{R}}_0 = 4.3$ without bednets, we see similar relative reductions in $\tilde{\mathcal{R}}_0$. However, given the lower baseline $\tilde{\mathcal{R}}_0$, even weakly effective nets give $\tilde{\mathcal{R}}_0 = 1.3$ under 80% bednet coverage, near the elimination threshold, and both moderately and highly effective nets push $\tilde{\mathcal{R}}_0$ well below zero. Bednet coverage of 20%, in this case, improves malaria control, but is insufficient for elimination.

The widespread use of insecticide-based vector control interventions, including pyrethroid based insecticide-treated nets (ITNs; later replaced by long-lasting insecticidal nets (LLINs)) has resulted in the emergence of vector resistance to nearly every currently-available agent used in the insecticides (Alout et al., 2017; Dondorp et al., 2009; Imwong et al., 2017; WHO, 2017b) with pyrethroid resistance now widely observed across the African continent (Hemingway et al., 2016). Most nets distributed to-date are pyrethroid-only nets (although pyrethroid nets with the syn-

ergist PBO and pyrethroid nets with a second active ingredient are now available), and pyrethroid-only nets will likely remain a core vector control intervention over the next few years. As such it is critical to understand their current impact - now resistance to their active ingredients is so widespread - on malaria epidemiology. This study suggests that high coverage of weakly effective (i.e. low killing efficiency) nets is better than low coverage with highly effective (i.e. high killing efficiency) nets.

The impact of the deterrence property of LLINs to repel mosquitoes from entering protected house has also been examined, and we find, perhaps unexpectedly, that higher deterrence almost uniformly increases $\tilde{\mathcal{R}}_0$. This is likely because mosquitoes repelled from protected persons now focus their efforts on the unprotected subpopulation, thus increasing transmission within this group and potentially hampering elimination efforts.

The transmission cycle of malaria is greatly affected by changes in the environment. In particular, the life-cycles of the malaria vector (adult female *Anopheles* mosquito) and parasites (*Plasmodium*) are both strongly affected by changes in ambient temperature, while suitable aquatic habitat is necessary for immature mosquito development. Therefore, we have examined how malaria burden changes with mean ambient temperature, and how this interacts with bednet coverage. We find $\tilde{\mathcal{R}}_0$ and EIR to both peak at just under 30°C, with this true regardless of bednet coverage levels. Indeed, we observe bednet coverage and temperature to essentially independently influence $\tilde{\mathcal{R}}_0$. Thus, somewhat colder regions, such as the eastern African highlands, may see an increase in malaria potential with climate change, while warmer western regions may be little affected.

Chapter 4

IMPACT OF STERILE INSECT TECHNOLOGY ON THE ECOLOGY OF MALARIA MOSQUITOES

4.1 Introduction

As stated in chapter 1, mosquitoes are the principal vectors of numerous MBDs, such as malaria, dengue, West Nile virus, Zika, Yellow fever and Chikungunya. Further, about 200 of the 3500 adult mosquito species can transmit MBD to humans. The control of MBDs (such as malaria) in endemic areas relies mainly on the implementation of mosquito-reduction strategies, such as larviciding, the use of LLINs and IRS and the treatment of confirmed cases (Mutabingwa, 2005). However, adult female mosquitoes have developed resistance to all five chemicals currently being used in the production of IRS and LLINs (see Figure 1.8 and (Alout et al., 2017; Dondorp et al., 2009; Imwong et al., 2017; WHO, 2017b)). Furthermore, in the context of malaria, the *Plasmodium* parasite has started developing resistance to the *artemisinin*-based therapy (Lubell et al., 2014; Ouji et al., 2018; Yeung et al., 2004). Hence, there is urgent need to explore other measures for vector control. Biological controls, such as sterile insect technology (SIT) (fre, 2017; Benelli et al., 2016; Cai et al., 2014; Huang et al., 2017; Patil et al., 2015; Thomé et al., 2010; Zheng et al., 2019), are being used to achieve this objective.

SIT is based on the repeated release of large numbers of sterile male mosquitoes aimed at disrupting the natural reproductive process of mosquitoes (Benelli et al., 2016; Cai et al., 2014; Thomé et al., 2010). One key feature of SIT is that female mosquitoes that mate only with sterile males will produce no offspring. If sufficient

numbers of wild females mate with sterile males, the target population will decline and possibly collapse. Sterile male mosquitoes can be mass produced using several different techniques, including exposure of male pupae to sterilizing radiation and infection with sterilizing vertically-transmitted bacteria such as *Wolbachia* (Benelli et al., 2016; Cai et al., 2014; Esteva and Yang, 2005; Thomé et al., 2010). Although controversial, certain forms of gene drive, engineered using CRISPR-CAS9 technology, may also lead to population declines through male sterility (Noble et al., 2017).

SIT was first successfully implemented in Florida, USA, in 1958 to eradicate screw-worm flies *Cochliomya omnivorax* (Bartlett and Staten; Benelli et al., 2016; Esteva and Yang, 2005; Knipling, 1979). In this instance, about 50 million sterile flies were released each week over an 18 month period within an 85,000 square mile area (Esteva and Yang, 2005). The technique has also been successfully used against a range of agricultural pest insects, such as fruit flies, moths and tsetse flies (Dyck VA and AS, 2005). Sterile mosquitoes have so far been used in the Cayman Islands, Brazil, USA, Panama and India (Patil et al., 2015).

Recently, the company Verily (formerly Google Life Sciences) released 20 million sterile male mosquitoes in two neighborhoods in Fresno County over a period of 20 weeks in an effort to reduce the population of *Aedes aegypti* mosquitoes (the primary vector of dengue, chikungunya, yellow fever and Zika viruses) which have been present in California's central valley since 2013 (fre, 2017). Zheng et al. (2019) recently studied the combined impact of using incompatible insect techniques (IIT) and SIT to control the population abundance of *Aedes albopictus* mosquitoes in Guangzhou province of China during the peak mosquito breeding seasons between 2016 and 2017 (based on the weekly release of over 160,000 of these mosquitoes *per* hectare).

Although the use of SIT has been proven to be effective (in reducing the abundance of the targeted mosquito species population in a community) under certain conditions,

it comes with a number of challenges (Benelli et al., 2016; Cai et al., 2014; Esteva and Yang, 2005; Gentile et al., 2015; Patil et al., 2015; White et al., 2010; Zheng et al., 2019). Depending on the distribution and abundance of the target species, large numbers of sterile males may have to be reared and released over a large area (Esteva and Yang, 2005; Gentile et al., 2015; Patil et al., 2015; White et al., 2010; Zheng et al., 2019). Even larger numbers of sterile males will be required if sterilization also reduces male mating fitness, since this will increase the likelihood of adult female mosquitoes mating with fertile adult wild male mosquitoes (Gentile et al., 2015). Furthermore, although SIT is highly species-specific and, therefore, less likely to have unintentional adverse environmental consequences (Benelli et al., 2016; Cai et al., 2014; Esteva and Yang, 2005; Gentile et al., 2015; Patil et al., 2015; White et al., 2010; Zheng et al., 2019), this specificity may be problematic in settings where there are multiple competent vector species requiring control.

As stated in chapters 1 and 3, another important factor that affects the dynamics of mosquito population is the seasonal variabilities in climate factors, such as temperature and precipitation (Abdelrazec and Gumel, 2017; Agusto et al., 2015; Eikenberry and Gumel, 2018; Githeko et al., 1992; Iboi and Gumel, 2018; Imbahale et al., 2011; Lambrechts et al., 2011; Okuneye and Gumel, 2017; Okuneye et al., 2019; Parham and Michael, 2010; Polwiang, 2015; Scott et al., 2000; SE and AB, 2019). In particular, changes in temperature is known to significantly affect the distribution and ecology of *Anopheles* mosquitoes by altering their maturation, survival and biting rates (Abdelrazec and Gumel, 2017; Eikenberry and Gumel, 2018; Githeko et al., 1992; Imbahale et al., 2011; Okuneye et al., 2019; Polwiang, 2015; SE and AB, 2019). Consequently, this chapter will additionally assess how such seasonal variability will affect the effectiveness of the SIT program in curtailing the abundance of the targeted mosquito population.

4.2 Main Objectives

The primary objective of this chapter is to use mathematical modeling and simulations to assess the impact of the periodic release of sterile male mosquitoes (using SIT) on the local abundance of *Anopheles* mosquitoes. The potential impact of seasonal variations in temperature on the population-level effectiveness of the SIT control strategy will also be assessed. In other words, we will seek to determine whether or not local (seasonal) changes in temperature might affect the utility of the SIT vector control strategy. To achieve these objectives, an improved mathematical model, which takes the form of an impulsive, deterministic system of nonlinear differential equations, will be developed.

4.3 Literature Review of Modeling of Sterile Insect Technology

Numerous mathematical models have been developed and used to assess the population-level effectiveness of SIT on the population abundance and dynamics of mosquito populations (see, for instance, (Anguelov et al., 2012; Cai et al., 2014; Dumont and Tchuenche, 2012; Esteva and Yang, 2005; Gentile et al., 2015; Thomé et al., 2010; White et al., 2010)). Anguelov et al. (2012) used a deterministic model to analyze the impact of the SIT as a measure for the control of *Anopheles* mosquito. Cai et al. (2014) formulated a model of the interactive dynamics of wild and sterile mosquitoes by incorporating different strategies in releasing sterile mosquitoes. Dumont and Tchuenche (2012) formulated and analysed a model of SIT to prevent, reduce, eliminate or stop an epidemic of Chikungunya.

Esteva and Yang (2005) proposed a model to assess the effect of irradiated (or transgenic) male insect introduction in a previously infested region. Gentile et al. (2015) used agent-based modelling of emerging and theoretical implementations of

transgenic SIT in *Anopheles gambiae* for the control of malaria. Thomé et al. (2010) presented a mathematical model to describe the dynamics of mosquito population when sterile male mosquitoes (produced by irradiation) are introduced as a biological control along with the application of insecticide. Finally, White et al. (2010) used a stage-structured model to explore the impact of pulsed releases of sterile males on a mosquito population in which sterilized males suffer a reduction in mating fitness.

4.4 Mathematical Formulation

The improved model to be formulated in this chapter is based on the dynamics of *Anopheles* mosquitoes. The total mosquito (immature and mature) population at time t, denoted by $N_V(t)$, is subdivided into subpopulations of eggs ($E(t)$), larvae ($L(t)$), pupae ($P(t)$), unmated female adult mosquitoes ($F_u(t)$), female adult mosquitoes that mated with fertile wild males ($F_{m,w}(t)$), female adult mosquitoes that mated with sterile males ($F_{m,s}(t)$), wild adult male mosquitoes ($M_w(t)$) and sterile adult male mosquitoes ($M_s(t)$). Hence,

$$N_V(t) = E(t) + \sum_{j=1}^{4} L_j(t) + P(t) + F_u(t) + F_{m,w}(t) + F_{m,s}(t) + M_w(t) + M_s(t).$$

First of all, upon emergence, adult female mosquitoes search for male mosquitoes to mate (Mike, 2008). Let β represent this (mating) rate. The mean time required for an adult female mosquito to find a mating partner (i.e., an adult male mosquito) is inversely proportional to the local density of adult male mosquitoes that are able to mate (J. Rankin and Kokko, 2007; Stone, 2013; White et al., 2010). It is assumed that while all wild-type adult male mosquitoes are able to mate, only a fraction, $0 < \eta \leq 1$, of adult sterile male mosquitoes are able to mate (this is due to a number of factors, such as development, culturing and production processes, including storage temperature and compaction rate (Chung et al., 2018; Dame et al., 2009;

Dyck VA and AS, 2005; Munhenga et al., 2016; White et al., 2010; Zheng et al., 2019)). Therefore, once an adult male mosquito is found, it is assumed that the mating process is completed within ζ units of time (Aldersley and Cator, 2019). Hence, the mean time for an adult female mosquito to find an adult male mosquito (and mate with it), denoted by $\mathcal{H}_{mean}$, is given by:

$$\mathcal{H}_{mean} = \zeta + \frac{1}{\beta(M_w + \eta M_s)}.$$

Furthermore, the *per capita* rate at which adult female mosquitoes mate with adult male mosquitoes (denoted by $\mathcal{Y}_a(t)$) is inversely proportional to this time. That is,

$$\mathcal{Y}_a(t) = -F_u \frac{1}{\mathcal{H}_{mean}} = -F_u \frac{\beta(M_w + \eta M_s)}{1 + \beta\zeta(M_w + \eta M_s)}.$$

Likewise, the rates at which adult female mosquitoes mate with adult male wild-type (denoted by $\mathcal{Y}_b(t)$) or sterile male mosquitoes (denoted by $\mathcal{Y}_c(t)$) are given, respectively, by

$$\mathcal{Y}_b(t) = \beta \left[\frac{M_w}{1 + \beta\zeta(M_w + \eta M_s)}\right] F_u \text{ and } \mathcal{Y}_c(t) = \beta \left[\frac{\eta M_s}{1 + \beta\zeta(M_w + \eta M_s)}\right] F_u.$$

Figure 4.1 depicts the possible mating outcomes between sterile male mosquitoes and adult wild female mosquitoes. It is worth emphasizing that the model to be designed in this study accounts for the seasonal fluctuations in temperature. In particular, fluctuations in both ambient/air temperature (denoted by $T_A(t)$) and water temperature (denoted by $T_W(t)$) will be incorporated into the model.

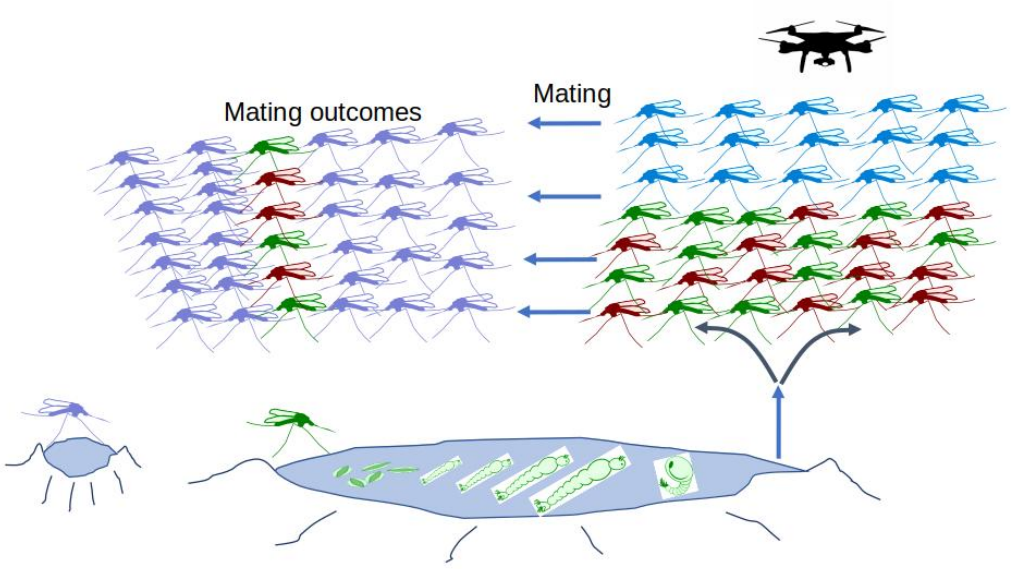

Figure 4.1: Mating Outcomes Between Sterile Male Mosquitoes and Wild Adult Female Mosquitoes. Colors: Blue–Sterile Male Mosquitoes; Brown–Wild male Mosquitoes; Green–Unmated Female Mosquitoes; Purple–Mated Female Mosquitoes that Would be Laying (Nonhatching) Eggs.

The model for the population dynamics of *Anopheles* mosquitoes, which incorporates, in addition to mosquito lifecycle dynamics, the intermittent release of sterile male mosquitoes and the seasonal fluctuation in temperature, is given by the following deterministic, impulsive, non-autonomous system of non-linear differential equations

(where a dot represents differentiation with respect to time t) (Iboi et al., 2019a):

$$
\begin{cases}
\left.\begin{aligned}
\dot{E} &= \phi_E \psi_E \left(1-\tfrac{E}{K_E}\right)_* F_{m,w} - \left[\sigma_E(T_W)+\mu_E(T_W)\right] E,\\
\dot{L}_1 &= \sigma_E(T_W)E - \left[\sigma_{L_1}(T_W)+\mu_L(T_W)+\delta_L L\right] L_1,\\
\dot{L}_j &= \sigma_{L_{j-1}}(T_W)L_{j-1} - \left[\sigma_{L_j}(T_W)+\mu_L(T_W)+\delta_L L\right] L_j,\\
\dot{P} &= \sigma_{L4}(T_W)L_4 - \left[\sigma_P(T_W)+\mu_P(T_W)\right] P,\\
\dot{F}_u &= r\sigma_P(T_W)P - \left[\tfrac{\beta(M_w+\eta M_s)}{1+\beta\zeta(M_w+\eta M_s)}+\mu_q(T_A)\right] F_u,\\
\dot{M}_w &= (1-r)\sigma_P(T_W)P - \mu_q(T_A)M_w,\\
\dot{F}_{m,w} &= \left[\tfrac{\beta M_w}{1+\beta\zeta(M_w+\eta M_s)}\right] F_u - \mu_q(T_A)F_{m,w},\\
\dot{F}_{m,s} &= \left[\tfrac{\beta\eta M_s}{1+\beta\zeta(M_w+\eta M_s)}\right] F_u - \mu_q(T_A)F_{m,s},\\
\dot{M}_s &= -\mu_q M_s,
\end{aligned}\right\} t \neq n\tau\\
\left.\begin{aligned}
E(n\tau^+) &= E(n\tau),\\
L_1(n\tau^+) &= L_1(n\tau),\\
L_j(n\tau^+) &= L_j(n\tau),\\
P(n\tau^+) &= P(n\tau),\\
F_u(n\tau^+) &= F_u(n\tau),\\
M_w(n\tau^+) &= M_w(n\tau),\\
F_{m,w}(n\tau^+) &= F_{m,w}(n\tau),\\
F_{m,s}(n\tau^+) &= F_{m,s}(n\tau),\\
M_s(n\tau^+) &= M_s(n\tau)+C_R,
\end{aligned}\right\} t = n\tau,\ n = 0,1,2,\cdots .
\end{cases}
\tag{4.4.1}
$$

It is convenient to define $L = \sum_{j=1}^{4} L_j$. A schematic diagram of the model (4.4.1) is depicted in Figure 4.2, and the state variables and parameters of the model are described in Table 4.1.

In the formulation of the model (4.4.1), it is assumed, first of all, that only adult female mosquitoes that have mated with wild male mosquitoes (i.e., $F_{m,w}$ mosquitoes) lay eggs (i.e., adult female mosquitoes that mate with sterile male mosquitoes will not lay eggs, owing to the assumed 100% effectiveness of SIT to inhibit egg laying (Anguelov et al., 2012; Esteva and Yang, 2005)). Eggs laying occurs at a logistic rate $\phi_E \psi_E \left(1 - \frac{E}{K_E}\right)_*$, where ϕ_E is the egg oviposition rate, ψ_E is the number of eggs laid *per* oviposition and K_E (the notation $r_* = \max\{0, r\}$ is used to ensure the non-negativity of the logistic term) is the carrying capacity for eggs (a measure of the exhaustion of space for laying the eggs) (Horsfall, 1955; Hoshen and Morse, 2004; Iboi and Gumel, 2018; Imbahale et al., 2011; Okuneye and Gumel, 2017).

Eggs hatch into larvae at a temperature-dependent rate $\sigma_E(T_W)$, larvae mature into pupae at temperature-dependent rates $\sigma_{Lj}(T_W)$ (with $j = 1, 2, 3, 4$ accounting for the four larval instar stages), and pupae mature into adult mosquitoes at a temperature-dependent rate $\sigma_P(T_W)$. Among these newly emerging adult mosquitoes, it is assumed that a proportion, $r\,(0 < r < 1)$, are females (and the remaining proportion, $1 - r$, are males). Natural mortality occurs in all mosquito life stages at a temperature-dependent rates $\mu_E(T_W), \mu_L(T_W), \mu_P(T_W)$ and $\mu_q(T_A)$, respectively, while larvae are also additionally lost due to density-dependent mortality at a rate $\delta_L L$ (Abdelrazec and Gumel, 2017) (where $\delta_L = 1/K_L$, with K_L being the carrying capacity of larvae).

Finally, sterile adult male mosquitoes are released to the environment periodically. That is (Dumont and Tchuenche, 2012; Gentile et al., 2015),

$$M_s(n\tau^+) = M_s(n\tau) + C_R,$$

where τ is the time lag between successive sterile male mosquito releases and $n\tau^+$ is the moment immediately after the nth sterile release. At each release time $n\tau$, a constant number of sterile male mosquitoes (C_R) are released to the environment. For instance, during the summer of 2015, a joint US-China research team released 7,000 to 10,000 sterile male mosquitoes in the Sand island (a small island in Guandong province of China) thrice a week in March (Huang et al., 2017). Similarly, in a more recent field study in Guangzhou province of China (Zheng et al., 2019), over 160,000 sterile male mosquitoes were released *per* hectare every week (during the peak mosquito breeding seasons between 2016 and 2017). Sterile male mosquitoes are typically released in areas where the density of wild female mosquitoes reaches a certain threshold level (Huang et al., 2017).

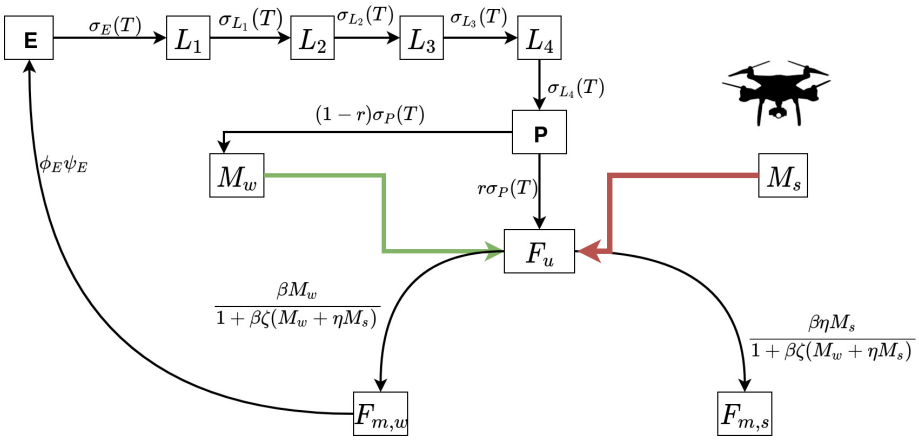

Figure 4.2: Flow Diagram of the Model.

The model (4.4.1) extends numerous mathematical models that incorporate the implementation of SIT vector control strategy, such as those in (Anguelov et al., 2012; Cai et al., 2014; Dumont and Tchuenche, 2012; Esteva and Yang, 2005; Gentile et al.,

2015; Thomé et al., 2010; White et al., 2010), in several ways. In particular,

(i) it extends the models in (Anguelov et al., 2012; Cai et al., 2014; Dumont and Tchuenche, 2012; Esteva and Yang, 2005; Gentile et al., 2015; Thomé et al., 2010; White et al., 2010) by including the dynamics of immature mosquitoes (i.e., the compartments E, $L_j (j = 1, 2, 3, 4)$ and P);

(ii) it extends the models in (Anguelov et al., 2012; Cai et al., 2014; Esteva and Yang, 2005; Gentile et al., 2015; Thomé et al., 2010) by including periodic releases of sterile male mosquitoes (i.e., $M_s(n\tau^+) = M_s(n\tau) + C_R$);

(iii) it extends the models in (Anguelov et al., 2012; Cai et al., 2014; Dumont and Tchuenche, 2012; Esteva and Yang, 2005; Gentile et al., 2015; Thomé et al., 2010; White et al., 2010) by including a novel mating function that realistically accounts for the detailed mating processes and outcomes;

(iv) it extends all of the aforementioned studies by incorporating the effect of local (seasonal) temperature variability on the dynamics of the mosquito population (in fact, to the best of the authors' knowledge, seasonal variation in temperature has not previously been investigated in SIT-based mosquito control modeling studies, despite the fact that mosquito and many other arthropod populations are strongly affected by seasonal changes in temperature and precipitation) (Abdelrazec and Gumel, 2017; Afrane et al., 2005; Agusto et al., 2015; Bayoh and Lindsay, 2003; Cailly et al., 2012; Iboi and Gumel, 2018; Mordecai et al., 2013; Wu et al., 2009).

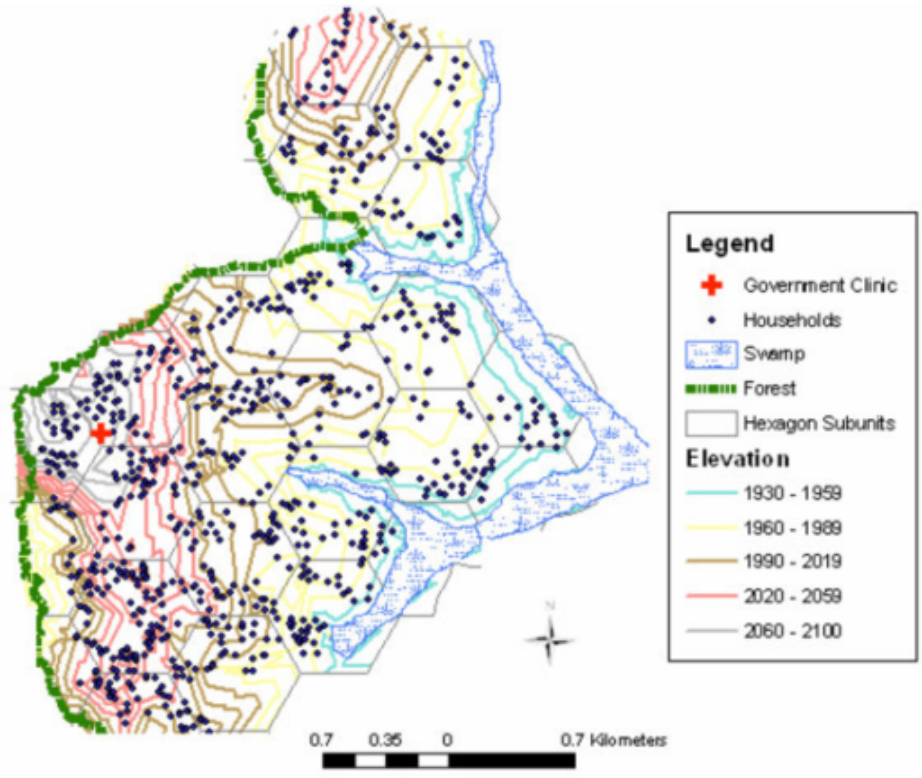

Figure 4.3: Geography and Household Locations in Kipsamoite Area (Within Nandi Hills District) of Kenya (Ernst et al., 2006).

4.4.1 Formulation of Thermal-Response Functions

The functional forms of the temperature-dependent parameters in the model (4.4.1) are based on the biology of *Anopheles* mosquitoes, and are formulated as follows. First of all, we adopt the relationship between water temperature and overall time from egg to adult, $\mathcal{D}_{EA}(T_W)$, given by Bayoh and Lindsay (Bayoh and Lindsay, 2003) (based on laboratory data):

$$\frac{1}{\mathcal{D}_{EA}(T_W)} = -0.05 + 0.005T_W - 2.139 \times 10^{-16} e^{T_W} - 2.81357 \times 10^{5} e^{-T_W}.$$

For the parameters related to the mosquito development rates in the immature stages, we determined stage-specific development times as a function of water temperature from Figure 1 of Bayoh and Lindsay (Bayoh and Lindsay, 2003), as shown

in Figure 3.4. It can be seen from Figure 5 that the development times are similar across all immature stages of the mosquito lifecycle, with appreciable overlap in the temperature-dependent curves. Hence, it is assumed that the average duration in all immature stages are the same. Further, the uniform temperature-dependent development rates are given as (recalling that $L = L_1 + L_2 + L_3 + L_4$):

$$\sigma_E(T_W) = \sigma_P(T_W) = \sigma_L(T_W) = 6\frac{1}{\mathcal{D}_{EA}(T_W)}. \tag{4.4.2}$$

It is worth mentioning that some field studies suggest that the distribution of hatching time in *Anopheles gambiae* is relatively constant (Dao et al., 2006).

The functional forms of the *per capita* death rates (μ_E for eggs; μ_L for larvae and μ_P for pupae) are obtained by fitting the data on larval survival times reported by Bayoh and Lindsay (Bayoh and Lindsay, 2003), to the following quartic polynomial (note that survival time is the inverse of death rate):

$\mu_i(T_W) = 8.929 \times 10^{-6}T_W^4 - 9.271 \times 10^{-4}T_W^3 + 3.536 \times 10^{-2}T_W^2 - 0.5814T_W + 3.509;$

$i = E, L, P$. The temperature-dependent mortality rate of adult mosquitoes ($\mu_q(T_A)$) is given by (Bayoh, 2001):

$$\frac{1}{\mu_q(T_A)} = \max(-11.8239 + 3.3292T_A - 0.0771T_A^2, 0.1).$$

In the formulation of the model (4.4.1), it is assumed, for simplicity, that near the surface of the water, air and water temperature are approximately equal (Agusto et al., 2015; Iboi and Gumel, 2018) (so that, $T_A(t) = T_W(t) = T(t)$). The following piecewise-constant function is proposed to model temperature variability:

$$T(t) = v(T_{obs} - T_{mean}) + T_{mean}, \tag{4.4.3}$$

where T_{mean} is the mean annual temperature in the chosen community, T_{obs} is the observed mean monthly temperature and v is a parameter that governs the amplitude

of seasonal fluctuations around the mean annual temperature. The observed mean monthly temperature for Kipsamoite area of Kenya for the year 2016 is tabulated in Table 4.2 (Lag, 2017). This formulation allows us to study the impact of increasing seasonal variation in temperature using temperature profiles typical of areas with moderate to high densities of wild adult female *Anopheles* mosquitoes. In particular, we note that the model (4.4.1) reduces to a non-seasonally-forced model when the parameter v is set to 0.

4.4.2 Timing of Release of Sterile Male Mosquitoes

Following White et al. (2010), we define the *release effect statistic*, denoted by $R(t)$, given by:

$$R(t) = \frac{\int_{\tau}^{t+\tau} N_1(s)ds}{\int_{\tau}^{t+\tau} N_0(s)ds}, \tag{4.4.4}$$

where N_1 is the total abundance of adult females over a period of time with the control (SIT) and N_0 is the total abundance of adult females over that same period without the control. Following White et al. (2010), Equation (4.4.4) yields the following three ecological interpretations for the release statistic R:

(i) If $R(t) < 1$, then the sterile male release (i.e., SIT control) has a negative (desirable) effect on the wild adult female mosquito population (i.e., the SIT control decreases the population abundance of the wild adult female mosquito).

(ii) If $R(t) = 1$, then the SIT control has no relative effect on the wild adult female mosquito population (i.e., SIT control does not increase or decrease the wild adult female mosquito population).

(iii) If $R(t) > 1$, then the SIT control has a positive (detrimental) effect on the wild adult female mosquito population (i.e., SIT increases the population abundance

of the wild adult female mosquitoes).

In other words, an SIT-based mosquito control strategy that has an associated release effect statistic value less than unity will lead to an effective control of the local abundance of the targeted (wild) adult mosquito population.

4.4.3 Basic Qualitative Properties of the Model

The basic qualitative properties of the model (4.4.1) will now be analysed. Let $\mathbb{R}_+ = [0, \infty)$, $\mathbb{R}_+^{11} = \{\mathcal{B} \in \mathbb{R}_+^{11} : \mathcal{B} \geq 0\}$, where

$$\mathcal{B} = (E(t), L_j(t), P(t), F_u(t), F_{m,w}(t), F_{m,s}(t), M_w(t), M_s(t)); \ j = 1, 2, 3, 4.$$

Consider the following ecologically-feasible region of the model (4.4.1):

$$\begin{aligned}\Omega = \big\{\mathcal{B} \in \mathbb{R}_+^{11} : E(t) \leq K_E, L_1(t) \leq L_1^\diamond, L_2(t) \leq L_2^\diamond, L_3(t) \leq L_3^\diamond, L_4(t) \leq L_4^\diamond, \\ P(t) \leq P^\diamond, F_u \leq F_u^\diamond, M_w \leq M_w^\diamond, F_{m,w} \leq F_{m,w}^\diamond, F_{m,s} \leq F_{m,s}^\diamond, M_s \leq M_s^\diamond\big\},\end{aligned}$$

where,

$$\begin{aligned}&L_1^\diamond = \frac{\sigma_E K_E}{\sigma_{L_1} + \mu_L}, \ L_2^\diamond = \frac{\sigma_{L_1} L_1^\diamond}{\sigma_{L_2} + \mu_L}, \ L_3^\diamond = \frac{\sigma_{L_2} L_2^\diamond}{\sigma_{L_3} + \mu_L}, \ L_4^\diamond = \frac{\sigma_{L_3} L_3^\diamond}{\sigma_{L_4} + \mu_L}, \ P^\diamond = \frac{\sigma_{L_4} L_4^\diamond}{\sigma_P + \mu_P}, \\ &M_w^\diamond = \frac{(1-r)\sigma_P P^\diamond}{\mu_q}, \ F_u^\diamond = \frac{r\sigma_P P^\diamond}{Q_1}, \ F_{m,s}^\diamond = \frac{Q_2}{\mu_q}, \ F_{m,w}^\diamond = \frac{Q_3}{\mu_q}, \ M_s^\diamond = \frac{C_R e^{-\mu_q(t-n\tau)}}{1 - e^{-\mu_q \tau}}, \\ &\left[\frac{\beta(M_w^\diamond + \eta M_s^\diamond)}{1 + \beta\zeta(M_w^\diamond + \eta M_s^\diamond)} + \mu_q\right] \leq Q_1, \ \frac{\beta M_w^\diamond}{1 + \beta\zeta(M_w^\diamond + \eta M_s^\diamond)} \leq Q_2, \text{ and} \\ &\frac{\beta\eta M_s^\diamond}{1 + \beta\zeta(M_w^\diamond + \eta M_s)} \leq Q_3.\end{aligned} \tag{4.4.5}$$

Furthermore, it is worth recalling the following definitions:

Definition 4.4.1. (Huang et al., 2017; Lakshmikantham V and PS, 1989). Let $r(t) = r(t, t_0, x_0)$ be a solution of (4.4.1) on $[t_0, t_0 + a)$. Then $r(t)$ is said to be a maximal

solution of (4.4.1), if for any solution $x(t) = x(t, t_0, x_0)$ of (4.4.1) existing on $[t_0, t_0+a)$, the inequality

$$x(t) \leq r(t), t \in [t_0, t_0 + a) \tag{4.4.6}$$

holds. A minimal solution $\rho(t)$ may be defined in a similar way by reversing the inequality of (4.4.6)

Definition 4.4.2. (Huang et al., 2017; Lakshmikantham V and PS, 1989). Let $V : \mathbb{R}_+ \times \mathbb{R}_+^{11} \longrightarrow \mathbb{R}_+$. Then V is said to belong to a class V_0 if V satisfies:

1. V is continuous on $(n\tau, (n+1)\tau] \times \mathbb{R}_+^{11}$ and $\lim_{(t,y)\to(n\tau^+,x)} V(t, x) = V(n\tau^+, x)$ for every $x \in \mathbb{R}_+^{11}, n \in N$;

2. V is locally Lipschitz continuous with respect to x.

Definition 4.4.3. (Huang et al., 2017; Lakshmikantham V and PS, 1989). Let $V \in V_0$, for $(t, x) \in (n\tau, (n+1)\tau] \times R^{11}$. Define the upper right derivative with respect to (2.4.1) as

$$D^+V(t, x) = \lim_{h\to 0^+} \sup \frac{1}{h}[V(t + h, x + hf(t, x)) - V(t, x)].$$

Theorem 4.4.1. *(Huang et al., 2017; Lakshmikantham V and PS, 1989). Let $V : \mathbb{R}_+ \times \mathbb{R}_+^{11} \longrightarrow R_+$, $V \in V_0$. Suppose*

$$\begin{aligned} D^+V(t, x) &\leq g(t, V(t, x)),\ t \neq t_n,\ n = 1, 2, \cdots, \\ V(t_n^+) &\leq m_n(V(t_k)),\ t = t_n,\ n = 1, 2, \cdots, \end{aligned} \tag{4.4.7}$$

where $g \in C(R_+ \times \mathbb{R}_+, \mathbb{R}), m_k \in C(\mathbb{R}, \mathbb{R})$ and $m_n(u)$ is non-decreasing in u for each $n = 1, 2, ...$ Let $r(t)$ be the maximal solution of the scalar impulsive differential equation

$$\begin{aligned} \dot{u}(t) &= g(t, u),\ t \neq t_n, \\ u(t_n^+) &= m_n(u(t_n)),\ t = t_n \\ u(t_0) &= u_0, \end{aligned} \tag{4.4.8}$$

which exists on $[t_0, \infty)$. *Then,* $V(t_0^+, x_0) \leq u_0$ *implies that* $V(t, x(t)) \leq r(t)$ *for* $t \geq t_0$ *where* $x(t) = x(t, t_0, x_0)$ *is any solution of* (4.4.1) *on* $[t_0, \infty)$. *Similar result can be obtained when all the directions of the inequalities in Theorem 4.4.1 are reversed and* $m_n(u)$ *is non-increasing.*

Remark 4.4.1. *In Theorem 4.4.1, the function g must be smooth enough to guarantee the existence and uniqueness of solution for* (4.4.8). *Hence,* $r(t)$ *is indeed the unique solution of* (4.4.8).

Let $x(t) = (E(t), L_j(t), P(t), F_u(t), F_{m,w}(t), F_{m,s}(t), M_w(t), M_s(t))^T$, with $j = 1, 2, 3, 4$, be a continuous solution of the model (4.4.1) on $(n\tau, (n+1)\tau], n \in Z_+$, and $x(n\tau^+) = \lim_{t \to n\tau^+} x(t)$ exists. Then, the global existence and uniqueness of solutions of the model (4.4.1) is determined by the smoothness of $f = (\mathbf{g})^T$ where $\mathbf{g}$ is the right-hand side vector of the model (4.4.1).

Consider, now, the impulsive component of the model (4.4.1), given by:

$$\begin{aligned} \dot{M}_s &= -\mu_s M_s, \qquad t \neq n\tau, \\ M_s(n\tau^+) &= M_s(n\tau) + C_R, \quad t = n\tau, \\ M_s(0^+) &\geq 0. \end{aligned} \tag{4.4.9}$$

We claim the following result.

Lemma 4.4.1. *The impulsive system* (4.4.9) *has a unique positive periodic solution and* $M_s^\diamond(t)$ *is globally-asymptotically stable, where*

$$\begin{aligned} M_s^\diamond(t) &= \frac{C_R e^{-\mu_q(t-n\tau)}}{1 - e^{-\mu_q \tau}}, \quad n\tau < t \leq (n+1)\tau, \\ M_s^\diamond(0^+) &= \frac{C_R}{1 - e^{-\mu_q \tau}}. \end{aligned} \tag{4.4.10}$$

Proof. It follows from the first equation of system (4.4.9) that,

$$M_s(t) = M_s(n\tau^+) e^{-\mu_q(t-n\tau)}, \quad n\tau < t \leq (n+1)\tau.$$

The following stroboscopic map can be established using the second equation of (4.4.9)(Yang et al., 2013):

$$M_s[(n+1)\tau^+] = M_s[(n+1)\tau] + C_R = M_s(n\tau^+). \tag{4.4.11}$$

Hence, the unique positive (periodic) solution of (4.4.9) is given by

$$\begin{aligned} M_s^\diamond(t) &= \frac{C_R e^{-\mu_q(t-n\tau)}}{1-e^{-\mu_q\tau}}, \quad n\tau < t \leq (n+1)\tau, \\ M_s^\diamond(0^+) &= \frac{C_R}{1-e^{-\mu_q\tau}}. \end{aligned} \tag{4.4.12}$$

□

We further claim the following positivity result.

Theorem 4.4.2. Consider the model (4.4.1). *Each component of the solution of the model, with non-negative initial conditions, remains positive and bounded for all time $t > 0$.*

Proof. The positivity of $M_s(t)$ follows from Lemma 4.4.1. It should be noted that the right-hand side of each of the first ten equations of the model (4.4.1) is continuous and locally-Lipschitz at $t = 0$. Hence, a solution of the model with non-negative initial conditions exists and is unique for all time $t > 0$. Now, to show that the periodic solution $M_s(t)$ is bounded, it can be recalled from Lemma 4.4.1 that system (E.0.3) has a globally-asymptotically stable positive periodic solution. This solution satisfies $\lim_{t\to\infty} M_s(t) \leq M_s^\diamond(t)$. Furthermore, since $\phi_E\psi_E\left(1-\frac{E}{K_E}\right)_* \geq 0$, it follows from the first equation of the model (4.4.1) that $E(t) \leq K_E$ for all time $t > 0$.

Similarly, it follows from the second equation of the model (4.4.1) that

$$\dot{L}_1 = \sigma_E E - (\sigma_{L_1} + \mu_L) L_1 \leq \sigma_E K_E - (\sigma_{L_1} + \mu_L) L_1,$$

so that $\limsup_{t\to\infty} L_1(t) \leq \frac{\sigma_E K_E}{\sigma_{L_1}+\mu_L} = L_1^\diamond$. Using a similar approach, it can be shown that $\limsup_{t\to\infty} L_2(t) \leq \frac{\sigma_{L_1} L_1^\diamond}{\sigma_{L_2}+\mu_L} = L_2^\diamond$, $\limsup_{t\to\infty} L_3(t) \leq \frac{\sigma_{L_2} L_2^\diamond}{\sigma_{L_3}+\mu_L} = L_3^\diamond$, $\limsup_{t\to\infty} L_4(t) \leq \frac{\sigma_{L_3} L_3^\diamond}{\sigma_{L_4}+\mu_L} = L_4^\diamond$, $\limsup_{t\to\infty} P(t) \leq \frac{\sigma_{L_4} L_4^\diamond}{\sigma_P+\mu_P} = P^\diamond$, $\limsup_{t\to\infty} M_w(t) \leq \frac{(1-r)\sigma_P P^\diamond}{\mu_q} = M_w^\diamond$, $\limsup_{t\to\infty} F_u(t) \leq \frac{r\sigma_P P^\diamond}{Q_1} = F_u^\diamond$, $\limsup_{t\to\infty} F_{m,s}(t) \leq \frac{Q_2}{\mu_q} = F_{m,s}^\diamond$, $\limsup_{t\to\infty} F_{m,w}(t) \leq \frac{Q_3}{\mu_q} = F_{m,w}^\diamond$, where

$$\left[\frac{\beta(M_w^\diamond+\eta M_s^\diamond)}{1+\beta\zeta(M_w^\diamond+\eta M_s^\diamond)}+\mu_q\right] \leq Q_1,\ \frac{\beta M_w^\diamond}{1+\beta\zeta(M_w^\diamond+\eta M_s^\diamond)} \leq Q_2 \text{ and}$$
$$\frac{\beta\eta M_s^\diamond}{1+\beta\zeta(M_w^\diamond+\eta M_s)} \leq Q_3.$$

Hence, all solutions of the model (4.4.1) are bounded for all time $t > 0$. □

In summary, it follows from the above analyses that the model (4.4.1) is well-posed mathematically. Hence, it is sufficient to study its dynamics in the invariant region Ω.

4.5 Numerical Simulations

The model (4.4.1) will now be simulated, using the mosquito ecology data in Table 4.3 (together with the mean monthly temperature data for the Kipsamoite area in the Nandi Hills District of Kenya in Table 4.2), to gain insight into the local mosquito dynamics in the absence or presence of SIT and seasonal variation in local temperature.

4.5.1 Mosquito Ecology in the Absence of SIT and Seasonality

Here, the model (4.4.1) is simulated in the absence of SIT (i.e., $C_R = 0$) and seasonal variation in temperature (i.e., $v = 0$). These simulations allow for the determination of the worst-case mosquito abundance (since $C_R = 0$) for the case where the mean

annual temperature is used (i.e., no seasonal variation in temperature). That is, for these simulations, the temperature-dependent parameters of the model (4.4.1), given in Section 2, are computed using the mean annual temperature for the Kipsamoite area (which is 22.2°C (Lag, 2017)). The simulation results obtained show that the population of mosquitoes (both immature and adult) rapidly reaches a non-trivial (endemic) steady-state (Figures 4.4a-e). Since no sterile male mosquitoes are released in these simulations, the release effect statistic (R) is unity (Figure 4.4f).

The effect of mean monthly temperature on the local population abundance of immature and adult mosquitoes is monitored by simulating the model (4.4.1), using the various values of the mean monthly temperature for the Kipsamoite area given in Table 4.2. The results obtained (depicted in Figure 4.5) show that the maximum abundance of both the immature and adult mosquitoes is achieved when the mean monthly temperature is about 30°C (which is 7.2°C higher than the current mean annual temperature for the Kipsamoite area or Nandi Hill region (Lag, 2017)).

4.5.2 Assessment of the Impact of SIT on Mosquito Abundance

The model (4.4.1) is also simulated to assess the impact of SIT-based vector control on the local population abundance of the wild adult female *Anopheles* mosquitoes. The model is, first of all, ran for a period of one year (so that the system settles at its non-trivial (endemic) steady-state). A fixed number of sterile male mosquitoes (C_R) are then released after every release period (τ). For these simulations, C_R is initially set at 10,000 sterile male mosquitoes. Further, three periods of release (τ) are chosen, namely weekly (in line with the SIT-IIT implementation in two islands in Guangzhou province of China during peak mosquito seasons in 2016-2017 (Zheng et al., 2019)), bi-weekly and every three weeks. For these simulations, we consider the cases with and without seasonal variation in temperature, as described below.

No seasonal variation in temperature ($v = 0$)

The model (4.4.1) is simulated using the parameter values tabulated in Table 4.3, for the case with no seasonal variation in temperature (i.e., $v = 0$). Furthermore, the temperature-dependent parameters of the model are evaluated at the mean annual temperature of 22.2°C. As stated above, the model, under this setting, is initially ran for a period of one year before the sterile male mosquitoes are released for another one year duration (Figure 4.6a). For these simulations, C_R is initially set to 10,000 sterile male mosquitoes.

The simulation results obtained show a dramatic decrease in the population of eggs and the first three larval instars (from the pre-SIT baseline equilibrium values), before settling down to a positive (mosquito-persistent) steady-state following the release of the sterile male mosquitoes for a period of one year (Figures 4.6b-c). Surprisingly, such weekly release (of 10,000 sterile male mosquitoes) resulted in an increase (from the pre-SIT baseline) in the fourth larval instar and pupal stages, leading to convergence to a stable endemic level (Figure 4.6c).

Furthermore, an increase in the population abundance of the mated adult female mosquitoes was observed (Figure 4.6d). This is a direct consequence of the decrease in the population of fertilized wild adult female mosquitoes, and the increase in the population of fertilized female mosquitoes that would be laying nonhatching eggs (Figure 4.6e). Finally, for these simulations, the release effect statistic (R) exceeds unity (Figure 4.6f). Thus, it follows from the simulations in Figure 4.6 that the weekly release of 10,000 sterile male mosquitoes ($C_R = 10,000$ with $\tau = 7$) in the community, for the case when seasonal variation in temperature is not accounted for (i.e., $v = 0$), increases the population abundance of adult female mosquitoes. Hence, this level of sterile male release and frequency of release ($C_R = 10,000$ and $\tau = 7$) induces

detrimental effect to the community (by increasing the local abundance of the mated adult mosquito population..... since both classes of mated adult female mosquitoes can transmit disease to humans, the epidemiological consequence of this SIT-induced increase in the mated adult female mosquito population is a corresponding increase in malaria burden in the community). Qualitatively similar trends were observed when the period of release is increased to bi-weekly, every three or four weeks (Figure 4.7). This result differs from one of the main conclusions in the White *et al.* study (White et al., 2010), which suggests that the control of the *Anopheles* population is more effective when smaller numbers of sterile male mosquitoes are released more frequently (as against releasing larger numbers less frequently).

Additional simulations were carried out for the case when the number of sterile male mosquitoes released (C_R) is increased (from C_R = 10,000) to $C_R = 100,000$ (Figure 4.8a). These simulations (depicted in Figure 4.8) show qualitatively different dynamics, in comparison to the simulation results depicted in Figures 4.6 and 4.7. In particular, these simulations show a rapid decrease in the population of the immature mosquitoes, leading to extinction (Figures 4.8b and 4.8c). Furthermore, the population of mated adult female mosquitoes initially increases (during the first three to four months of SIT implementation), followed by a rapid decline leading to extinction (Figure 4.8d). This is a consequence of the rapid decrease in the population of the mated wild adult female mosquitoes, and the gradual decline (after three to four months of SIT implementation) in the population of mated adult female mosquitoes that will be laying nonhatching eggs (Figure 4.8e). Additionally, the release effect statistic (R) increases during the first three to four months of the one year SIT implementation period, and then significantly decreases for the remaining SIT implementation duration (Figure 4.8f).

In summary, the above simulations show that, when a large number of sterile male

mosquitoes are released (e.g., $C_R = 100,000$) for a weekly period ($\tau = 7$ days), there is an initial time-lag (of about three to four months, on a one year SIT release protocol), before the full population-level impact of the SIT release (*vis a vis* reduction in local mosquito abundance) is achieved. In fact, this combination of C_R and τ values can lead to the extinction of the adult mosquito population if implemented weekly for a one year period (Figure 4.8). Unlike for the case where only 10,000 sterile male mosquitoes were released (Figures 4.6-4.7), the weekly release of 100,000 sterile male mosquitoes can significantly reduce (and potentially lead to the extinction of) the adult mosquito population (while the former cannot eliminate the adult mosquito population).

It is worth mentioning that White *et al.* (White et al., 2010) and Dumont and Tchuenche (Dumont and Tchuenche, 2012) also showed that the control of the wild adult female mosquito population is highly dependent on the rate at which the sterile male mosquitoes are released, with only high release rates giving sufficient control. Our result is also consistent with that reported in the field study conducted in Guangzhou province of China by Zheng *et al.* (Zheng et al., 2019) (based on the weekly release of over 160,000 sterile male mosquitoes during the SIT implementation period).

Although similar qualitative trends were observed when the period between releases (τ) is increased from weekly to bi-weekly, every three and four weeks (Figure 4.9), such scenario, while greatly reducing the population abundance of the adult mosquitoes, does not lead to the extinction of the adult mosquito population. In general, the simulations in Figures 4.6-4.9 show that, for the case when no seasonal variation in temperature is allowed, releasing more sterile male mosquitoes (e.g., $C_R = 100,000$) over a one year period with relatively shorter duration between releases (e.g., weekly, bi-weekly or even monthly) does better (in terms of reducing

the population abundance of mosquitoes) than releasing smaller numbers of sterile male mosquitoes (e.g., $C_R = 10,000$) over the same time period and frequency of release. The modeling studies in (Dumont and Tchuenche, 2012; Huang et al., 2017; White et al., 2010) also advocate for more frequent (but smaller) sterile male releases.

The effect of density-dependent mortality in the larval stage (δ_L)on the population dynamics of the mosquito and the effectiveness of SIT is monitored by simulating the model (4.4.1) using various values of δ_L for different quantities of sterile male mosquito released (C_R). The results obtained, depicted in Figure 4.10, show that, for relatively small values of δ_L (such as $\delta_L = 0.00002$), the biweekly release of the sterile male mosquitoes (below a certain threshold value) initially increases the total mated female population until a peak is reached and decreases briefly before settling to a positive (mosquito persistent) state. However, when larval density-dependent mortality is increased (e.g, to $\delta_L = 0.0001$ or $\delta_L = 0.001$), the release also led to a dramatic increase in the population abundance, but followed by a rapid decrease, which may result in extinction depending on the amount released. Furthermore, much higher values of sterile release amount (C_R) are needed to achieve mosquito elimination for small values of δ_L. In particular, while about $300,000$ mosquitoes need to be released to achieve elimination when $\delta_L = 0.00002$ (Figure 4.10a), only about $50,000$ need to be released to achieve such elimination if δ_L is increased to $\delta_L = 0.0001$ (Figure 4.10b). For $\delta_L = 0.001$, however, elimination can be achieved by releasing only $10,000$ sterile male mosquitoes weekly for one year (Figure 4.10c). In other words, this study shows that larval density-dependent mortality decreases the number of sterile male mosquitoes that need to be released to achieve effective mosquito control or extinction. Hence, SIT-based mathematical models for mosquito (immature and adult) population dynamics that do not incorporate density-dependence in the larval stage of the immature mosquito lifecycle may under-estimate or over-estimate the

effectiveness of SIT implementation on the local mosquito population abundance.

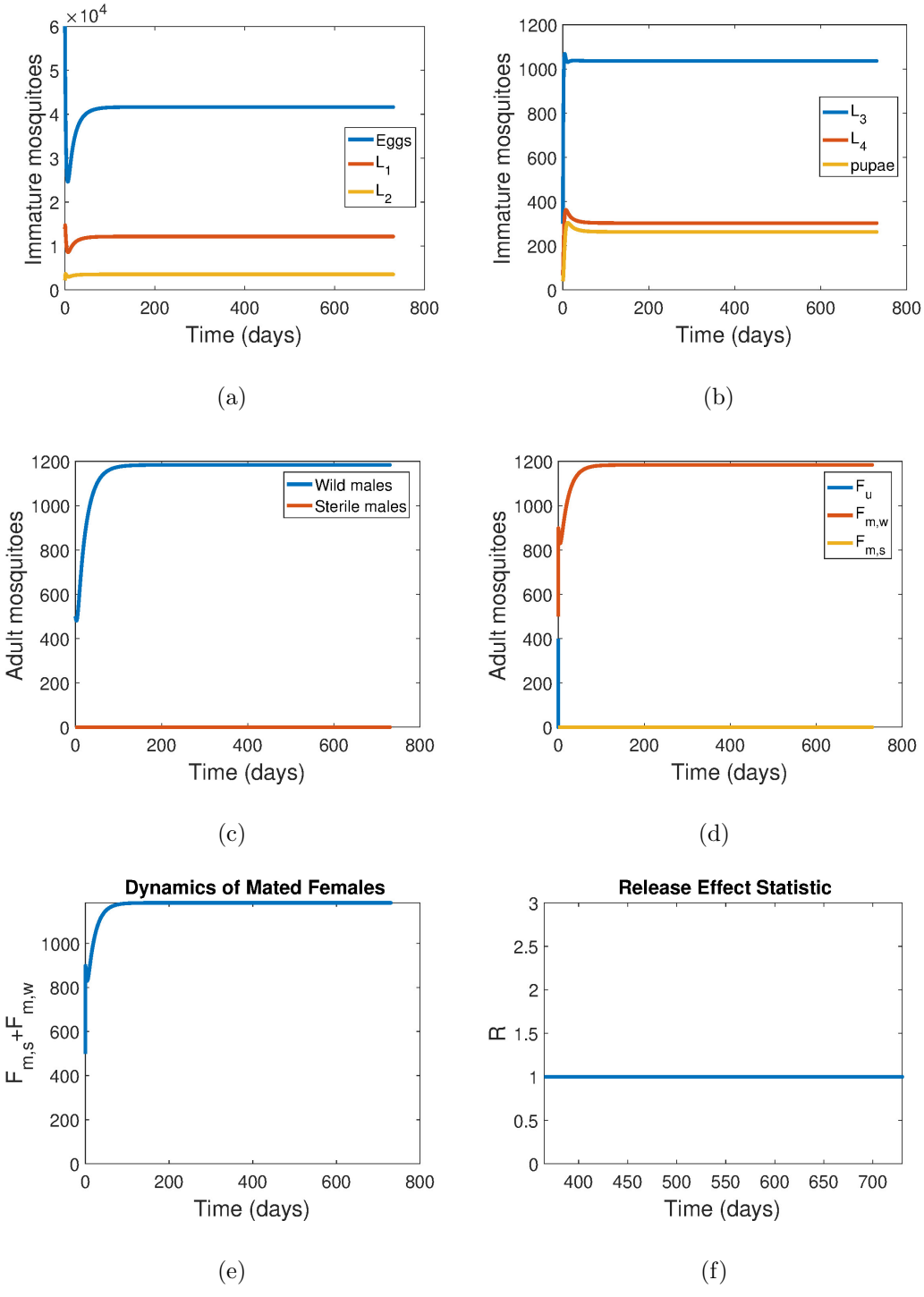

Figure 4.4: Simulations of the Model (4.4.1), Showing the Dynamics of the Various Mosquito Lifecycle Stages in the Absence of SIT (i.e., $C_R = 0$) and Seasonal Variation in Temperature (i.e., $v = 0$), as a Function of Time. Other Parameter Values Used are as Given in Table 4.3.

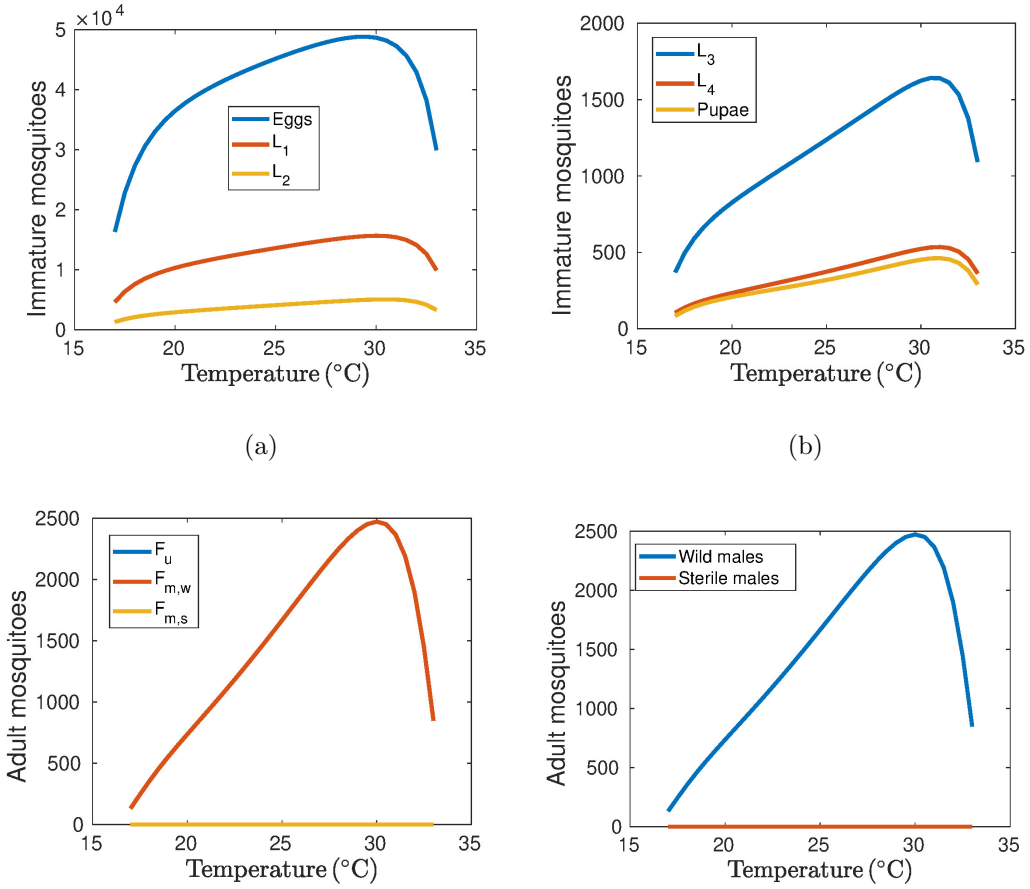

Figure 4.5: Simulations of the Model (4.4.1), Showing the Dynamics of the Various Mosquito Lifecycle Stages as a Function of the Mean Monthly Temperature (for Kipsamoite Area of Kenya) in the Absence of SIT Release (i.e., $C_R = 0$) and Seasonal Variation in Temperature (i.e., $v = 0$). Other Parameter Values Used are as Given in Table 4.3.

Seasonal variation in temperature ($v \neq 0$)

The effect of SIT implementation will now be assessed for the case when the assumption for no seasonal variation in temperature ($v = 0$) is relaxed. That is, the model (4.4.1) will now be simulated for the case when $v \neq 0$. In particular, we set $v = 1$ (i.e., the temperature at time t equals the actual observed temperature at time t, as given in equation (4.4.3)). Here, too, the model is, first of all, simulated for one year prior to the release of the sterile male mosquitoes, followed by the release of $10,000$ sterile male mosquitoes weekly for a one year duration (Figure 4.11a).

The simulation results obtained, depicted in Figures 4.11b-e, show oscillatory dynamics in the mosquito population (unlike the monotone dynamics observed in Figures 4.6-4.9). Further, although this strategy leads to the overall decline in some of the mosquito populations (Figures 4.11b-c), it also resulted in an overall increase in some of the other mosquito populations (Figures 4.11c-e). For these simulations, the release effect statistic (R) always exceeds unity (Figure 4.11e). Thus, for the case when seasonal variation in temperature is accounted for (i.e., $v \neq 0$), the weekly release of 10,000 sterile male mosquitoes will not lead to the effective control of the mosquito population (since it resulted in an overall increase in the mated adult female mosquito population). Similar trends were observed when the period between releases was increased to bi-weekly and every three weeks (Figure 4.12).

However, when the number of sterile male mosquitoes released is increased to $100,000$, the simulation results obtained show that mosquito extinction is feasible if such release is made on a weekly basis for one year (Figure 4.13a). However, when such release is made bi-weekly (Figure 4.13b), every three (Figure 4.13c) or every four (Figure 4.13d) weeks, these simulation results show that mosquito extinction is not feasible. Thus, this study shows that seasonal fluctuation in mean monthly tem-

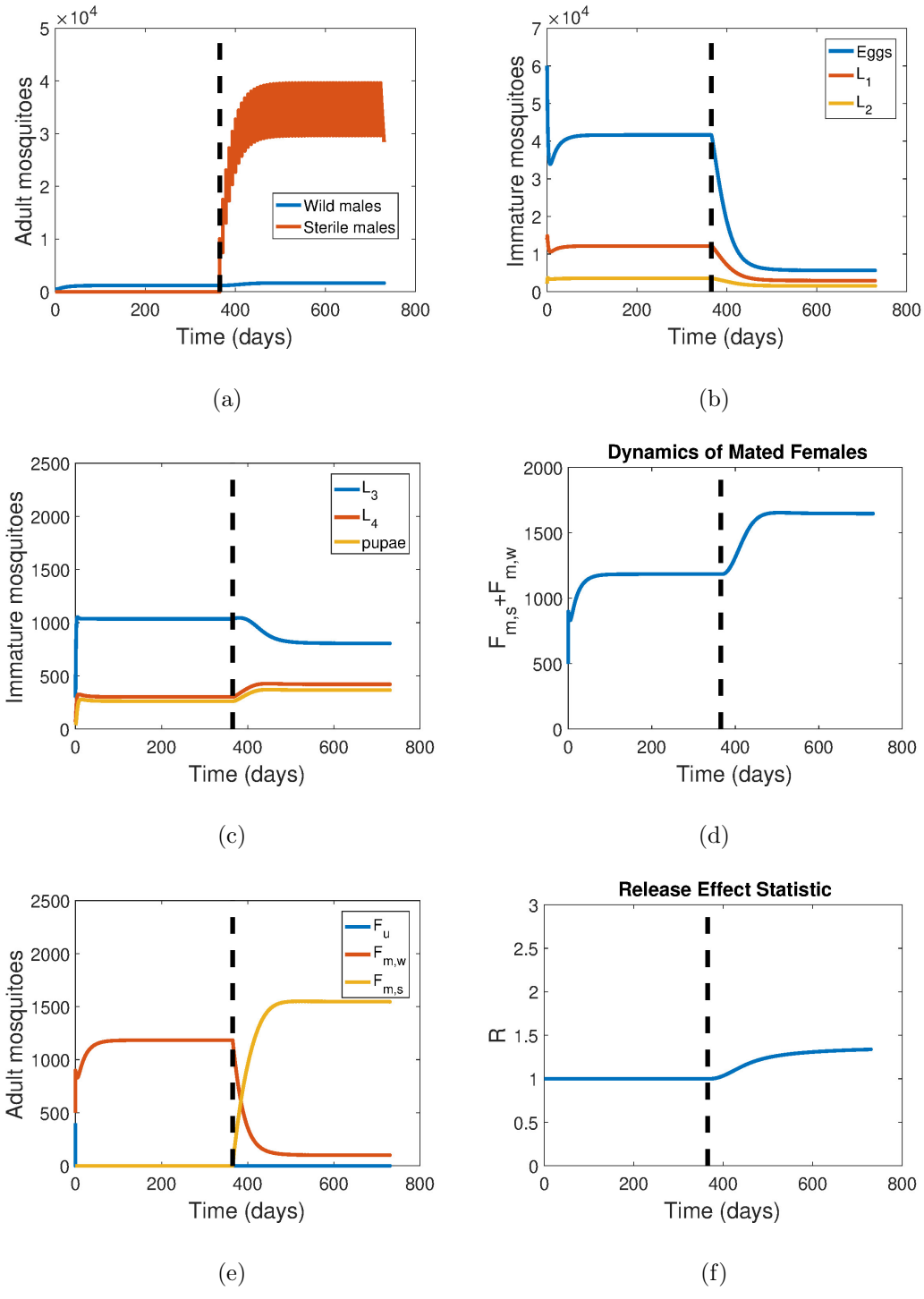

Figure 4.6: Simulations of the Model (4.4.1), Showing the Dynamics of the Various Mosquito Lifecycle Stages in the Presence of SIT (with $C_R = 10,000$), no Seasonal Variation in Temperature ($v = 0$), and ($\tau = 7$ days). Parameter Values Used are as Given in Table 4.3.

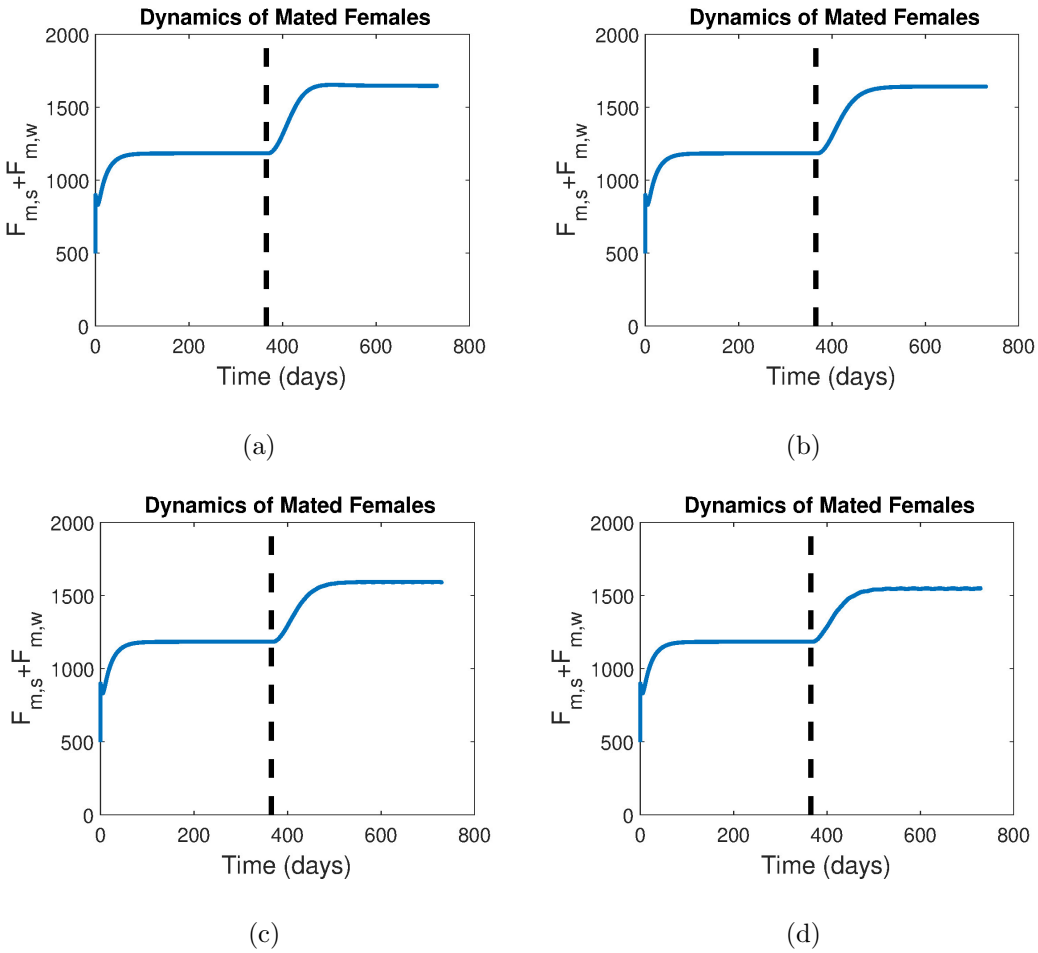

Figure 4.7: Simulations of the Model (4.4.1), Showing the Effect of the Frequency of Release of Sterile Male Mosquitoes (τ) on the Dynamics of Mated Female Mosquitoes. (a) $\tau = 7$ days (b) $\tau = 14$ days (c) $\tau = 21$ days and (d) $\tau = 28$ days. The Simulations were ran for One Year Without the Release of the Sterile Male Mosquitoes, Followed by the Release of Sterile Male Mosquitoes for a Period of 1 Year. Parameter Values Used are as Given in Table 4.3, with $C_R = 10,000$ and $v = 0$.

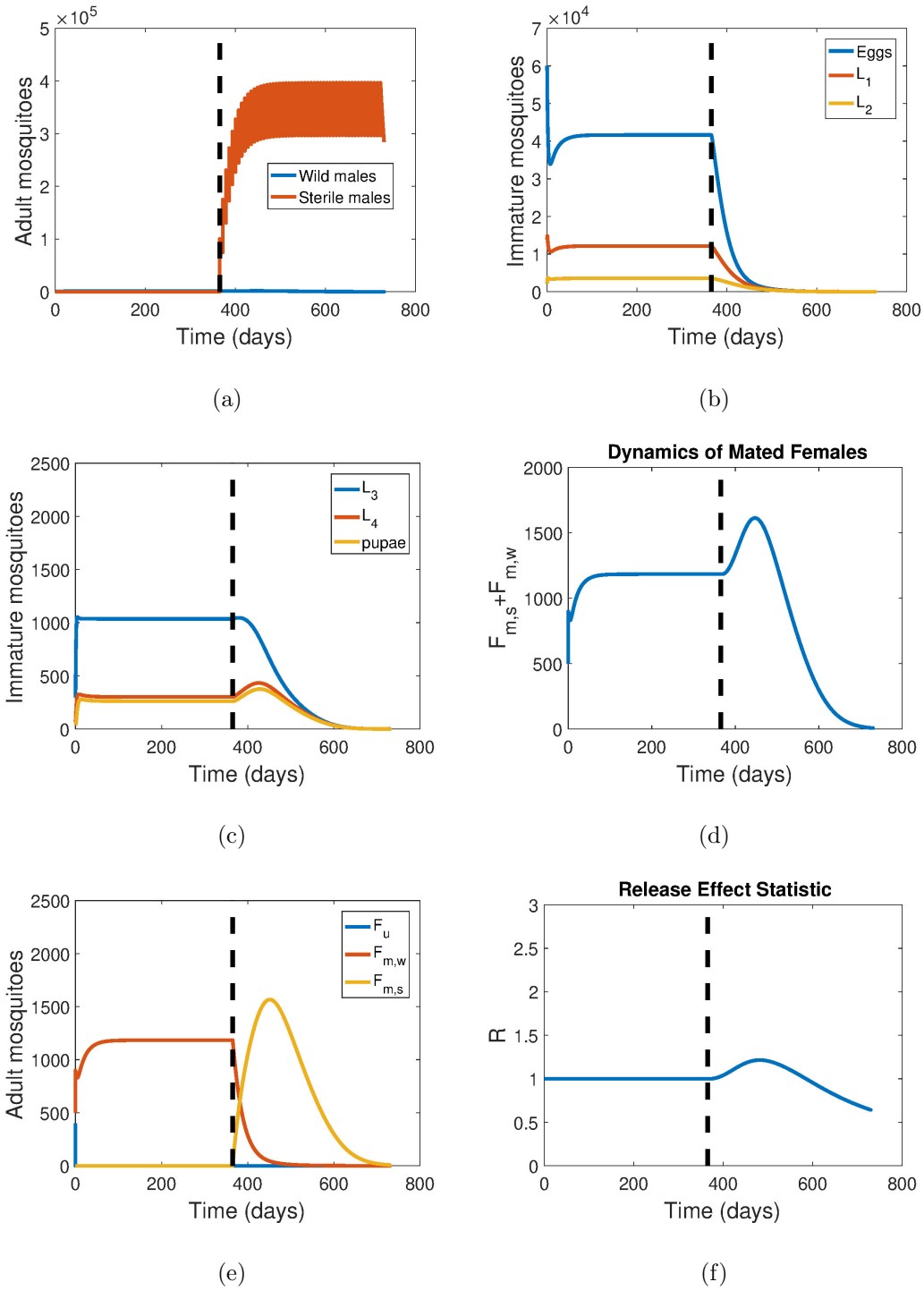

Figure 4.8: Simulations of the Model (4.4.1), Showing the Dynamics of the Various Mosquito Lifecycle Stages in the Presence of SIT (with $C_R = 100,000$) and the Seasonal Variation in Temperature ($v = 0$). Other Parameter Values Used are as Given in Table 4.3, with $\tau = 7$ days.

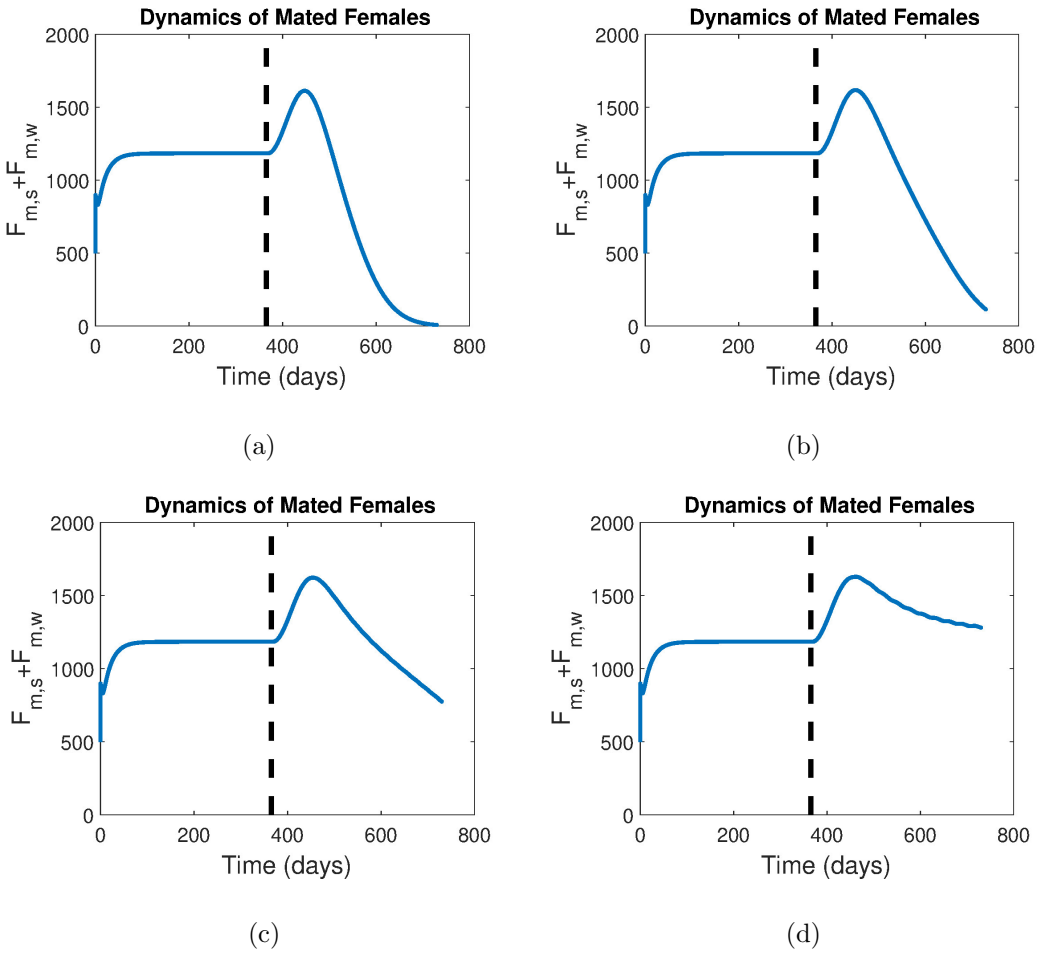

Figure 4.9: Simulations of the Model (4.4.1), Showing the Effect of the Frequency of Release of Sterile Male Mosquitoes (τ) on the Dynamics of Mated Female Mosquitoes. (a) $\tau = 7$ days (b) $\tau = 14$ days (c) $\tau = 21$ days and (d) $\tau = 28$ days. The Simulations were ran for One Year without the Release of the Sterile Male Mosquitoes, Followed by the Release of Sterile Male Mosquitoes for a Period of 1 Year. Parameter Values Used are as Given in Table 4.3, with $C_R = 100,000$ and $v = 0$.

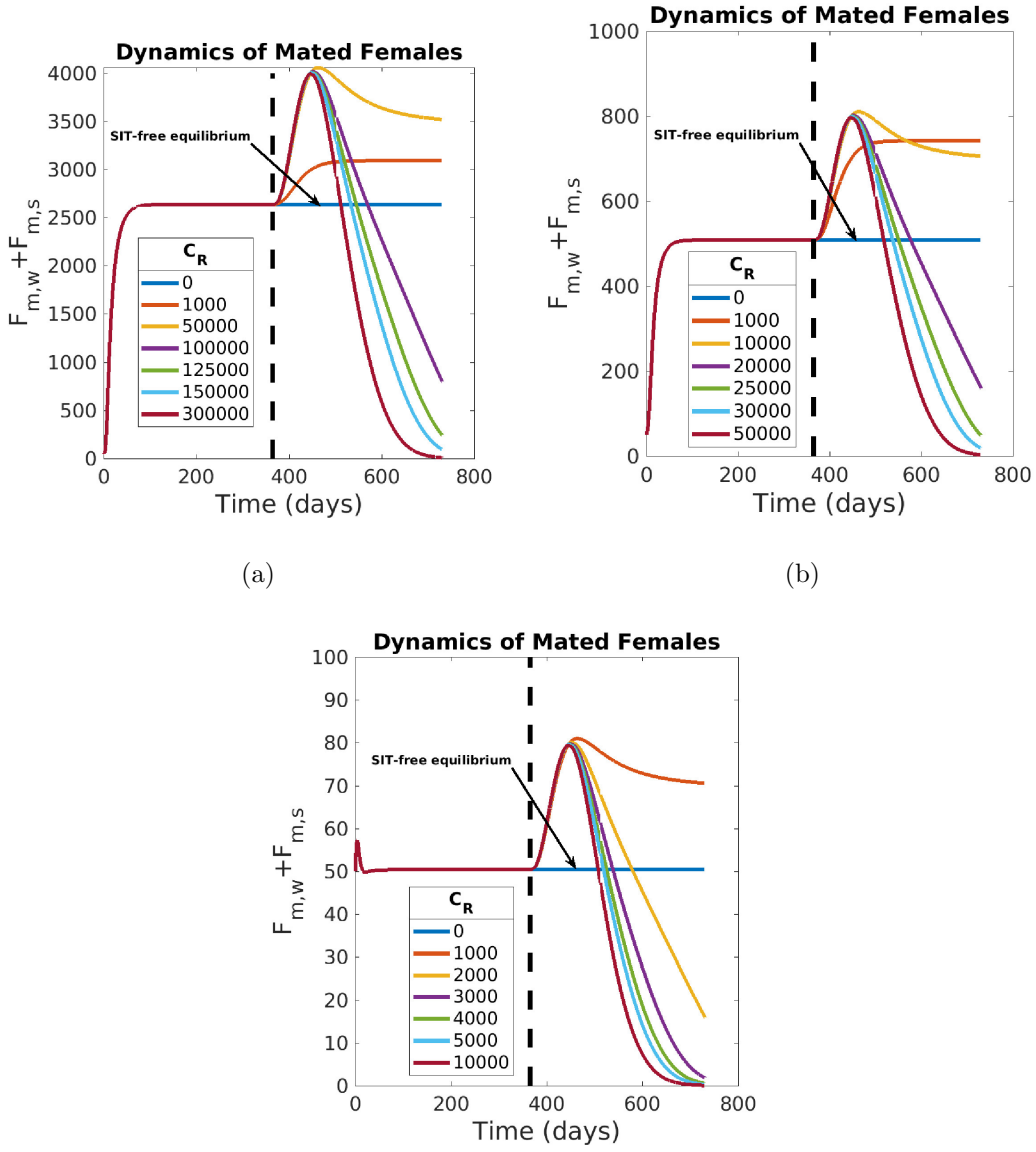

Figure 4.10: Simulations of the Model (4.4.1), Showing the Dynamics of the Total Number of Mated Female Mosquitoes for Several Different Choices of C_R. (a) $\delta_L = 0.00002$. (b) $\delta_L = 0.0001$ and (c) $\delta_L = 0.001$. The Simulations were ran for One Year Without the Release of the Sterile Male Mosquitoes (to reach the mosquito-present endemic equilibrium), Followed by the Release of Sterile Male Mosquitoes for a Period of One Year. Other Parameter Values Used are as Given in Table 4.3.

perature ($v \neq 0$) necessitates more frequent releases of the sterile male mosquitoes (in comparison to the corresponding case where such seasonal variation is not incorporated into the numerical simulation of the model) to achieve effective control or extinction of the local mosquito population.

4.6 Discussion and Conclusions

Diseases caused by mosquitoes, such as chikungunya, dengue fever, malaria, West Nile virus and Zika, continue to pose major public health challenges in areas inhabited by more than one-third of the world's population. These diseases are transmitted to humans *via* the bite of infected adult female mosquitoes (in search of blood needed for egg development and oviposition). Malaria is the deadliest of all mosquito-borne diseases (accounting for over 500,000 deaths every year, mostly in children under the age of five (Huang et al., 2017)).

In the absence of a safe and effective vaccine for use in humans against some of these diseases (particularly malaria), control measures against diseases vectored by the mosquito are mostly limited to implementing strategies that target the mosquito population. These strategies primarily include the use of insecticides (for example, in the form of IRS and LLINs in the context of malaria) to reduce the local population abundance of the mosquito in the targeted community. Unfortunately, the widespread use of these insecticides in endemic areas has resulted in the emergence of insecticide resistance in the adult mosquito population (Figure 1.8). Consequently, other alternative methods for mosquito control (notably using biological measures (fre, 2017; Cai et al., 2014; Patil et al., 2015; Thomé et al., 2010; Zheng et al., 2019)) are urgently needed

Sterile insect technology (SIT), based on the release of sterile male mosquitoes into a wild adult female mosquito population, is one of the promising mosquito-

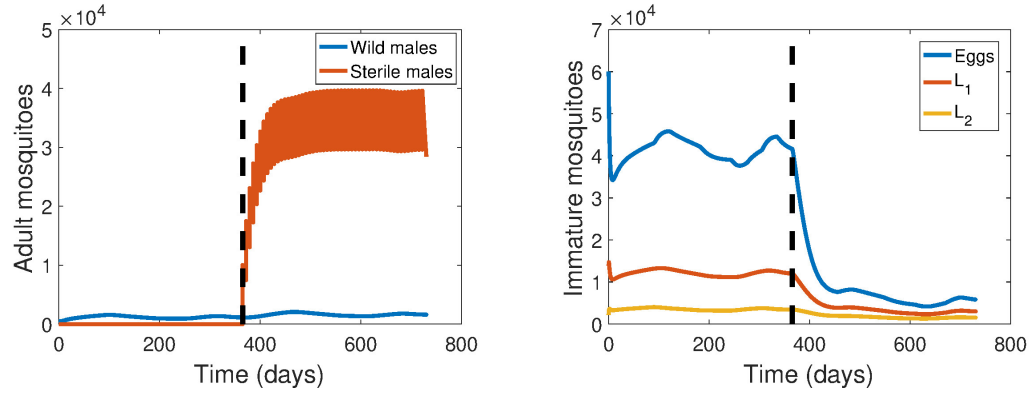

(a)

(b)

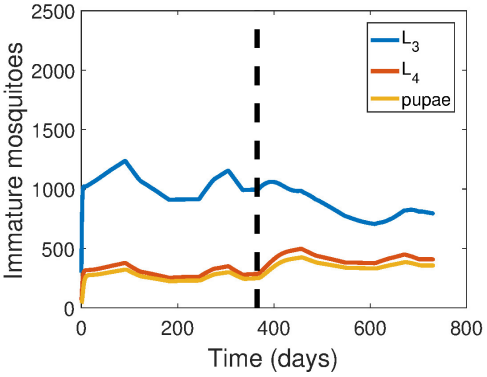

(c)

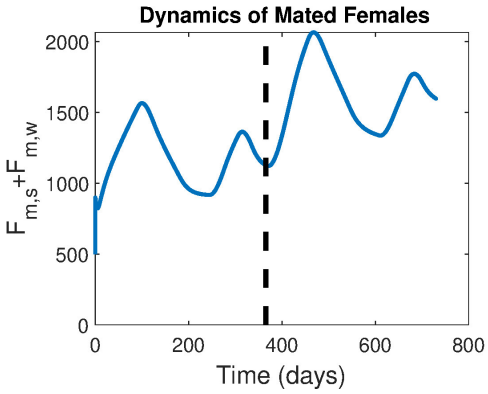

(d)

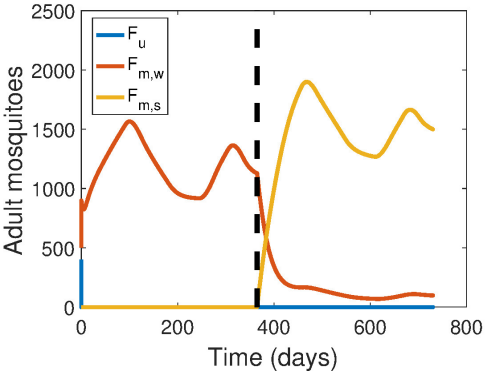

(e)

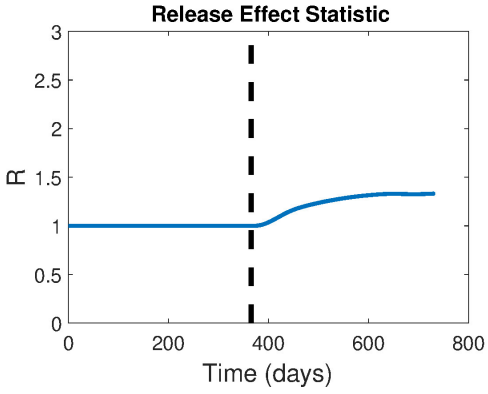

(f)

Figure 4.11: Simulations of the Model (4.4.1), Showing the Effect of Seasonal Fluctuation in Temperature ($v = 1$), and SIT (with $C_R = 10,000$) on Mosquito Abundance. Parameter Values Used are as Given in Table 4.3, with $\tau = 7$ days.

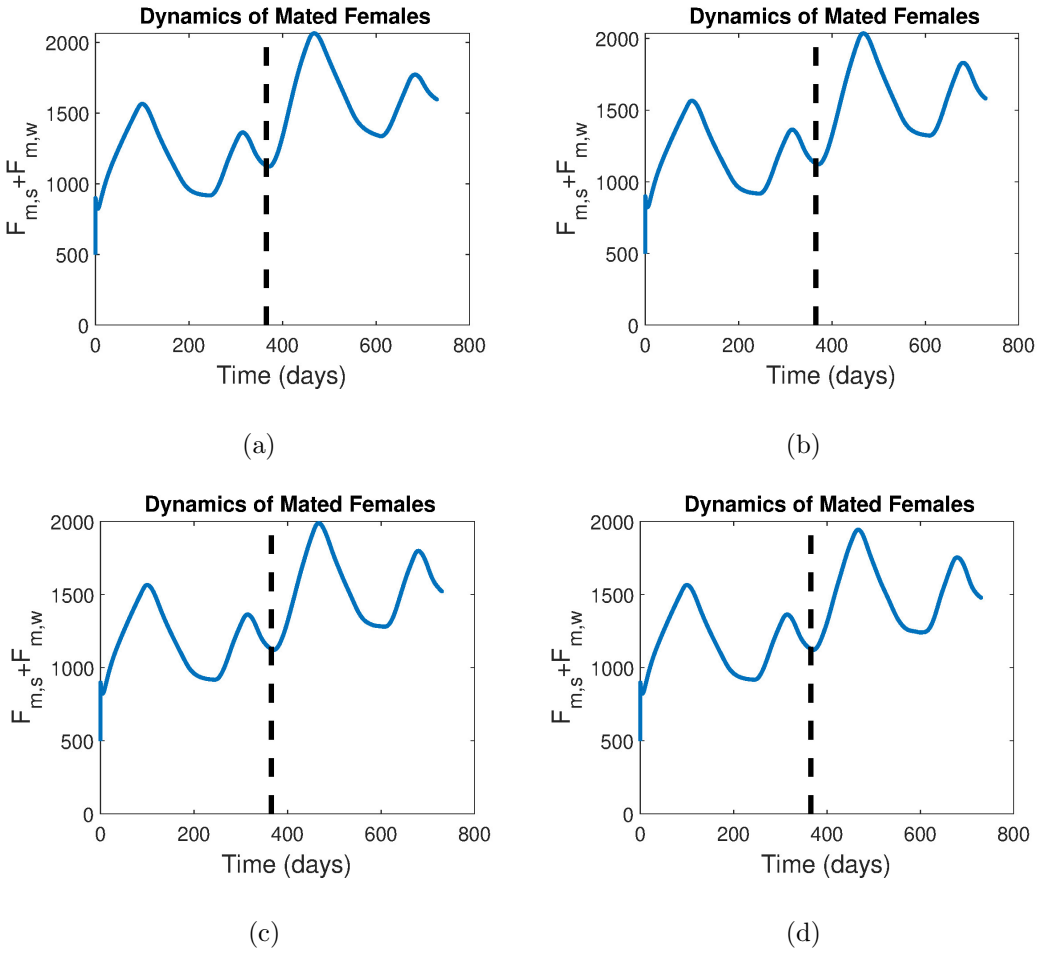

Figure 4.12: Simulations of the Model (4.4.1), Showing the Effect of the Frequency of Release of Sterile Male Mosquitoes (τ) on the Dynamics of Mated Female mosquitoes. (a) $\tau = 7$ days (b) $\tau = 14$ days (c) $\tau = 21$ days and (d) $\tau = 28$ days. Parameter Values Used are as Given in Table 4.3, with $C_R = 10,000$ and $v = 1$.

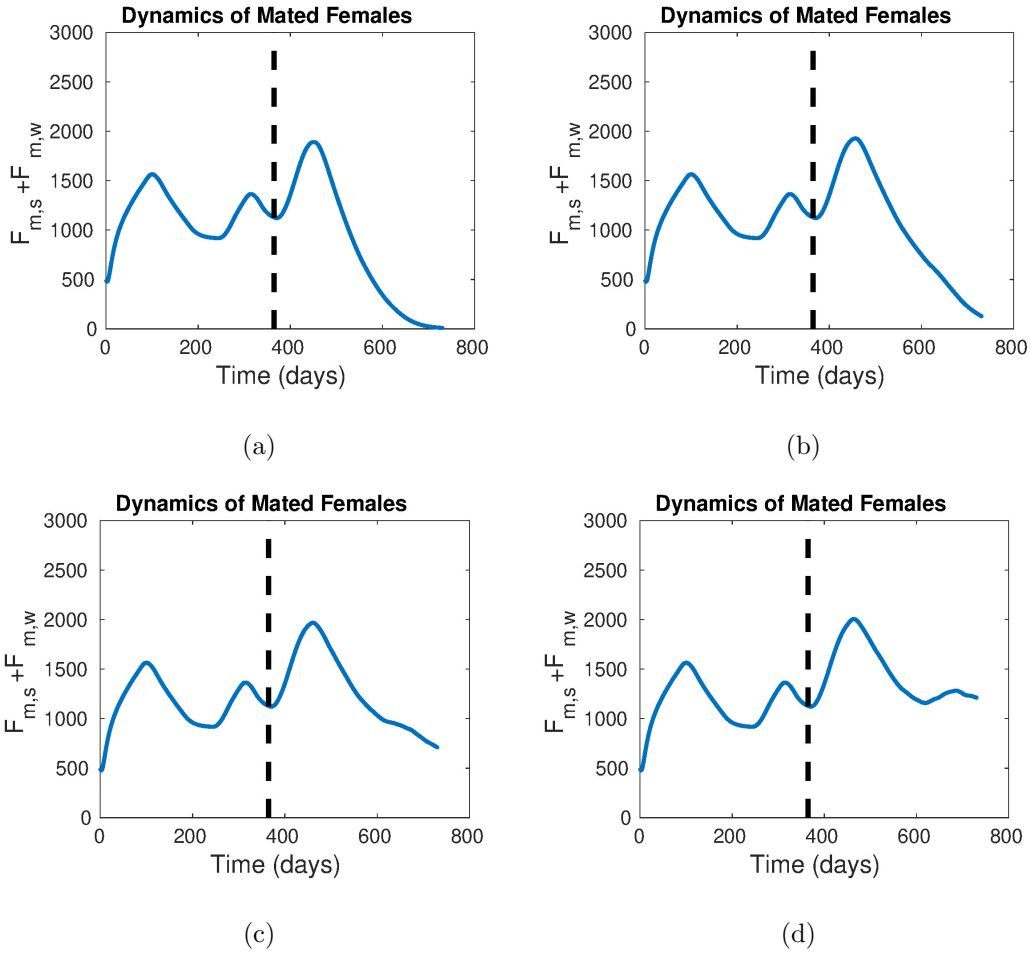

Figure 4.13: Simulations of the Model (4.4.1), Showing the Effect of the Frequency of Release of Sterile Male Mosquitoes (τ) on the Dynamics of Mated Female Mosquitoes. (a) $\tau = 7$ days (b) $\tau = 14$ days (c) $\tau = 21$ days and (d) $\tau = 28$ days. The Simulations were ran for One Year Without the Release of the Sterile Male Mosquitoes, Followed by the Release of Sterile Male Mosquitoes for a Period of 1 Year. Parameter Values Used are as Given in Table 4.3, with $C_R = 100,000$ and $v = 1$.

reduction strategies being advocated in many endemic regions for mosquito-borne diseases (Cai et al., 2014; Thomé et al., 2010). SIT which entails the periodic release of sterile male mosquitoes, into the wild mosquito population, targets the population of the wild (i.e., susceptible to biological control) adult female mosquitoes. SIT is a biological control mechanism that entails the alteration of the natural reproductive process of the target mosquito population (by chemical or physical means (Huang et al., 2017)). In particular, it is associated with the genetic modification of adult male mosquitoes to be sterile, while still being able to be sexually active. The sterile male mosquitoes are then periodically released into the environment, typically into areas with abundance of adult wild female mosquitoes, and the expectation is that an adult wild female mosquito that mates with the released sterile adult male mosquito will either not reproduce at all or produce eggs that do not hatch into larvae (Huang et al., 2017). Ultimately, the hope is that the release of the sterile male mosquitoes may eventually lead to the effective control of the abundance of (or even eliminating) the adult wild female mosquitoes (thereby eliminating the disease(s) they vector).

This Chapter aimed to provide insight into the effectiveness of such biological control strategy in combating the targeted mosquito population. This was achieved *via* the development, analysis and simulations of a novel mathematical model for the temporal dynamics of the mosquito (both immature and adult) population in a community. In addition to incorporating many pertinent features of the mosquito population dynamics (such as the entire lifecycle of the mosquito, density-dependent larval mortality etc.), the model developed in this study also incorporated the effect of seasonality in the mosquito dynamics (to account for the fact that seasonal variations in local climate variables, such as temperature, significantly affect many aspects of the mosquito dynamics, such as reproduction, parasite development, larval and adult survival etc. (Abdelrazec and Gumel, 2017; Agusto et al., 2015; Cailly et al., 2012;

Huang et al., 2017; Iboi and Gumel, 2018; Mordecai et al., 2013; Wu et al., 2009).

The novel model developed in this chapter was used to assess the impact of such changes on the population abundance of mosquitoes in Kipsamoite area of Kenya. The simulation results obtained show that maximum population of both the immature and adult female mosquito is recorded in the Kipsamoite area whenever the mean monthly temperature is about 30°C. This value is 7.2°C greater than the current mean annual temperature for the province. The implication of this result is that increases in mean annual temperature (due to global warming) could make the province more vulnerable to increased malaria burden.

The model developed in this chapter was also used to assess the population-level impact of the release of a certain number of sterile male mosquitoes (with a certain frequency) on the population biology of *Anopheles* mosquitoes in a malaria-endemic community. Simulations were carried out for the case where local seasonal variation in temperature is (or is not) accounted for. In the absence of the seasonal variation in temperature, numerical simulations of the model showed that the weekly release of 10,000 sterile male mosquitoes, over a one year period, induces a detrimental effect to the malaria-endemic community. This is because such release resulted in an increase in the population of mated adult female mosquitoes. Similar qualitative result was obtained when the release period was increased to bi-weekly or every three or four weeks. This result differs from that reported by White *et al.* (White et al., 2010), which showed that control is more effective if smaller numbers of sterile male mosquitoes are released more frequently (rather than larger and less frequent releases). However, when the number of sterile male mosquitoes released was increased to 100,000, the population of the mated adult female mosquitoes initially increased (for a period of 3 to 4 months) followed by a rapid decline (leading to extinction) for the reminder of the one year sterile release duration. The ecological implication

of this result is that, when seasonal variation in temperature is not accounted for, effective control or extinction of the mosquito population is feasible by releasing a large number of sterile male mosquitoes for a very short frequency of release period (e.g., weekly). White *et al.* (White et al., 2010) and Dumont and Tchuenche (Dumont and Tchuenche, 2012) also emphasized the importance of larger sterile male releases on mosquito control. Although (for this level of sterile male release) the population of mosquitoes is greatly reduced when the frequency of release is increased from weekly to bi-weekly or every three weeks or monthly, such does not result in mosquito extinction.

The model was also used to study the effect of density-dependent larval mortality on the population abundance of mosquitoes and the effectiveness of the SIT-based mosquito control strategy. Such density-dependence occurs when larvae compete for space and nutrients (Abdelrazec and Gumel, 2017; Iboi and Gumel, 2018). Simulations of the model, for the case with no seasonal variations in temperature, showed that for small values of the larval density-dependent mortality, the bi-weekly release of sterile male mosquitoes resulted in an increase in the population abundance of mated adult female mosquitoes. On the other hand, higher values of density-dependent mortality rates could lead to mosquito extinction depending on the number of the sterile male mosquitoes released. The implication of this result is that the effect of (higher values of) larval density-dependent mortality is to decrease the number of sterile male mosquitoes that need to be released in order to achieve effective control or extinction of the mosquito population.

For the case where seasonal variation in temperature is accounted for, the simulations of the model showed very different qualitative dynamics than the case without such variation. For instance, unlike the monotone dynamics observed for the case with no seasonal variations, rich oscillatory dynamics were observed when such variations

are taken into account. Here, too, the release of 10,000 sterile male mosquitoes failed to result in the extinction of the mosquito population. However, when 100,000 sterile male mosquitoes were released (under this scenario with seasonal temperature variation), our simulation results showed that mosquito extinction is feasible if the sterile male mosquitoes are released weekly (such extinction is not feasible if the frequency of release exceeds a week). The implication of this result is that incorporating seasonal variation in temperature necessitate more frequent releases of the (large number) of the sterile male mosquitoes. In summary, our simulations for the population-level impact of SIT suggest that the prospects of an SIT-based mosquito control strategy (for a one-year duration) are very bright if large numbers of the sterile male mosquitoes ($C_R = 100,000$) are released.

Table 4.1: Description of State Variables and Parameters for the Model (4.4.1)

Variables	**Interpretation**
E	Total number of eggs
$L = \sum_{j=1}^{4} L_j$	Total number of larvae
P	Total number of pupae
F_u	Population of new unmated wild adult female mosquitoes
M_w	Population of wild adult male mosquitoes
$F_{m,w}$	Population of fertilized wild adult female mosquitoes that have mated
$F_{m,s}$	Population of fertilized female mosquitoes that would be laying (nonhatching) eggs
M_s	Population of sterile male mosquitoes released
Parameters	**Interpretation**
β	Mating rate of wild female mosquitoes with males (either M_w or M_s)
η	Fraction of sterile males that are able to mate
ζ	Time required for mating to be completed
r	Proportion of new adult mosquitoes (based on gender status)
ϕ_E	Egg oviposition rate
ψ_E	Number of eggs laid *per* oviposition
$\sigma_E(T_W)$	Maturation rate from egg to larvae
$\sigma_L(T_W)$	Maturation rate from larvae to pupae
$\sigma_P(T_W)$	Maturation rate from pupae to adult mosquitoes
$\mu_E(T_W)$	Natural mortality rate of eggs
$\mu_L(T_W)$	Natural mortality rate of larvae
$\mu_P(T_W)$	Natural mortality rate of pupae
δ_L	Density-dependent mortality rate of larvae
$\mu_q(T_A)$	Natural mortality rate of adult female and male mosquitoes
C_R	Rate of release of sterile male mosquitoes

Month	Jan	Feb	Mar	Apr	May	Jun	Jul	Aug	Sep	Oct	Nov	Dec
Temperature (^{0}C)	24	26	25	23	21	20	20	21	21	22	21	22

Table 4.2: Mean Monthly Temperature (in ^{0}C) for Kipsamoite, Kenya for the Year 2019 (Lag, 2017).

Parameters	Values	Reference
ψ_E	65	(Afrane et al., 2005; Takken et al., 1998)
ϕ_E	0.4	(Afrane et al., 2005; Takken et al., 1998)
β	0.7	(Esteva and Yang, 2005)
ζ	0.000174	Estimated
η	0.75	(White et al., 2010)
C_R	10^4	Variable
δ_L	0.00005	Assumed
r	0.5	(Okuneye et al., 2019)

Table 4.3: Values of Temperature-independent Parameters of the Model (4.4.1).

REFERENCES

World health organization. draft global technical strategy. sixty-eighth world health assembly, march 20, 2015.

Kipsamoite monthly climate average, nandi hills district of kenya, 2017. URL https://www.worldweatheronline.com/nandi-weather-averages/rift-valley/ke.aspx.

Imgur. google's life science division to release 20 million infected mosquitoes in california, 2017. URL https://imgur.com/gallery/aMBAZ.

A. Abdelrazec and A. B. Gumel. Mathematical assessment of the role of temperature and rainfall on mosquito population dynamics. *Journal of mathematical biology*, 74(6):1351–1395, 2017.

Y. A. Afrane, B. W. Lawson, A. K. Githeko, and G. Yan. Effects of microclimatic changes caused by land use and land cover on duration of gonotrophic cycles of anopheles gambiae (diptera: Culicidae) in western kenya highlands. *Journal of medical entomology*, 42(6):974–980, 2005.

Aguiar. The dengue vaccine dilemma, 2018. URL http://www.thelancet.com/journals/laninf/article/PIIS1473-3099(18)30023-9/fulltext.

F. Agusto, A. Gumel, and P. Parham. Qualitative assessment of the role of temperature variations on malaria transmission dynamics. *Journal of Biological Systems*, 23(04):1550030, 2015.

A. Aldersley and L. J. Cator. Female resistance and harmonic convergence influence male mating success in aedes aegypti. *Scientific reports*, 9(1):1–12, 2019.

H. Alles, K. Mendis, and R. Carter. Malaria mortality rates in south asia and in africa: implications for malaria control. *Parasitology Today*, 14(9):369–375, 1998.

Alliance. The alliance for malaria prevention. "net mapping q2 2018", 2018. URL http://allianceformalariaprevention.com/net-mapping-project/.

H. Alout, B. Roche, R. K. Dabire, and A. Cohuet. Consequences of insecticide resistance on malaria transmission. *PLoS pathogens*, 13(9), 2017.

R. Anderson and R. May. *Population Biology of Infectious Diseases*, volume 2. Springer-Verlag, Berlin, Heilderberg, New York, 1982.

R. Anderson and R. May. *Infectious Disease of Humans, Dynamics and Control*, volume 2. Oxford University Press, 1991.

M. Andraud, N. Hens, C. Marais, and P. Beutels. Dynamic epidemiological models for dengue transmission: a systematic review of structural approaches. *PloS one*, 7(11), 2012a.

M. Andraud, N. Hens, C. Marais, and P. Beutels. Dynamic epidemiological models for dengue transmission: a systematic review of structural approaches. *PloS one*, 7(11), 2012b.

R. Anguelov, Y. Dumont, and J. Lubuma. Mathematical modeling of sterile insect technology for control of anopheles mosquito. *Computers & Mathematics with Applications*, 64(3):374–389, 2012.

S. Antinori, L. Galimberti, L. Milazzo, and M. Corbellino. Biology of human malaria plasmodia including plasmodium knowlesi. *Mediterranean journal of hematology and infectious diseases*, 4(1), 2012.

A. Asale, Y. Getachew, W. Hailesilassie, N. Speybroeck, L. Duchateau, and D. Yewhalaw. Evaluation of the efficacy of ddt indoor residual spraying and long-lasting insecticidal nets against insecticide resistant populations of anopheles arabiensis patton (diptera: Culicidae) from ethiopia using experimental huts. *Parasites & vectors*, 7(1):131, 2014.

E. A. Ashley and N. J. White. The duration of plasmodium falciparum infections. *Malaria journal*, 13(1):500, 2014.

A. N. Asidi, R. N'Guessan, R. A. Hutchinson, M. Traoré-Lamizana, P. Carnevale, and C. Curtis. Experimental hut comparisons of nets treated with carbamate or pyrethroid insecticides, washed or unwashed, against pyrethroid-resistant mosquitoes. *Medical and veterinary entomology*, 18(2):134–140, 2004.

A. N. Asidi, R. N'Guessan, A. A. Koffi, C. F. Curtis, J.-M. Hougard, F. Chandre, V. Corbel, F. Darriet, M. Zaim, and M. W. Rowland. Experimental hut evaluation of bednets treated with an organophosphate (chlorpyrifos-methyl) or a pyrethroid (lambdacyhalothrin) alone and in combination against insecticide-resistant anopheles gambiae and culex quinquefasciatus mosquitoes. *Malaria journal*, 4(1):25, 2005.

T. Bancroft. On the aetiology of dengue fever. *Australian Medical Gazette*, 25:17–18, 1906.

S. Barbosa and I. M. Hastings. The importance of modelling the spread of insecticide resistance in a heterogeneous environment: the example of adding synergists to bed nets. *Malaria journal*, 11(1):258, 2012.

A. C. Bartlett and R. T. Staten. The sterile insect release method and other genetic control strategies.

K. Bayili, S. N'do, M. Namountougou, R. Sanou, A. Ouattara, R. K. Dabiré, A. G. Ouédraogo, D. Malone, and A. Diabaté. Evaluation of efficacy of interceptor® g2, a long-lasting insecticide net coated with a mixture of chlorfenapyr and alpha-cypermethrin, against pyrethroid resistant anopheles gambiae sl in burkina faso. *Malaria journal*, 16(1):190, 2017.

M. N. Bayoh. *Studies on the development and survival of Anopheles gambiae sensu stricto at various temperatures and relative humidities*. PhD thesis, Durham University, 2001.

M. N. Bayoh and S. W. Lindsay. Effect of temperature on the development of the aquatic stages of anopheles gambiae sensu stricto (diptera: Culicidae). *Bulletin of entomological research*, 93(5):375–381, 2003.

M. N. Bayoh and S. W. Lindsay. Temperature-related duration of aquatic stages of the afrotropical malaria vector mosquito anopheles gambiae in the laboratory. *Medical and veterinary entomology*, 18 2:174–9, 2004.

G. Benelli, C. L. Jeffries, and T. Walker. Biological control of mosquito vectors: past, present, and future. *Insects*, 7(4):52, 2016.

S. Bhatt, D. Weiss, E. Cameron, D. Bisanzio, B. Mappin, U. Dalrymple, K. Battle, C. Moyes, A. Henry, P. Eckhoff, et al. The effect of malaria control on plasmodium falciparum in africa between 2000 and 2015. *Nature*, 526(7572):207–211, 2015.

P. L. Birget and J. C. Koella. A genetic model of the effects of insecticide-treated bed nets on the evolution of insecticide-resistance. *Evolution, medicine, and public health*, 2015(1):205–215, 2015a.

P. L. Birget and J. C. Koella. An epidemiological model of the effects of insecticide-treated bed nets on malaria transmission. *PloS one*, 10(12), 2015b.

K. W. Blayneh, A. B. Gumel, S. Lenhart, and T. Clayton. Backward bifurcation and optimal control in transmission dynamics of west nile virus. *Bulletin of mathematical biology*, 72(4):1006–1028, 2010.

S. Blower, T. Porco, and G. Darby. Predicting and preventing the emergence of antiviral drug resistance in hsv-2. *Nature medicine*, 4(6):673–678, 1998.

S. M. Blower and H. Dowlatabadi. Sensitivity and uncertainty analysis of complex models of disease transmission: an hiv model, as an example. *International Statistical Review/Revue Internationale de Statistique*, pages 229–243, 1994.

J.-F. Briere, P. Pracros, A.-Y. Le Roux, and J.-S. Pierre. A novel rate model of temperature-dependent development for arthropods. *Environmental Entomology*, 28(1):22–29, 1999.

T. Brinkhoff. City population, 2017. URL https://www.citypopulation.de/Mexico-Cities.html.

Z. S. Brown, K. L. Dickinson, and R. A. Kramer. Insecticide resistance and malaria vector control: the importance of fitness cost mechanisms in determining economically optimal control trajectories. *Journal of economic entomology*, 106(1):366–374, 2013.

D. S. Burke, A. Nisalak, D. E. Johnson, and R. M. Scott. A prospective study of dengue infections in bangkok. *The American journal of tropical medicine and hygiene*, 38(1):172–180, 1988.

L. Cai, S. Ai, and J. Li. Dynamics of mosquitoes populations with different strategies for releasing sterile mosquitoes. *SIAM Journal on Applied Mathematics*, 74(6): 1786–1809, 2014.

P. Cailly, A. Tran, T. Balenghien, G. L'Ambert, C. Toty, and P. Ezanno. A climate-driven abundance model to assess mosquito control strategies. *Ecological Modelling*, 227:7–17, 2012.

S. Camara, L. P. A. Alou, A. A. Koffi, Y. C. M. Clegban, J.-P. Kabran, F. M. Koffi, K. Koffi, and C. Pennetier. Efficacy of interceptor® g2, a new long-lasting insecticidal net against wild pyrethroid-resistant anopheles gambiae ss from côte d'ivoire: a semi-field trial. *Parasite*, 25, 2018.

M. R. Capeding, N. H. Tran, S. R. S. Hadinegoro, H. I. H. M. Ismail, T. Chotpitayasunondh, M. N. Chua, C. Q. Luong, K. Rusmil, D. N. Wirawan, R. Nallusamy, et al. Clinical efficacy and safety of a novel tetravalent dengue vaccine in healthy children in asia: a phase 3, randomised, observer-masked, placebo-controlled trial. *The Lancet*, 384(9951):1358–1365, 2014.

J. Cariboni, D. Gatelli, R. Liska, and A. Saltelli. The role of sensitivity analysis in ecological modelling. *Ecological modelling*, 203(1-2):167–182, 2007.

J. Carr. *Application of Centre Manifold Theory*. Springer-Verlag, 1981.

R. Carter and K. N. Mendis. Evolutionary and historical aspects of the burden of malaria. *Clinical microbiology reviews*, 15(4):564–594, 2002.

C. Castillo-Chavez and B. Song. Dynamical models of tuberculosis and their applications. *Mathematical Biosciences & Engineering*, 1(2):361, 2004.

L. J. Cator, P. A. Lynch, A. F. Read, and M. B. Thomas. Do malaria parasites manipulate mosquitoes? *Trends in parasitology*, 28(11):466–470, 2012.

CDC. Center for disease control and prevention. malaria biology, 2019a. URL https://www.cdc.gov/malaria/about/biology/mosquitoes/.

CDC. Dengue vaccine globally, 2019b. URL https://www.cdc.gov/dengue/prevention/dengue-vaccine.html.

F. Chandre, F. Darriet, S. Duchon, L. Finot, S. Manguin, P. Carnevale, and P. Guillet. Modifications of pyrethroid effects associated with kdr mutation in anopheles gambiae. *Medical and veterinary entomology*, 14(1):81–88, 2000.

D. L. Chao, S. B. Halstead, M. E. Halloran, and I. M. Longini Jr. Controlling dengue with vaccines in thailand. *PLoS Negl Trop Dis*, 6(10):e1876, 2012.

J. Charlwood, T. Smith, P. Billingsley, W. Takken, E. Lyimo, and J. Meuwissen. Survival and infection probabilities of anthropophagic anophelines from an area of high prevalence of plasmodium falciparum in humans. *Bulletin of Entomological Research*, 87(5):445–453, 1997.

N. Chitnis, T. Smith, and R. Steketee. A mathematical model for the dynamics of malaria in mosquitoes feeding on a heterogeneous host population. *Journal of Biological Dynamics*, 2(3):259–285, 2008.

G. Chowell, P. Diaz-Duenas, J. Miller, A. Alcazar-Velazco, J. Hyman, P. Fenimore, and C. Castillo-Chavez. Estimation of the reproduction number of dengue fever from spatial epidemic data. *Mathematical biosciences*, 208(2):571–589, 2007.

H.-N. Chung, S. D. Rodriguez, K. K. Gonzales, J. Vulcan, J. J. Cordova, S. Mitra, C. G. Adams, N. Moses-Gonzales, N. Tam, J. W. Cluck, et al. Toward implementation of mosquito sterile insect technique: the effect of storage conditions on survival of male aedes aegypti mosquitoes (diptera: Culicidae) during transport. *Journal of insect science*, 18(6):2, 2018.

N. Clements. *The Biology of Mosquitoes: Sensory, Reception, and Behaviour*. CABI Publishing, Eastbourne, 1999.

A. Cohuet, C. Harris, V. Robert, and D. Fontenille. Evolutionary forces on anopheles: what makes a malaria vector? *Trends in parasitology*, 26(3):130–136, 2010.

V. Corbel, F. Chandre, C. Brengues, M. Akogbéto, F. Lardeux, J. M. Hougard, and P. Guillet. Dosage-dependent effects of permethrin-treated nets on the behaviour of anopheles gambiae and the selection of pyrethroid resistance. *Malaria journal*, 3(1):22, 2004.

V. Corbel, J. Chabi, R. K. Dabiré, J. Etang, P. Nwane, O. Pigeon, M. Akogbeto, and J.-M. Hougard. Field efficacy of a new mosaic long-lasting mosquito net (permanet® 3.0) against pyrethroid-resistant malaria vectors: a multi centre study in western and central africa. *Malaria journal*, 9(1):113, 2010.

L. Coudeville and G. P. Garnett. Transmission dynamics of the four dengue serotypes in southern vietnam and the potential impact of vaccination. *PloS one*, 7(12), 2012.

D. A. Dame, C. F. Curtis, M. Q. Benedict, A. S. Robinson, and B. G. Knols. Historical applications of induced sterilisation in field populations of mosquitoes. *Malaria journal*, 8(2):S2, 2009.

A. Dao, A. Adamou, J. E. Crawford, J. M. Ribeiro, R. Gwadz, S. F. Traoré, T. Lehmann, et al. The distribution of hatching time in anopheles gambiae. *Malaria journal*, 5(1):19, 2006.

T. S. Detinova, D. Bertram, W. H. Organization, et al. *Age-grouping methods in Diptera of medical importance, with special reference to some vectors of malaria*. World Health Organization, 1962.

O. Diekmann, J. A. P. Heesterbeek, and J. A. Metz. On the definition and the computation of the basic reproduction ratio r 0 in models for infectious diseases in heterogeneous populations. *Journal of mathematical biology*, 28(4):365–382, 1990.

A. Djènontin, L. P. A. Alou, A. Koffi, B. Zogo, E. Duarte, R. N'Guessan, N. Moiroux, and C. Pennetier. Insecticidal and sterilizing effect of olyset duo®, a permethrin and pyriproxyfen mixture net against pyrethroid-susceptible and-resistant strains of anopheles gambiae ss: a release-recapture assay in experimental huts. *Parasite*, 22, 2015.

B. Djènontin, Moiroux and Cédric. Field efficacy of a new deltamethrin long lasting insecticidal net (lifenet®) against wild pyrethroid-resistant anopheles gambiae in benin. *Public Health*, 18, 2018.

T. T. T. Do, P. Martens, N. H. Luu, P. Wright, and M. Choisy. Climatic-driven seasonality of emerging dengue fever in hanoi, vietnam. *BMC public health*, 14(1): 1078, 2014.

A. M. Dondorp, F. Nosten, P. Yi, D. Das, A. P. Phyo, J. Tarning, K. M. Lwin, F. Ariey, W. Hanpithakpong, S. J. Lee, et al. Artemisinin resistance in plasmodium falciparum malaria. *New England Journal of Medicine*, 361(5):455–467, 2009.

A. M. Dondorp, C. I. Fanello, I. C. Hendriksen, E. Gomes, A. Seni, K. D. Chhaganlal, K. Bojang, R. Olaosebikan, N. Anunobi, K. Maitland, et al. Artesunate versus quinine in the treatment of severe falciparum malaria in african children (aquamat): an open-label, randomised trial. *The Lancet*, 376(9753):1647–1657, 2010.

Y. Dumont and F. Chiroleu. Vector control for the chikungunya disease. *Mathematical Biosciences & Engineering*, 7(2):313, 2010.

Y. Dumont and J. Tchuenche. Mathematical studies on the sterile insect technique for the chikungunya disease and aedes albopictus. *Journal of mathematical Biology*, 65(5):809–854, 2012.

H. J. Dyck VA and R. AS. *Sterile Insect Technique: Principles and Practice in Area-wide Integrated Pest Management*. Springer, 2005.

S. E. Eikenberry and A. B. Gumel. Mathematical modeling of climate change and malaria transmission dynamics: a historical review. *Journal of mathematical biology*, 77(4):857–933, 2018.

K. C. Ernst, S. O. Adoka, D. O. Kowuor, M. L. Wilson, and C. C. John. Malaria hotspot areas in a highland kenya site are consistent in epidemic and non-epidemic years and are associated with ecological factors. *Malaria journal*, 5(1):78, 2006.

L. Esteva and C. Vargas. Influence of vertical and mechanical transmission on the dynamics of dengue disease. *Math Biosci.*, 67:51–64, 2000.

L. Esteva and H. M. Yang. Mathematical model to assess the control of aedes aegypti mosquitoes by the sterile insect technique. *Mathematical biosciences*, 198(2):132–147, 2005.

C. Fanello, J. Kolaczinski, D. Conway, P. Carnevale, and C. Curtis. The kdr pyrethroid resistance gene in anopheles gambiae: tests of non-pyrethroid insecticides and a new detection method for the gene. *Parassitologia*, 41(1-3):323–326, 1999.

X. Feng, S. Ruan, Z. Teng, and K. Wang. Stability and backward bifurcation in a malaria transmission model with applications to the control of malaria in china. *Mathematical biosciences*, 266:52–64, 2015.

Z. Feng and J. X. Velasco-Hernández. Competitive exclusion in a vector-host model for the dengue fever. *Journal of mathematical biology*, 35(5):523–544, 1997.

N. M. Ferguson, I. Rodríguez-Barraquer, I. Dorigatti, L. Mier-y Teran-Romero, D. J. Laydon, and D. A. Cummings. Benefits and risks of the sanofi-pasteur dengue vaccine: Modeling optimal deployment. *Science*, 353(6303):1033–1036, 2016.

J. A. Filipe, E. M. Riley, C. J. Drakeley, C. J. Sutherland, and A. C. Ghani. Determination of the processes driving the acquisition of immunity to malaria using a mathematical transmission model. *PLoS computational biology*, 3(12), 2007.

F. Forouzannia and A. B. Gumel. Mathematical analysis of an age-structured model for malaria transmission dynamics. *Mathematical biosciences*, 247:80–94, 2014.

S. M. Garba and A. B. Gumel. Effect of cross-immunity on the transmission dynamics of two strains of dengue. *International Journal of Computer Mathematics*, 87(10): 2361–2384, 2010.

S. M. Garba, A. B. Gumel, and M. A. Bakar. Backward bifurcations in dengue transmission dynamics. *Mathematical biosciences*, 215(1):11–25, 2008.

B. Gates. We can eradicate malaria within a generation, 2016. URL https://www.gatesnotes.com/Malaria.

J. E. Gentile, S. S. Rund, and G. R. Madey. Modelling sterile insect technique to control the population of anopheles gambiae. *Malaria journal*, 14(1):92, 2015.

J. Gerardin, P. Eckhoff, and E. A. Wenger. Mass campaigns with antimalarial drugs: a modelling comparison of artemether-lumefantrine and dha-piperaquine with and without primaquine as tools for malaria control and elimination. *BMC infectious diseases*, 15(1):144, 2015.

P. W. Gething, D. L. Smith, A. P. Patil, A. J. Tatem, R. W. Snow, and S. I. Hay. Climate change and the global malaria recession. *Nature*, 465(7296):342–345, 2010.

P. W. Gething, A. P. Patil, D. L. Smith, C. A. Guerra, I. R. Elyazar, G. L. Johnston, A. J. Tatem, and S. I. Hay. A new world malaria map: Plasmodium falciparum endemicity in 2010. *Malaria journal*, 10(1):378, 2011.

P. W. Gething, D. C. Casey, D. J. Weiss, D. Bisanzio, S. Bhatt, E. Cameron, K. E. Battle, U. Dalrymple, J. Rozier, P. C. Rao, et al. Mapping plasmodium falciparum mortality in africa between 1990 and 2015. *New England Journal of Medicine*, 375 (25):2435–2445, 2016.

A. Githeko, A. Brandling-Bennett, M. Beier, F. Atieli, M. Owaga, and F. Collins. The reservoir of plasmodium falciparum malaria in a holoendemic area of western kenya. *Transactions of the Royal Society of Tropical Medicine and Hygiene*, 86(4): 355–358, 1992.

K. D. Glunt, M. Coetzee, S. Huijben, A. A. Koffi, P. A. Lynch, R. N'Guessan, W. A. Oumbouke, E. D. Sternberg, and M. B. Thomas. Empirical and theoretical investigation into the potential impacts of insecticide resistance on the effectiveness of insecticide-treated bed nets. *Evolutionary applications*, 11(4):431–441, 2018.

W. Gu and R. J. Novak. Predicting the impact of insecticide-treated bed nets on malaria transmission: the devil is in the detail. *Malaria Journal*, 8(1):256, 2009.

D. Gubler and G. Kuno. *Dengue and Dengue Hemorrhagic Fever*. CAB International, London, 1997.

S. R. Hadinegoro, J. L. Arredondo-García, M. R. Capeding, C. Deseda, T. Chotpitayasunondh, R. Dietze, H. Hj Muhammad Ismail, H. Reynales, K. Limkittikul, D. M. Rivera-Medina, et al. Efficacy and long-term safety of a dengue vaccine in regions of endemic disease. *New England Journal of Medicine*, 373(13):1195–1206, 2015.

J. Hale and S. Verduyn Lunel. *Introduction to Functional Differential Equations*. Springer, New York, 1993.

S. Halstead, S. Nimmannitya, and S. Cohen. Observations related to pathogenesis of dengue hemorrhagic fever. iv. relation of disease severity to antibody response and virus recovered. *The Yale journal of biology and medicine*, 42(5):311, 1970.

S. B. Halstead. Immune enhancement of viral infection. In *Immunity and Concomitant Immunity in Infectious Diseases*, volume 31, pages 301–364. Karger Publishers, 1982.

W. A. Hawley, F. O. TER KUILE, R. S. Steketee, B. L. Nahlen, D. J. Terlouw, J. E. Gimnig, Y. P. Shi, J. M. Vulule, J. A. Alaii, A. W. Hightower, et al. Implications of the western kenya permethrin-treated bed net study for policy, program implementation, and future research. *The American journal of tropical medicine and hygiene*, 68(4_suppl):168–173, 2003.

J. Hemingway, H. Ranson, A. Magill, J. Kolaczinski, C. Fornadel, J. Gimnig, M. Coetzee, F. Simard, D. K. Roch, C. K. Hinzoumbe, et al. Averting a malaria disaster: will insecticide resistance derail malaria control? *The Lancet*, 387(10029):1785–1788, 2016.

H. W. Hethcote. The mathematics of infectious diseases. *SIAM review*, 42(4):599–653, 2000.

S. Hews, S. Eikenberry, J. D. Nagy, and Y. Kuang. Rich dynamics of a hepatitis b viral infection model with logistic hepatocyte growth. *Journal of mathematical biology*, 60(4):573–590, 2010.

Y. E.-S. Himeidan and E. Kweka. Malaria in east african highlands during the past 30 years: impact of environmental changes. *Frontiers in physiology*, 3:315, 2012.

T. J. Hladish, C. A. Pearson, D. L. Chao, D. P. Rojas, G. L. Recchia, H. Gómez-Dantés, M. E. Halloran, J. R. Pulliam, and I. M. Longini. Projected impact of dengue vaccination in yucatán, mexico. *PLoS neglected tropical diseases*, 10(5), 2016.

B. R. Holzer, M. Egger, T. Teuscher, S. Koch, D. M. Mboya, and G. D. Smith. Childhood anemia in africa: to transfuse or not transfuse? *Acta tropica*, 55(1-2): 47–51, 1993.

W. Horsfall. *Mosquitoes: Their Bionomics and Relation to Disease*. Hafner Publishing Company, New York, 1955.

M. B. Hoshen and A. P. Morse. A weather-driven model of malaria transmission. *Malaria journal*, 3(1):32, 2004.

M. Huang, X. Song, and J. Li. Modelling and analysis of impulsive releases of sterile mosquitoes. *Journal of biological dynamics*, 11(1):147–171, 2017.

S. Huijben and K. P. Paaijmans. Putting evolution in elimination: winning our ongoing battle with evolving malaria mosquitoes and parasites. *Evolutionary applications*, 11(4):415–430, 2018.

N. Hussaini, J. M. Lubuma, K. Barley, and A. Gumel. Mathematical analysis of a model for avl–hiv co-endemicity. *Mathematical biosciences*, 271:80–95, 2016.

Iboi, Gumel, and Taylor. Mathematical assessment of the impact of periodic release of sterile male mosquitoes and seasonality on the population abundance of malaria mosquitoes. 2019a.

E. Iboi, K. Okuneye, O. Sharomi, and A. Gumel. Comments on "a mathematical study to control visceral leishmaniasis: An application to south sudans. *Bulletin of mathematical biology*, 80(4):825–839, 2018.

E. Iboi, Gumel, Huijben, and Paaijmans. Long-lasting insecticidal nets and the quest for malaria eradication: A mathematical modeling approach. 2019b.

E. A. Iboi and A. B. Gumel. Mathematical assessment of the role of dengvaxia vaccine on the transmission dynamics of dengue serotypes. *Mathematical biosciences*, 304: 25–47, 2018.

S. S. Imbahale, K. P. Paaijmans, W. R. Mukabana, R. Van Lammeren, A. K. Githeko, and W. Takken. A longitudinal study on anopheles mosquito larval abundance in distinct geographical and environmental settings in western kenya. *Malaria journal*, 10(1):81, 2011.

M. Imwong, K. Suwannasin, C. Kunasol, K. Sutawong, M. Mayxay, H. Rekol, F. M. Smithuis, T. M. Hlaing, K. M. Tun, R. W. van der Pluijm, et al. The spread of artemisinin-resistant plasmodium falciparum in the greater mekong subregion: a molecular epidemiology observational study. *The Lancet Infectious Diseases*, 17(5): 491–497, 2017.

irmapper. The dengue vaccine dilemma, 2019. URL http://anopheles.irmapper.com/.

D. J. Rankin and H. Kokko. Do males matter? the role of males in population dynamics. *Oikos*, 116(2):335–348, 2007.

G. M. Jeffery and D. E. Eyles. The duration in the human host of infections with a panama strain of plasmodium falciparum. *The American journal of tropical medicine and hygiene*, 3(2):219–224, 1954.

J. Jiang, Z. Qiu, J. Wu, and H. Zhu. Threshold conditions for west nile virus outbreaks. *Bulletin of mathematical biology*, 71(3):627–647, 2009.

G. L. Johnston, D. L. Smith, and D. A. Fidock. Malaria's missing number: calculating the human component of r0 by a within-host mechanistic model of plasmodium falciparum infection and transmission. *PLoS computational biology*, 9(4), 2013.

B. Kabula, W. Kisinza, P. Tungu, C. Ndege, B. Batengana, D. Kollo, R. Malima, J. Kafuko, M. Mohamed, and S. Magesa. Co-occurrence and distribution of east (l1014s) and west (l1014f) a frican knock-down resistance in a nopheles gambiae sensu lato population of t anzania. *Tropical Medicine & International Health*, 19 (3):331–341, 2014.

J. C. Kamgang and G. Sallet. Computation of threshold conditions for epidemiological models and global stability of the disease-free equilibrium (dfe). *Mathematical biosciences*, 213(1):1–12, 2008.

I. Kawaguchi, A. Sasaki, and M. Boots. Why are dengue virus serotypes so distantly related? enhancement and limiting serotype similarity between dengue virus strains. *Proceedings of the Royal Society of London. Series B: Biological Sciences*, 270(1530):2241–2247, 2003.

G. K. Ketoh, K. M. Ahadji-Dabla, J. Chabi, A. D. Amoudji, G. Y. Apetogbo, F. Awokou, and I. A. Glitho. Efficacy of two pbo long lasting insecticidal nets against natural populations of anopheles gambiae sl in experimental huts, kolokopé, togo. *PloS one*, 13(7), 2018.

G. F. Killeen and T. A. Smith. Exploring the contributions of bed nets, cattle, insecticides and excitorepellency to malaria control: a deterministic model of mosquito host-seeking behaviour and mortality. *Transactions of the Royal Society of Tropical Medicine and Hygiene*, 101(9):867–880, 2007.

G. F. Killeen, N. Chitnis, S. J. Moore, and F. O. Okumu. Target product profile choices for intra-domiciliary malaria vector control pesticide products: repel or kill? *Malaria journal*, 10(1):207, 2011.

I. Kleinschmidt, J. Bradley, T. B. Knox, A. P. Mnzava, H. T. Kafy, C. Mbogo, B. A. Ismail, J. D. Bigoga, A. Adechoubou, K. Raghavendra, et al. Implications of insecticide resistance for malaria vector control with long-lasting insecticidal nets: a who-coordinated, prospective, international, observational cohort study. *The Lancet infectious diseases*, 18(6):640–649, 2018.

E. F. Knipling. *The basic principles of insect population suppression and management*. Number 512. US Department of Agriculture, 1979.

A. A. Koffi, L. P. A. Alou, A. Djenontin, J.-P. K. Kabran, Y. Dosso, A. Kone, N. Moiroux, and C. Pennetier. Efficacy of olyset® duo, a permethrin and pyriproxyfen mixture net against wild pyrethroid-resistant anopheles gambiae ss from côte d'ivoire: an experimental hut trial. *Parasite*, 22, 2015.

E. J. Kweka, L. J. Lyaruu, and A. M. Mahande. Efficacy of permanet® 3.0 and permanet® 2.0 nets against laboratory-reared and wild anopheles gambiae sensu lato populations in northern tanzania. *Infectious diseases of poverty*, 6(1):11, 2017.

J. L. Kyle and E. Harris. Global spread and persistence of dengue. *Annu. Rev. Microbiol.*, 62:71–92, 2008.

V. Lakshmikantham and S. Leela. *Differential and Integral Inequalities: Theory and Applications*. Academic Press, New York, 1969.

B. D. Lakshmikantham V and S. PS. *Theory of Impulsive Differential Equations*. Word Scientific Publishing, 1989.

L. Lambrechts, K. P. Paaijmans, T. Fansiri, L. B. Carrington, L. D. Kramer, M. B. Thomas, and T. W. Scott. Impact of daily temperature fluctuations on dengue virus transmission by aedes aegypti. 108(18):7460–7465, 2011. doi: 10.1073/pnas.1101377108.

J. LaSalle and S. Lefschetz. *The Stability of Dynamical Systems*. SIAM, Philadelphia, 1976.

A. Le Menach, S. Takala, F. E. McKenzie, A. Perisse, A. Harris, A. Flahault, and D. L. Smith. An elaborated feeding cycle model for reductions in vectorial capacity of night-biting mosquitoes by insecticide-treated nets. *Malaria journal*, 6(1):10, 2007.

L. Levitz, M. Janko, K. Mwandagalirwa, K. L. Thwai, J. L. Likwela, A. K. Tshefu, M. Emch, and S. R. Meshnick. Effect of individual and community-level bed net usage on malaria prevalence among under-fives in the democratic republic of congo. *Malaria journal*, 17(1):39, 2018.

M. Lewis, J. Rencławowicz, and P. Van den Driessche. Traveling waves and spread rates for a west nile virus model. *Bulletin of mathematical biology*, 68(1):3–23, 2006.

J. Lines, T. Wilkes, and E. Lyimo. Human malaria infectiousness measured by age-specific sporozoite rates in anopheles gambiae in tanzania. *Parasitology*, 102(2): 167–177, 1991.

D. E. Loy, W. Liu, Y. Li, G. H. Learn, L. J. Plenderleith, S. A. Sundararaman, P. M. Sharp, and B. H. Hahn. Out of africa: origins and evolution of the human malaria parasites plasmodium falciparum and plasmodium vivax. *International journal for parasitology*, 47(2-3):87–97, 2017.

Y. Lubell, A. Dondorp, P. J. Guérin, T. Drake, S. Meek, E. Ashley, N. P. Day, N. J. White, and L. J. White. Artemisinin resistance–modelling the potential human and economic costs. *Malaria journal*, 13(1):452, 2014.

J. Lyons. Mosquito-borne diseases, 2015. URL https://www.rentokil.com/blog/mosquito-borne-diseases/#.XlpgS_R7nIU.

G. Macdonald. *The Epidemiology and Control of Malaria*. Oxford University Press, 1957.

R. Malima, P. K. Tungu, V. Mwingira, C. Maxwell, S. M. Magesa, H. Kaur, M. J. Kirby, and M. Rowland. Evaluation of the long-lasting insecticidal net interceptor ln: laboratory and experimental hut studies against anopheline and culicine mosquitoes in northeastern tanzania. *Parasites & vectors*, 6(1):296, 2013.

R. C. Malima, S. M. Magesa, P. K. Tungu, V. Mwingira, F. S. Magogo, W. Sudi, F. W. Mosha, C. F. Curtis, C. Maxwell, and M. Rowland. An experimental hut evaluation of olyset® nets against anopheline mosquitoes after seven years use in tanzanian villages. *Malaria journal*, 7(1):38, 2008.

S. Marino, I. B. Hogue, C. J. Ray, and D. E. Kirschner. A methodology for performing global uncertainty and sensitivity analysis in systems biology. *Journal of theoretical biology*, 254(1):178–196, 2008.

K. Marsh. Malaria disaster in africa. *The Lancet*, 352(9132):924, 1998.

J. P. Messina, O. J. Brady, T. W. Scott, C. Zou, D. M. Pigott, K. A. Duda, S. Bhatt, L. Katzelnick, R. E. Howes, K. E. Battle, et al. Global spread of dengue virus types: mapping the 70 year history. *Trends in microbiology*, 22(3):138–146, 2014.

Mike. Cambridge university. medical entomology for students, third edition - mike w. introduction to mosquitoes (culicidae), 2008. URL http://assets.cambridge.org/97805215/47758/excerpt/9780521547758_excerpt.pdf.

N. Minakawa, C. M. Mutero, J. I. Githure, J. C. Beier, and G. Yan. Spatial distribution and habitat characterization of anopheline mosquito larvae in western kenya. *The American journal of tropical medicine and hygiene*, 61(6):1010–1016, 1999.

N. Minakawa, G. Sonye, M. Mogi, and G. Yan. Habitat characteristics of anopheles gambiae s.s. larvae in a kenyan highland. *Medical and Veterinary Entomology*, 18 (3):301–305, 2004.

N. Minakawa, S. Munga, F. Atieli, E. Mushinzimana, G. Zhou, A. K. Githeko, and G. Yan. Spatial distribution of anopheline larval habitats in western kenyan highlands: effects of land cover types and topography. *The American journal of tropical medicine and hygiene*, 73(1):157–165, 2005.

J. Mohammed-Awel and E. Numfor. Optimal insecticide-treated bed-net coverage and malaria treatment in a malaria-hiv co-infection model. *Journal of biological dynamics*, 11(sup1):160–191, 2017.

M. Mohammed-Awel, Agusto and Gumel. Mathematical assessment of the role of vector insecticide resistance and feeding/resting behavior on malaria transmission dynamics: optimal control analysis. *Infectious Disease Modelling*, 3:301–321, 2018.

N. G. Morales, M. Núñez-López, J. Ramos-Castañeda, and J. Velasco-Hernández. Transmission dynamics of two dengue serotypes with vaccination scenarios. *Mathematical biosciences*, 287:54–71, 2017.

E. A. Mordecai, K. P. Paaijmans, L. R. Johnson, C. Balzer, T. Ben-Horin, E. de Moor, A. McNally, S. Pawar, S. J. Ryan, T. C. Smith, et al. Optimal temperature for malaria transmission is dramatically lower than previously predicted. *Ecology letters*, 16(1):22–30, 2013.

G. Munhenga, B. D. Brooke, J. R. Gilles, K. Slabbert, A. Kemp, L. C. Dandalo, O. R. Wood, L. N. Lobb, D. Govender, M. Renke, et al. Mating competitiveness of sterile genetic sexing strain males (gama) under laboratory and semi-field conditions: steps towards the use of the sterile insect technique to control the major malaria vector anopheles arabiensis in south africa. *Parasites & vectors*, 9(1):122, 2016.

T. K. Mutabingwa. Artemisinin-based combination therapies (acts): best hope for malaria treatment but inaccessible to the needy! *Acta tropica*, 95(3):305–315, 2005.

J. A. Nájera, M. González-Silva, and P. L. Alonso. Some lessons for the future from the global malaria eradication programme (1955–1969). *PLoS medicine*, 8(1), 2011.

R. N'Guessan, F. Darriet, J. Doannio, F. Chandre, and P. Carnevale. Olyset net® efficacy against pyrethroid-resistant anopheles gambiae and culex quinquefasciatus after 3 years' field use in côte d'ivoire. *Medical and veterinary entomology*, 15(1): 97–104, 2001.

C. Ngufor, R. N'Guessan, P. Boko, A. Odjo, E. Vigninou, A. Asidi, M. Akogbeto, and M. Rowland. Combining indoor residual spraying with chlorfenapyr and long-lasting insecticidal bed nets for improved control of pyrethroid-resistant anopheles gambiae: an experimental hut trial in benin. *Malaria journal*, 10(1):343, 2011.

C. Ngufor, R. N'Guessan, J. Fagbohoun, A. Odjo, D. Malone, M. Akogbeto, and M. Rowland. Olyset duo®(a pyriproxyfen and permethrin mixture net): an experimental hut trial against pyrethroid resistant anopheles gambiae and culex quinquefasciatus in southern benin. *PloS one*, 9(4), 2014.

C. Ngufor, R. N'Guessan, J. Fagbohoun, D. Todjinou, A. Odjo, D. Malone, H. Ismail, M. Akogbeto, and M. Rowland. Efficacy of the olyset duo net against insecticide-resistant mosquito vectors of malaria. *Science translational medicine*, 8 (356):356ra121–356ra121, 2016.

A. M. Niger and A. B. Gumel. Mathematical analysis of the role of repeated exposure on malaria transmission dynamics. *Differential Equations and Dynamical Systems*, 16(3):251–287, 2008.

C. Noble, J. Olejarz, K. M. Esvelt, G. M. Church, and M. A. Nowak. Evolutionary dynamics of crispr gene drives. *Science advances*, 3(4):e1601964, 2017.

R. N'Guessan, V. Corbel, M. Akogbéto, and M. Rowland. Reduced efficacy of insecticide-treated nets and indoor residual spraying for malaria control in pyrethroid resistance area, benin. *Emerging infectious diseases*, 13(2):199, 2007.

R. N'Guessan, A. Asidi, P. Boko, A. Odjo, M. Akogbeto, O. Pigeon, and M. Rowland. An experimental hut evaluation of permanet® 3.0, a deltamethrin—piperonyl butoxide combination net, against pyrethroid-resistant anopheles gambiae and culex quinquefasciatus mosquitoes in southern benin. *Transactions of the Royal Society of Tropical Medicine and Hygiene*, 104(12):758–765, 2010.

F. O. Okumu and S. J. Moore. Combining indoor residual spraying and insecticide-treated nets for malaria control in africa: a review of possible outcomes and an outline of suggestions for the future. *Malaria journal*, 10(1):208, 2011.

F. O. Okumu, S. S. Kiware, S. J. Moore, and G. F. Killeen. Mathematical evaluation of community level impact of combining bed nets and indoor residual spraying upon malaria transmission in areas where the main vectors are anopheles arabiensis mosquitoes. *Parasites & vectors*, 6(1):17, 2013.

K. Okuneye and A. B. Gumel. Analysis of a temperature-and rainfall-dependent model for malaria transmission dynamics. *Mathematical biosciences*, 287:72–92, 2017.

K. Okuneye, S. E. Eikenberry, and A. B. Gumel. Weather-driven malaria transmission model with gonotrophic and sporogonic cycles. *Journal of biological dynamics*, 13 (sup1):288–324, 2019.

M. Ouji, J.-M. Augereau, L. Paloque, and F. Benoit-Vical. Plasmodium falciparum resistance to artemisinin-based combination therapies: A sword of damocles in the path toward malaria elimination. *Parasite*, 25, 2018.

R. M. Oxborough, J. Kitau, J. Matowo, E. Feston, R. Mndeme, F. W. Mosha, and M. W. Rowland. Itn mixtures of chlorfenapyr (pyrrole) and alphacypermethrin (pyrethroid) for control of pyrethroid resistant anopheles arabiensis and culex quinquefasciatus. *PLoS One*, 8(2), 2013.

K. P. Paaijmans, S. Blanford, A. S. Bell, J. I. Blanford, A. F. Read, and M. B. Thomas. Influence of climate on malaria transmission depends on daily temperature variation. 107(34):15135–15139, 2010. doi: 10.1073/pnas.1006422107.

P. E. Parham and E. Michael. Modeling the effects of weather and climate change on malaria transmission. *Environmental health perspectives*, 118(5):620–626, 2010.

P. B. Patil, B. Niranjan Reddy, K. Gorman, K. Seshu Reddy, S. R. Barwale, U. B. Zehr, D. Nimmo, N. Naish, and L. Alphey. Mating competitiveness and life-table comparisons between transgenic and indian wild-type aedes aegypti l. *Pest management science*, 71(7):957–965, 2015.

L. M. Paul, E. R. Carlin, M. M. Jenkins, A. L. Tan, C. M. Barcellona, C. O. Nicholson, S. F. Michael, and S. Isern. Dengue virus antibodies enhance zika virus infection. *Clinical & translational immunology*, 5(12):e117, 2016.

C. Pennetier, A. Bouraima, F. Chandre, M. Piameu, J. Etang, M. Rossignol, I. Sidick, B. Zogo, M.-N. Lacroix, R. Yadav, et al. Efficacy of olyset® plus, a new long-lasting insecticidal net incorporating permethrin and piperonil-butoxide against multi-resistant malaria vectors. *PLoS One*, 8(10), 2013.

C. N. Podder and A. B. Gumel. Qualitative dynamics of a vaccination model for hsv-2. *IMA Journal of Applied Mathematics*, 75(1):75–107, 2010.

S. Polwiang. The seasonal reproduction number of dengue fever: impacts of climate on transmission. *PeerJ*, 3:e1069, 2015.

N. Protopopoff, J. F. Mosha, E. Lukole, J. D. Charlwood, A. Wright, C. D. Mwalimu, A. Manjurano, F. W. Mosha, W. Kisinza, I. Kleinschmidt, et al. Effectiveness of a long-lasting piperonyl butoxide-treated insecticidal net and indoor residual spray interventions, separately and together, against malaria transmitted by pyrethroid-resistant mosquitoes: a cluster, randomised controlled, two-by-two factorial design trial. *The Lancet*, 391(10130):1577–1588, 2018.

S. Randriamaherijaona, O. J. BriŰt, S. Boyer, A. Bouraima, R. N'Guessan, C. Rogier, and V. Corbel. Do holes in long-lasting insecticidal nets compromise their efficacy against pyrethroid resistant anopheleságambiae and culexáquinquefasciatus? results from a release–recapture study in experimental huts. *Malaria journal*, 14(1): 332, 2015.

N. G. Reich, S. Shrestha, A. A. King, P. Rohani, J. Lessler, S. Kalayanarooj, I.-K. Yoon, R. V. Gibbons, D. S. Burke, and D. A. Cummings. Interactions between serotypes of dengue highlight epidemiological impact of cross-immunity. *Journal of The Royal Society Interface*, 10(86):20130414, 2013.

H. Reyburn, R. Mbatia, C. Drakeley, J. Bruce, I. Carneiro, R. Olomi, J. Cox, W. Nkya, M. Lemnge, B. M. Greenwood, et al. Association of transmission intensity and age with clinical manifestations and case fatality of severe plasmodium falciparum malaria. *Jama*, 293(12):1461–1470, 2005.

L. S. Rickman, T. R. Jones, G. W. Long, S. Paparello, I. Schneider, C. F. Paul, R. L. Beaudoin, and S. L. Hoffman. Plasmodium falciparum-infected anopheles stephensi inconsistently transmit malaria to humans. *The American journal of tropical medicine and hygiene*, 43(5):441–445, 1990.

I. Rodriguez-Barraquer, L. Mier-y Teran-Romero, I. B. Schwartz, D. S. Burke, and D. A. Cummings. Potential opportunities and perils of imperfect dengue vaccines. *Vaccine*, 32(4):514–520, 2014.

W. Sama, G. Killeen, and T. Smith. Estimating the duration of plasmodium falciparum infection from trials of indoor residual spraying. *The American journal of tropical medicine and hygiene*, 70(6):625–634, 2004.

T. W. Scott, P. H. Amerasinghe, A. C. Morrison, L. H. Lorenz, G. G. Clark, D. Strickman, P. Kittayapong, and J. D. Edman. Longitudinal studies of aedes aegypti (diptera: Culicidae) in thailand and puerto rico: blood feeding frequency. *Journal of medical entomology*, 37(1):89–101, 2000.

E. SE and G. AB. *Mathematics of Malaria and Climate Change. Book Chapter in Mathematics of Planet Earth: Protecting Our Planet, Learning from the Past, Safeguarding the Future*. Springer International Publishing AG, 2019.

C. Shekhar. Deadly dengue: new vaccines promise to tackle this escalating global menace. *Chemistry & biology*, 14(8):871–872, 2007.

M. E. Sinka, M. J. Bangs, S. Manguin, M. Coetzee, C. M. Mbogo, J. Hemingway, A. P. Patil, W. H. Temperley, P. W. Gething, C. W. Kabaria, et al. The dominant anopheles vectors of human malaria in africa, europe and the middle east: occurrence data, distribution maps and bionomic précis. *Parasites & vectors*, 3(1):117, 2010.

D. L. Smith, S. I. Hay, A. M. Noor, and R. W. Snow. Predicting changing malaria risk after expanded insecticide-treated net coverage in africa. *Trends in parasitology*, 25 (11):511–516, 2009.

C. M. Stone. Transient population dynamics of mosquitoes during sterile male releases: modelling mating behaviour and perturbations of life history parameters. *PloS one*, 8(9), 2013.

W. Takken, M. Klowden, and G. Chambers. Effect of body size on host seeking and blood meal utilization in anopheles gambiae sensu stricto (diptera: Culicidae): the disadvantage of being small. *Journal of medical entomology*, 35(5):639–645, 1998.

R. C. Thomé, H. M. Yang, and L. Esteva. Optimal control of aedes aegypti mosquitoes by the sterile insect technique and insecticide. *Mathematical Biosciences*, 223(1): 12–23, 2010.

K. Toe, P. Müller, A. Badolo, A. Traore, N. Sagnon, R. Dabiré, and H. Ranson. Do bednets including piperonyl butoxide offer additional protection against populations of anopheles gambiae sl. that are highly resistant to pyrethroids? an experimental hut evaluation in burkina fasov. *Medical and veterinary entomology*, 32(4): 407–416, 2018.

P. Tungu, S. Magesa, C. Maxwell, R. Malima, D. Masue, W. Sudi, J. Myamba, O. Pigeon, and M. Rowland. Evaluation of permanet 3.0 a deltamethrin-pbo combination net against anopheles gambiae and pyrethroid resistant culex quinquefasciatus mosquitoes: an experimental hut trial in tanzania. *Malaria Journal*, 9(1):21, 2010.

P. van den Driessche and J. Watmough. Reproduction numbers and sub-threshold endemic equilibria for compartmental models of disease transmission. *Mathematical biosciences*, 180(1-2):29–48, 2002.

L. Villar, G. H. Dayan, J. L. Arredondo-García, D. M. Rivera, R. Cunha, C. Deseda, H. Reynales, M. S. Costa, J. O. Morales-Ramírez, G. Carrasquilla, et al. Efficacy of a tetravalent dengue vaccine in children in latin america. *New England Journal of Medicine*, 372(2):113–123, 2015.

H. Wan and H. Zhu. The backward bifurcation in compartmental models for west nile virus. *Mathematical Biosciences*, 227(1):20–28, 2010.

N. White, F. Nosten, S. Looareesuwan, W. Watkins, K. Marsh, R. Snow, G. Kokwaro, J. Ouma, T. Hien, M. Molyneux, et al. Averting a malaria disaster. *The Lancet*, 353(9168):1965–1967, 1999.

S. M. White, P. Rohani, and S. M. Sait. Modelling pulsed releases for sterile insect techniques: fitness costs of sterile and transgenic males and the effects on mosquito dynamics. *Journal of Applied Ecology*, 47(6):1329–1339, 2010.

WHO. World health organization. world malaria report 2012. geneva, switzerland, 2012.

WHO. World health organization. world malaria report 2015, 2015a. URL http://www.who.int/malaria/publications/world-malaria-report-2015/report/en/.

WHO. World health organization. global technical strategy for malaria 2016-2030, 2015b. URL http://www.who.int/malaria/publications/atoz/9789241564991/en/.

WHO. World health organization. global technical strategy for malaria 2016-2030, ed., world health organization, geneva, 2015, 2015c.

WHO. World health organization. world malaria report 2016, 2016. URL http://apps.who.int/iris/bitstream/10665/252038/1/9789241511711-eng.pdf?ua=1.

WHO. World health organization. malaria media center:fact sheet, updated april 2017, 2017a. URL http://www.who.int/mediacentre/factsheets/fs094/en/.

WHO. World health organization. global insecticide resistance database, 2017b. URL https://www.who.int/malaria/areas/vector_control/en/.

WHO. World health organization.achieving and maintaining universal coverage with long-lasting insecticidal nets for malaria control, ed., world health organization, geneva, 2017, 2017c.

WHO. World health organization. who recommended insecticides for indoor residual spraying against malaria vectors, 2018a. URL https://www.who.int/neglected_diseases/vector_ecology/vector-control/Insecticides_IRS_22_September_2018.pdf?ua=1.

WHO. World health organization. world malaria day 2018: Ready to beat malaria, 2018b. URL https://www.who.int/malaria/media/world-malaria-day-2018/en/.

WHO. Dengue and severe dengue, 2019. URL https://www.who.int/en/news-room/fact-sheets/detail/dengue-and-severe-dengue.

WHO et al. Dengue vaccine: Who position paper, july 2016–recommendations. *Vaccine*, 35(9):1200–1201, 2017.

D. W. Willis and N. Hamon. Eliminating malaria by 2040 among agricultural households in africa: potential impact on health, labor productivity, education and gender equality. *Gates open research*, 2, 2018.

P.-C. Wu, J.-G. Lay, H.-R. Guo, C.-Y. Lin, S.-C. Lung, and H.-J. Su. Higher temperature and urbanization affect the spatial patterns of dengue fever transmission in subtropical taiwan. *Science of the total Environment*, 407(7):2224–2233, 2009.

L. Yakob and T. Walker. Zika virus outbreak in the americas: the need for novel mosquito control methods. *The Lancet Global Health*, 4(3):e148–e149, 2016.

Y. Yang, Y. Xiao, and J. Wu. Pulse hiv vaccination: feasibility for virus eradication and optimal vaccination schedule. *Bulletin of mathematical biology*, 75(5):725–751, 2013.

S. Yeung, W. Pongtavornpinyo, I. M. Hastings, A. J. Mills, and N. J. White. Antimalarial drug resistance, artemisinin-based combination therapy, and the contribution of modeling to elucidating policy choices. *The American journal of tropical medicine and hygiene*, 71(2_suppl):179–186, 2004.

X. Zheng, D. Zhang, Y. Li, C. Yang, Y. Wu, X. Liang, Y. Liang, X. Pan, L. Hu, Q. Sun, et al. Incompatible and sterile insect techniques combined eliminate mosquitoes. *Nature*, 572(7767):56–61, 2019.

APPENDIX A

NEXT GENERATION MATRICES FOR MODEL (2.4.1)

$$F_1 = \begin{bmatrix} 0 & 0 & 0 & 0 & 0 & 0 & 0 & \frac{\beta_H b_M S^*_{UH}}{N^*_H} & 0 \\ 0 & 0 & 0 & 0 & 0 & 0 & 0 & 0 & 0 \\ 0 & 0 & 0 & 0 & 0 & 0 & 0 & 0 & 0 \\ 0 & 0 & 0 & 0 & 0 & 0 & 0 & 0 & 0 \\ 0 & 0 & 0 & 0 & 0 & 0 & 0 & 0 & \frac{\beta_H b_M S^*_{UH}}{N^*_H} \\ 0 & 0 & 0 & 0 & 0 & 0 & 0 & 0 & 0 \\ 0 & 0 & 0 & 0 & 0 & 0 & 0 & 0 & 0 \\ 0 & 0 & 0 & 0 & 0 & 0 & 0 & 0 & 0 \\ 0 & 0 & 0 & 0 & 0 & 0 & 0 & \frac{\beta_H b_M (1-\varepsilon_1) S^*_{VH}}{N^*_H} & 0 \end{bmatrix},$$

$$F_2 = \begin{bmatrix} 0 & 0 & 0 & 0 & 0 & 0 & 0 & 0 & 0 \\ 0 & 0 & 0 & 0 & 0 & 0 & 0 & 0 & 0 \\ 0 & 0 & 0 & 0 & 0 & 0 & 0 & 0 & 0 \\ 0 & 0 & 0 & 0 & 0 & 0 & 0 & 0 & 0 \\ 0 & 0 & 0 & 0 & 0 & 0 & 0 & 0 & 0 \\ 0 & 0 & 0 & 0 & 0 & 0 & 0 & 0 & 0 \\ 0 & 0 & 0 & 0 & 0 & 0 & 0 & 0 & 0 \\ 0 & \frac{\beta_M b_M S^*_M}{N^*_H} & 0 & \frac{\beta_H b_M \theta_{12} S^*_M}{N^*_H} & 0 & 0 & 0 & 0 & 0 \\ 0 & 0 & 0 & 0 & 0 & \frac{\beta_M b_M S^*_M}{N^*_H} & 0 & \frac{\beta_M b_M \theta_{21} S^*_M}{N^*_H} & 0 \end{bmatrix},$$

$$F_3 = \begin{bmatrix} 0 & 0 & 0 & 0 & 0 & 0 & 0 & 0 & 0 \\ 0 & 0 & 0 & 0 & 0 & 0 & 0 & 0 & 0 \\ 0 & 0 & 0 & 0 & 0 & 0 & 0 & 0 & 0 \\ 0 & 0 & 0 & 0 & 0 & 0 & 0 & 0 & \frac{\beta_H b_M (1-\varepsilon_2) S^*_{VH}}{N_H} \\ 0 & 0 & 0 & 0 & 0 & 0 & 0 & 0 & 0 \\ 0 & 0 & 0 & 0 & 0 & 0 & 0 & 0 & 0 \\ 0 & 0 & 0 & 0 & 0 & 0 & 0 & 0 & 0 \\ \frac{\beta_M b_M \theta_{V1} S^*_M}{N^*_H} & 0 & \frac{\beta_M b_M \theta_1 S^*_M}{N^*_H} & 0 & 0 & 0 & 0 & 0 & 0 \\ 0 & 0 & 0 & 0 & \frac{\beta_M b_M \theta_{V2} S^*_M}{N^*_H} & 0 & \frac{\beta_M b_M \theta_2 S^*_M}{N^*_H} & 0 & 0 \end{bmatrix},$$

$$V_1 = \begin{bmatrix} K_3 & 0 & 0 & 0 & 0 & 0 & 0 & 0 & 0 \\ -\sigma_{U1} & K_4 & 0 & 0 & 0 & 0 & 0 & 0 & 0 \\ 0 & 0 & K_5 & 0 & 0 & 0 & 0 & 0 & 0 \\ 0 & 0 & -\alpha_{12} & K_6 & 0 & 0 & 0 & 0 & 0 \\ 0 & 0 & 0 & 0 & K_7 & 0 & 0 & 0 & 0 \\ 0 & 0 & 0 & 0 & -\sigma_{U2} & K_8 & 0 & 0 & 0 \\ 0 & 0 & 0 & 0 & 0 & 0 & K_9 & 0 & 0 \\ 0 & 0 & 0 & 0 & 0 & 0 & -\alpha_{21} & K_{10} & 0 \\ 0 & 0 & 0 & 0 & 0 & 0 & 0 & 0 & K_{11} \end{bmatrix},$$

$$V_2 = \begin{bmatrix} 0 & 0 & 0 & 0 & 0 & 0 & 0 & 0 & -\sigma_{V1} \\ 0 & 0 & 0 & 0 & 0 & 0 & 0 & 0 & 0 \\ 0 & 0 & 0 & 0 & 0 & 0 & 0 & 0 & 0 \\ 0 & 0 & 0 & 0 & 0 & 0 & 0 & 0 & 0 \\ 0 & 0 & 0 & 0 & 0 & 0 & 0 & 0 & 0 \\ 0 & 0 & 0 & 0 & 0 & 0 & 0 & 0 & 0 \\ 0 & 0 & 0 & 0 & 0 & 0 & 0 & 0 & 0 \\ 0 & 0 & 0 & 0 & 0 & 0 & 0 & 0 & 0 \\ 0 & 0 & 0 & 0 & 0 & 0 & 0 & 0 & 0 \end{bmatrix},$$

$$V_3 = \begin{bmatrix} K_{11} & 0 & 0 & 0 & 0 & 0 & 0 & 0 & 0 \\ 0 & K_{13} & 0 & 0 & 0 & 0 & 0 & 0 & 0 \\ 0 & -\sigma_{V12} & K_{14} & 0 & 0 & 0 & 0 & 0 & 0 \\ 0 & 0 & 0 & K_{15} & 0 & 0 & 0 & 0 & 0 \\ 0 & 0 & 0 & -\sigma_{V2} & K_{16} & 0 & 0 & 0 & 0 \\ 0 & 0 & 0 & 0 & 0 & K_{17} & 0 & 0 & 0 \\ 0 & 0 & 0 & 0 & 0 & -\sigma_{V21} & K_{18} & 0 & 0 \\ 0 & 0 & 0 & 0 & 0 & 0 & 0 & \mu_M & 0 \\ 0 & 0 & 0 & 0 & 0 & 0 & 0 & 0 & \mu_M \end{bmatrix}.$$

APPENDIX B

PROOF OF THEOREM 2.5.2

Consider the the model (2.4.1) with $\delta_{UHi} = \delta_{Uij} = \delta_{VHi} = \delta_{Vij} = \delta_H$, $\eta_{ij} = \eta_{Vij} = 0\,(i, j = 1, 2;\, i \neq j)$ and $\tilde{\mathcal{R}}_{vac} \leq 1$. Further, let $\delta_H > \delta_H^c$ and $\varepsilon_1 = \varepsilon_2 = 1$. It is convenient to carry out the following change of variables: $S_{UH} = x_1$, $S_{VH} = x_2$, $E_{UH1} = x_3$, $I_{UH1} = x_4$, $W_{U12} = x_5$, $E_{U12} = x_6$, $I_{U12} = x_7$, $E_{UH2} = x_8$, $I_{UH2} = x_9$, $W_{U21} = x_{10}$, $E_{U21} = x_{11}$, $I_{U21} = x_{12}$, $E_{VH1} = x_{13}$, $I_{VH1} = x_{14}$, $W_{V12} = x_{15}$, $E_{V12} = x_{16}$, $I_{V12} = x_{17}$, $E_{VH2} = x_{18}$, $I_{VH2} = x_{19}$, $W_{V21} = x_{20}$, $E_{V21} = x_{21}$, $I_{V21} = x_{22}$, $W = x_{23}$, $L_M = x_{24}$, $S_M = x_{25}$, $I_{M1} = x_{26}$, $I_{M2} = x_{27}$. Using the vector notation $X = (x_1, ...x_{27})^T$ and $F = (f_1, ...f_{27})^T$, the aforementioned special case of the model (2.4.1), can then be written in the form $\frac{dX}{dt} = (f_1, ...f_{27})^T$, as follows:

$$
\begin{aligned}
\dot{x}_1 &\equiv f_1 = \Pi_H + \omega x_2 - \sum_{i=1}^{2} \lambda_{Hi} x_1 - K_1 x_1, \\
\dot{x}_2 &\equiv f_2 = \xi x_1 - K_2 x_2, \\
\dot{x}_3 &\equiv f_3 = \lambda_{H1} x_1 - K_3 x_3, \\
\dot{x}_4 &\equiv f_4 = \sigma_{U1} x_3 - K_4 x_4, \\
\dot{x}_5 &\equiv f_5 = \gamma_{U1} x_4 - \eta_{12} \lambda_{H2} x_5 - \mu_H x_5, \\
\dot{x}_6 &\equiv f_6 = \eta_{12} \lambda_{H2} x_5 - K_5 x_6, \\
\dot{x}_7 &\equiv f_7 = \alpha_{12} x_6 - K_6 x_7, \\
\dot{x}_8 &\equiv f_8 = \lambda_{H2} x_1 - K_7 x_8, \\
\dot{x}_9 &\equiv f_9 = \sigma_{U2} x_8 - K_8 x_9, \\
\dot{x}_{10} &\equiv f_{10} = \gamma_{U2} x_9 - \eta_{21} \lambda_{H1} x_{10} - \mu_H x_{10}, \\
\dot{x}_{11} &\equiv f_{11} = \eta_{21} \lambda_{H1} x_{10} - K_9 x_{11}, \\
\dot{x}_{12} &\equiv f_{12} = \alpha_{21} x_{11} - K_{10} x_{12}, \\
\dot{x}_{13} &\equiv f_{13} = -K_{11} x_{13}, \\
\dot{x}_{14} &\equiv f_{14} = \sigma_{V1} x_{13} - K_{12} x_{14}, \\
\dot{x}_{15} &\equiv f_{15} = \gamma_{V1} x_{14} - \mu_H x_{15}, \\
\dot{x}_{16} &\equiv f_{16} = -K_{13} x_{16}, \\
\dot{x}_{17} &\equiv f_{17} = \alpha_{V12} x_{16} - K_{14} x_{17}, \\
\dot{x}_{18} &\equiv f_{18} = -K_{15} x_{18}, \\
\dot{x}_{19} &\equiv f_{19} = \sigma_{V2} x_{18} - K_{16} x_{19}, \\
\dot{x}_{20} &\equiv f_{20} = \gamma_{V2} x_{19} - \mu_H x_{20}, \\
\dot{x}_{21} &\equiv f_{21} = -K_{17} x_{21}, \\
\dot{x}_{22} &\equiv f_{22} = \alpha_{V21} x_{21} - K_{18} x_{22}, \\
\dot{x}_{23} &\equiv f_{23} = \tau_{12} x_7 + \tau_{21} x_{12} + \tau_{V12} x_{17} + \tau_{V21} x_{22} - \mu_H x_{23}, \\
\dot{x}_{24} &\equiv f_{24} = \alpha_L \left(1 - \frac{x_{24}}{K_M}\right)(x_{25} + x_{26} + x_{27}) - K_{19} x_{24}, \\
\dot{x}_{25} &\equiv f_{25} = f \psi_L x_{24} - \sum_{i=1}^{2} \lambda_{Mi} x_{25} - \mu_M x_{25}, \\
\dot{x}_{26} &\equiv f_{26} = \lambda_{M1} x_{25} - \mu_M x_{26}, \\
\dot{x}_{27} &\equiv f_{27} = \lambda_{M2} x_{25} - \mu_M x_{27},
\end{aligned}
\tag{B.0.1}
$$

with the infection rates, λ_{Hi} and λ_{Mi} $(i = 1, 2)$, now given, respectively, by (with $N_H = \sum_{i=1}^{23} x_i$):

$$
\lambda_{H1} = \frac{\beta_H b_M x_{26}}{N_H}, \lambda_{H2} = \frac{\beta_H b_M x_{27}}{N_H},
$$

$$\lambda_{M1} = \frac{\beta_M b_M(x_4 + \theta_{12}x_7 + \theta_{V1}x_{14} + \theta_1 x_{17})}{N_H},$$
$$\lambda_{M2} = \frac{\beta_M b_M((x_9 + \theta_{21}x_{12} + \theta_{V2}x_{19} + \theta_2 x_{22})}{N_H}.$$

Without loss of generality, consider $\tilde{\mathcal{R}}_{vac} = \max\{\tilde{\mathcal{R}}_{vac1}, \tilde{\mathcal{R}}_{vac2}\} = 1$ when $\tilde{\mathcal{R}}_{vac1} = 1$ and $\tilde{\mathcal{R}}_{vac2} < 1$ (the same approach also works if $\tilde{\mathcal{R}}_{vac2} = 1$ and $\tilde{\mathcal{R}}_{vac1} < 1$ are chosen). Suppose, further, that $\beta_H = \beta_H^*$ is chosen as a bifurcation parameter. Solving for $\beta_H = \beta_H^*$ from $\tilde{\mathcal{R}}_{vac} = \max\{\tilde{\mathcal{R}}_{vac1}, \tilde{\mathcal{R}}_{vac2}\} = 1$ gives

$$\beta_H = \beta_H^* = \frac{\Pi_H^2 \beta_M b_M^2 x_{25}^* \sigma_{U1} x_1^*}{K_3 K_4 \mu_H^2 \mu_M}.$$

The Jacobian of the transformed system (H.0.1), evaluated at the DFE ($\mathcal{T}_1$) with $\beta_H = \beta_H^*$, is given by

$$J(\beta_H^*) = \begin{bmatrix} J_1 & \mathbf{0}_{10\times 10} & J_2 \\ \mathbf{0}_{10\times 10} & J_3 & \mathbf{0}_{10\times 7} \\ J_4 & J_5 & J_6 \end{bmatrix},$$

$$J_1 = \begin{bmatrix} -K_1 & \omega & 0 & 0 & 0 & 0 & 0 & 0 & 0 & 0 \\ \xi & -K_2 & 0 & 0 & 0 & 0 & 0 & 0 & 0 & 0 \\ 0 & 0 & -K_3 & 0 & 0 & 0 & 0 & 0 & 0 & 0 \\ 0 & 0 & \sigma_{U1} & -K_4 & 0 & 0 & 0 & 0 & 0 & 0 \\ 0 & 0 & 0 & \gamma_{U1} & -\mu_H & 0 & 0 & 0 & 0 & 0 \\ 0 & 0 & 0 & 0 & 0 & -K_5 & 0 & 0 & 0 & 0 \\ 0 & 0 & 0 & 0 & 0 & \alpha_{12} & -K_6 & 0 & 0 & 0 \\ 0 & 0 & 0 & 0 & 0 & 0 & 0 & -K_7 & 0 & 0 \\ 0 & 0 & 0 & 0 & 0 & 0 & 0 & \sigma_{U2} & -K_8 & 0 \\ 0 & 0 & 0 & 0 & 0 & 0 & 0 & 0 & \gamma_{U2} & -\mu_H \end{bmatrix},$$

$$J_2 = \begin{bmatrix} 0 & 0 & 0 & 0 & 0 & -\frac{\beta_H^* b_M x_1^*}{x_1^* + x_2^*} & -\frac{\beta_H^* b_M x_1^*}{x_1^* + x_2^*} \\ 0 & 0 & 0 & 0 & 0 & 0 & 0 \\ 0 & 0 & 0 & 0 & 0 & \frac{\beta_H^* b_M x_1^*}{x_1^* + x_2^*} & 0 \\ 0 & 0 & 0 & 0 & 0 & 0 & 0 \\ 0 & 0 & 0 & 0 & 0 & 0 & 0 \\ 0 & 0 & 0 & 0 & 0 & 0 & 0 \\ 0 & 0 & 0 & 0 & 0 & 0 & 0 \\ 0 & 0 & 0 & 0 & 0 & 0 & \frac{\beta_H^* b_M x_1^*}{x_1^* + x_2^*} \\ 0 & 0 & 0 & 0 & 0 & 0 & 0 \\ 0 & 0 & 0 & 0 & 0 & 0 & 0 \end{bmatrix},$$

$$J_3 = \begin{bmatrix} -K_9 & 0 & 0 & 0 & 0 & 0 & 0 & 0 & 0 & 0 \\ \alpha_{21} & -K_{10} & 0 & 0 & 0 & 0 & 0 & 0 & 0 & 0 \\ 0 & 0 & -K_{11} & 0 & 0 & 0 & 0 & 0 & 0 & 0 \\ 0 & 0 & \sigma_{V1} & -K_{12} & 0 & 0 & 0 & 0 & 0 & 0 \\ 0 & 0 & 0 & \gamma_{V1} & -\mu_H & 0 & 0 & 0 & 0 & 0 \\ 0 & 0 & 0 & 0 & 0 & -K_{13} & 0 & 0 & 0 & 0 \\ 0 & 0 & 0 & 0 & 0 & \alpha_{V12} & -K_{14} & 0 & 0 & 0 \\ 0 & 0 & 0 & 0 & 0 & 0 & 0 & -K_{15} & 0 & 0 \\ 0 & 0 & 0 & 0 & 0 & 0 & 0 & \sigma_{V2} & -K_{16} & 0 \\ 0 & 0 & 0 & 0 & 0 & 0 & 0 & 0 & \gamma_{V2} & -\mu_H \end{bmatrix},$$

$$J_4 = \begin{bmatrix} 0 & 0 & 0 & 0 & 0 & 0 & 0 & 0 & 0 & 0 \\ 0 & 0 & 0 & 0 & 0 & 0 & 0 & 0 & 0 & 0 \\ 0 & 0 & 0 & 0 & 0 & 0 & \tau_{12} & 0 & 0 & 0 \\ 0 & 0 & 0 & 0 & 0 & 0 & 0 & 0 & 0 & 0 \\ 0 & 0 & 0 & -\frac{\beta_M b_M x_{25}^*}{x_1^*+x_2^*} & 0 & 0 & -\frac{\beta_M b_M x_{25}^* \theta_{12}}{x_1^*+x_2^*} & 0 & -\frac{\beta_M b_M x_{25}^*}{x_1^*+x_2^*} & 0 \\ 0 & 0 & 0 & \frac{\beta_M b_M x_{25}^*}{x_1^*+x_2^*} & 0 & 0 & \frac{\beta_M b_M x_{25}^* \theta_{12}}{x_1^*+x_2^*} & 0 & 0 & 0 \\ 0 & 0 & 0 & 0 & 0 & 0 & 0 & 0 & \frac{\beta_M b_M x_{25}^*}{x_1^*+x_2^*} & 0 \end{bmatrix},$$

$$J_5 = \begin{bmatrix} 0 & 0 & 0 & 0 & 0 & 0 & 0 & 0 & 0 & 0 \\ 0 & 0 & 0 & 0 & 0 & 0 & 0 & 0 & 0 & 0 \\ 0 & \tau_{21} & 0 & 0 & 0 & 0 & \tau_{V12} & 0 & 0 & 0 \\ 0 & 0 & 0 & 0 & 0 & 0 & 0 & 0 & 0 & 0 \\ 0 & -\frac{\beta_M b_M x_{25}^* \theta_{21}}{x_1^*+x_2^*} & 0 & -\frac{\beta_M b_M x_{25}^* \theta_{V1}}{x_1^*+x_2^*} & 0 & 0 & -\frac{\beta_M b_M x_{25}^* \theta_1}{x_1^*+x_2^*} & 0 & -\frac{\beta_M b_M x_{25}^* \theta_{V2}}{x_1^*+x_2^*} & 0 \\ 0 & 0 & 0 & \frac{\beta_M b_M x_{25}^* \theta_{V1}}{x_1^*+x_2^*} & 0 & 0 & \frac{\beta_M b_M x_{25}^* \theta_1}{x_1^*+x_2^*} & 0 & 0 & 0 \\ 0 & \frac{\beta_M b_M x_{25}^* \theta_{21}}{x_1^*+x_2^*} & 0 & 0 & 0 & 0 & 0 & 0 & \frac{\beta_M b_M x_{25}^* \theta_{V2}}{x_1^*+x_2^*} & 0 \end{bmatrix},$$

$$J_6 = \begin{bmatrix} -K_{17} & 0 & 0 & 0 & 0 & 0 & 0 \\ \alpha_{V21} & -K_{18} & 0 & 0 & 0 & 0 & 0 \\ 0 & \tau_{V21} & -\mu_H & 0 & 0 & 0 & 0 \\ 0 & 0 & 0 & -\frac{\alpha_L L_M^*}{K_M} - K_{19} & \alpha_L\left(1-\frac{L_M^*}{K_M}\right) & \alpha_L\left(1-\frac{L_M^*}{K_M}\right) & \alpha_L\left(1-\frac{L_M^*}{K_M}\right) \\ 0 & -\frac{\beta_M b_M x_{25}^* \theta_2}{x_1^*+x_2^*} & 0 & f\psi_L & -\mu_L & 0 & 0 \\ 0 & 0 & 0 & 0 & 0 & -\mu_M & 0 \\ 0 & \frac{\beta_M b_M x_{25}^* \theta_2}{x_1^*+x_2^*} & 0 & 0 & 0 & 0 & -\mu_M \end{bmatrix}.$$

The Jacobian $J(\beta_H^*)$ has a simple zero eigenvalue (and all other eigenvalues having negative real parts). Hence, the center manifold theory (Carr, 1981; Castillo-Chavez and Song, 2004; van den Driessche and Watmough, 2002) can be used to analyse the dynamics of (H.0.1) near $\beta_H = \beta_H^*$. This entails carrying out the following computations. **Eigenvectors of** $J(\mathcal{T}_1)\,|_{\beta_H=\beta_H^*}$ The Jacobian of the transformed system

(H.0.1), evaluated at the DFE ($\mathcal{T}_1$) with $\beta_H = \beta^*$, has a right eigenvector (associated with the zero eigenvalue) given by

$$\mathbf{w} = (w_1, ..., w_{27})^T,$$

where,

$$w_1 = \frac{\beta_H^* x_1^* b_M^2 \sigma_{U1} \beta_M x_{25}^* w_3 K_2}{\mu_M K_4 \left(x_1^* + x_2^*\right)^2 (\omega\,\xi - K_1 K_2)},\ w_2 = \frac{\xi\,\beta_H^* x_1^* b_M^2 \sigma_{U1} \beta_M x_{25}^* w_3}{\mu_M K_4 \left(x_1^* + x_2^*\right)^2 (\omega\,\xi - K_1 K_2)},$$

$$w_3 = w_3 > 0,\ w_4 = \frac{\sigma_{U1} w_3}{K_4},\ w_5 = \frac{\gamma_{U1}\sigma_{U1} w_3}{\mu_H K_4},$$

$$w_6 = w_7 = w_8 = w_9 = w_{10} = w_{11} = w_{12} = 0,$$

$$w_{13} = w_{14} = w_{15} = w_{16} = w_{17} = w_{18} = w_{19} = w_{20} = w_{21} = w_{22} = w_{23} = w_{24} = 0,$$

$$w_{25} = -\frac{\sigma_{U1} \beta_M x_{25}^* w_3 b_M}{\mu_M K_4 \left(x_1^* + x_2^*\right)},\ w_{26} = \frac{\sigma_{U1} \beta_M x_{25}^* w_3 b_M}{\mu_M K_4 \left(x_1^* + x_2^*\right)},\ w_{27} = 0,$$

with $\omega\,\xi - K_1 K_2 = -\mu_H(\xi + \omega + \mu_H) < 0$.

The matrix $J(\mathcal{T}_1)\mid_{\beta_H = \beta_H^*}$ has a left eigenvector $\mathbf{v} = (v_1, ..., v_{27})$, associated with the zero eigenvalue, given by

$$v_1 = v_2 = 0,\ v_3 = v_3,\ v_4 = \frac{\beta_M \beta_H^* x_{25}^* x_1^* v_3 b_M^2}{\mu_M K_4 \left(x_1^* + x_2^*\right)^2},\ v_5 = 0,\ v_6 = \frac{\theta_{12}\alpha_{12}\beta_M \beta_H^* x_{25}^* x_1^* v_3 b_M^2}{\mu_M K_6 K_5 \left(x_1^* + x_2^*\right)^2},$$

$$v_7 = \frac{\theta_{12}\beta_M \beta_H^* x_{25}^* x_1^* v_3 b_M^2}{\mu_M K_6 \left(x_1^* + x_2^*\right)^2},\ v_8 = v_9 = v_{10} = v_{11} = v_{12} = 0,\ v_{13} = \frac{\theta_{V1}\sigma_{V1}\beta_M \beta_H^* x_{25}^* x_1^* v_3 b_M^2}{\mu_M K_{12} K_{11}\left(x_1^* + x_2^*\right)^2},$$

$$v_{14} = \frac{\theta_{V1}\beta_M \beta_H^* x_{25}^* x_1^* v_3 b_M^2}{\mu_M K_{12} \left(x_1^* + x_2^*\right)^2},\ v_{15} = 0,\ v_{16} = \frac{\alpha_{V12}\theta_1\beta_M \beta_H^* x_{25}^* x_1^* v_3 b_M^2}{\mu_M K_{14} K_{13} \left(x_1^* + x_2^*\right)^2},$$

$$v_{17} = \frac{\theta_1\beta_M \beta_H^* x_{25}^* x_1^* v_3 b_M^2}{\mu_M K_{14} \left(x_1^* + x_2^*\right)^2},\ v_{18} = v_{19} = v_{20} = v_{21} = v_{22} = v_{23} = v_{24} = v_{25} = 0,$$

$$v_{26} = \frac{\beta_H^* b_M x_1^* v_3}{\mu_M \left(x_1^* + x_2^*\right)},\ v_{27} = 0.$$

Computations of bifurcation coefficients of a and b :

By computing the associated non-zero partial derivatives of $F(x)$ evaluated the DFE, it follows from Theorem 4.1 in (Castillo-Chavez and Song, 2004) that the associated

bifurcation coefficients, a and b, are given, respectively, by

$$\begin{aligned}
a =& 2\,\frac{v_3\beta_H^* x_1^* b_M^3 {\sigma_{U1}}^2 \beta_M^2 (x_{25}^*)^2 {w_3}^2 K_2}{{\mu_M}^2 {K_4}^2 \left(x_1^*+x_2^*\right)^3 (\omega\,\xi - K_1K_2)}\left(\frac{\beta_H^* b_M}{x_1^*+x_2^*} - \frac{\beta_H^* b_M x_1^*}{\left(x_1^*+x_2^*\right)^2}\right)\\
&- 4\,\frac{v_3\xi\,{\beta_H^*}^2 (x_1^*)^2 b_M^4 \sigma_{U1}^2 \beta_M^2 x_{25}^2 w_3^2}{\mu_M^2 {K_4}^2 \left(x_1^*+x_2^*\right)^5 (\omega\,\xi - K_1K_2)}\\
&- 4\,\frac{v_3 w_3^2 \sigma_{U1}\beta_M x_{25}^* b_M^2 \beta_H^* x_1^*}{\mu_M K_4 \left(x_1^*+x_2^*\right)^3} - 4\,\frac{v_3\sigma_{U1}^2 w_3^2 \beta_M x_{25}^* b_M^2 \beta_H^* x_1^*}{{K_4}^2 \mu_M \left(x_1^*+x_2^*\right)^3} - 4\,\frac{v_3\sigma_{U1}^2 w_3^2 \beta_M x_{25}^* b_M^2 \beta_H^* x_1^*}{\mu_H {K_4}^2 \mu_M \left(x_1^*+x_2^*\right)^3}\\
&- 2\,\frac{{\beta_H^*}^2 b_M^4 x_1^2 v_3 \sigma_{U1}^2 {\beta_M^*}^2 (x_{25}^*)^2 w_3^2 K_2}{\mu_M^2 K_4^2 \left(x_1^*+x_2^*\right)^5 (\omega\,\xi - K_1K_2)} - 2\,\frac{\beta_H^* b_M^3 x_1^* v_3 \sigma_{U1}^2 w_3^2 \beta_M^2 x_{25}^*}{\mu_M^2 \left(x_1^*+x_2^*\right)^3 K_4^2},
\end{aligned} \tag{B.0.2}$$

and,

$$b = \frac{v_3\sigma_{U1}\beta_M x_{25}^* w_3 b_M^2 x_1^*}{\mu_M K_4 \left(x_1^*+x_2^*\right)^2} > 0. \tag{B.0.3}$$

Hence, it follows from Theorem 4.1 of (Castillo-Chavez and Song, 2004) that the transformed model (H.0.1) undergoes a backward bifurcation at $\tilde{\mathcal{R}}_{vac1} = 1$ and $\tilde{\mathcal{R}}_{vac2} < 1$ if the bifurcation coefficient a (given by (H.0.2)) is positive. Solving the Inequality $a > 0$, in terms of the disease-induced mortality in the host population (δ_H), gives $a > 0$ whenever

$$\delta_H > \frac{-[2a_1(1+\mu_H)+a_4] - \sqrt{[2a_1(1+\mu_H)+a_4]^2 - 4a_1[a_1(1+\mu_H)^2 + a_4(1+\mu_H)+a_2+a_3]}}{2a_1} = \delta_H^c,$$

where,

$$\begin{aligned}
a_1 &= -4v_3 w_3^2 \sigma_{U1}^2 \beta_M^2 (S_M^*)^2 b_M^4 \Pi_H^2 (S_{UH}^*)^2 K_3 \mu_H^3 \mu_M^2 (S_{UH}^* + S_{VH}^*)^2 (\xi + \mu_H + \omega) < 0,\\
a_2 &= 4\,v_3 \Pi_H^4 \beta_M^4 b_M^8 \sigma_{U1}^4 (S_{UH}^*)^4 (S_M)^4 w_3^2 \xi,\\
a_3 &= 2\,v_3 \Pi_H^4 \beta_M^4 b_M^8 \sigma_{U1}^4 (S_{UH}^*)^3 (S_M^*)^4 w_3^2 K_2 \left(S_{UH}^* - S_{VH}^*\right),\\
a_4 &= -2\,v_3 w_3^2 \sigma_{U1}^3 \beta_M^2 (S_M^*)^2 b_M^4 \Pi_H^2 (S_{UH}^*)^2 K_3 \mu_H^2 \mu_M^2 (S_{UH}^* + S_{VH}^*)^2 \left[b_M\beta_M\mu_H + 2\mu_M + 2\mu_H\mu_M\right] < 0.
\end{aligned} \tag{B.0.4}$$

APPENDIX C

PROOF OF THEOREM 2.5.3

Consider the special case of the model (2.4.1) with $\eta_{ij} = \eta_{Vij}\,(i,j=1,2;\, i \neq j) = 0$, $\delta_H = 0$ and $\varepsilon_1 \neq 1$ and $\varepsilon_1 \neq 1$. It can be shown, using the approach in Appendix B1, that the associated bifurcation coefficient (a) is given by

$$
\begin{aligned}
a = &-2\,\frac{v_3(\beta_H^*)^2\mu_H^4 b_M^4\left[\omega\, x_2^*(1-\varepsilon_1)+K_2x_1^*\right]{\sigma_{U1}}^2\beta_M^2(x_{25}^*)^2K_{12}^2K_{11}^2w_3^2}{K_4^2\left[b_M^2\beta_H^*\beta_M\mu_H^2\sigma_{V1}\theta_{V1}x_2^*x_{25}^*(\varepsilon_1-1)+K_{11}K_{12}\Pi_H^2\mu_M\right]^2(\omega\,\xi-K_1K_2)}\\
&+2\,\frac{(\beta_H^*)^3\mu_H^6x_1v_3b_M^6\theta_{V1}\sigma_{V1}\beta_M{}^3(x_{25}^*)^3{\sigma_{U1}}^2K_{12}^2K_{11}^2w_3^2\left(-K_1x_2^*\varepsilon_1+\xi\,x_1+K_1x_2^*\right)(1-\varepsilon_1)}{\left[b_M^2\beta_H^*\beta_M\mu_H^2\sigma_{V1}\theta_{V1}x_2^*x_{25}^*(\varepsilon_1-1)+K_{11}K_{12}\Pi_H{}^2\mu_M\right]^3K_4^2(\omega\,\xi-K_1K_2)}\\
&-2\,\frac{\beta_H^*\mu_H^3\Pi_HK_{12}^2K_{11}^2x_1^*v_3b_M^3{\sigma_{U1}}^2w_3^2\beta_M^2x_{25}^*}{\left[b_M^2\beta_H^*\beta_M\mu_H^2\sigma_{V1}\theta_{V1}x_2^*x_{25}^*(\varepsilon_1-1)+K_{11}K_{12}\Pi_H^2\mu_M\right]^2K_4^2}\\
&+2\,\frac{(\beta_H^*)^2\mu_H^5\Pi_HK_{12}^2K_{11}^2x_1^*v_3b_M^5\sigma_{V1}x_2\left(-1+\varepsilon_1\right){\sigma_{U1}}^2\beta_M^3(x_{25}^*)^2w_3^2\theta_{V1}}{\left[b_M^2\beta_H^*\beta_M\mu_H^2\sigma_{V1}\theta_{V1}x_2^*x_{25}^*(\varepsilon_1-1)+K_{11}K_{12}\Pi_H^2\mu_M\right]^3K_4^2},
\end{aligned}
\tag{C.0.1}
$$

so that the model undergoes a backward bifurcation at

$$\mathcal{R}_{vac}^* = \mathcal{R}_{vac}|_{\delta_H=\eta_{ij}=\eta_{Vij}\,(i,j=1,2;\,i\neq j)=0} = 1$$

if the bifurcation coefficient, a (given by B-5) is positive.

APPENDIX D

PROOF OF THEOREM 2.5.5

Consider the model (2.4.1) with $\varepsilon_1 = \varepsilon_2 = 1$, $\delta_H = 0$ and $\eta_{ij} = \eta_{Vij} = 0\,(i, j = 1, 2; i \neq j)$. Let $\mathcal{R}^{**}_{vac} < 1$. The proof is based on the approach in (Dumont and Chiroleu, 2010; Kamgang and Sallet, 2008). It is convenient to re-write this special case of the model in the form;

$$\begin{aligned} \dot{X}_S &= A_1(X)(X_S - X_{NDFE,S}) + A_{12}(X)X_I, \\ \dot{X}_I &= A_2(X)X_I, \end{aligned} \tag{D.0.1}$$

where X_S represents the non-transmitting compartments and X_I represents the infected compartments (Kamgang and Sallet, 2008). That is,

$$\begin{aligned} X_S &= (S_{UH}, S_{VH}, W_{Vij}, W_{Uij}, W, L_M, S_M)^T, \\ X_I &= (E_{VHi}, E_{UHi}, E_{ji}, E_{Vij}, I_{VHi}, I_{Vij}, I_{UHi}, I_{ij}, I_{Mi})^T, \\ X_{NDFE,S} &= (S^*_{UH}, S^*_{VH}, 0, 0, 0, 0, 0, L^*_M, S^*_M)^T, \end{aligned}$$

with,

$$A_1(X) = \begin{bmatrix} A^*_1 & \mathbf{0}_{9\times 9} \\ \mathbf{0}_{9\times 9} & \mathbf{0}_{9\times 9} \end{bmatrix},$$

$$A^*_1(X) = \begin{bmatrix} -K_1 & \omega & 0 & 0 & 0 & 0 & 0 & 0 & 0 \\ \xi & -K_2 & 0 & 0 & 0 & 0 & 0 & 0 & 0 \\ 0 & 0 & -\mu_H & 0 & 0 & 0 & 0 & 0 & 0 \\ 0 & 0 & 0 & -\mu_H & 0 & 0 & 0 & 0 & 0 \\ 0 & 0 & 0 & 0 & -\mu_H & 0 & 0 & 0 & 0 \\ 0 & 0 & 0 & 0 & 0 & -\mu_H & 0 & 0 & 0 \\ 0 & 0 & 0 & 0 & 0 & 0 & -\mu_H & 0 & 0 \\ 0 & 0 & 0 & 0 & 0 & 0 & 0 & -(\frac{\alpha_L S^*_M}{K_M} + \psi_L + \mu_L) & \alpha_L\Big(1 - \frac{L_M}{K_M}\Big) \\ 0 & 0 & 0 & 0 & 0 & 0 & 0 & f\psi_L & -\mu_M \end{bmatrix},$$

$$A_{12}(X) = \begin{bmatrix} A^1_{12} & A^2_{12} \\ \mathbf{0}_{9\times 9} & \mathbf{0}_{9\times 9} \end{bmatrix},$$

$$A^1_{12}(X) = \begin{bmatrix} 0 & 0 & 0 & 0 & 0 & 0 & 0 & 0 & 0 \\ 0 & 0 & 0 & 0 & 0 & 0 & 0 & 0 & 0 \\ 0 & \gamma_{U1} & 0 & 0 & 0 & 0 & 0 & 0 & 0 \\ 0 & 0 & 0 & 0 & 0 & \gamma_{U2} & 0 & 0 & 0 \\ 0 & 0 & 0 & 0 & 0 & 0 & 0 & 0 & 0 \\ 0 & 0 & 0 & 0 & 0 & 0 & 0 & 0 & 0 \\ 0 & 0 & 0 & \tau_{12} & 0 & 0 & 0 & \tau_{21} & 0 \\ 0 & 0 & 0 & 0 & 0 & 0 & 0 & 0 & 0 \\ 0 & -\frac{\beta_M b_M S_M}{N_H} & 0 & -\frac{\beta_M b_M \theta_{12} S_M}{N_H} & 0 & -\frac{\beta_M b_M S_M}{N_H} & 0 & -\frac{\beta_M b_M \theta_{21} S_M}{N_H} & 0 \end{bmatrix},$$

$$A^2_{12}(X) = \begin{bmatrix} 0 & 0 & 0 & 0 & 0 & 0 & 0 & -\frac{\beta_M b_M S_{UH}}{N_H} & -\frac{\beta_M b_M S_{UH}}{N_H} \\ 0 & 0 & 0 & 0 & 0 & 0 & 0 & 0 & 0 \\ 0 & 0 & 0 & 0 & 0 & 0 & 0 & 0 & 0 \\ 0 & 0 & 0 & 0 & 0 & 0 & 0 & 0 & 0 \\ \gamma_{V1} & 0 & 0 & 0 & 0 & 0 & 0 & 0 & 0 \\ 0 & 0 & 0 & 0 & \gamma_{V2} & 0 & 0 & 0 & 0 \\ 0 & 0 & \tau_{V12} & 0 & 0 & 0 & \tau_{V21} & 0 & 0 \\ 0 & 0 & 0 & 0 & 0 & 0 & 0 & \alpha_L\Big(1 - \frac{L_M}{K_M}\Big)S_M & \alpha_L\Big(1 - \frac{L_M}{K_M}\Big)S_M \\ -\frac{\beta_M b_M \theta_{V1} S_M}{N_H} & 0 & -\frac{\beta_M b_M \theta_1 S_M}{N_H} & 0 & -\frac{\beta_M b_M \theta_{V2} S_M}{N_H} & 0 & -\frac{\beta_M b_M \theta_2 S_M}{N_H} & 0 & 0 \end{bmatrix},$$

$$A_2(X) = \begin{bmatrix} A_2^1 & A_2^2 \\ A_2^3 & A_2^4 \end{bmatrix},$$

where,

$$A_2^1(X) = \begin{bmatrix} -K_3 & 0 & 0 & 0 & 0 & 0 & 0 & 0 & 0 \\ \sigma_{U1} & -K_4 & 0 & 0 & 0 & 0 & 0 & 0 & 0 \\ 0 & 0 & -K_5 & 0 & 0 & 0 & 0 & 0 & 0 \\ 0 & 0 & \alpha_{12} & -K_6 & 0 & 0 & 0 & 0 & 0 \\ 0 & 0 & 0 & 0 & -K_7 & 0 & 0 & 0 & 0 \\ 0 & 0 & 0 & 0 & \sigma_{U2} & -K_8 & 0 & 0 & 0 \\ 0 & 0 & 0 & 0 & 0 & 0 & -K_9 & 0 & 0 \\ 0 & 0 & 0 & 0 & 0 & 0 & \alpha_{21} & -K_{10} & 0 \\ 0 & 0 & 0 & 0 & 0 & 0 & 0 & 0 & -K_{11} \end{bmatrix},$$

$$A_2^2(X) = \begin{bmatrix} 0 & 0 & 0 & 0 & 0 & 0 & 0 & \frac{\beta_H b_M S_{UH}}{N_H} & 0 \\ 0 & 0 & 0 & 0 & 0 & 0 & 0 & 0 & 0 \\ 0 & 0 & 0 & 0 & 0 & 0 & 0 & 0 & 0 \\ 0 & 0 & 0 & 0 & 0 & 0 & 0 & 0 & 0 \\ 0 & 0 & 0 & 0 & 0 & 0 & 0 & 0 & \frac{\beta_H b_M S_{UH}}{N_H} \\ 0 & 0 & 0 & 0 & 0 & 0 & 0 & 0 & 0 \\ 0 & 0 & 0 & 0 & 0 & 0 & 0 & 0 & 0 \\ 0 & 0 & 0 & 0 & 0 & 0 & 0 & 0 & 0 \\ 0 & 0 & 0 & 0 & 0 & 0 & 0 & 0 & 0 \end{bmatrix},$$

$$A_2^3(X) = \begin{bmatrix} 0 & 0 & 0 & 0 & 0 & 0 & 0 & 0 & 0 \\ 0 & 0 & 0 & 0 & 0 & 0 & 0 & 0 & 0 \\ 0 & 0 & 0 & 0 & 0 & 0 & 0 & 0 & 0 \\ 0 & 0 & 0 & 0 & 0 & 0 & 0 & 0 & 0 \\ 0 & 0 & 0 & 0 & 0 & 0 & 0 & 0 & 0 \\ 0 & 0 & 0 & 0 & 0 & 0 & 0 & 0 & 0 \\ 0 & 0 & 0 & 0 & 0 & 0 & 0 & 0 & 0 \\ 0 & \frac{\beta_M b_M S_M}{N_H} & 0 & \frac{\beta_M b_M \theta_{12} S_M}{N_H} & 0 & 0 & 0 & 0 & 0 \\ 0 & 0 & 0 & 0 & 0 & \frac{\beta_M b_M S_M}{N_H} & 0 & \frac{\beta_M b_M \theta_{21} S_M}{N_H} & 0 \end{bmatrix},$$

and,

$$A_2^4(X) = \begin{bmatrix} -K_{12} & 0 & 0 & 0 & 0 & 0 & 0 & 0 & 0 \\ 0 & -K_{13} & 0 & 0 & 0 & 0 & 0 & 0 & 0 \\ 0 & \alpha_{V12} & -K_{14} & 0 & 0 & 0 & 0 & 0 & 0 \\ 0 & 0 & 0 & -K_{15} & 0 & 0 & 0 & 0 & 0 \\ 0 & 0 & 0 & \sigma_{V2} & -K_{16} & 0 & 0 & 0 & 0 \\ 0 & 0 & 0 & 0 & 0 & -K_{17} & 0 & 0 & 0 \\ 0 & 0 & 0 & 0 & 0 & \alpha_{V21} & -K_{18} & 0 & 0 \\ \frac{\beta_M b_M \theta_{V1} S_M}{N_H} & 0 & \frac{\beta_M b_M \theta_1 S_M}{N_H} & 0 & 0 & 0 & 0 & -\mu_M & 0 \\ 0 & 0 & 0 & \frac{\beta_M b_M \theta_{V2} S_M}{N_H} & 0 & 0 & \frac{\beta_M b_M \theta_2 S_M}{N_H} & 0 & -\mu_M \end{bmatrix}.$$

It can be seen that the eigenvalues of the Metzler matrix (i.e., M-matrix) $A_1(X)$ are real and negative. Hence, the system $\dot{X}_S = A_1(X)(X_S - X_{NDFE,S})$ is GAS at the non-trivial DFE, $X_{NDFE,S}$ (Kamgang and Sallet, 2008). It should be noted that the matrix $A_2(X)$ is also an M-matrix (since its off diagonal entries are non-negative). The result below is needed to complete the proof of Theorem 2.5.5.

Theorem D.0.1. *(Dumont and Chiroleu, 2010). Let $\mathcal{D} \subset \mathcal{U} = \mathbb{R}^{18} \times \mathbb{R}^9$. The system (11) is of class C^1, defined on $\mathcal{U}$, if:*

1. *$\mathcal{D}$ is positively invariant relative to (11),*
2. *The system $\dot{X}_S = A_1(X)(X_S - X_{NDFE,S})$ is GAS at $X_{NDFE,S}$,*
3. *For any $x \in \mathcal{D}$, the matrix $A_2(X)$ is Metzler irreducible,*
4. *There exist a matrix $\bar{A}_2$, which is an upper bound of the set $\mathcal{M} = \{A_2(X) \in \mathcal{M}_{18}(\boldsymbol{R}) : x \in \mathcal{D}\}$ with the property that if $A_2 \in \mathcal{M}$, for any $\bar{x} \in \mathcal{D}$ such that $A_2(\bar{x}) = \bar{A}_2$, then $\bar{x} \in \boldsymbol{R}^9 \times \{0\}$,*
5. *The stability modulus of $\bar{A}_2$ satisfies $\gamma(\bar{A}_2) \leq 0$.*

Condition 1 of Theorem C.1 is automatically satisfied by model (2.4.1) (since, by Lemma 2.4.1, $\mathcal{D}$ is positively-invariant). Furthermore, Condition 2 holds since the eigenvalues of the M-matrix $A_1(X)$ are real and negative. Similarly, Condition 3 holds since the matrix $A_2(X)$ is Metzler irreducible. For Condition 4, it is convenient to define an upper bound for the set of matrices $\mathcal{M}$. This upper bound (in our notation) is the matrix $\bar{A}_2(X)$, given by (where $\bar{N}_H$ is bounded above by $\frac{\Pi_H}{\mu_H}$)

$$\bar{A}_2(X) = \begin{bmatrix} \bar{A}_2^1 & \bar{A}_2^2 \\ \bar{A}_2^3 & \bar{A}_2^4 \end{bmatrix},$$

where,

$$\bar{A}_2^1(X) = \begin{bmatrix} -K_3 & 0 & 0 & 0 & 0 & 0 & 0 & 0 & 0 \\ \sigma_{U1} & -K_4 & 0 & 0 & 0 & 0 & 0 & 0 & 0 \\ 0 & 0 & -K_5 & 0 & 0 & 0 & 0 & 0 & 0 \\ 0 & 0 & \alpha_{12} & -K_6 & 0 & 0 & 0 & 0 & 0 \\ 0 & 0 & 0 & 0 & -K_7 & 0 & 0 & 0 & 0 \\ 0 & 0 & 0 & 0 & \sigma_{U2} & -K_8 & 0 & 0 & 0 \\ 0 & 0 & 0 & 0 & 0 & 0 & -K_9 & 0 & 0 \\ 0 & 0 & 0 & 0 & 0 & 0 & \alpha_{21} & -K_{10} & 0 \\ 0 & 0 & 0 & 0 & 0 & 0 & 0 & 0 & -K_{11} \end{bmatrix},$$

$$\bar{A}_2^2(X) = \begin{bmatrix} 0 & 0 & 0 & 0 & 0 & 0 & 0 & \frac{\beta_H b_M S_{UH} \mu_H}{\Pi_H} & 0 \\ 0 & 0 & 0 & 0 & 0 & 0 & 0 & 0 & 0 \\ 0 & 0 & 0 & 0 & 0 & 0 & 0 & 0 & 0 \\ 0 & 0 & 0 & 0 & 0 & 0 & 0 & 0 & 0 \\ 0 & 0 & 0 & 0 & 0 & 0 & 0 & 0 & \frac{\beta_H b_M S_{UH} \mu_H}{\Pi_H} \\ 0 & 0 & 0 & 0 & 0 & 0 & 0 & 0 & 0 \\ 0 & 0 & 0 & 0 & 0 & 0 & 0 & 0 & 0 \\ 0 & 0 & 0 & 0 & 0 & 0 & 0 & 0 & 0 \\ 0 & 0 & 0 & 0 & 0 & 0 & 0 & 0 & 0 \end{bmatrix},$$

$$\bar{A}_2^3(X) = \begin{bmatrix} 0 & 0 & 0 & 0 & 0 & 0 & 0 & 0 & 0 \\ 0 & 0 & 0 & 0 & 0 & 0 & 0 & 0 & 0 \\ 0 & 0 & 0 & 0 & 0 & 0 & 0 & 0 & 0 \\ 0 & 0 & 0 & 0 & 0 & 0 & 0 & 0 & 0 \\ 0 & 0 & 0 & 0 & 0 & 0 & 0 & 0 & 0 \\ 0 & 0 & 0 & 0 & 0 & 0 & 0 & 0 & 0 \\ 0 & 0 & 0 & 0 & 0 & 0 & 0 & 0 & 0 \\ 0 & \frac{\beta_M b_M S_M \mu_H}{\Pi_H} & 0 & \frac{\beta_M b_M S_M \theta_{12} \mu_H}{\Pi_H} & 0 & 0 & 0 & 0 & 0 \\ 0 & 0 & 0 & 0 & 0 & \frac{\beta_M b_M S_M \mu_H}{\Pi_H} & 0 & \frac{\beta_M b_M S_M \theta_{21} \mu_H}{\Pi_H} & 0 \end{bmatrix},$$

and,

$$\bar{A}_2^4(X) = \begin{bmatrix} -K_{12} & 0 & 0 & 0 & 0 & 0 & 0 & 0 & 0 \\ 0 & -K_{13} & 0 & 0 & 0 & 0 & 0 & 0 & 0 \\ 0 & \alpha_{V12} & -K_{14} & 0 & 0 & 0 & 0 & 0 & 0 \\ 0 & 0 & 0 & -K_{15} & 0 & 0 & 0 & 0 & 0 \\ 0 & 0 & 0 & \sigma_{V2} & K_{16} & 0 & 0 & 0 & 0 \\ 0 & 0 & 0 & 0 & 0 & -K_{17} & 0 & 0 & 0 \\ 0 & 0 & 0 & 0 & 0 & \alpha_{V21} & -K_{18} & 0 & 0 \\ \frac{\beta_M b_M S_M \theta_{V1} \mu_H}{\Pi_H} & 0 & \frac{\beta_M b_M S_M \theta_1 \mu_H}{\Pi_H} & 0 & 0 & 0 & 0 & -\mu_M & 0 \\ 0 & 0 & 0 & \frac{\beta_M b_M \mu_H S_M \theta_{V2}}{\Pi_H} & 0 & 0 & \frac{\beta_M b_M S_M \theta_2 \mu_H}{\Pi_H} & 0 & -\mu_M \end{bmatrix}.$$

To check for Condition 5, it is convenient to use Proposition 3.1 in (Kamgang and Sallet, 2008), which is a characterization of Metzler stable matrices (reproduced below):

Lemma D.0.1. *(Kamgang and Sallet, 2008) Let $\boldsymbol{M}$ be a Metzler matrix, which is block decomposed:*

$$\boldsymbol{M} = \begin{bmatrix} \boldsymbol{A} & \boldsymbol{B} \\ \boldsymbol{C} & \boldsymbol{D} \end{bmatrix}$$

where $\boldsymbol{A}$ and $\boldsymbol{D}$ are square matrices. Then $\boldsymbol{M}$ is Metzler stable if and only if $\boldsymbol{A}$ and $\boldsymbol{D} - \boldsymbol{C}\boldsymbol{A}^{-1}\boldsymbol{B}$ are Metzler stable.

It should be noted that the matrix $\mathbf{A}$ (which is the same as the M-matrix $\bar{A}_2^1(X)$ in our notation) is Metzler stable (since all the elements on the diagonal of $\bar{A}_2^1(X)$ are negative). It follows then (after some algebraic computations) that $\mathbf{D} - \mathbf{C}\mathbf{A}^{-1}\mathbf{B}$ (which is equivalent to $\bar{A}_2^4(X) - \bar{A}_2^3(X)[\bar{A}_2^1(X)]^{-1}\bar{A}_2^2(X)$) is a stable Metzler matrix if and only if

$$\mathcal{R}_G = \max\{\mathcal{R}_{G_1}, \mathcal{R}_{G_2}\} \leq 1, \tag{D.0.2}$$

where,

$$\mathcal{R}_{G_1} = \frac{\beta_H \beta_M b_M^2 \sigma_{U1} S_{UH}^* S_M^* \mu_H^2}{K_3 K_4 \mu_M \Pi_H^2} \text{ and } \mathcal{R}_{G_2} = \frac{\beta_H \beta_M \sigma_{U2} b_M^2 S_{UH}^* S_M^* \mu_H^2}{K_7 K_8 \mu_M \Pi_H^2}.$$

APPENDIX E

PROOF OF LEMMA 3.4.1

(a) It should be noted, first of all, that the right-hand side of each of the equations of the model {(3.4.1), (3.4.2),(3.4.4)} is continuous and locally-Lipschitz at $t = 0$. Hence, a solution of the model with non-negative initial conditions exists and is unique in $\Omega = \Omega_1 \times \Omega_2 \times \Omega_3$ for all time $t > 0$ (see also (Iboi et al., 2018; Okuneye et al., 2019)). Furthermore, since $\left(1 - \frac{E}{K_E}\right)_+ \geq 0$, it follows from the first equation of the sub-system (3.4.1) that $E(t) \leq K_E$ for all time $t > 0$. Similarly, it follows from the second equation of the sub-system (3.4.1) that

$$\dot{L}_1 = \sigma_E E - (\sigma_{L_1} + \mu_L) L_1 \leq \sigma_E K_E - (\sigma_{L_1} + \mu_L) L_1,$$

so that $\limsup_{t\to\infty} L_1(t) \leq \frac{\sigma_E K_E}{\sigma_{L_1} + \mu_L} = L_1^\diamond$. Using a similar approach, it can be shown that $\limsup_{t\to\infty} L_2(t) \leq \frac{\sigma_{L_1} L_1^\diamond}{\sigma_{L_2} + \mu_L} = L_2^\diamond$, $\limsup_{t\to\infty} L_3(t) \leq \frac{\sigma_{L_2} L_2^\diamond}{\sigma_{L_3} + \mu_L} = L_3^\diamond$, $\limsup_{t\to\infty} L_4(t) \leq \frac{\sigma_{L_3} L_3^\diamond}{\sigma_{L_4} + \mu_L} = L_4^\diamond$ and $\limsup_{t\to\infty} P(t) \leq \frac{\sigma_{L_4} L_4^\diamond}{\sigma_P + \mu_P} = P^\diamond$. That is, all solutions of the sub-system (3.4.1) are bounded for all time $t > 0$.

For the boundedness of the solutions of the sub-system (3.4.2), we consider the following equation (for the rate of change of the total adult mosquito population):

$$\dot{N}_M = f\sigma_P P - \mu_X S_X - \mu_X E_X - \mu_X I_X - \mu_M N_M + b_H(Q_2 + Q_3 - Q_1 + R_1 + R_2)A_X, \tag{E.0.1}$$

where, $N_M = A_X + A_Y + A_Z$ (with $A_X, A_Y, A_Z, Q_1, Q_2, Q_3, R_1$ and R_2 are as defined in Section 2). It can be shown that $Q_2 + Q_3 - Q_1 + R_1 + R_2 < 0$. Hence, Equation (E.0.1) can be re-written as

$$\begin{aligned} \dot{N}_M &= f\sigma_P P - \mu_X S_X - \mu_X E_X - \mu_X I_X - \mu_M N_M \\ &\quad + b_H(Q_2 + Q_3 - Q_1 + R_1 + R_2)A_X \leq f\sigma_P P - \mu_M N_M, \end{aligned} \tag{E.0.2}$$

so that,

$$\limsup_{t\to\infty} N_M(t) \leq \frac{f\sigma_P P^\diamond}{\mu_M}.$$

Hence, the solutions of the equations of the sub-system (3.4.2) are bounded for all time $t > 0$. Similarly, consider the equation for the rate of change of the total human population, given by:

$$\dot{N}_H = \Pi - \mu_H N_H - \delta_H(I_{H_p} + I_{H_u}) \leq \Pi - \mu_H N_H, \tag{E.0.3}$$

from which it follows that $\limsup_{t\to\infty} N(t) \leq \frac{\Pi}{\mu_H}$. Thus, the solutions of the sub-system (3.4.4) are bounded for all $t > 0$. Since the solutions of the three sub-systems of the model {(3.4.1), (3.4.2),(3.4.4)} are bounded, it follows that the solutions of the model are bounded. This concludes the proof of Item (a).

(b) The proof for the invariance of the region Ω_1 follows from the bounds established in Item (a) (i.e., $0 < \limsup_{t\to\infty} L_1(t) \leq L_1^\diamond$, $0 < \limsup_{t\to\infty} L_j(t) \leq L_j^\diamond$ and $0 < \limsup_{t\to\infty} P(t) \leq$

$P^{\diamond}$) and the fact that $\dot{E}(t) < 0$ whenever $E(t) > K_E$, $\dot{L}_1(t) < 0$ whenever $L_1(t) > L_1^{\diamond}$ and $\dot{L}_j(t) < 0$ whenever $L_j(t) > L_1^{\diamond}$ $(j = 2, 3, 4)$, respectively.

For the invariance of the region Ω_2, it is convenient to consider the following equation for the rate of change of the total mosquito population given by:

$$\begin{aligned}\dot{N}_M &= f\sigma_P P - \mu_X S_X - \mu_X E_X - \mu_X I_X - \mu_M N_M \\ &\quad + b_H(Q_2 + Q_3 - Q_1 + R_1 + R_2)A_X \leq f\sigma_P P - \mu_M N_M.\end{aligned}$$

It follows that $\dot{N}_M < 0$ whenever $N_M(t) > \frac{f\sigma_P P^{\diamond}}{\mu_M}$. Thus, the region Ω_2 is invariant with respect to the sub-system (3.4.2) of the model {(3.4.1), (3.4.2),(3.4.4)}.

Finally, consider the equation for the total human population given by

$$\dot{N}_H = \Pi - \mu_H N_H - \delta_H(I_{Hp} + I_{Hu}) \leq \Pi - \mu_H N_H.$$

It follows that $\dot{N}_H < 0$ whenever $N_H(t) > \frac{\Pi}{\mu_H}$. Thus, the region Ω_3 is invariant with respect to the sub-system (3.4.4) of the model {(3.4.1), (3.4.2),(3.4.4)}. Since the regions Ω_1, Ω_2 and Ω_3 are positively-invariant and attracting, it follows that $\Omega = \Omega_1 \times \Omega_2 \times \Omega_3$ is positively-invariant and attracting for the model {(3.4.1), (3.4.2),(3.4.4)}. This concludes the proof of Item (b).

APPENDIX F

COEFFICIENTS OF EQUATION (3.5.5)

$$
\begin{aligned}
C_1 &= b_H\left\{\pi_p(1-\varepsilon_{deter})[(1-\varepsilon_{die,p})\varepsilon_{bite|\sim die,p}+\varepsilon_{die,p}]+\pi_u[(1-\varepsilon_{die,u})\varepsilon_{bite|\sim die,u}+\varepsilon_{die,u}]\right\}+\mu_X+\mu_M>0,\\
C_2 &= b_H[\pi_p(1-\varepsilon_{deter})(1-\varepsilon_{die,p})\varepsilon_{bite|\sim die,p}+\pi_u(1-\varepsilon_{die,u})\varepsilon_{bite|\sim die,u}]>0,\\
C_3 &= b_H\left\{\pi_p(1-\varepsilon_{deter})[(1-\varepsilon_{die,p})\varepsilon_{bite|\sim die,p}+\varepsilon_{die,p}]+\pi_u[(1-\varepsilon_{die,u})\varepsilon_{bite|\sim die,u}+\varepsilon_{die,u}]\right\}\\
&\quad +\kappa_V+\mu_X+\mu_M>0,\\
C_4 &= \left\{\pi_p(1-\varepsilon_{deter})[\varepsilon_{die,p}(1-\varepsilon_{bite|\sim die,p})+\varepsilon_{bite|\sim die,p}]+\pi_u[\varepsilon_{die,u}(1-\varepsilon_{bite|\sim die,u})+\varepsilon_{bite|\sim die,u}]\right\}\kappa_V^2>0,\\
C_5 &= 2\kappa_V\left(\mu_M+\frac{\theta_Y}{2}+\frac{\varphi_Z}{2}\right)C_4>0,\\
C_6 &= \pi_p(1-\varepsilon_{deter})\left\{[\varepsilon_{die,p}(1-\varepsilon_{bite|\sim die,p})+\varepsilon_{bite|\sim die,p}]\mu_M^2+(\theta_Y+\varphi_Z)[\varepsilon_{die,u}(1-\varepsilon_{bite|\sim die,u})+\varepsilon_{bite|\sim die,u}]\mu_M+\varepsilon_{bite|\sim die,p}\theta_Y\varphi_Z\right\}>0,\\
C_7 &= \pi_u\left\{[\varepsilon_{die,u}(1-\varepsilon_{bite|\sim die,u})+\varepsilon_{bite|\sim die,u}]\mu_M^2+(\theta_Y+\varphi_Z)[\varepsilon_{die,u}(1-\varepsilon_{bite|\sim die,u})+\varepsilon_{bite|\sim die,u}]\mu_M+\varepsilon_{bite|\sim die,u}\theta_Y\varphi_Z\right\}>0,\\
C_8 &= (\mu_M+\kappa_V)K_{10}K_{12},\\
C_9 &= \varphi_Z+\theta_Y+b_H\left\{\pi_p(1-\varepsilon_{deter})[1-(1-\varepsilon_{die,p})(1-\varepsilon_{bite|\sim die,p})]+\pi_u[1-(1-\varepsilon_{die,u})(1-\varepsilon_{bite|\sim die,u})]\right\}>0,\\
C_{10} &= \theta_Y\varphi_Z+b_H(\theta_Y+\varphi_Z)\left\{\pi_p(1-\varepsilon_{deter})[1-(1-\varepsilon_{die,p})(1-\varepsilon_{bite|\sim die,p})]+\pi_u[1-(1-\varepsilon_{die,u})(1-\varepsilon_{bite|\sim die,u})]\right\}>0,\\
C_{11} &= b_H\theta_Y\varphi_Z[\pi_p\varepsilon_{die,p}(1-\varepsilon_{deter})+\varepsilon_{die,u}\pi_u]>0.
\end{aligned}
$$

APPENDIX G

EQUATIONS OF THE MODEL (3.4.1),(3.4.2),(3.4.4) WITHOUT BEDNETS INTERVENTION

In the absence of the bednet-based intervention, the sub-systems of the model involving the adults and human dynamics, given by Equations (3.4.2) and (3.4.4), reduce, respectively, to the following sub-systems:

$$\text{Stage I}\begin{cases}\dot{S}_X &= f\sigma_P P + \varphi_Z S_Z + b_H Q_3 S_X - (b_H + \mu_X + \mu_M)\, S_X,\\ \dot{E}_X &= \varphi_Z E_Z + b_H Q_3 E_X - (b_H + \kappa_V + \mu_X + \mu_M)\, E_X,\\ \dot{I}_X &= \varphi_Z I_Z + \kappa_V E_X + b_H Q_3 I_X - (b_H + \mu_X + \mu_M)\, I_X.\end{cases}$$

$$\text{Stage II}\begin{cases}\dot{S}_Y &= (1-\beta_V\omega) R_2 S_X - (\theta_Y + \mu_M)\, S_Y,\\ \dot{E}_Y &= b_H\beta_V\omega R_2 S_X + b_H R_2 E_X - (\theta_Y + \kappa_V + \mu_M)\, E_Y,\\ \dot{I}_Y &= \kappa_V E_Y + b_H R_2 I_X - (\theta_Y + \mu_M)\, I_Y.\end{cases} \tag{G.0.1}$$

$$\text{Stage III}\begin{cases}\dot{S}_Z &= \theta_Y S_Y - (\varphi_Z + \mu_M)\, S_Z,\\ \dot{E}_Z &= \theta_Y E_Y - (\varphi_Z + \kappa_V + \mu_M)\, E_Z,\\ \dot{I}_Z &= \theta_Y I_Y + \kappa_V E_Z - (\varphi_Z + \mu_M)\, I_Z,\end{cases}$$

$$\text{Human}\begin{cases}\dot{S}_H &= \Pi - (\lambda_{VH} + \mu_H) S_H + \eta_H R_H,\\ \dot{E}_H &= \lambda_{VH} S_H - (\gamma_H + \mu_H) E_H,\\ \dot{I}_H &= \gamma_H E_H - (\alpha_H + \delta_H + \mu_H) I_H,\\ \dot{R}_H &= \alpha_H I_H - (\eta_H + \mu_H) R_H.\end{cases} \tag{G.0.2}$$

The equations for the aquatic dynamics, given by (3.4.1), remain unchanged. Hence, the reduced (no-bednets) model consist of the equations $\{(3.4.1), (3.4.2), (G.0.2)\}$.

It can be shown, using the next generation operator method (as in Section 3), that the basic reproduction number of the reduced model $\{(3.4.1), (3.4.2),\ (G.0.2)\}$ is given by

$$\tilde{\mathcal{R}}_{0*} = \sqrt{\frac{b_H\beta_V J_1 J_3 S_X^0 \beta_M \gamma_H \theta_Y \varphi_Z \kappa_V [(K_9 + K_{12}) J_5 + K_9 K_{11}]}{K_{13} K_{14} N_H^* (J_5 K_{10} K_{12} - J_6\theta_Y\varphi_Z)(J_4 K_9 K_{11} - J_6\theta_Y\varphi_Z)}}, \tag{G.0.3}$$

where,

$$J_1 = b_H\left[\varepsilon_{bite|die,u}\,\varepsilon_{die,u} + \varepsilon_{bite|\sim die,u}(1-\varepsilon_{die,u})\right],\ J_2 = (1-\varepsilon_{die,u})(1-\varepsilon_{bite|\sim die,u}),$$
$$N_H^* = \frac{\Pi}{\mu_H},\ J_3 = (1-\varepsilon_{die,u})\varepsilon_{bite|\sim die,u},\ J_4 = (b_H+\mu_X+\mu_M) - b_H J_2,$$
$$J_5 = (b_H+\kappa_V+\mu_X+\mu_M) - b_H J_2,\ J_6 = b_H J_3,\ \mathcal{N}_{0*} = \frac{(\psi_E\varphi_Z\sigma_E f\sigma_P\theta_Y J_6)\prod_{i=1}^{4}\sigma_{L_i}}{(J_4K_9K_{11} - J_6\theta_Y\varphi_Z)\prod_{i=1}^{6}K_i},$$
$$S_X^0 = \frac{\left[f\sigma_E\sigma_P K_E\left(1-\frac{1}{\mathcal{N}_{0*}}\right)K_9K_{11}\right]\prod_{i=1}^{4}\sigma_{L_i}}{(J_4K_9K_{11} - J_6\theta_Y\varphi_Z)\prod_{i=2}^{6}K_i}.$$

Substituting the baseline parameter values in Table 4 (for the holo-endemic setting) shows that the worst-case scenario basic reproduction number ($\tilde{\mathcal{R}}_0$) of the model {(3.4.1), (3.4.2), (3.4.4)}, or, equivalently, the reduced model {(3.4.2), (G.0.2)}, given by (G.0.3), is $\tilde{\mathcal{R}}_{0*} = 11.4$.

APPENDIX H

PROOF OF THEOREM 3.5.2

The proof of Theorem 3.5.2 is based on using center manifold theory (Carr, 1981; Castillo-Chavez and Song, 2004). It is convenient to define the following change of variables for the model {(3.4.1), (3.4.2), (3.4.4)}: $E = x_1$, $L_1 = x_2$, $L_2 = x_3$, $L_3 = x_4$, $L_4 = x_5$, $P = x_6$, $S_X = x_7$, $E_X = x_8$, $I_X = x_9$, $S_Y = x_{10}$, $E_Y = x_{11}$, $I_Y = x_{12}$, $S_Z = x_{13}$, $E_Z = x_{14}$, $I_Z = x_{15}$, $S_{Hp} = x_{16}$, $E_{Hp} = x_{17}$, $I_{Hp} = x_{18}$, $R_{Hp} = x_{19}$, $S_{Hu} = x_{20}$, $E_{Hu} = x_{21}$, $I_{Hu} = x_{22}$, $R_{Hu} = x_{23}$. Using the vector notation $X = (x_1, ...x_{23})^T$ and $F = (f_1, ...f_{23})^T$, the model can then be written in the form $\frac{dX}{dt} = (f_1, ...f_{23})^T$, as follows:

$$
\begin{aligned}
\dot{x}_1 \equiv f_1 &= \psi_E \varphi_Z \left(1 - \frac{x_1}{K_E}\right)_+ (x_{13} + x_{14} + x_{15}) - (\sigma_E + \mu_E)\, x_1, \\
\dot{x}_2 \equiv f_2 &= \sigma_E x_1 - (\sigma_{L_1} + \mu_L)\, x_2, \\
\dot{x}_3 \equiv f_3 &= \sigma_{L_1} x_2 - (\sigma_{L_2} + \mu_L)\, x_3, \\
\dot{x}_4 \equiv f_4 &= \sigma_{L_2} x_3 - (\sigma_{L_3} + \mu_L)\, x_4, \\
\dot{x}_5 \equiv f_5 &= \sigma_{L_3} x_4 - (\sigma_{L_4} + \mu_L)\, x_5, \\
\dot{x}_6 \equiv f_6 &= \sigma_{L_4} x_5 - (\sigma_P + \mu_P)\, x_6, \\
\dot{x}_7 \equiv f_7 &= f\sigma_P x_6 + \varphi_Z x_{13} + b_H(Q_2 + Q_3)x_7 - (b_H Q_1 + \mu_X + \mu_M)\, x_7, \\
\dot{x}_8 \equiv f_8 &= \varphi_Z x_{14} + b_H(Q_2 + Q_3)x_8 - (b_H Q_1 + \kappa_V + \mu_X + \mu_M)\, x_8, \\
\dot{x}_9 \equiv f_9 &= \varphi_Z x_{15} + \kappa_V x_8 + b_H(Q_2 + Q_3)x_9 - (b_H Q_1 + \mu_X + \mu_M)\, x_9, \\
\dot{x}_{10} \equiv f_{10} &= b_H[(1 - \beta_V \omega_p)R_1 + (1 - \beta_V \omega_u)R_2]x_7 - (\theta_Y + \mu_M)\, x_{10}, \\
\dot{x}_{11} \equiv f_{11} &= b_H(\beta_V \omega_p R_1 + \beta_V \omega_u R_2)x_7 + b_H(R_1 + R_2)x_8 - (\theta_Y + \kappa_V + \mu_M)\, x_{11}, \\
\dot{x}_{12} \equiv f_{12} &= \kappa_V x_{11} + b_H(R_1 + R_2)x_9 - (\theta_Y + \mu_M)\, x_{12}, \\
\dot{x}_{13} \equiv f_{13} &= \theta_Y x_{10} - (\varphi_Z + \mu_M)\, x_{13}, \\
\dot{x}_{14} \equiv f_{14} &= \theta_Y x_{11} - (\varphi_Z + \kappa_V + \mu_M)\, x_{14}, \\
\dot{x}_{15} \equiv f_{15} &= \theta_Y x_{12} + \kappa_V x_{14} - (\varphi_Z + \mu_M)\, x_{15}, \\
\dot{x}_{16} \equiv f_{20} &= \Pi \pi_p - (\lambda_{VH_p} + \mu_H)x_{16} + \eta_H x_{19}, \\
\dot{x}_{17} \equiv f_{21} &= \lambda_{VH_p} x_{16} - (\gamma_H + \mu_H)x_{17}, \\
\dot{x}_{18} \equiv f_{22} &= \gamma_H x_{17} - (\alpha_H + \delta_H + \mu_H)x_{18}, \\
\dot{x}_{19} \equiv f_{23} &= \alpha_H x_{18} - (\eta_H + \mu_H)x_{19}, \\
\dot{x}_{20} \equiv f_{24} &= \Pi \pi_u - (\lambda_{VH_u} + \mu_H)x_{20} + \eta_H x_{23}, \\
\dot{x}_{21} \equiv f_{25} &= \lambda_{VH_u} x_{20} - (\gamma_H + \mu_H)x_{21}, \\
\dot{x}_{22} \equiv f_{26} &= \gamma_H x_{21} - (\alpha_H + \delta_H + \mu_H)x_{22}, \\
\dot{x}_{23} \equiv f_{27} &= \alpha_H x_{22} - (\eta_H + \mu_H)x_{23},
\end{aligned}
\tag{H.0.1}
$$

where,

$$\begin{aligned}
\text{EIR}_p &= b_H \frac{x_9}{N_{H_p}} \pi_p (1-\varepsilon_{deter}) \left[\varepsilon_{bite|die,p}\varepsilon_{die,p} + \epsilon_{bite|\sim die,p}(1-\varepsilon_{die,p})\right], \\
\text{EIR}_u &= b_H \frac{x_9}{N_{H_u}} \pi_u \left[\varepsilon_{bite|die,u}\varepsilon_{die,u} + \varepsilon_{bite|\sim die,u}(1-\varepsilon_{die,u})\right], \\
\lambda_{VH_p} &= \beta_M \,\text{EIR}_p, \\
\lambda_{VH_u} &= \beta_M \,\text{EIR}_u, \\
\omega_p &= \frac{x_{18}}{N_{H_p}},\ \omega_u = \frac{x_{22}}{N_{H_u}}.
\end{aligned}$$

Let $\mathcal{R}_0 = 1$ and suppose, further, that $\beta_M = \beta_M^*$ is chosen as a bifurcation parameter. Solving for $\beta_M = \beta_M^*$ from $\mathcal{R}_0 = 1$ gives

$$\beta_M = \beta_M^* = \frac{\Pi \pi_p \pi_u \left(C_3 K_{10} K_{12} - C_2 \theta_Y \varphi_Z\right)\left(C_1 K_9 K_{11} - C_2 \theta_Y \varphi_Z\right)}{\mu_H^2 b_H x_7^* \kappa_V \varphi_Z \theta_Y [(K_9 + K_{12})C_3 + K_9 K_{11}](\mathcal{R}_{H_p V} + \mathcal{R}_{H_u V})}.$$

The Jacobian of the transformed system (H.0.1), evaluated at the DFE ($\mathcal{T}_2$) with $\beta_M = \beta_M^*$, is given by

$$J(\beta_M^*) = \begin{bmatrix} J_1 & J_2 \\ J_3 & J_4 \end{bmatrix},$$

where,

$$J_1 = \begin{bmatrix}
-\frac{\psi_E \varphi_Z x_{13}^*}{K_E} - K_1 & 0 & 0 & 0 & 0 & 0 & 0 & 0 & 0 & 0 & 0 & 0 \\
\sigma_E & -K_2 & 0 & 0 & 0 & 0 & 0 & 0 & 0 & 0 & 0 & 0 \\
0 & \sigma_{L_1} & -K_3 & 0 & 0 & 0 & 0 & 0 & 0 & 0 & 0 & 0 \\
0 & 0 & \sigma_{L_2} & -K_4 & 0 & 0 & 0 & 0 & 0 & 0 & 0 & 0 \\
0 & 0 & 0 & \sigma_{L_3} & -\mu_H & 0 & 0 & 0 & 0 & 0 & 0 & 0 \\
0 & 0 & 0 & 0 & \sigma_{L_4} & -K_5 & 0 & 0 & 0 & 0 & 0 & 0 \\
0 & 0 & 0 & 0 & 0 & f\sigma_P & -C_1 & 0 & 0 & 0 & 0 & 0 \\
0 & 0 & 0 & 0 & 0 & 0 & 0 & -C_3 & 0 & 0 & 0 & 0 \\
0 & 0 & 0 & 0 & 0 & 0 & 0 & \kappa_V & -C_1 & 0 & 0 & 0 \\
0 & 0 & 0 & 0 & 0 & 0 & C_2 & 0 & 0 & -K_9 & 0 & 0 \\
0 & 0 & 0 & 0 & 0 & 0 & 0 & C_2 & 0 & 0 & -K_{10} & 0 \\
0 & 0 & 0 & 0 & 0 & 0 & 0 & 0 & C_2 & 0 & \kappa_V & -K_9
\end{bmatrix},$$

$$J_2 = \begin{bmatrix}
\psi_E \varphi_Z (1-\frac{x_1^*}{K_E}) & \psi_E \varphi_Z (1-\frac{x_1^*}{K_E}) & \psi_E \varphi_Z (1-\frac{x_1^*}{K_E}) & 0 & 0 & 0 & 0 & 0 & 0 & 0 & 0 \\
0 & 0 & 0 & 0 & 0 & 0 & 0 & 0 & 0 & 0 & 0 \\
0 & 0 & 0 & 0 & 0 & 0 & 0 & 0 & 0 & 0 & 0 \\
0 & 0 & 0 & 0 & 0 & 0 & 0 & 0 & 0 & 0 & 0 \\
0 & 0 & 0 & 0 & 0 & 0 & 0 & 0 & 0 & 0 & 0 \\
0 & 0 & 0 & 0 & 0 & 0 & 0 & 0 & 0 & 0 & 0 \\
\varphi_Z & 0 & 0 & 0 & 0 & 0 & 0 & 0 & 0 & 0 & 0 \\
0 & \varphi_Z & 0 & 0 & 0 & 0 & 0 & 0 & 0 & 0 & 0 \\
0 & 0 & \varphi_Z & 0 & 0 & 0 & 0 & 0 & 0 & 0 & 0 \\
0 & 0 & 0 & 0 & 0 & -\frac{b_H R_1 \beta_V x_7^*}{x_{16}^*} & 0 & 0 & 0 & -\frac{b_H R_2 \beta_V x_7^*}{x_{20}^*} & 0 \\
0 & 0 & 0 & 0 & 0 & \frac{b_H R_1 \beta_V x_7^*}{x_{16}^*} & 0 & 0 & 0 & \frac{b_H R_2 \beta_V x_7^*}{x_{20}^*} & 0 \\
0 & 0 & 0 & 0 & 0 & 0 & 0 & 0 & 0 & 0 & 0
\end{bmatrix},$$

$$J_3 = \begin{bmatrix} 0 & 0 & 0 & 0 & 0 & 0 & 0 & 0 & \theta_Y & 0 & 0 \\ 0 & 0 & 0 & 0 & 0 & 0 & 0 & 0 & 0 & \theta_Y & 0 \\ 0 & 0 & 0 & 0 & 0 & 0 & 0 & 0 & 0 & 0 & \theta_Y \\ 0 & 0 & 0 & 0 & 0 & 0 & 0 & -\beta_M Q_p & 0 & 0 & 0 \\ 0 & 0 & 0 & 0 & 0 & 0 & 0 & \beta_M Q_p & 0 & 0 & 0 \\ 0 & 0 & 0 & 0 & 0 & 0 & 0 & 0 & 0 & 0 & 0 \\ 0 & 0 & 0 & 0 & 0 & 0 & 0 & 0 & 0 & 0 & 0 \\ 0 & 0 & 0 & 0 & 0 & 0 & 0 & -\beta_M Q_u & 0 & 0 & 0 \\ 0 & 0 & 0 & 0 & 0 & 0 & 0 & \beta_M Q_u & 0 & 0 & 0 \\ 0 & 0 & 0 & 0 & 0 & 0 & 0 & 0 & 0 & 0 & 0 \\ 0 & 0 & 0 & 0 & 0 & 0 & 0 & 0 & 0 & 0 & 0 \end{bmatrix},$$

and,

$$J_4 = \begin{bmatrix} -K_{11} & 0 & 0 & 0 & 0 & 0 & 0 & 0 & 0 & 0 & 0 \\ 0 & -K_{12} & 0 & 0 & 0 & 0 & 0 & 0 & 0 & 0 & 0 \\ 0 & \kappa_V & -K_{11} & 0 & 0 & 0 & 0 & 0 & 0 & 0 & 0 \\ 0 & 0 & 0 & -\mu_H & 0 & 0 & \eta_H & 0 & 0 & 0 & 0 \\ 0 & 0 & 0 & 0 & -K_{13} & 0 & 0 & 0 & 0 & 0 & 0 \\ 0 & 0 & 0 & 0 & \gamma_H & -K_{14} & 0 & 0 & 0 & 0 & 0 \\ 0 & 0 & 0 & 0 & 0 & \alpha_H & -K_{15} & 0 & 0 & 0 & 0 \\ 0 & 0 & 0 & 0 & 0 & 0 & 0 & -\mu_H & 0 & 0 & \eta_H \\ 0 & 0 & 0 & 0 & 0 & 0 & 0 & 0 & -K_{13} & 0 & 0 \\ 0 & 0 & 0 & 0 & 0 & 0 & 0 & 0 & \gamma_H & -K_{14} & 0 \\ 0 & 0 & 0 & 0 & 0 & 0 & 0 & 0 & 0 & \alpha_H & -K_{15} \end{bmatrix}.$$

The Jacobian $J(\beta_M^*)$ has a simple zero eigenvalue (and all other eigenvalues having negative real parts). Hence, the center manifold theory (Carr, 1981; Castillo-Chavez and Song, 2004) can be used to analyse the dynamics of (H.0.1) near $\beta_M = \beta_M^*$. This entails carrying out the following computations.

Eigenvectors of $J(\mathcal{T}_2)\mid_{\beta_M=\beta_M^*}$: The Jacobian of the transformed system (H.0.1), evaluated at the DFE ($\mathcal{T}_2$) with $\beta_M = \beta_M^*$, has a right and left eigenvectors (associated with the zero eigenvalue) (the expression for the eigenvector w_i and v_i, $i = 1, 2, .., 23$, are given in the Supplementary Material).

Computations of bifurcation coefficients of a and b :

By computing the associated non-zero partial derivatives of $F(x)$ evaluated the the DFE, it follows from Theorem 4.1 in (Castillo-Chavez and Song, 2004) that the associated bifurcation coefficients, a and b, are given, respectively, by

$$\begin{aligned} a =& -2b_H \left[\frac{(-w_{22}R_2w_7v_{11}\beta_V + v_{21}Q_u\beta_M w_9(w_{22}+w_{21}+w_{23}))x_{20}^* + w_{22}\beta_V R_2 x_7^* v_{11}(w_{20}+w_{21}+w_{22}+w_{23})}{(x_{20}^*)^2} \right] \\ & -2b_H \left[\frac{(-w_{18}\beta_V R_1 w_7 v_{11} + Q_p\beta_M w_9(w_{18}+w_{19}+1))x_{16}^* + w_{18}(x_{20}^*)^2\beta_V R_1 x_7^* v_{11}(w_{16}+w_{18}+w_{19}+1)}{(x_{16}^*)^2} \right], \end{aligned} \tag{H.0.2}$$

and,

$$b = b_H w_9 \left(Q_u v_{21} + Q_p\right) > 0. \tag{H.0.3}$$

Hence, it follows from Theorem 4.1 of (Castillo-Chavez and Song, 2004) that the transformed model (H.0.1) undergoes a backward bifurcation at $\mathcal{R}_0 = 1$ if the bifurcation coefficient a (given by (H.0.2)) is positive.

APPENDIX I

PROOF OF THEOREM 3.5.3.

Consider the special case of the model {(3.4.1), (3.4.2), (3.4.4)} without disease-induced mortality in the host population (i.e., $\delta_H = 0$). Further, let $\mathcal{N}_0 > 1$ (so that the NDFE, $\mathcal{T}_2$, exists) and $\tilde{\mathcal{R}}_0 \leq 1$. Setting $\delta_H = 0$ in the model {(3.4.1), (3.4.2), (3.4.4)} gives $N_H(t) \to \frac{\Pi}{\mu_H}$ as $t \to \infty$, and $\bar{K}_{14} = \alpha_H + \mu_H$. Hence, from now on, $N_H(t)$ is replaced by its limiting value, $\frac{\Pi}{\mu_H}$. Furthermore, consider the following linear Lyapunov function:

$$\mathcal{F} = g_1 E_{Hp} + g_2 I_{Hp} + g_3 E_{Hu} + g_4 I_{Hu} + g_5 E_X + g_6 I_X + g_7 E_Y + g_8 I_Y + g_9 E_Z + g_{10} I_Z,$$

where,

$$\begin{aligned}
g_1 &= \beta_V N_{Hu} \gamma_H b_H R_1 S_X \kappa_V \varphi_Z \theta_Y \left(C_3 \left(K_9 + K_{12}\right) + K_9 K_{11}\right), \\
g_2 &= \beta_V N_{Hu} b_H R_1 S_X \kappa_V \varphi_Z \theta_Y \left(C_3 \left(K_9 + K_{12}\right) + K_9 K_{11}\right) K_{13}, \\
g_3 &= \beta_V N_{Hp} \gamma_H b_H R_2 S_X \kappa_V \varphi_Z \theta_Y \left(C_3 \left(K_9 + K_{12}\right) + K_9 K_{11}\right), \\
g_4 &= \beta_V N_{Hp} b_H R_2 S_X \kappa_V \varphi_Z \theta_Y \left(C_3 \left(K_9 + K_{12}\right) + K_9 K_{11}\right) K_{13}, \\
g_5 &= \frac{C_2 \beta_M \gamma_H \theta_Y^2 \varphi_Z^2 \kappa_V^2 S_X \beta_V (C_3(K_9+K_{12})+K_9 K_{11})^2 \left(N_{Hp} Q_u R_2 S_{Hu} + N_{Hu} Q_p R_1 S_{Hp}\right)}{(C_3 K_{10} K_{12} - C_2 \theta_Y \varphi_Z)(C_1 K_9 K_{11} - C_2 \theta_Y \varphi_Z) C_3} \\
&\quad + \frac{K_9 K_{11} K_{13} \bar{K}_{14} N_{Hp} N_{Hu} \left(C_3 K_{10} K_{12} - C_2 \theta_Y \varphi_Z\right) \kappa_V}{C_3}, \\
g_6 &= K_9 K_{11} K_{13} \bar{K}_{14} N_{Hp} N_{Hu} \left(C_3 K_{10} K_{12} - C_2 \theta_Y \varphi_Z\right), \\
g_7 &= \frac{\beta_M \gamma_H \theta_Y^2 \varphi_Z^2 \kappa_V^2 S_X \beta_V (C_3(K_9+K_{12})+K_9 K_{11})^2 \left(N_{Hp} Q_u R_2 S_{Hu} + N_{Hu} Q_p R_1 S_{Hp}\right)}{(C_3 K_{10} K_{12} - C_2 \theta_Y \varphi_Z)(C_1 K_9 K_{11} - C_2 \theta_Y \varphi_Z)}, \\
g_8 &= \theta_Y K_{13} \bar{K}_{14} \varphi_Z N_{Hp} N_{Hu} \left(C_3 K_{10} K_{12} - C_2 \theta_Y \varphi_Z\right), \\
g_9 &= \frac{C_2 \beta_M \gamma_H \theta_Y^2 \varphi_Z^3 \kappa_V^2 S_X \beta_V (C_3(K_9+K_{12})+K_9 K_{11})^2 \left(N_{Hp} Q_u R_2 S_{Hu} + N_{Hu} Q_p R_1 S_{Hp}\right)}{(C_3 K_{10} K_{12} - C_2 \theta_Y \varphi_Z)(C_1 K_9 K_{11} - C_2 \theta_Y \varphi_Z) K_{12} C_3} \\
&\quad + \frac{\varphi_Z K_9 K_{13} \bar{K}_{14} N_{Hp} N_{Hu} \left(C_3 K_{10} K_{12} - C_2 \theta_Y \varphi_Z\right) \kappa_V \left(K_{11} + C_3\right)}{K_{12} C_3}, \\
\text{and, } g_{10} &= \varphi_Z K_9 K_{13} \bar{K}_{14} N_{Hp} N_{Hu} \left(C_3 K_{10} K_{12} - C_2 \theta_Y \varphi_Z\right).
\end{aligned}$$

The Lyapunov derivative of $\mathcal{F}$ (where a dot represents differentiation with respect to

t) is given by:

$$\begin{aligned}
\dot{\mathcal{F}} &= g_1\dot{E}_{Hp} + g_2\dot{I}_{Hp} + g_3\dot{E}_{Hu} + g_4\dot{I}_{Hu} + g_5\dot{E}_X + g_6\dot{I}_X + g_7\dot{E}_Y + g_8\dot{I}_Y + g_9\dot{E}_Z + g_{10}\dot{I}_Z,\\
&= g_1(\lambda_{VH_p}S_{H_p} - K_{13}E_{H_p}) + g_2(\gamma_H E_{H_p} - \bar{K}_{14}I_{H_p}) + g_3(\lambda_{VH_u}S_{H_u} - K_{13}E_{H_u})\\
&+ g_4(\gamma_H E_{H_u} - \bar{K}_{14}I_{Hu}) + g_5(\varphi_Z E_Z - C_3E_X) + g_6(\varphi_Z I_Z + \kappa_V E_X - C_1 I_X)\\
&+ g_7[(b_H\beta_V\omega_p R_1 + b_H\beta_V\omega_u R_2)S_X + C_2E_X - K_{10}E_Y] + g_8(\kappa_V E_Y + C_2 I_X - K_9 I_Y)\\
&+ g_9(\theta_Y E_Y - K_{12}E_Z) + g_{10}(\theta_Y I_Y + \kappa_V E_Z - K_{11}I_Z),\\
&= \left(\frac{g_1\beta_M Q_p S_{Hp}}{N_{Hp}} + \frac{g_3\beta_M Q_u S_{Hu}}{N_{Hu}} - g_6C_1 + g_8C_2\right)I_X + \left(\frac{g_7 b_H\beta_V R_1 S_X}{N_{Hp}} - g_2\bar{K}_{14}\right)I_{Hp}\\
&+ \left(\frac{g_7 b_H\beta_V R_2 S_X}{N_{Hu}} - g_4\bar{K}_{14}\right)I_{Hu} + \left(-g_1K_{13} + g_2\gamma_H\right)E_{Hp} + \left(-g_3K_{13} + g_4\gamma_H\right)E_{Hu}\\
&+ \left(-g_5C_3 + g_6\kappa_V + g_7C_2\right)E_X + \left(-g_7K_{10} + g_8\kappa_V + g_9\theta_Y\right)E_Y\\
&+ \left(-g_9K_{12} + g_{10}\kappa_V + g_5\varphi_Z\right)E_Z\\
&+ (-g_8K_9 + g_{10}\theta_Y)I_Y + (-g_{10}K_{11} + g_6\varphi_Z)I_Z.
\end{aligned}$$

Since $S_{Hp}(t) \leq N_{Hp}$, $S_{Hu}(t) \leq N_{Hu}$, $N_{Hp}(t) = \frac{\Pi\pi_p}{\mu_H}$ and $N_{Hu}(t) = \frac{\Pi\pi_u}{\mu_H}$ in Ω for all $t > 0$, it follows that:

$$\begin{aligned}
\dot{\mathcal{F}} =& \leq K_{13}\bar{K}_{14}N_{Hp}N_{Hu}(C_1K_9K_{11} - C_2\theta_Y\varphi_Z)(C_3K_{10}K_{12} - C_2\theta_Y\varphi_Z)(\tilde{\mathcal{R}}_0^2 - 1)I_X\\
&+ \beta_V N_{Hu} b_H R_1 S_X \kappa_V\varphi_Z\theta_Y\left(C_3\left(K_9 + K_{12}\right) + K_9K_{11}\right)K_{13}K_{14}(\tilde{\mathcal{R}}_0^2 - 1)I_{Hp}\\
&+ \beta_V N_{Hp} b_H R_2 S_X \kappa_V\varphi_Z\theta_Y\left(C_3\left(K_9 + K_{12}\right) + K_9K_{11}\right)K_{13}K_{14}(\tilde{\mathcal{R}}_0^2 - 1)I_{Hu}\\
&+ \frac{\varphi_Z^2\left(N_{Hp}Q_uR_2S_{Hu} + N_{Hu}Q_pR_1S_{Hp}\right)\kappa_V^2\beta_V(C_3(K_9+K_{12}) + K_9K_{11})^2\theta_Y^2 S_X\gamma_H\beta_M}{b_H K_{12}C_3(C_1K_9K_{11} - C_2\theta_Y\varphi_Z)}\left(1 - \frac{1}{\tilde{\mathcal{R}}_0^2}\right)E_Y.
\end{aligned}$$

Hence, $\dot{\mathcal{F}} \leq 0$ if $\tilde{\mathcal{R}}_0 < 1$ with $\dot{\mathcal{F}} = 0$ if and only if $I_X = I_{Hp} = I_{Hu} = E_Y = 0$. Therefore, $\mathcal{F}$ is a Lyapunov function in Ω and it follows from LaSalle's Invariance Principle (LaSalle and Lefschetz, 1976) that every solution to the equations in {(3.4.1), (3.4.2), (3.4.4)} (with $\delta_H = 0$ and initial conditions in Ω) converges to $\mathcal{T}_2$ as $t \to \infty$ That is,

$$\begin{aligned}
&(E_X(t), I_X(t), E_Y(t), I_Y(t), E_Z(t), I_Z(t), E_{Hp}(t), I_{Hp}(t), R_{Hp}(t), E_{Hu}(t), I_{Hu}(t), R_{Hu}(t))\\
&\to (0,0,0,0,0,0,0,0,0,0,0,0) \text{ as } t \to \infty.
\end{aligned}$$

$$\text{Thus, } \mathcal{X}(t) \to \left(E^*, L_1^*, L_2^*, L_3^*, L_4^*, P^*, S_X^*, 0, 0, S_Y^*, 0, 0, S_Z^*, 0, 0, \frac{\Pi\pi_p}{\mu_H}, 0, 0, 0, \frac{\Pi\pi_u}{\mu_H}, 0, 0, 0\right)$$

as $t \to \infty$ for $\tilde{\mathcal{R}}_0 \leq 1$. Hence, the NDFE, $\mathcal{T}_2$, is globally-asymptotically stable in Ω if $\tilde{\mathcal{R}}_0 \leq 1$ for the special case of the model {(3.4.1), (3.4.2), (3.4.4)} with $\delta_H = 0$.